Fall 2013

Kinetics of human and bovine insulin amyloid fibril formation in the presence of solid/liquid interfaces

Paulina Barranco Morales

Department:

KINETICS OF HUMAN AND BOVINE INSULIN AMYLOID FIBRIL FORMATION IN THE PRESENCE OF SOLID/LIQUID INTERFACES

by

PAULINA BARRANCO MORALES

A THESIS

Presented to the Faculty of the Graduate School of the

MISSOURI UNIVERSITY OF SCIENCE AND TECHNOLOGY

In Partial Fulfillment of the Requirements for the Degree

MASTER OF SCIENCE IN CHEMICAL ENGINEERING

2013

Approved by

Dr. Daniel Forciniti, Advisor
Dr. Douglas Ludlow
Dr. Parthasakha Neogi

ABSTRACT

The purpose of this thesis was to study the rate and extent of aggregation of human and bovine insulin in bulk and in the presence of either polystyrene microspheres with different surface chemistries or liposomes of different composition. Insulin aggregation was followed by turbidimetry, Fourier transform infrared spectroscopy (FTIR), and dynamic light scattering. The Congo red assay was used to corroborate the presence of amyloid deposits and transmission electron microscopy (TEM) was used to analyze the morphology of the amyloid deposits.

Our results show that not all the surfaces shortened the lag time. On the other hand, most surfaces had an impact (either significant or minute) on the growth rate of both insulins. Faster nucleation was observed at all times for both insulins when incubated at 60 ˚C vs. 37 ˚C, 230 rpm. Furthermore, considerable secondary structure changes (from random coils and α-helices to β sheets and turns) in both insulins during fibrillation were observed.

Both, human and bovine insulin exhibited analogous fibril morphologies (i.e. similar length, width, and structure) when treated under the same conditions in the presence and in the absence of surfaces with the exception of incubation at 37 ˚C, 230 rpm stirring for 55 hours. In addition, when human and bovine insulin were subjected to mechanical stresses the fibrils appear “fragmented” and hence their size is smaller when compared to insulin that has not been agitated. Bovine insulin fibrils are longer and thinner under these incubation conditions (37 ˚C, 230 rpm) than human insulin fibrils. Incubation temperatures were different between agitated insulin (37 ˚C) and non-agitated insulin (60 ˚C). It is also noticeable that at 60 ˚C larger fibrils formed at longer incubation times, for both insulins. The width of the fibrils ranged between 10 to 20 nm, there is not a noticeable dependence/correlation between fibril length and width for human or bovine insulin. On the other hand, based on the obtained images, the statistical analysis, and in agreement with literature the incubation methods utilized determined the fibril morphologies.

ACKNOWLEDGEMENTS

First, I would like to thank my family for their continuous support and encouragement. I would like to express my sincere gratitude to my advisor, Dr. Daniel Forciniti, for his guidance throughout my graduate studies and for giving me a chance when most doors seemed closed.

I would also like to express my deepest gratitude to Dr. Douglas Ludlow and Dr. Parthasakha Neogi for their time and endeavor in serving as committee members and reviewing this thesis. Special thanks to my friends, especially Mariana Escalona, for their wonderful support.

Finally, I am very thankful to my Mother, Martha Morales, for her endless love and support throughout my life. This thesis is dedicated to her.

This material is based upon work supported by the National Science Foundation under Grant No. 0933468.

TABLE OF CONTENTS

LIST OF ILLUSTRATIONS

LIST OF TABLES

1. INTRODUCTION

Amyloid fibrils are ordered aggregates of peptides or proteins that are associated with many diseases such as Alzheimer's, Parkinson's, and Huntington's diseases, type 2 diabetes mellitus, etc. (Nilsson, 2004). Amyloid diseases are apparently unconnected; however, intermolecular secondary structure (mainly β-sheet) is present in all amyloid aggregates. A number of factors that contribute to the formation of amyloid fibrils include, but are not limited to, temperature, protein concentration, pH, ionic strength, and amino acid sequence. There are three criteria that define a protein aggregate as an amyloid fibril: fibrillar morphology, green birefringence upon staining with Congo Red, and β-sheet secondary structure (Nilsson, 2004).

We have chosen insulin to study amyloid fibril formation in bulk and in the presence of interfaces because (i) insulin is a well-studied protein that is known to develop structurally similar cross-β-sheet plaques to those found in other amyloid-forming proteins (ii) insulin is readily available in large amounts at a reasonable price and (iii) its amino acid sequence is highly conserved from species to species, which facilitates the study of minute changes in amino-acid sequence on fibrillation. Insulin is a glucose regulatory hormone composed of two polypeptide chains: the A-chain, which consists of 21 amino acids, and the B-chain, which consists of 30 amino acids. Insulin has a helical native structure, with its two polypeptide chains linked together by two interchain and one intra-chain disulfide bonds (Brange et al., 1997). In solution, this protein is found as an equilibrium mixture of monomers, dimers, tetramers, and hexamers (which vary according to pH and concentration, among other factors) (Klunk et al., 1989).

Insulin is mainly stored as a zinc-coordinated hexamer while zinc-free insulin is a dimer at low protein concentration over the pH 2-8 range, changing to a tetramer at protein concentrations above 1.5 mg/ml (Brange et al., 1987). Nielsen et al. (2001b) studied the effect of pH on the association of human and bovine insulin. At pH 7.4 insulin is hexameric and it dissociates upon decreasing the pH. At pH 3 insulin exists as a tetramer, at pH 2.0 is monomeric in acetic acid and at pH 1.6 insulin is dimeric. Despite the fact that insulin aggregation has been extensively studied, the differences in the

aggregation behavior between proteins from different species have not been deeply investigated. The aggregation behavior of human and bovine insulin in vitro in bulk and at solid/liquid interfaces is explored in this thesis.

The amino acid sequences of human and bovine insulin are different in positions 8 and 10 of the A-chain and in position 30 of the B- chain. Threonine (Thr), a polar amino acid in position 8 of the A chain in human insulin is substituted in bovine insulin by alanine (Ala), a nonpolar amino acid. Isoleucine (Ile), a nonpolar amino acid in position 10 of the A chain of human insulin, is substituted in bovine insulin by valine (Val), a nonpolar amino acid as well. Finally, threonine (Thr), in position 30 of human insulin, is substituted in bovine by alanine (Ala).

Formation of insulin fibrils is a physical process in which non-native molecules interact with each other to form linear, biologically inactive aggregates (Brange et al., 1997). In vitro insulin fibril formation has been shown to result in the formation of insoluble aggregates which are rich in β-sheet structures (Nielsen et al., 2001a). Numerous studies, reviewed below, have shown that once insulin has been exposed to elevated temperatures, mechanical stresses, organic solvents, and low pH is prone to fibrillation.

It has been shown by Waugh (1940, 1941) that the formation of insulin fibrils occurs before precipitation and that the heat treatment does not completely modify the globular nature of the insulin molecule. Waugh later demonstrated that heat precipitation consists of three steps: 1) nucleation (formation of active centers), 2) growth (elongation of these centers to fibrils), and 3) precipitation/equilibrium (floccule formation) (Waugh, 1946a; Waugh 1946b; Waugh et al., 1953). These steps involve interactions between nonpolar side chains (hydrophobic interactions) (Nielsen et al., 2001a; Bryant et al., 1993; Waugh, 1946a). Although nucleation appears to need temperatures above ambient, the growth into fibrils can happen at ambient or lower temperatures and, depending on the conditions, the growth leads to long fibrils or to shorter fibrils with a propensity to assemble radially to spherulites with precipitation as the result (Waugh et al., 1953; Waugh, 1957).

The concentration dependence of bovine insulin aggregation was studied by Sluzky et al. (1991). They concluded that the aggregation process is kinetically

controlled, with rates of aggregation proportional to protein concentration. Their study also demonstrated the importance of mechanical stresses by showing that an increase in the agitation rate decreased the initial lag phase and that the rate of aggregation became steeper.

Nielsen et al. (2001a) investigated the effect of insulin concentration, pH, ionic strength, agitation, anions (i.e. 1-anilinonaphthalene-8-sulfonic acid (ANS)), the use of denaturants (such as urea), stabilizers (like sucrose) and seeding of fibrils on the kinetics of fibril formation. In agreement with Sluzky et al. (1991), they found that higher insulin concentrations lead to shorter lag times and faster growth. Their studies also demonstrated that shorter lag times and faster growth of fibrils are attained at acidic pH compared to neutral pH, while an increase in ionic strength yielded shorter lag times and slower growth. According to their results, there was no clear connection between the rate of fibril elongation and ionic strength. Furthermore, they concluded that strong agitation (960 rpm) was the dominant effect on the kinetics of insulin aggregation. The presence of the anion (ANS) and the stabilizer (sucrose) increased the lag time while the presence of the denaturant (urea) decreased it. Finally, they showed that the addition of seeds eliminated the lag time.

Waugh (1946a) observed the formation of small spherulites produced in 2% insulin/1% sodium chloride solution in hydrochloric acid at pH 1.8 incubated at 100 ˚C for 3 minutes. According to him, the structure of the spherite (as it was called then) is one of statistical orientation of the constituent fibrils. He also suggested that a new fibril entering the association has to diffuse into the region of the growing spherite and become correctly oriented. We obtained spherical aggregates by the method (see description in Appendix A) of Burke and Rougvie (1972). Figure 1.1 shows amyloid spherulites by themselves and amyloid spherulites coexisting with amyloid fibrils obtained by this method which is similar to that of Waugh. All the micrographs were obtained from the same sample and were prepared in 0.025 M HCl and 0.1 M NaCl (pH 1.6).

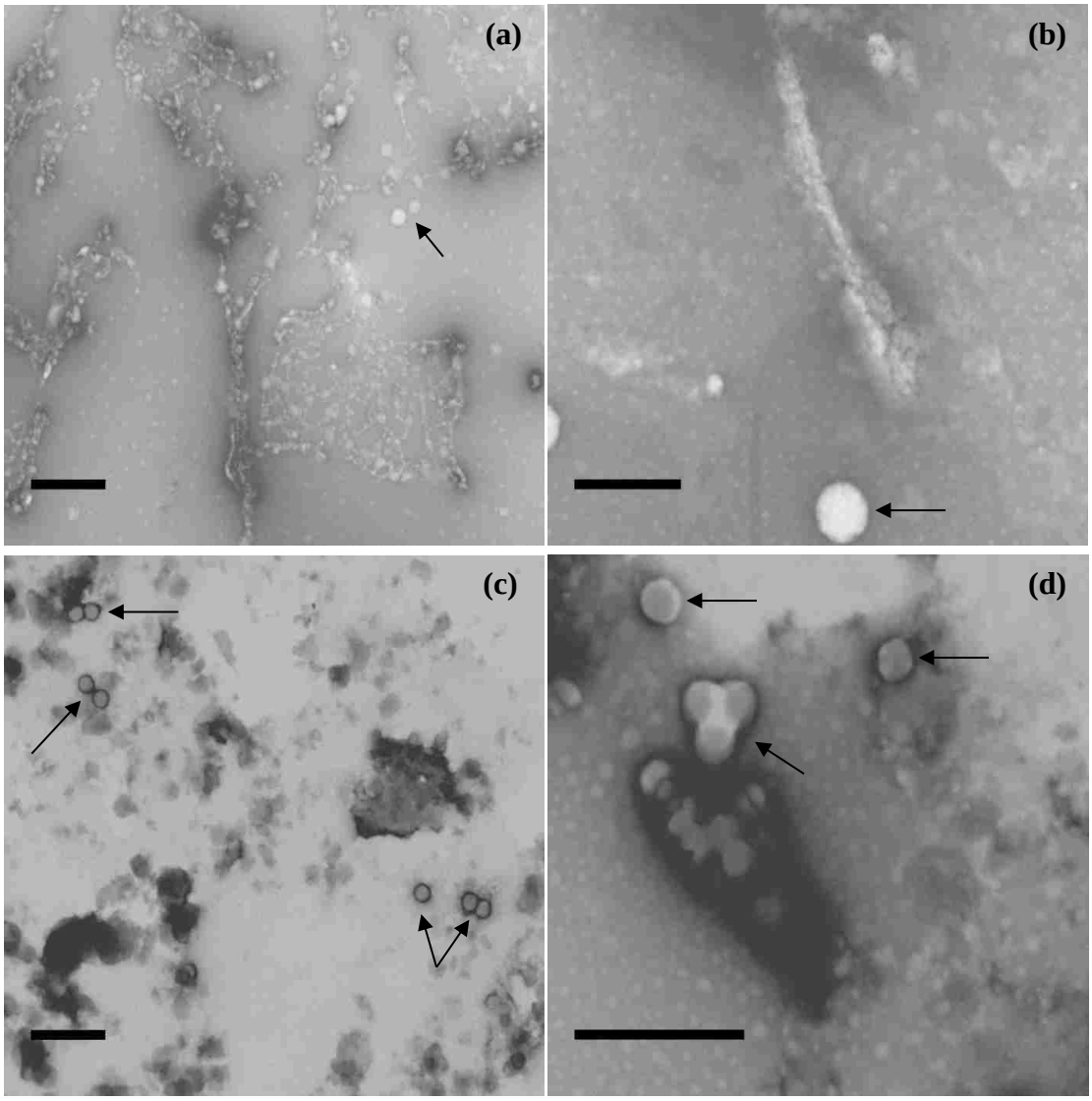

Figure 1.1. Negative staining scanning electron images of bovine insulin fibrils and spherulites obtained by the method of Burke and Rougvie (1972). (a) and (b) may suggest that fibril formation and random coil aggregation occur at the same time under certain conditions. (c) and (d) illustrate the presence of spherulites. The scale bar represents 500 nm.

The presence of solid/liquid or liquid/air interfaces affects the formation of fibrils. The following studies have shown that the physicochemical nature of the surface plays a critical role in amyloid fibril formation and impacts the kinetics, the size and the shape of amyloid aggregates and fibrils. Sluzky et al. (1991) observed an increase in bovine insulin aggregation rate in the presence of hydrophobic Teflon surfaces. Brange et al.

(1997) suggested that insulin denatures and aggregates at the liquid/air interface generated during vigorous agitation (Aggregation of proteins at the liquid/air interface is a well-known phenomenon). The effect of roughness and surface wettability on human insulin fibrillation was studied by Nayak et al. (2008) by atomic force microscopy and UV-vis absorption spectroscopy. They noticed a decrease of the lag phase in the presence of different polymeric surfaces such as regenerated cellulose, polyethylene, and poly ethersulfone). They concluded that the nucleation rate increased with increasing surface roughness and decreasing surface wettability. The effect of lipid/water interfaces on protein fibrillation has also been investigated (Sharp et al., 2002; McLaurin et al., 2002). Sharp and coworkers utilized lipid-coated polystyrene surfaces (such as 1,2-dioleoyl-3-trimethylammonium propane (DOTAP, cationic headgroup) and 1,2-dioleoyl-sn-glycerol-3-[phosphor-rac-(1-glycerol)] (DOPG, anionic headgroup)) to study surface denaturation and amyloid fibril formation of bovine insulin. Their results show that both negatively (containing DOPG) and positively (containing DOTAP) charged liposomes accelerate the rate of unfolding and of beta sheet formation. DOPG containing liposomes were less effective than DOTAP containing ones. McLaurin et al., (2002) explored the role of cholesterol in bulk in Aβ40/42 fibrillogenesis. They observed fibril formation in the case of Aβ40 but not with Aβ42, which forms amorphous aggregates.

The molecular mechanism of amyloid fibril formation is not fully understood. Several mechanisms that may lead to the formation of aggregates are under discussion. The more widespread one is nucleated polymerization. In this mechanism an uncommon event leads to the formation of a nucleus (frequently considered to be a small oligomer, but it could be an unusual monomer conformation). Once this nucleus forms, it leads to the development of the formation of a fibril. Protofilaments (thought to consist of two β-sheets running in parallel) can wrap up around each other to form protofibrils or mature fibrils, which are generally considered to be composed of two to six protofilaments.

It is now believe that protein folding does not involve a sequence of steps from an specific partially folded state to another one but rather it would involve a stochastic search of the several conformations accessible to a polypeptide chain (Dobson et al., 1998; Wolynes et al., 1995). People have suggested that aggregation of insulin occurs by exposing the hydrophobic residues that are usually buried within the protein's structure,

this destabilizes the protein and aggregation begins. Mass spectrometry of amyloid insulin fibrils has confirmed that the disulfide bonds of the native protein are retained in the amyloid structure (Nettleton et al., 1998).

It has been suggested by Ahmad et al. (2003) that the first step in insulin fibrillation is the formation of a non-native, partially unfolded, monomeric intermediate. Nielsen et al. (2001b) proposed a model for insulin fibril formation in which the formation of amyloid fibrils starts with hexamer/trimer/dimer units followed by the dissociation of these units into the monomer which has to unfold to some extent to form the intermediate necessary to produce the nucleus from which amyloid fibrils can grow. Vestergaard et al. (2007) suggested that the main elongation mechanism of insulin fibrils consists of the addition of oligomers to the growing fibril. They demonstrated that the growth rate is proportional to the number of oligomers and that the amount of monomers in solution is close to zero during the later phases of fibril formation.

A left-handed helical twist has been described for all of the amyloid fibrils for which the hand has been confirmed such as human calcitonin (hCT) peptide hormone, and human amylin (Bauer, et al., 1995, Goldsbury et al., 1997). Based on this evidence and on the fact that the twist between β-sheets and β-strands is also left-handed, a model for the protofilaments' twist was suggested by Jimenez et al. (2002) in which the protofilaments must be left-handed and must follow the overall twist of the fibril. In contrast to previous models based on a β-coil structure (Blake & Serpell, 1996). Jimenez and coworkers also indicated that the β-sheets in amyloid protofilaments have to accompany the overall fibril twist.

2. MATERIALS AND METHODS

2.1 MATERIALS

Human and bovine insulin were used without further purification. Table 2.1 is a list of the different insulins used.

Table 2.1. Insulin sources.

Insulin (source)		Vendor	Catalog No.	Lot No.	Zinc content (%)
(1)	Human	SACF Biosciences	91077C	10L918	Unknown
(2)		SIGMA	I2643	096K03811V	0.4
(3)		SIGMA	I2643	SLBC1253V	0.4
(4)	Bovine	Sigma-Aldrich	15500	019K17765V	0.5
(5)		SIGMA	I1882	099K8702	0.5
(6)		CELL Applications, INC	128	104	Unknown

The latexes used were: (1) monodisperse polystyrene (PS) (average particle diameter: 107 nm, concentration: 2.64 w/v %) latex, (2) polystyrene hydroxylate (PS-OH) (average particle diameter: 193 nm, concentration: 2.63 w/v %), (3) polystyrene carboxylate (PS-COOH) (average particle diameter: 107 nm, concentration: 2.57 w/v %), and (4) polystyrene amino (PS-NH_2) (average particle diameter: 108 nm, concentration: 2.63 w/v %). All the latexes were purchased from Polysciences, Inc. Warrington, PA.

Five different types of liposomes were prepared. Lipids were dissolved at a concentration of 30 mg/ml in tert-butyl alcohol. The lipids, cholesterol (≈99%), L-α-phosphatidylcholine from egg yolk (≈99%), L-α- phosphatidylethanolamine from egg yolk (≈98%), L-α-phosphatidyl-DL-glycerol, and L-α- phosphatidyl-L-serine from glycine max (soybean) were purchased from Sigma (St. Louis, MO) and used without further purification. Nanopure water was used in all experiments. The compositions of the liposomes are shown in Table 2.2.

Table 2.2. Composition of liposomes.

Liposome	Composition		Abbreviation
1	80%/20%	PC/PS	C: Cholesterol
2	20%/80%	PC/C	PC: Phosphatidylcholine
3	80%/20%	PC/C	PE: Phosphatidylethanolamine
4	2:2:1:1	C/PC/PG/PE	PG: Phosphatidylglycerol
5	10:5:7.5:16	PC/PE/PS/C	PS: Phosphatidylserine
6	50%/50%	PC/C	

Congo red dye (C6277, Lot# MKBB0292) was purchased from Sigma-Aldrich, Saint Louis, MO.

2.2 METHODS

2.2.1. Preparation of Insulin Fibrils. All solutions were freshly prepared before each experiment. The solution consisted of 25 mM HCl, 100 mM NaCl adjusted to pH 1.6 (insulin is dimeric under these conditions). This solution was filtered through a Whatman 0.45 μm polysulfone membrane filter and then filtered again through a Whatman 0.2 μm polyethersulfone membrane filter. Stock protein solutions were prepared in this buffer at a concentration of 2 mg/ml. For bulk insulin samples, the required amount of sample was withdrawn from the stock solution and no further sample preparation was performed.

For insulin samples in the presence of surfaces, enough solution was withdrawn from the stock solution to prepare two samples (i.e. duplicates) but only one sample was prepared and then this sample was split in two to obtain "identical duplicates". All samples consisted of 1 to 2 ml (depending on the cuvette size) of 2 mg/ml insulin at a surface concentration of 12 cm^2/mg of insulin, with the exception of the control samples which contained only human or bovine insulin (also with duplicates). The samples were then transferred to disposable poly(methyl)methacrylate square cells. Two different incubation conditions were used for turbidimetry, FTIR, and dynamic light scattering

(DLS): 1) 37 ˚C at 230 rpm up to 55 hours, and 2) 60 ˚C for 4 to 6 hours. For TEM, the previous incubation conditions were used plus incubation at 60 ˚C for 40 hours. The samples were removed from the incubator at appropriate time intervals for analysis and were immediately placed back in the incubator.

2.2.2. Preparation of Liposomes. Liposomes were prepared by the freeze drying method (Li and Deng, 2004). 20 mg of lipid was dissolved in 1 ml of tert-Butyl Alcohol (TBA). Then, 150 mg of sucrose was dissolved in 1 ml of water. These two solutions were mixed at a volume ratio between 1:1 and 1:2. After mixing the solution remained optically clear. The mixture was further sonicated for less than a minute in order to assure proper mixing. The solution was then filtered through a Whatman 0.22 μm polyethersulfone membrane filter. The sample was then freeze-dried. After drying, the sample was stored in the freezer. The dried solid was dissolved in the appropriate amount of buffer before using.

2.2.3. Turbidity. The formation of fibrils was followed by monitoring the turbidity of the sample at 600 nm (OD600). The absorbance at 600 nm was measured using a Hitachi U-2900 Double-Beam UV/Vis spectrophotometer (Hitachi High Technologies America, Inc). Measurements were taken at multiple times.

2.2.4. Fourier Transform Infrared (FTIR) Spectroscopy. Analysis of the samples was performed in a Thermo Scientific Nicolet 6700 FTIR. At proper time intervals, the sample was gently shaken to distribute fibrils uniformly in the microtube before withdrawing aliquots of 8-10 μl. The sample was placed on a CaF_2 window and left to dry under the hood (drying took no more than 2 minutes). The sample chamber of the FTIR was purged with dry, CO_2 free, air for a few minutes before and after loading the sample. A scan of the CaF_2 window (without sample) was used as the background (Fandrich and Dobson, 2002; Kong and Yu, 2007; Nilsson, 2004). A total of 32 scans per sample were taken at a resolution of 4 cm^{-1}. A few runs were done with native insulin in a KBr pellet and the results were identical to those obtained by placing a solution of the hormone on the CaF_2 window and measuring after evaporation of the water.

2.2.5. Dynamic Light Scattering (DLS). The experiments were performed on a fiber-optic quasi-elastic light scattering (FOQELS) instrument from Brookhaven

Instruments Corp (Brookhaven). Measurements were done at 830 nm, at a 135.70° scattering angle, at 37 ˚C or 60 ˚C. Samples were measured for 30 seconds.

2.2.6. Congo Red Histological Dye Binding to Insulin Fibrils. The method of Klunk et al. (1989) was used. A stock solution of Congo red was prepared by dissolving 7 mg of the dye in 1ml of a buffer solution consisting of 0.15 M sodium chloride and 5 mM potassium phosphate, adjusted to pH 7.4. This solution was filtered twice through a Whatman 0.2-μm polyethersulfone membrane filter. 1 ml of the described buffer was added to a disposable poly(methyl)methacrylate square cell and the Hitachi U-2900 Double-Beam UV/Vis spectrophotometer (Hitachi High Technologies America, Inc) was zeroed with this solution between 400 and 700 nm at room temperature. Next, 5 μl of the Congo red dye stock solution was added to the cell, a spectrum was recorded between 400 and 700 nm. Lastly, 10 μl of the protein sample was added to the same cell and another spectrum was recorded between 400 and 700 nm. After each addition, the cuvette was tilted a few times to mix its contents. Congo red tests were performed on all samples at the end of each experiment. A maximal spectral difference at 540 nm indicated the presence of amyloid fibrils.

2.2.7. Imaging by Transmission Electron Microscopy (TEM) and Scanning Electron Microscopy (SEM). The morphology of insulin fibrils under different conditions was examined with a FEI Tecnai F20 transmission electron microscope with an accelerating voltage of 120 kV or with a Helios NanoLab 600 Dual Beam (FIB/STEM) FEI Microscope operated under STEM mode at 30kV. A drop of water-diluted suspension of insulin fibrils (100 ml of the 2 mg/ml solution were diluted with 300 ml of water) was placed on a 200-mesh formvar copper grid (EMS, USA) and allowed to dry for 3 minutes. The excess solution was gently wicked off. Subsequently, the grid was negatively stained with a 5% (w/v) aqueous solution of uranyl acetate and left to dry for 3 minutes. Once again, the excess solution was gently wicked off.

3. RESULTS AND DISCUSSION

The rate and extent of aggregation of human and bovine insulin in bulk and in the presence of either polystyrene microspheres with different surface chemistries or liposomes of different compositions were studied. Insulin aggregation was followed by turbidimetry, Fourier transform infrared spectroscopy (FTIR), and dynamic light scattering (DLS). The Congo red assay was used to corroborate the presence of amyloid deposits and electron microscopy was used to analyze the morphology of the amyloid deposits.

Due to a scarcity of both insulins during this study different vendors and batches of human and bovine insulin were utilized in this work. This should be kept in mind when looking at the results since different batches may yield different results. The insulin source (a number) is given for each and every result from which the details of the insulin used (vendor information, catalog number, etc) can be found on Table 2.1.

3.1. MONITORING THE PROGRESS OF AGGREGATION BY TURBIDITY

Figures 3.1 to 3.8 show the kinetics of fibril formation followed by absorbance at 600 nm. Each data set is the average of two runs. The aggregation kinetics shows a pronounced lag phase that is followed by a sigmoidal increase (aggregate growth) and ends on a plateau which corresponds to the formation of mature fibrils. These features are usually assigned to a nucleation-dependent aggregation mechanism that consists of a nucleation, growth and precipitation/equilibrium phases (Jarrett and Lansbury, 1993).

The results are presented first for human and bovine insulin in bulk followed by insulin in the presence of liposomes and polystyrene beads (incubation conditions: (1) 60 ˚C (Figures 3.1 – 3.6) and (2) 37 ˚C and 230 rpm (Figures 3.1, 3.7 and 3.8). The graphs are shown in accordance with the way the experiments were run, i.e. for the first experiments (and graphs) a set of bulk insulin solutions was prepared per surface. For the later experiments (and graphs) a single bulk insulin solution was prepared for the entire run.

The lag times and the apparent rate constants of both insulins in bulk and in the presence of surfaces can be found in Tables 3.1 and 3.2, and 3.3 respectively.

When incubated at 60 ˚C, the lag times of human and bovine insulin in bulk are 3.2 and 1.7 hr (sources 1 and 3) and 1.0 and 2.1 hr (sources 4 and 6), respectively. The lag times of human and bovine insulin, when incubated at 37 ^{o}C and 230 rpm, are 4.0 and 11.0 hr, respectively (sources 2 and 6) (Figure 3.1, Table 3.1). However, under both incubation conditions, the growth rate is faster for bovine insulin than for human insulin. Furthermore, the higher the temperature the shorter the lag time and the faster the growth rate occurs.

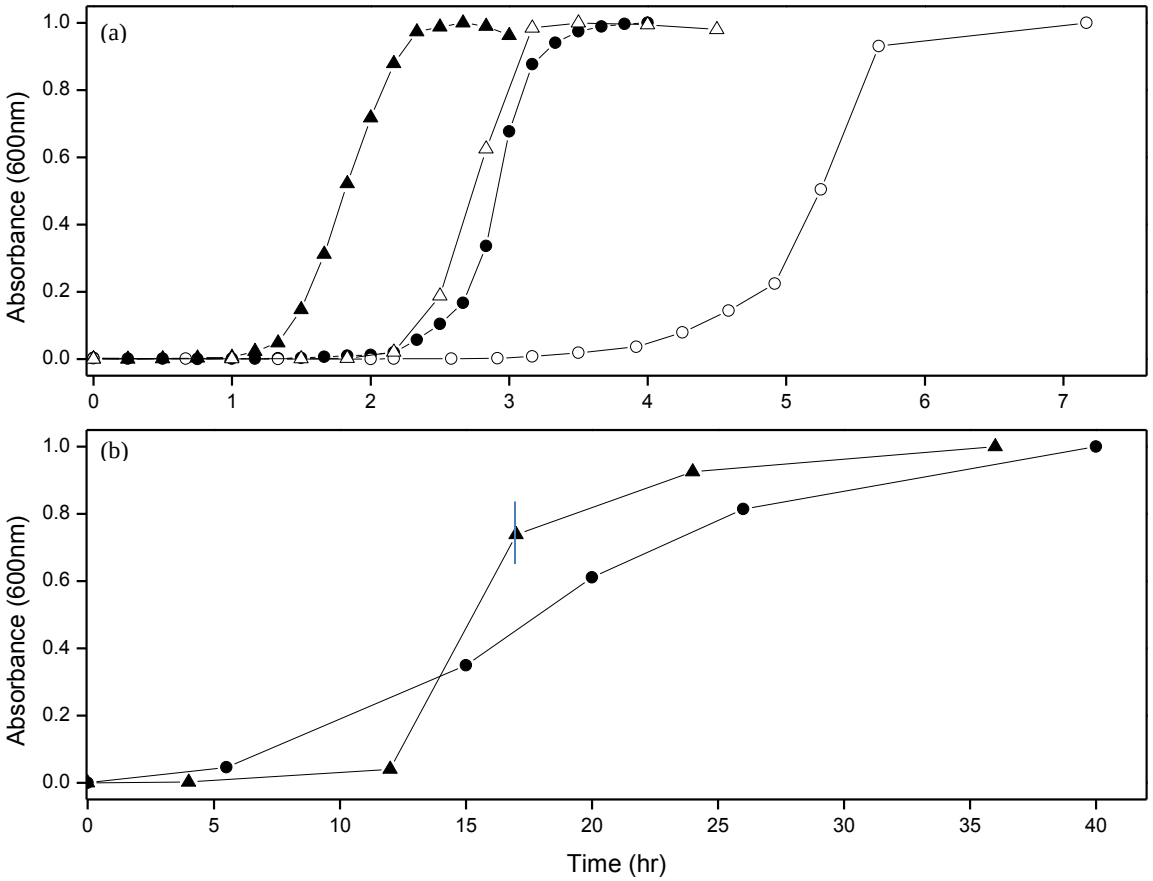

Figure 3.1. Fibril formation of human and bovine insulin in bulk incubated at 60 ˚C followed by absorbance at 600 nm. (a): insulin species were human insulin from source 1 (●), human insulin from source 3 (○), bovine insulin from source 4 (▲) and bovine insulin from source 6 (Δ) Incubation at 37 ˚C and 230 rpm (b): insulin species were human insulin from source 2 (●) and bovine insulin from source 6 (▲). The absorbance was normalized on a scale from zero to one.

Table 3.1. Lag time of human and bovine insulin in bulk.

60 ˚C			
Human insulin Source	**Lag time (hr)**		**Bovine insulin Source**
1	2.39	0.58	4
3	4.73	2.44	6
37 ˚C and 230 rpm			
2	7.05	13.31	6

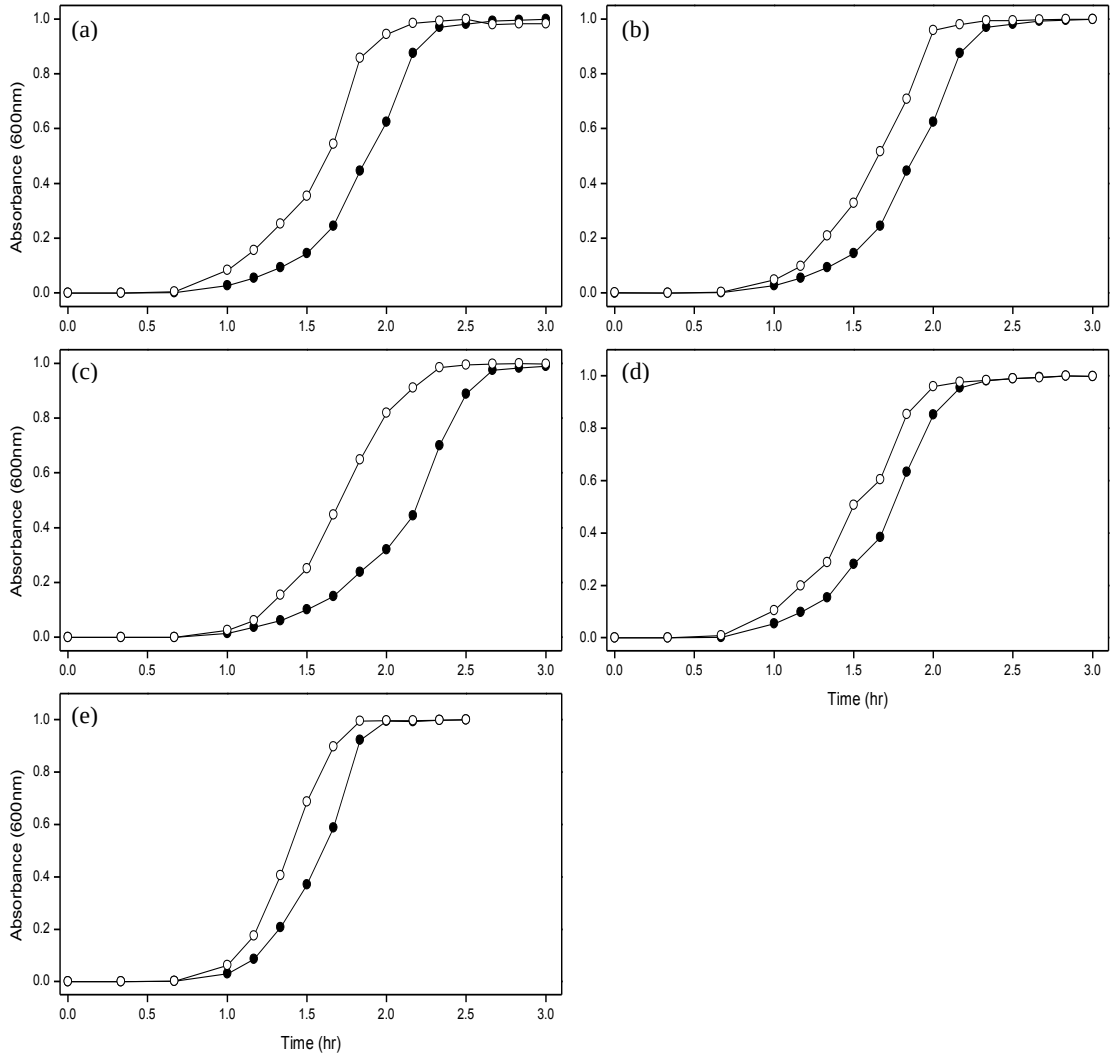

Figure 3.2. Fibril formation of human insulin in bulk and in the presence of liposomes incubated at 60˚ C followed by absorbance at 600 nm. Human insulin (source 1): in bulk (●) and in the presence of liposome s (○). (a) liposome 1 (80/20 PC/PS), (b) liposome 2 (20/80 PC/C), (c) liposome 3 (80/20 PC/C), (d) liposome 4 (2:2:1:1 C/PC/PG/PE) and € liposome 5 (10/5/7.5/16 PC/PE/PS/C).

Figure 3.2 shows that the only liposomes that have an impact on the lag time of human insulin are liposomes 4 (2:2:1:1 C/PC/PG/PE) and 5 (10/5/7.5/16 PC/PE/PS/C). From panel d, the lag time of human insulin in bulk (source 1) is 0.67 hr while in the presence of liposome 4 is 0.60 hr. The lag time of human insulin in bulk is 0.75 hr and in the presence of liposome 5 is 0.67 hr (panel e). Nonetheless, all the liposomes accelerate the aggregation of human insulin with liposome 3 (80/20 PC/C) having the greatest impact.

The data shown in Figure 3.3 shows that liposomes affect the overall kinetics of bovine insulin (source 4) more than that of human insulin (source 1, Figure 3.2). It is also noticeable that liposome 3 (80/20 PC/C) shortens the lag time and accelerates the growth rate of bovine insulin more than any other liposome (1.10 hr vs. 0.67 hr in bulk, panel c). Liposomes 1 (80/20 PC/PS) and 5 (10/5/7.5/16 PC/PE/PS/C) have a minor effect on the lag time and the growth rate of bovine insulin while liposomes 2 (20/80 PC/C) and 4 (2:2:1:1 C/PC/PG/PE) reduced the lag time significantly. The lag time for bovine insulin in bulk is 0.95 hr (panel b) and 0.85 hr (panel d) whereas in the presence of liposomes 2 and 4 the lag time is 0.67 hr, panels b and d respectively.

Both, human (panel a) and bovine (panel b) insulin from sources 3 and 6 (Figure 3.4) have slower kinetics than the insulins from sources 1 and 4, respectively. Liposome 2 had the biggest impact on the lag time (2.05 hr) and growth rate of human insulin; conversely, this liposome had the least impact on the lag time (1.85 hr) and growth rate of bovine insulin. Liposomes 3 (80/20 PC/C) and 6 (50/50 PC/C) affected the lag time of human insulin to the same extent (2.50 hr) but liposome 6 causes a faster growth rate. For bovine insulin, liposomes 3 and 6 had the same lag time (1.75 hr); in addition, their growth rates were almost identical.

Figure 3.5 shows the aggregation kinetics of human and bovine insulin (sources 1 and 4) in the presence of polystyrene (PS) beads. The lag time of human insulin in the presence of all polystyrene beads is the same (1.75 hr) as in bulk (panel a); however, the growth rates are different: PS-COOH causes the fastest growth rate followed by PS-NH_2 and PS-OH.

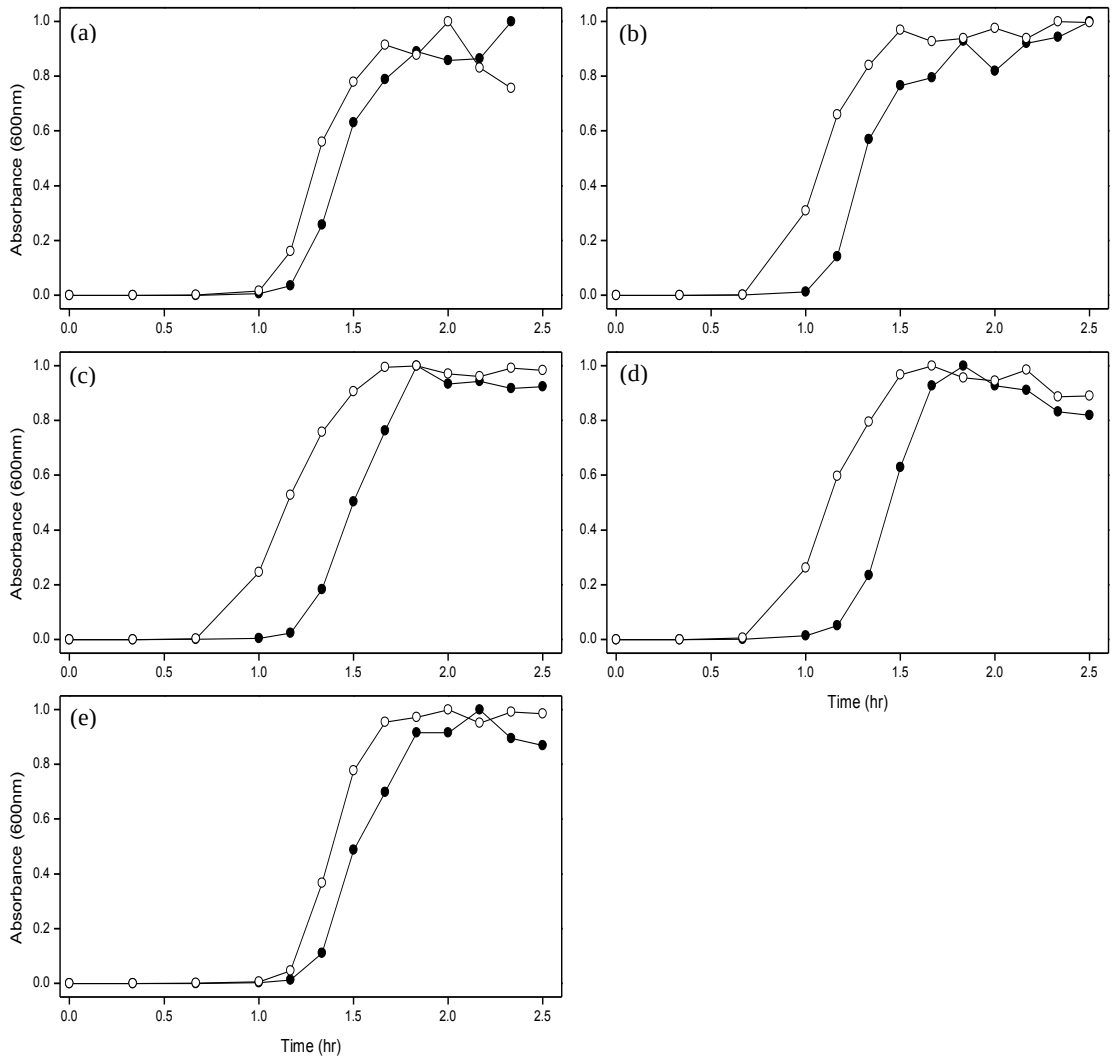

Figure 3.3. Fibril formation of bovine insulin in bulk and in the presence of liposomes incubated at 60˚ C followed by absorbance at 600 nm. All insulin species were from source 4. Bovine insulin: in bulk (●) and in the presence of liposome surface (○). Results shown are for: liposome 1 (80/20 PC/PS) (a), liposome 2 (20/80 PC/C) (b), liposome 3 (80/20 PC/C) (c), liposome 4 (2:2:1:1 C/PC/PG/PE) (d) and liposome 5 (10/5/7.5/16 PC/PE/PS/C) (e). The absorbance was normalized on a scale from zero to one.

An interesting phenomenon occurs in the growth rates of human insulin in bulk and in the presence of PS: the growth rate is faster for human insulin in bulk until it reaches 50% of the absorbance then the growth rate of human insulin in the presence of PS becomes faster than that of human insulin in bulk. All the polystyrenes, but PS-NH_2, extend the lag time of bovine insulin (bulk value: 0.70 hr, panel b): PS (0.90 hr), PS-

COOH (0.85 hr) and PS-OH (0.75 hr). The lag time is the same for bovine insulin in bulk and bovine insulin in the presence of PS-NH_2 (0.70 hr). The growth rates of bovine insulin followed the same trends as the lag times: i.e., from slowest to fastest: PS, PS-COOH and PS-OH. Bovine insulin in bulk and in the presence of $PSNH_2$ have the same growth rate until they reach about 40% of the absorbance but they behave quite differently after that point.

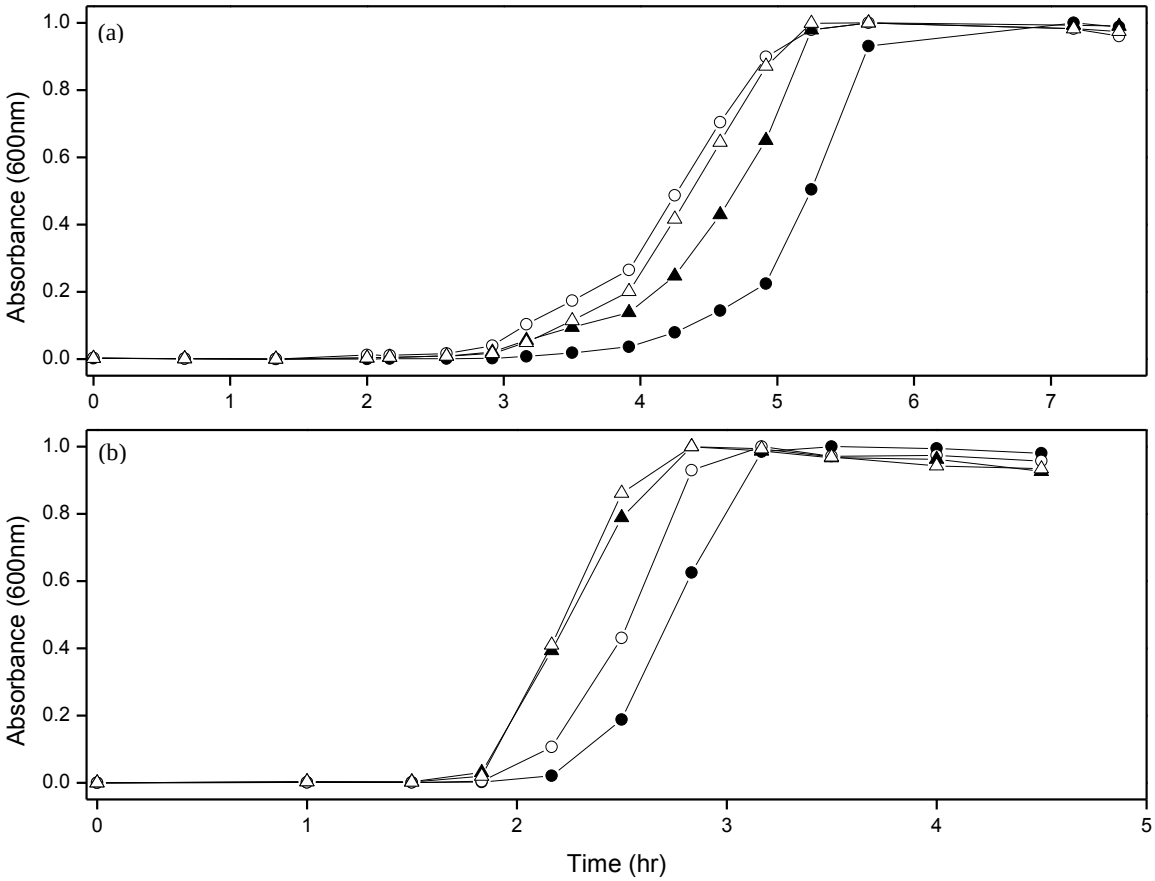

Figure 3.4. Fibril formation of human and bovine insulin in bulk and in the presence of liposomes incubated at 60 ˚C followed by absorbance at 600 nm. All human insulin species were from source 3 and all bovine insulin was from source 6. Results shown are for human insulin, panel (a) and bovine insulin, panel (b): in bulk (●), in the presence of: liposome 2 (20/80 PC/C) (○), liposome 3 (80/20 PC/C) (▲) and liposome 6 (50/50PC/C) (Δ). The absorbance was normalized on a scale from zero to one.

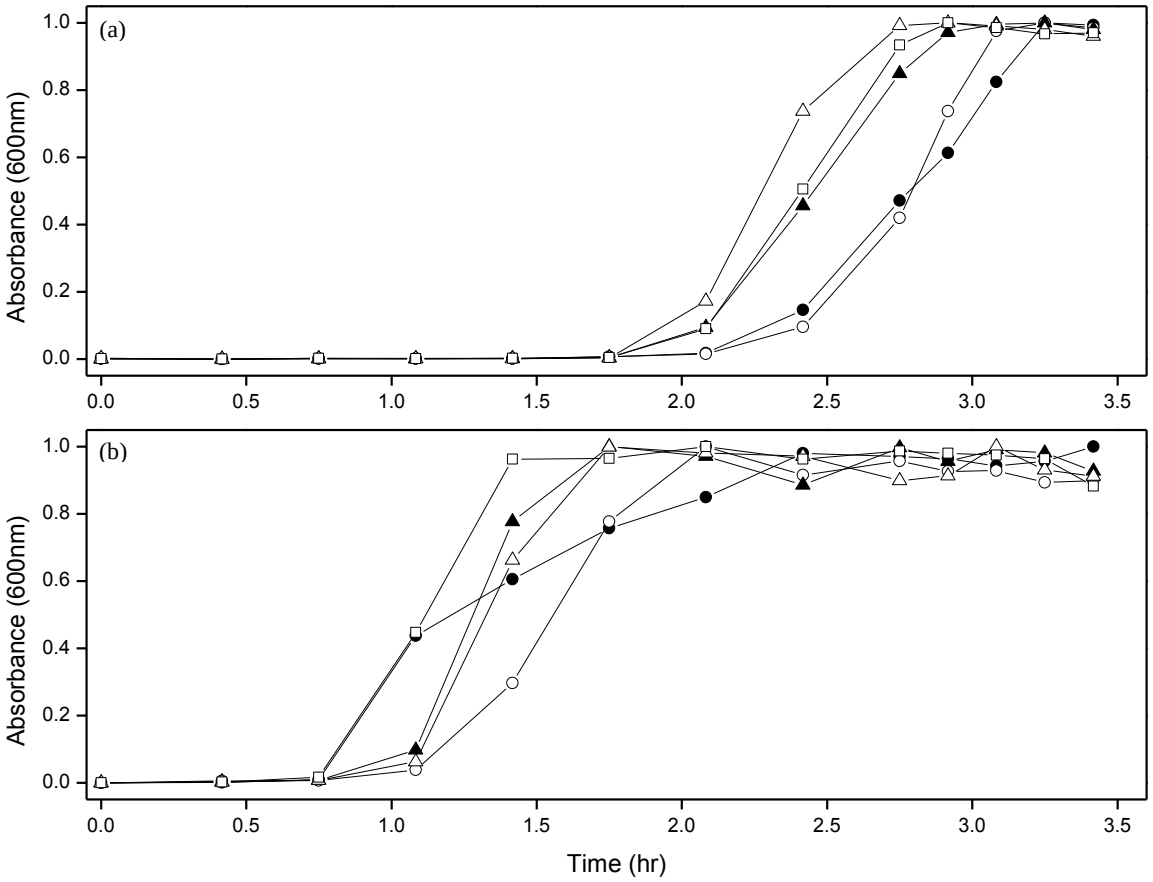

Figure 3.5. Fibril formation of human and bovine insulin in bulk and in the presence of polystyrene beads incubated at 60 ˚C followed by absorbance at 600 nm. All human insulin species were from source 1 and all bovine insulin was from source 4. Results shown are for human insulin, panel (a) and bovine insulin, panel (b): in bulk (●), in the presence of: PS (○), PS-OH (▲), PS-COOH (Δ) and PS-NH2 (□). The absorbance was normalized on a scale from zero to one.

The growth rate of bovine insulin in bulk seems to overshoot until it reaches the elongation phase while the growth rate of bovine insulin in the presence of PS-NH_2 continues to increase linearly until it reaches the elongation phase.

As previously discussed, human and bovine insulin from sources 3 and 6 have slower aggregation kinetics than the insulins from sources 1 and 4, respectively. Figure 3.6 shows that the lag time of human insulin (panel a) in bulk (3.20 hr) was not affected by PS-NH_2 (3.20 hr) while PS-COOH shortened the lag time (2.95 hr). The growth rates in both polystyrenes were faster than human insulin in bulk with PS-COOH being slightly faster than PS-NH_2. The lag time of bovine insulin in bulk (panel b) is 2.05 hr

while that of bovine insulin in the presence of PS-COOH (slowest growth rate) and PS-NH_2 (fastest growth rate) is 2.10 hr.

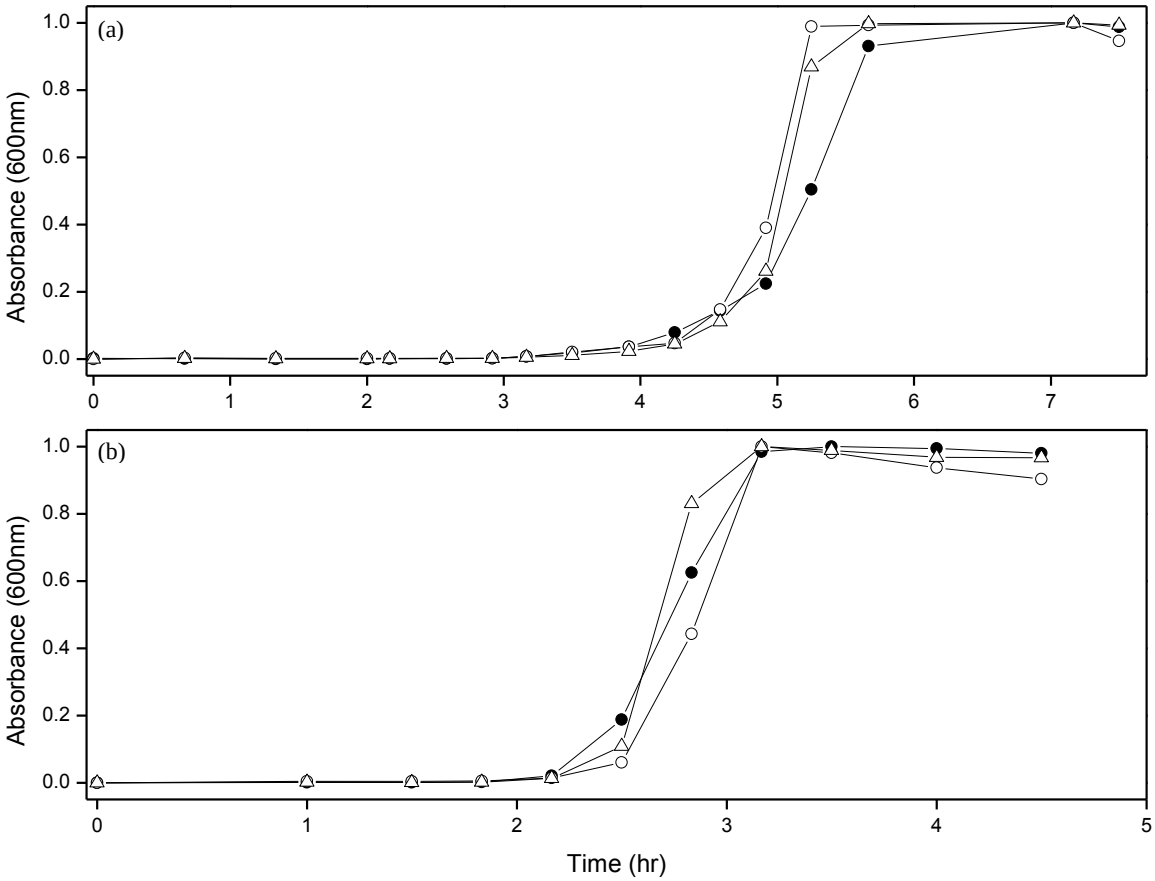

Figure 3.6. Fibril formation of human and bovine insulin in bulk and in the presence of polystyrene beads incubated at 60 ˚C followed by absorbance at 600 nm. All human insulin species were from source 3 and all bovine insulin was from source 6. Results shown are for human insulin, panel (a) and bovine insulin, panel (b): in bulk (●), in the presence of: PS-COOH (○) and PS-NH2 (Δ). The absorbance was normalized on a scale from zero to one.

Figure 3.7 shows the aggregation kinetics of human (panel a) and bovine (panel b) insulin (sources 2 and 6) incubated at 37 ˚C and 230 rpm in the presence of liposomes. The lag time of human insulin in bulk is 4.00 hr while that of bovine insulin in bulk is 11.0 hr. All the liposomes but 6 (50/50 PC/C) had an impact on the lag time of human insulin. Liposome 5 (10:5:7.5:16 PC/PE/PS/C) completely eliminated the lag phase, the

presence of liposomes 2 (20/80 PC/C) and 3 (80/20 PC/C) produced lag times of 2.00 hr and 3.50 hr, respectively. The growth rates follow the same trends as the lag times with liposome 5 causing the fastest rates followed by liposomes 2, 6, 4 and lastly human insulin in bulk.

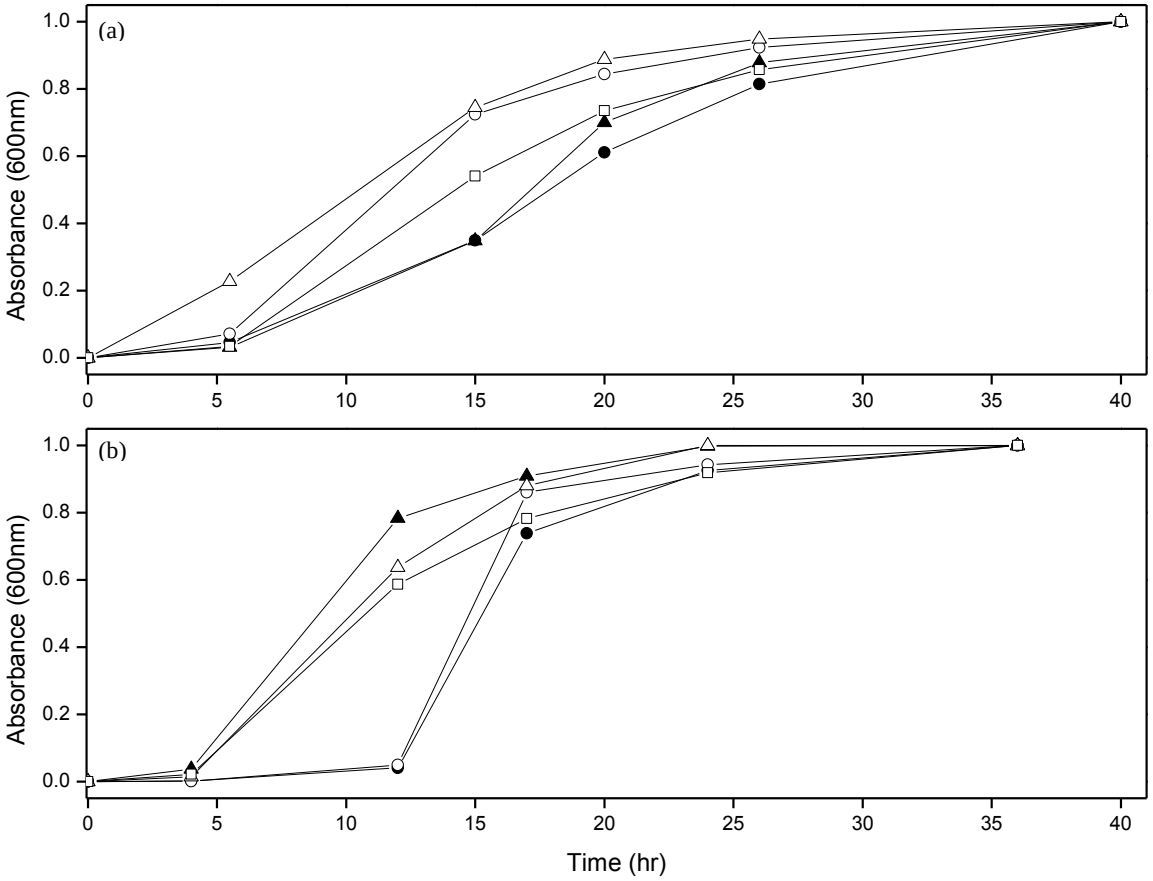

Figure 3.7. Fibril formation of human and bovine insulin in bulk and in the presence of liposomes incubated at 37 ˚C and 230 rpm followed by absorbance at 600 nm. All human insulin species were from source 2 and all bovine insulin was from source 6. Results shown are for human insulin, panel (a) and bovine insulin, panel (b): in bulk (●), in the presence of: liposome 2 (20/80 PC/C) (○), liposome 3 (80/20 PC/C) (▲), liposome 5 (10:5:7.5:16 PC/PE/PS/C) (Δ) and liposome 6 (50/50PC/C) (□). The absorbance was normalized on a scale from zero to one.

All the liposomes but 2 (20/80 PC/C) affected the lag time of bovine insulin. Insulin has the shortest lag time (3.00 hr) in the presence of liposome 3 it has the same lag time in the presence of liposomes 5 and 6 (3.50 hr). The growth rates show the same correlation with the various liposomes as the lag times. The growth rates of bovine

insulin in bulk and in the presence of liposome seem to be faster than those of human insulin.

Figure 3.8 shows the aggregation kinetics of human (panel a) and bovine (panel b) insulin (sources 2 and 6) incubated at 37 ˚C and 230 rpm in the presence of polystyrene

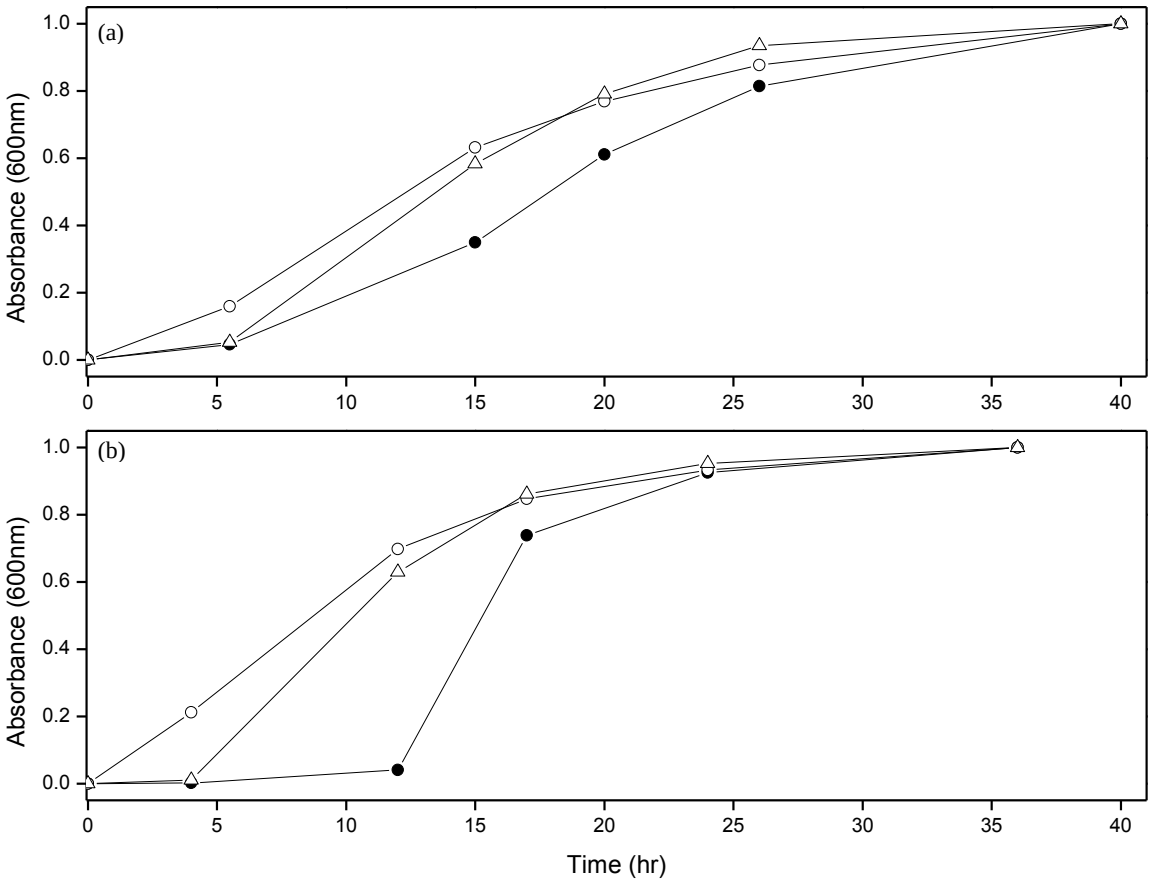

Figure 3.8. Fibril formation of human and bovine insulin in bulk and in the presence of polystyrene beads incubated at 37 ˚C and 230 rpm followed by absorbance at 600 nm. All human insulin species were from source 2 and all bovine insulin was from source 6. Results shown are for human insulin, panel (a) and bovine insulin, panel (b): in bulk (●), in the presence of: PS-COOH (○) and of PS-NH2 (Δ). The absorbance was normalized on a scale from zero to one.

beads. The lag time of human insulin in bulk is 4.00 hr while that of bovine insulin in bulk is 11.0 hr. PS-COOH eliminated the lag phase for both insulins. The lag time of human and bovine insulin in the presence of PS-NH_2 is 2.75 hr and 4.00 hr, respectively.

The growth rates of bovine insulin in bulk and in the presence of liposome are faster than those of human insulin. Table 3.2 contains a summary of the obtained lag times.

Table 3.2. Lag time of human and bovine insulin in the presence of surfaces.

60 ˚C						
Surface used	**Human**			**Bovine**		
		Lag Time (hr)			**Lag Time (hr)**	
	Source	**Bulk**	**Surface**	**Source**	**Bulk**	**Surface**
Liposome 1	1	1.52	1.23	4	1.22	2.49
Liposome 2	1	1.52	1.27	4	1.10	0.85
Liposome 3	1	1.72	1.31	4	1.28	0.87
Liposome 4	1	1.34	1.09	4	1.27	0.88
Liposome 5	1	1.28	1.11	4	1.30	1.21
PS	1	2.39	2.54	4	0.58	1.26
PS-OH	1	2.39	2.12	4	0.58	1.11
PS-NH_2	1	2.39	2.16	4	0.58	0.96
PS-COOH	1	2.39	2.03	4	0.58	1.17
Liposome 2	3	4.74	3.54	6	2.44	2.27
Liposome 3	3	4.74	4.03	6	2.44	1.93
Liposome 6	3	4.74	3.73	6	2.44	1.96
PS-NH_2	3	4.74	4.80	6	2.44	2.51
PS-COOH	3	4.74	4.75	6	2.44	----
37 ˚C and 230 rpm						
Liposome 2	2	7.05	5.09	6	13.31	12.95
Liposome 3	2	7.05	9.50	6	13.31	5.21
Liposome 5	2	7.05	0.00	6	13.31	5.25
Liposome 6	2	7.05	3.92	6	13.31	3.06
PS-NH_2	2	7.05	5.24	6	13.31	5.18
PS-COOH	2	7.05	0.00	6	13.31	0.00

The previous results, Figures 3.1 (panel a) to 3.6, indicate that when human and bovine insulin, in bulk and in the presence of surfaces, are incubated at 60 ˚C, they follow, to some extent, the same aggregation mechanism: a lag phase (first stage of the fibrillation process in which the nuclei is formed, preceding the detection of fibrils), a growth (elongation) phase and an equilibrium (or precipitation) phase.

Table 3.3. Apparent aggregation rate constant of human and bovine insulin.

60 ˚C						
	Human			Bovine		
Surface used		k_{app} (1/hr)			k_{app} (1/hr)	
	Source	Bulk	Surface	Source	Bulk	Surface
Liposome 1	1	5.43	5.51	4	9.87	12.00
Liposome 2	1	5.43	5.32	4	10.15	8.64
Liposome 3	1	4.26	4.99	4	9.67	7.17
Liposome 4	1	5.19	4.64	4	12.84	8.83
Liposome 5	1	6.63	7.28	4	9.50	11.87
PS	1	4.54	8.06	4	3.11	7.61
PS-OH	1	4.54	6.15	4	3.11	11.08
PS-NH_2	1	4.54	7.97	4	3.11	15.11
PS-COOH	1	4.54	8.14	4	3.11	11.51
Liposome 2	3	4.13	2.80	6	6.56	7.92
Liposome 3	3	4.13	3.16	6	6.56	6.49
Liposome 6	3	4.13	3.17	6	6.56	8.01
PS-NH_2	3	4.13	8.26	6	6.56	11.48
PS-COOH	3	4.13	9.61	6	6.56	---
37 ˚C and 230 rpm						
Liposome 2	2	0.19	0.31	6	0.86	1.00
Liposome 3	2	0.19	0.27	6	0.86	0.49
Liposome 5	2	0.19	0.20	6	0.86	0.38
Liposome 6	2	0.19	0.20	6	0.86	0.27
PS-NH_2	2	0.19	0.24	6	0.86	0.38
PS-COOH	2	0.19	0.15	6	0.86	0.19

The lag times of both insulins incubated at 60 ˚C vary from insulin to insulin, even within the same batch: in some instances the lag time of human insulin from source 1 is faster than that of bovine insulin from source 4 but in some cases the opposite is true. The presence of "seeds" is likely to have caused this problem. Nonetheless, regardless of the insulin source and the lag times, the aggregation rates for bovine insulin are, for the most part, faster than those of human insulin. One can say that while the formation of the "active nucleus" (i.e. the lag time) varied from insulin to insulin, the elongation (growth phase) of such nucleus is faster for bovine insulin than for human insulin.

Figures 3.1 (panel b), 3.7 and 3.8 show that the aggregation of human and bovine insulin possibly follows the same mechanism irrespective of the incubation conditions (with a few exceptions). The lag phases are indeed longer for both insulins when the incubation temperature is lower. Shorter lag times for human insulin as compared to bovine insulin are evident but once again, the aggregation rates of bovine insulin are faster than those of human insulin indicating that while the formation of the "active nucleus" (i.e. the lag time) is faster for human insulin, the elongation (growth phase) of such nucleus is faster for bovine insulin.

A few exceptions regarding the sigmoidal shape (and hence the reaction mechanism) are evident for human and bovine insulin when incubated at 37 ˚C and 230 rpm. Such exceptions occur to human insulin in the presence of liposome 5 (10:5:7.5:16 PC/PE/PS/C) (Figure 3.7) and to both insulins in the presence of PS-COOH (Figure 3.8). Under these conditions (37 ˚C and 230 rpm) and in the presence of such surfaces, the lag time is completely eliminated changing the shape of the curve. Such processes are commonly encountered when "seeding" takes place. Seeding (heterogeneous or homogeneous) often occurs at concentrations above the critical concentration and the nucleation (i.e. lag time) phase is bypassed by the introduction of an external nucleus or seed (a seed provides a template on which further insulin molecules can assemble to create a nucleus) (Jarrett and Lansbury, 1993). As a result of seeding, the lag time is eliminated and a first-order growth process takes place (Naiki and Nakakuki, 1996). In our case, more likely the surfaces used (liposome 5 and PS-COOH) acted as seeds, serving as a template for the insulin molecules to further assemble into insulin fibers. Another explanation of this phenomenon is the combination of the surface that acted as a seed along with the mechanical stresses (230 rpm) that the insulin was subjected to while being incubated (37 ˚C). It is worth noting that agitation increases the contact of insulin with air.

The lag times of bovine insulin are plotted vs. the lag time of human insulin in Figure 3.9. It is obvious that the lag times of bovine insulin are shorter than the lag times of human insulin when the hormones are incubated at 60 ^{o}C (Panel (a)). The data at 37 ^{o}C are inconclusive. The apparent rate constants of bovine insulin fibrillation are plotted vs. the apparent rate constants of human insulin in Figure 3.10. Both panels show that

the rate constants for the fibrillation of bovine insulin are larger than the ones of human insulin irrespective of the incubation conditions.

The "Oosawa Model" is the simplest feasible kinetic model describing a nucleation–elongation polymerization (Oosawa and Asakura, 1975). This model applies when the nucleus (least stable species) is in thermodynamic (unfavorable) equilibrium with the monomeric protein. For this type of aggregation processes, the fibril mass should at all times be proportional to t^2 (i.e. a parabolic time pathway) at the beginning of the reaction, with essentially no lag phase. Moreover, a critical protein concentration must exist for the nucleation to take place. In the case of insulin fibrillation, this type of model is excluded due to the time dependence (clearly incompatible with a t^2 behavior) at the beginning of the kinetics, i.e. the lag phase. Nonetheless, this mechanism has been widely used to describe amyloid fibrillation processes (Jarrett and Lansbury, 1992; Naiki and Nakakuki, 1996; Nielsen et. al, 2001a).

The downhill polymerization or irreversible polymerization mechanism (a generalization of Oosawa's classical-nucleation polymerization model) has also been used to describe insulin aggregation (Librizzi and Rischel, 2005; Grudzielanek et al. 2005). This mechanism is different from the nucleation-dependent process in that the nucleation is not considered the rate-limiting step. Instead, they argue that earlier structural phases cause the lag phase (the generation of sufficient amounts of native monomeric protein or the initial unfolding event of the native species). Flyvbjerg et al. (1996) used this mechanism effectively to model the kinetics of tubulin polymerization. It has been suggest by Wang et al. (2010) that regardless of the chosen mechanism, several aggregation pathways may lead to the formation of a nucleus.

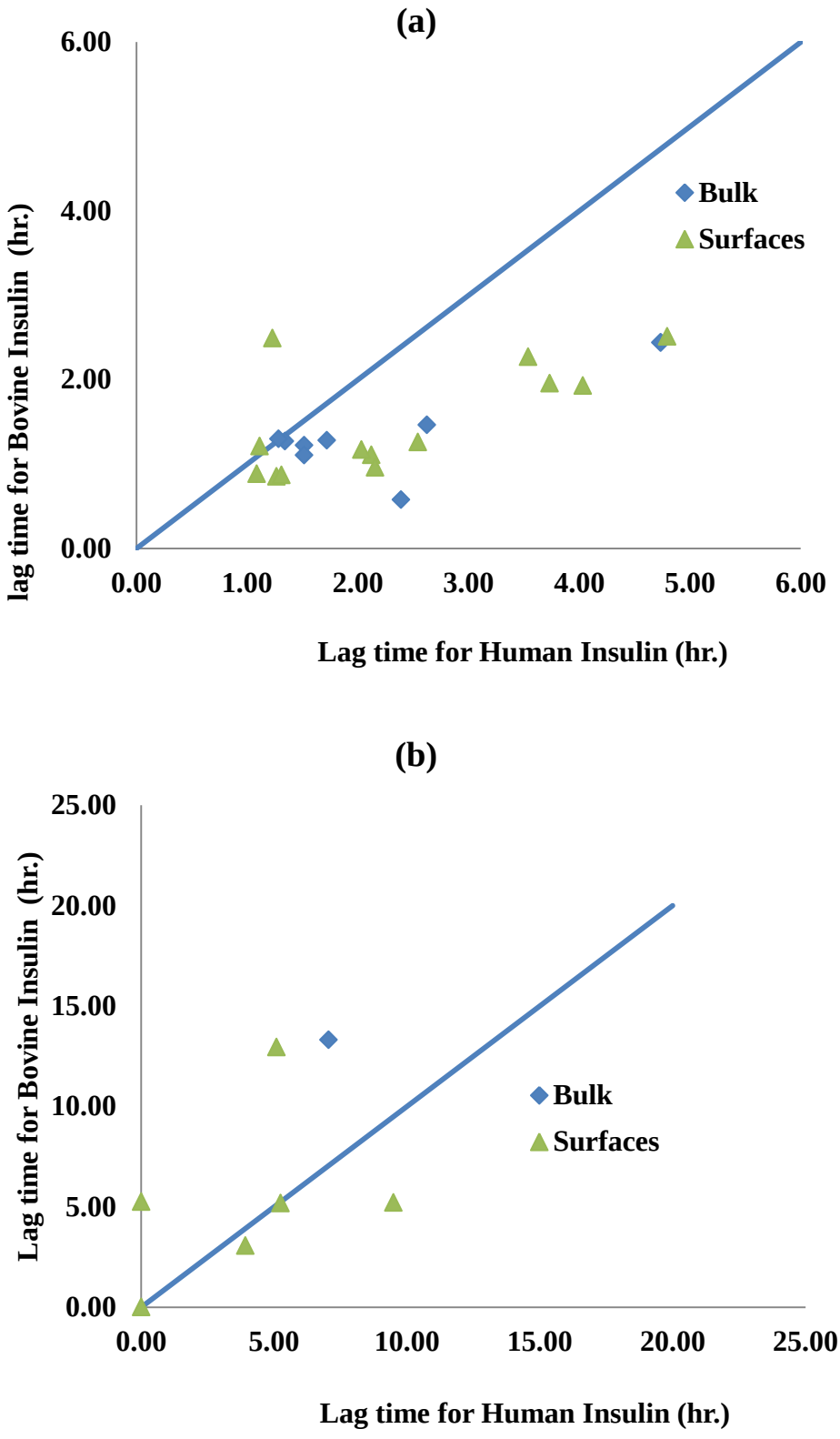

Figure 3.9. Lag time of bovine vs. human insulin. (a) Incubation at 60 ^{o}C and (b) Incubation at 37 ^{o}C and 230 rpm.

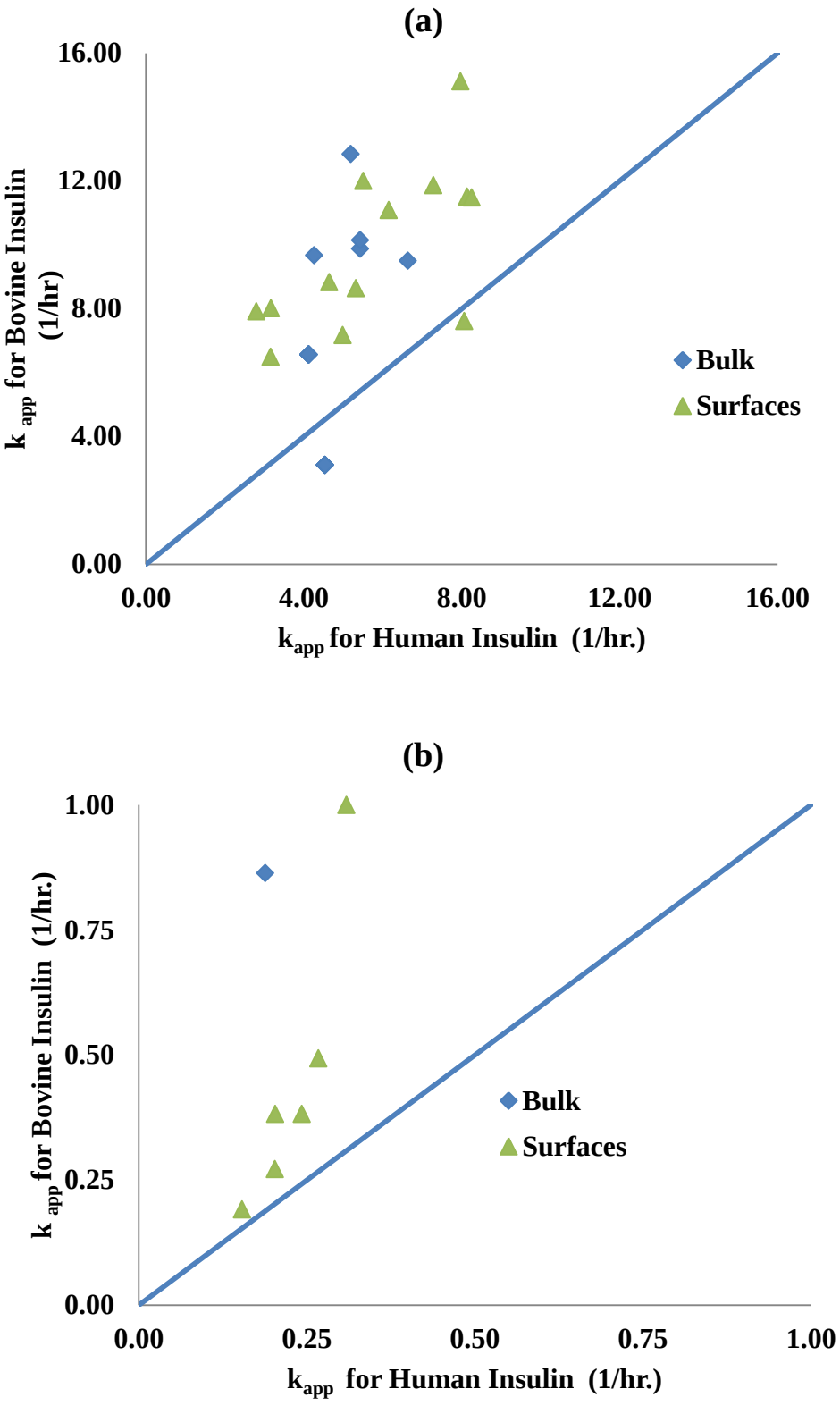

Figure 3.10. Apparent rate constant of bovine vs. human insulin. (a) Incubation at 60 ^{o}C and (b) Incubation at 37 ^{o}C and 230 rpm.

Sluzky et al. (1992) showed that bovine insulin aggregates faster (2 days) in the presence of solid Teflon as opposed to bovine insulin in the presence of much more hydrophilic glass beads (no aggregation was observed for more than a week). Their incubation conditions were 37 ˚C and 160 rpm at insulin concentration of 0.6 mg/ml. They also suggested that insulin stability could be increased by minimizing unfavorable contacts between the hormone and hydrophobic surfaces.

Nielsen et al. (2001b) conducted insulin aggregation studies with human insulin, bovine insulin and insulin mutants at various conditions, including incubation at 60 ˚C, pH 1.6 at insulin concentrations of 2 mg/ml. They concluded that the initial oligomeric state of the insulin has a major impact on the kinetics of nucleation, as reflected in the different lag times. All of their kinetic results (obtained from ThT fluorescence measurements) displayed a sigmoidal curve. They also concluded that bovine insulin is the fastest fibrillating native species under all their incubation conditions, including that at pH 7.4 and 37 ˚C in which bovine insulin is in its stable hexameric conformation. They claimed that substitution of Thr to Ala in position A8 in bovine insulin plays an important role for the greater propensity of bovine insulin to form fibrils. Ala^{A8} is located on the surface of the monomer of bovine insulin, and it has been suggested that the presence of this hydrophobic residue instead of Thr in human insulin might lead to the greater fibrillation tendency of bovine insulin. Lastly, their results suggest that insulin fibril formation, at least the initial nucleation, is primarily driven by hydrophobic interactions. A model for insulin fibrillation was proposed by them in which the formation of a partially folded intermediate is the precursor for associated species on the pathway to fibril formation.

Nayak et al. (2008) studied the effect of different surfaces such as hydrophilic regenerated cellulose and hydrophobic poly(tetrafluoroethyle) (PTFE) on the aggregation of human insulin (at a concentration of 2mg/ml) incubated at 65 ˚C. They concluded that no matter what surface is used, they always tend to induce faster nucleation (i.e. shorter lag times), unless they are purposely designed with inhibitory chemistries. In addition, they claimed that the growth rates of formation of fibrils are not significantly affected by the presence of the surfaces. Their conclusions and our findings are somewhat different. In our case, not all the surfaces accelerated the lag time (this is more evident for both

insulins incubated at 60 ˚C). On the other hand, most surfaces had an impact (either significant or minute) on the growth rate of both insulins.

3.2. FOURIER TRANSFORM INFRARED SPECTROSCOPY

FTIR was used to study the secondary structure changes of both insulins in bulk and in the presence of surfaces during fibrillation. An attempt was made to run turbidimetry and FTIR studies simultaneously but the sampling time of FTIR is much longer than that of turbidimetry when several samples are processed at once. The changes in secondary structure with respect to time are presented in the following tables (Tables 3.4 through 3.15). The time is corresponds to the time elapsed when the sample was removed and not the time of the measurement. Fibrillation likely continued at room temperature and in the absence of stirring. Figure 3.11 is a representation of the time evolution of the FTIR spectra (amide I region) of human insulin during fibril formation at 60 ˚C.

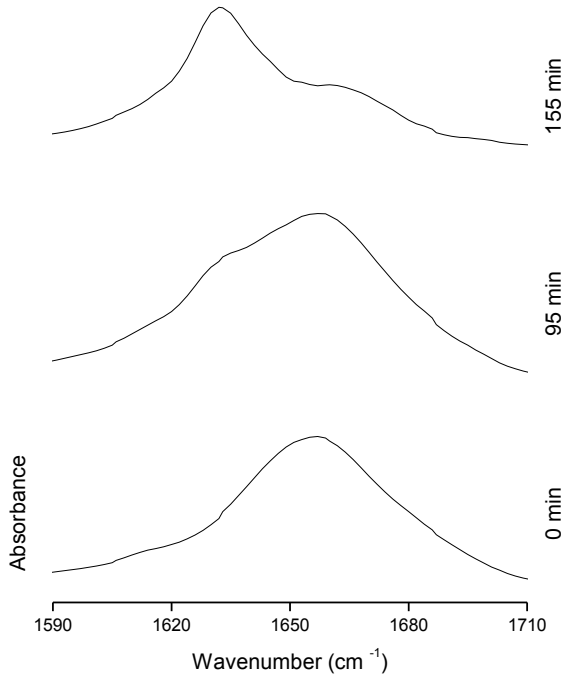

Figure 3.11. Time evolution of the FTIR spectra (amide I region) of human insulin (source 2) during fibril formation at 60 ˚C. Samples were collected before heating (0 min) and at numerous times during heating.

Before heating (time 0) human insulin, the amide I band is located at 1656.3 cm^{-1}. The shape and the location of the band are consistent with the presence of mostly helical and/or disordered structures. Heating the solution at 60 ˚C and for 95 min causes a shift in the amide I region toward lower frequencies and the appearance of a minute shoulder are evident (Figure 3.11). The shift of the band implies the presence of a higher amount of disordered structure and the shoulder of a small amount of β-sheet structure. After 155 minutes, new bands have emerged between 1,627 and 1665 cm^{-1} which indicate the presence of intermolecular β–sheet and β–turn structures.

Tables 3.4 to 3.15 show the secondary structure percentages obtained from the FT-IR spectra of human and bovine insulin in bulk and in the presence of surfaces under both incubation conditions (60 ˚C and 37 ˚C, 230 rpm). The reported values are averages of two experiments. Unfortunately, the time frames of the experiments for both insulin types are not the same. Nonetheless, a few time frames are similar and interesting information may be inferred from the data.

The secondary structures of both insulins incubated at 60 ˚C (sources 2 and 6) in bulk before heating (time 0) are very similar (Table 3.4). After approximately one hour, a considerable increase in α-helix content occurs in both insulins (88.7% and 84.3%). However, at longer times (125 and 120 min), a sharp decrease of α-helices and random coils takes place and a sharp increase of β-sheets occurs. It is also noticeable that after 120 minutes bovine insulin is richer than human insulin in β-sheet content (72.1 vs. 60.0%).

Before incubation at 37 ˚C and 230 rpm (Table 3.5), human insulin (source 1) in bulk contains more random coils (43.4%) than bovine insulin (33.7%) (source 6); on the other hand, human insulin contains no β-sheets. After 17 hours, human insulin still has no β-sheets but bovine insulin has reached its maximum (70.1%); on the other hand, human insulin still contains a high amount of random coils (42.2%) while bovine insulin has none. After 45 hours, the amount of α-helix decreased in human (48.5%) and bovine (50.4%) insulin. The amount of β-turn and β-sheet is 14.8% and 44.3% and 21.9% and 60.5% for human and bovine insulin, respectively.

Table 3.4. Secondary structure percentage of human and bovine insulin in bulk incubated at 60 ˚C.

Insulin type and source		Random coil	Side chain	α- Helix	β- Turn	β- Sheet	Time (min)
	Human, 2	32.7	5.3	49.4	10.0	2.7	0
		0.0	3.7	88.7	6.8	0.9	35
		0.0	2.6	86.3	7.4	3.7	65
		6.9	4.5	54.2	0.4	34.1	95
		10.9	1.4	13.3	14.3	60.0	125
		11.1	2.1	14.0	12.5	60.3	155
	Bovine, 6	33.0	3.7	49.9	7.5	6.0	0
		0.0	6.6	84.3	6.3	2.9	60
		2.3	4.6	0.3	20.8	72.1	120
		0.6	4.9	1.2	21.2	72.1	180
		0.6	3.4	1.4	21.2	73.4	240

Table 3.5. Secondary structure percentage of human and bovine insulin in bulk incubated at 37 ˚C and 230 rpm.

Insulin type and source		Random coil	Side chain	α- Helix	β- Turn	β- Sheet	Time (hr)
	Human, 1	43.4	0.0	48.5	8.1	0.0	0
		42.2	2.9	47.3	7.6	0.0	17
		0.0	0.0	91.9	6.0	2.1	25
		0.0	0.0	88.1	5.3	6.6	36
		7.4	23.3	10.3	14.8	44.3	45
	Bovine, 6	33.7	2.3	50.4	9.6	4.0	0
		0.3	3.7	12.7	16.1	67.1	10
		0.0	2.5	12.4	15.0	70.1	17
		0.0	2.6	5.6	22.0	69.8	24
		0.0	2.7	6.1	21.7	69.4	36
		0.0	2.8	5.8	21.9	69.5	45

The secondary structure of both insulins incubated at 60 ˚C (sources 2 and 6) in the presence of liposome 2 (20/80 PC/C) before heating (time 0) is very similar (Table 3.6). As time increases (65 and 60 min) a considerable increase in α-helices (85.1%) and the loss of random coils occur in human insulin but not in bovine insulin whose secondary structure remains nearly the same with a small decrease in α-helix content and

small increase in random coil content. However, at longer times (125 and 120 min) a sharp decrease of α-helices and a sharp increase of β-sheets take place in both insulins. It is also noticeable that after 120 minutes bovine insulin has more β-sheet content than human insulin (75.0 vs. 60.3%).

Table 3.6. Secondary structure percentage of human and bovine insulin in the presence of liposome 2 (20/80 PC/C) incubated at 60 ˚C.

Insulin type and source		Random coil	Side chain	α- Helix	β- Turn	β- Sheet	Time (min)
	Human, 2	35.1	2.9	50.7	7.5	3.7	0
		0.0	2.3	55.3	35.8	6.6	35
		0.0	4.3	85.1	5.2	5.4	65
		23.3	5.5	19.9	29.8	21.5	95
		10.9	1.6	13.0	14.2	60.3	125
		7.6	1.3	14.3	10.4	66.5	155
	Bovine, 6	33.1	5.1	47.1	9.0	5.6	0
		41.7	3.7	42.9	6.2	5.6	60
		0.0	2.3	0.8	21.9	75.0	120
		2.3	6.2	0.4	20.1	71.0	180
		0.0	5.5	0.7	21.2	72.6	240

Table 3.7. Secondary structure percentage of human and bovine insulin in the presence of liposome 3 (80/20 PC/C) incubated at 60 ˚C.

Insulin type and source		Random coil	Side chain	α- Helix	β- Turn	β- Sheet	Time (min)
	Human 2	32.7	4.4	39.0	17.8	6.0	0
		0.0	5.1	86.0	5.4	3.5	35
		0.0	5.3	85.3	5.2	4.2	65
		6.7	4.2	42.5	7.9	38.7	95
		12.4	0.8	13.5	13.3	60.1	125
		11.8	0.8	15.3	11.7	60.4	155
	Bovine 6	35.5	7.4	43.6	7.0	6.5	0
		36.2	5.1	44.8	6.6	7.3	60
		3.0	3.9	0.4	19.6	73.1	120
		2.4	5.4	0.6	20.4	71.2	180
		1.4	3.2	2.4	19.9	73.2	240

The secondary structures of both insulins incubated at 60 ˚C (sources 2 and 6) in the presence of liposome 3 (80/20 PC/C) before heating (time 0) are very similar (Table 3.7) with the exception of β-turn content: 17.8 % (human insulin) and 7.0 % (bovine insulin). As time increases (65 and 60 min), a considerable increase in α-helices (85.3%) and the loss of random coils occur in human insulin but the secondary structure of bovine insulin remains relatively the same. Nonetheless, at longer times (125 and 120 min), a sharp decrease of α-helices and a sharp increase of β-sheets occurs in both insulins. It is also noticeable that after 120 minutes bovine insulin has more β-sheets than human insulin (73.1 vs. 60.1%).

Table 3.8. Secondary structure percentage of human and bovine insulin in the presence of liposome 6 (50/50 PC/C) incubated at 60 ˚C.

Insulin type and source		Random coil	Side chain	α- Helix	β- Turn	β- Sheet	Time (min)
	Human, 2	19.4	5.3	24.0	36.3	15.1	0
		0.0	6.8	67.8	10.3	15.1	35
		0.0	4.0	38.9	36.6	20.4	65
		6.5	5.9	51.4	3.3	33.0	95
		12.0	1.6	10.9	15.7	59.7	125
		11.4	1.2	14.3	13.8	59.4	155
	Bovine, 6	34.2	6.1	49.9	6.1	3.7	0
		4.3	5.7	0.7	21.1	68.2	60
		1.8	5.7	2.1	21.6	68.8	120
		5.1	6.3	0.9	23.0	64.8	180
		0.0	4.3	3.1	23.4	69.2	240

The secondary structure of both insulins incubated at 60 ˚C (sources 2 and 6) in the presence of liposome 6 (50/50 PC/C) before heating (time 0) is very different. Human insulin contains a lot less random coils (19.4%) and α-helices (24.0%) than bovine insulin (34.2% and 49.9%, respectively). On the other hand, the β-turn and β-sheet contents are much higher in human insulin (36.3% and 15.1%, respectively) than in bovine insulin (6.1% and 3.7%, respectively) (Table 3.8). As time elapses (65 and 60 min), an increase in α-helices (38.9%) and β-sheets (20.4%) and the loss of random coils occur in human insulin; in bovine insulin, the amount of random coils (4.3%) and α-helices (49.9%)

decreases but β-turns and β-sheets increase (21.1% and 68.2%, respectively). At longer times (125 and 120 min), a decrease in α-helices and an increase in β-sheets are observed for both insulins. It is evident that after 120 minutes bovine insulin has higher β-sheet content than human insulin (68.8 vs. 59.7%).

The secondary structure of both insulins incubated at 60 ˚C (sources 2 and 6) in the presence of PS-NH_2 before heating (time 0) is different (Table 3.9); β-turn and β-sheet contents are higher in human insulin (22.9% and 11.5%, respectively) than in bovine insulin (7.1% and 7.9%, respectively) but the amounts of random coils and α-helices are lower in human insulin (23.6% and 39.1%, respectively) than bovine insulin (36.3% and 48.3%, respectively). At longer times (65 and 60 min), a considerable increase in α-helices (69.8%), the loss of random coils and a decrease in β-sheets (3.3%) occur in human insulin; the amount of random coils is also reduced in bovine insulin (3.0%) but a reduction of α-helices (0.8%) and an increase in β-turns (23.1%) and β-sheets (71.2%) take place. At longer times (125 and 120 min), a sharp decrease of α-helices (12.4%) and a sharp increase of β-sheets (57.7%) occur in human insulin; conversely, the secondary structure of bovine insulin remains constant. It is clear that after 120 minutes bovine insulin has a larger β-sheet content than human insulin (70.3% vs. 57.7%).

Table 3.9. Secondary structure percentage of human and bovine insulin in the presence of PS-NH_2 incubated at 60 ˚C.

Insulin type and source		Random coil	Side chain	α- Helix	β- Turn	β- Sheet	Time (min)
	Human, 2	23.6	2.9	39.1	22.9	11.5	0
		0.0	1.3	84.0	7.5	7.2	35
		0.0	0.3	69.8	26.6	3.3	65
		0.0	1.2	87.3	8.5	3.0	95
		8.3	8.8	12.4	12.7	57.7	125
		7.1	5.4	10.0	14.8	62.8	155
	Bovine, 6	36.3	0.4	48.3	7.1	7.9	0
		3.0	1.8	0.8	23.1	71.2	60
		3.0	4.8	0.3	21.6	70.3	120
		4.1	4.2	0.7	22.4	68.6	180
		0.3	3.0	1.4	22.9	72.4	240

The secondary structure of both insulins incubated at 60 ˚C (sources 2 and 6) in the presence of PS-COOH before heating (time 0) is different to some extent. Human insulin contains a lot less α-helices (21.0%) than bovine insulin (54.5); on the other hand, human insulin contains more β-turns (37.6%) and β-sheets (14.2%) than bovine insulin (6.3% and 6.7%, respectively); the amounts of random coils and side chains are similar in both insulins (Table 3.10). As time increases (65 and 60 min), a sharp increase in α-helices (87.6%) and the loss of random coils occur in human insulin whereas there is a decrease in random coils (9.5%) and α-helices (36.6%) but an increase in β-sheets (45.8%) in bovine insulin. At longer times (125 and 120 min), an abrupt decrease in α-helices and an increase in β-sheets take place in both insulins. After 120 minutes bovine insulin has more β-sheets than human insulin (69.3% vs. 60.1%).

Table 3.10. Secondary structure percentage of human and bovine insulin in the presence of PS-COOH incubated at 60 ˚C.

Insulin type and source		Random coil	Side chain	α- Helix	β- Turn	β- Sheet	Time (min)
	Human, 2	21.3	5.9	21.0	37.6	14.2	0
		0.0	1.3	85.4	6.9	6.3	35
		0.0	3.2	87.6	6.6	2.5	65
		0.0	2.8	84.1	6.1	7.0	95
		3.2	15.0	0.0	21.7	60.1	125
		6.7	3.0	7.7	18.4	64.3	155
	Bovine, 6	29.8	2.6	54.5	6.3	6.7	0
		9.5	4.0	36.6	4.1	45.8	60
		1.2	5.7	2.9	20.9	69.3	120
		0.7	6.3	0.9	22.4	69.6	180
		0.0	5.2	1.0	20.9	72.9	240

The secondary structure of both insulins incubated at 37 ˚C and 230 rpm (sources 1 and 6) in the presence of liposome 2 (20/80 PC/C) before heating (time 0) is relatively similar (Table 3.11. At longer times (17 hr), a decrease of random coils and α-helices occurs in both insulins. The amount of β-turns slightly decreases in human insulin (9.9%) but slightly increases in bovine insulin (18.5%). The amount of β-sheets increases in

human insulin (36.5%) and in bovine insulin (73.8%). At longer times (45 hr), a sharp decrease of α-helices (8.2%) and a sharp increase of β-sheets (69.7%) occur in human insulin while the secondary structure of bovine insulin remains the same. At this point both insulins have a similar amount of β-sheets but human insulin has more α-helices but less β-turns than bovine insulin.

Table 3.11. Secondary structure percentage of human and bovine insulin in the presence of liposome 2 (20/80 PC/C) incubated at 37 ˚C and 230 rpm.

Insulin type and source		Random coil	Side chain	α- Helix	β- Turn	β- Sheet	Time (hr)
	Human, 1	30.5	2.2	55.2	12.2	0.0	0
		12.7	0.2	40.7	9.9	36.5	17
		6.0	1.2	8.7	19.4	64.8	25
		4.0	0.0	8.6	17.6	69.8	36
		3.8	1.6	8.2	16.7	69.7	45
	Bovine, 6	32.8	7.0	49.3	7.9	3.1	0
		2.8	5.5	5.2	20.1	66.3	10
		2.0	2.8	2.8	18.5	73.8	17
		2.7	3.7	4.8	20.7	68.2	24
		2.4	5.3	3.8	20.3	68.2	36
		3.1	2.8	2.3	22.3	69.5	45

Table 3.12. Secondary structure percentage of human and bovine insulin in the presence of liposome 3 (80/20 PC/C) incubated at 37 ˚C and 230 rpm.

Insulin type and source		Random coil	Side chain	α- Helix	β- Turn	β- Sheet	Time (hr)
	Human, 1	28.4	1.4	57.7	12.4	0.0	0
		15.1	2.0	15.4	25.2	42.3	17
		4.7	0.0	8.7	18.0	68.6	25
		4.0	0.0	5.7	19.7	70.6	36
		4.3	0.0	8.7	17.1	69.8	45
	Bovine, 6	33.7	6.7	48.3	6.9	4.3	0
		19.5	5.2	20.1	15.6	39.5	10
		1.8	7.4	28.7	14.3	47.8	17
		7.1	4.8	9.3	22.5	56.2	24
		3.6	4.1	4.6	19.4	68.3	36
		0.0	3.0	3.7	22.0	71.2	45

Table 3.12 summarizes the secondary structure results obtained for both insulins incubated at 37 ˚C and 230 rpm (sources 1 and 6) in the presence of liposome 3 (80/20 PC/C). Before heating (time 0), the secondary structure of both preparations is similar. At longer times (17 hr), a decrease in the amounts of random coils and α-helices occur in human, 15.1% (random coil) and 15.4% (helix), and bovine, 1.8% (random coil) and 28.7% (helix), insulins. The amount of β-turns and β-sheets increases in human, 25.2% (turns) and 42.3% (sheets), and bovine, 14.3% (turns) and 47.8% (sheets), insulins. At even longer times (45 hr), a further decrease in α-helices takes place: 8.7% (human insulin) and 3.7% (bovine insulin) and a sharp increase of β-sheets occurs: 69.8% (human insulin) and 71.2% (bovine insulin). Both insulins have similar β-sheet contents at the end of the incubation time but human insulin has more α-helices but less β-turns than bovine insulin.

Table 3.13. Secondary structure percentage of human and bovine insulin in the presence of liposome 5 (10:5:7.5:16 PC/PE/PS/C) incubated at 37 ˚C and 230 rpm.

Insulin type and source		Random coil	Side chain	α- Helix	β- Turn	β- Sheet	Time (hr)
	Human, 1	0.0	10.4	33.9	2.3	53.4	0
		13.8	1.2	45.3	6.9	32.8	17
		13.5	2.0	14.5	23.5	46.5	25
		4.7	0.0	9.4	16.8	69.1	36
		8.2	2.1	9.0	17.2	63.5	45
	Bovine, 6	34.2	3.3	49.9	10.2	2.5	0
		0.0	4.3	6.5	20.1	69.2	10
		0.9	4.4	7.7	17.4	69.5	17
		0.0	2.8	4.8	22.5	69.8	24
		3.0	2.5	6.0	18.7	69.8	36
		0.1	4.0	3.9	22.8	69.2	45

The secondary structures of both insulins incubated at 37 ˚C and 230 rpm (sources 1 and 6) in the presence of liposome 5 (10:5:7.5:16 PC/PE/PS/C) before heating (time 0) are very different (Table 3.13). The side chain and β-sheet contents are higher in human (10.4% and 53.4%, respectively) than in bovine insulin (3.3% and 2.5%, respectively) but

the amounts of random coils, α-helices and β-turns are lower in human (0%, 33.9% and 2.3%, respectively) than in bovine insulin (34.2%, 49.9% and 10.2%, respectively). At longer times (17 hr), reductions in the percentage of side chains (1.2%) and β-sheets (32.8%) and increases in random coils (13.8%), α-helices (45.3%) and β-turns (6.9%) take place in human insulin. For bovine insulin, reductions in the percentage of random coils (0.9%) and α-helices (7.7%) and an increase in β-turns (17.4%) and β-sheets (69.5%) occur. At even longer times (45 hr), a sharp decrease of α-helices (9.0%) and a sharp increase of β-sheets (63.5%) occur in human insulin whereas the secondary structure contents of bovine insulin remain almost unchanged; α-helix: 3.9%, β-turn: 22.8% and β-sheet: 69.2%.

Table 3.14. Secondary structure percentage of human and bovine insulin in the presence of PS-NH_2 incubated at 37 ˚C and 230 rpm.

Insulin type and source		Random coil	Side chain	α- Helix	β- Turn	β- Sheet	Time (hr)
	Human, 1	32.4	1.4	54.3	11.9	0.0	0
		11.3	0.6	29.5	17.6	41.0	17
		1.3	0.0	8.7	17.3	72.7	25
		1.1	0.0	6.4	18.6	73.9	36
		0.6	0.0	8.2	15.7	75.5	45
	Bovine, 6	27.0	2.2	54.4	13.7	2.7	0
		11.5	4.1	4.7	19.6	60.0	10
		4.1	2.7	3.8	20.4	69.0	17
		2.4	4.4	3.2	21.6	68.3	24
		4.4	5.4	4.3	19.8	66.2	36
		0.0	1.8	5.8	22.5	69.9	45

Table 3.14 shows the secondary structure content of both insulins incubated at 37 ˚C and 230 rpm (sources 1 and 6) in the presence of PS-NH_2. Before heating (time 0), the distribution of secondary for both insulins is nearly the same. At longer times (17 hr), a decrease in the amount of random coils and α-helices and an increase of β-turns and β-sheets are observed for both insulins. At even longer times (45 hr), a further decrease in α-helix takes place for both insulins and a sharp increase in the amount of β-sheets occurs

in human insulin (75.5%). At the end of the incubation period the distribution of sencondary structures for both insulins is somehow similar (See table 3.14).

Table 3.15. Secondary structure percentage of human and bovine insulin in the presence of PS-COOH incubated at 37 ˚C and 230 rpm.

Insulin type and source		Random coil	Side chain	α- Helix	β- Turn	β- Sheet	Time (hr)
	Human, 1	37.1	2.4	53.6	6.9	0.0	0
		12.0	3.0	13.9	22.8	48.3	17
		2.1	0.0	11.7	14.6	71.7	25
		1.7	0.0	11.1	15.7	71.6	36
		2.1	0.0	9.9	14.7	73.3	45
	Bovine, 6	25.9	3.3	53.0	14.5	3.3	0
		10.0	4.2	12.3	16.7	56.7	10
		2.3	2.7	19.6	10.0	65.4	17
		4.2	1.1	9.1	17.4	68.2	24
		6.2	3.3	7.8	17.9	64.9	36
		2.4	2.3	15.6	12.5	67.1	45

The distribution of secondary structures of both insulins incubated at 37 ˚C and 230 rpm (sources 1 and 6) in the presence of PS-COOH before heating (time 0) is somewhat similar (Table 3.15). At longer times (17 hr), a decrease in random coil and α-helix content takes place for human (12.0% and 13.9% for coil and helix respectively) and bovine (10.0% and 12.3% for coil and helix respectively) insulins. An increase in the amount of β-turns is observed in human insulin (22.8%) but a decrease is observed in bovine insulin (10.0%). The β-sheet content increases in both human (48.3%) and bovine (65.4%) insulins. At longer times (45 hr), a further decrease in random coil (2.1%), α-helix (9.9%) and β-turn (14.7%) but a sharp increase in β-sheet (73.3%) contents is observed in human insulin whereas the secondary structure of bovine insulin remains almost unchanged.

Four transitions are evident for human insulin incubated at 60 ^{o}C (source 2) in bulk and in the presence of liposomes 2 (20/80 PC/C) and 3 (80/20 PC/C). The first transition (0-35 min) may correspond to the dissolution of the protein in which an

increase in α-helix and the total depletion of random coil structures take place. The second transition (35-65 min) may be attributed to the changes inside the dimeric insulin in the nucleation phase, along with a constant content of secondary structure (human insulin in bulk and in the presence of liposome 3) or a continuous increase of α-helix conformation (human insulin in the presence of liposome 2). The third transition (65-95 min) may correspond to the conversion of α-helices into random coils and β-sheets. After 125 minutes, the conformation of the insulin solution is predominantly β-sheet.

Only three transitions are observed for human insulin incubated at 60 ˚C (source 2) in the presence of PS-COOH beads. The first transition (0-35 min) is similar to that of human insulin in bulk and in the presence of liposomes 2 and 3 in which a tremendous increase in α-helix content and the complete depletion of random coils occur. Between 35 to 95 minutes (second transition) the secondary structure remains unchanged. However, after 95 minutes (third transition), an abrupt decrease in α-helix and a large increase in β-turns and β-sheets take place, after this point the secondary structure remains somewhat constant with a small reduction of β-turns and sheets.

Four transitions are observed when human insulin is incubated 60 ˚C (source 2) in the presence of liposome 6 (50/50 PC/C) or PS-NH_2 beads. Once more, the first transition (0-35 min) is similar to that of human insulin in bulk and in the presence of all the surfaces in which an increase in α-helix and the complete depletion of random coils take place. The second transition (35-65 min) consists of the replacement of α-helices by (mainly) β-turns and β-sheets. The third transition (65-95 min) consists of an increase in α-helices and a decrease in (mainly) β-turns and β-sheets. The fourth transition (95-125 min) consists of a replacement of α-helices by mostly β-sheets.

The sampling frames used with bovine insulin (source 6) are different from those used with human insulin (source 2), at the same incubation conditions (60 ^{o}C). In the case of bovine insulin in bulk and in the presence of surfaces some secondary structure changes could have been missed between 60-120 minutes. For bovine insulin in bulk, the first transition (0-60 min) is similar to that observed with human insulin in bulk and in the presence of surfaces; i.e. an increase in α-helices and the complete depletion of random coils. In the second transition (60-120 min), the complete conversion of α-helices into β-

turns and (mostly) β-sheets takes place. After 120 minutes the secondary structure of bovine insulin in bulk remains unchanged with a high content of β-sheets.

Only one transition is evident for bovine insulin incubated at 60˚C (source 6) in the presence of liposomes 2 (20/80 PC/C) or 3 (80/20 PC/C). For the most part, the secondary structure did not change much between 0-60 minutes; there was a slight increase in random coils and a small decrease in α-helices in the presence of liposome 2. Therefore, the first transition took place between 60-120 minutes in which a complete depletion (in the presence of liposome 2) or a significant reduction (in the presence of liposome 3) of random coils and a considerable reduction of α-helices occurs. The predominant structures at the end of the incubation were β-sheets and to a lesser extent β-turn.

Similarly, only one transition is observed for bovine insulin incubated at 60 ^{o}C (source 6) in the presence of liposome 6 (50/50 PC/C) or PS-NH_2 beads. The transition takes place within the first hour (0-60 min) in which the random coil and α-helix conformations are significantly reduced and replaced by mainly β-sheets. After 60 minutes, no more conformational changes are observed.

When incubated at 37 ˚C and 230 rpm, human insulin (source 1) in bulk shows two transitions. Its secondary structure remains virtually unchanged for the first 17 hours; hence, the initial transition takes place between 17-25 hours. During this time the dissolution of the protein may occur and a large increase in α-helix and the complete depletion of random coil conformations take place. After 36 hours, the secondary structure remains constant. Throughout the second transition (36-45 hr) a significant decrease in α-helix and an increase of side chains, β-turns and (mainly) β-sheet takes place.

Human insulin incubated at 37 ˚C and 230 rpm (source 1) in the presence of liposome 2 (20/80 PC/C), liposome 3 (80/20 PC/C), PS-NH_2 or PS-COOH goes through the same changes in secondary structure. During the first transition (0-17 hr) a reduction of random coils and α-helices and an increase of β-sheets takes place. A second transition takes place after 17 hours in which a further reduction in random coils and α-helices and a further increase of β-turns and β-sheets occur.

Human insulin incubated at 37 ˚C and 230 rpm (source 1) in the presence of liposome 5 (10:5:7.5:16 PC/PE/PS/C) shows three transitions in secondary structure. The first transition (0-17 hr) may correspond to the dissolution of the protein; interestingly, the β-sheet content at time 0 is really high (53.4%), during this time a depletion of β-sheet into random coil and α-helix structures takes place. The second transition (17-25 hr) consists of a reduction in α-helices and an increase in β-turns and β-sheets. After 25 hours (third transition), β-sheets are the predominantly structures.

When incubated at 37 ˚C and 230 rpm, bovine insulin (source 6) in bulk and in the presence of liposome 3 (80/20 PC/C) shows two transitions. During the initial transition (0-10 hr) a complete depletion of random coils, a reduction of α-helices, and an increase in the amounts β-sheets, and to a lesser extent turns, take place. The secondary structure remains somewhat stable between 10-17 hours. After 17 hours, the second transition takes place in which a further replacement of α-helices by β-turns takes place.

Only one transition is observed for bovine insulin incubated at 37 ˚C and 230 rpm (source 6) in the presence of liposomes 2 (20/80 PC/C), liposome 5 (10:5:7.5:16 PC/PE/PS/C), or PS-NH_2 beads. The transition takes place between 0-10 hours in which the amount of random coils and α-helices is significantly reduced with the simultaneous increase of β-sheets and turns. After 10 hours, no more conformational changes are observed.

Three transitions are observed for bovine insulin incubated at 37 ˚C and 230 rpm (source 6) in the presence of PS-COOH beads. Replacement of α-helices and random coils by β-sheet takes place during the first transition (0-10 hr). Between 10 and 17 hours (second transition) a replacement of β-turns and β-sheets by α-helices occurs. A decrease in α-helices and an increase in β-turns and β-sheets takes place after 17 hours (third transition); after this point the secondary structure remains fairly constant.

Bovine insulin amyloid fibril formation in bulk (incubated at 68 ˚C at pD 2.6, i.e. pH 2.2, at a concentration of 2.0 mM) was studied by Bouchard et al. (2000). Their sample preparation included leaving the protein at pD 1.9 at room temperature for 12 hours followed by lyophilization (this procedure was repeated until the labile hydrogen in the sample were completely replaced by deuterium). Their results show that before heating, bovine insulin is in a helical/disordered conformation with bands at about 1639

and 1652 cm^{-1}, respectively. Heating the sample for 1.5 hours results in a slight increase in the content of random coil structure, although the protein remains mostly helical. Similar to us, they also observed a shift of the IR band at about 1651 cm^{-1} with increasing incubation time toward lower frequencies and the appearance of a small shoulder on this band. After 18 hours of heating, the predominant secondary structure was β-sheet. Secondary structure percentages were not reported.

Nielsen et al. (2000) used bovine insulin in bulk (at a concentration of 20 mg/mL in 0.05 M HCl, pH 1.6 incubated at 50 °C for 7 hours or agitated at 37 °C for 24 hours) to investigate fibril formation of insulin in acid media. Their FTIR spectroscopy studies showed that the native secondary structure of insulin was identical in hydrochloric acid and acetic acid, whereas the secondary structure of fibrils formed in hydrochloric acid was different from that formed in acetic acid. Fibrils of bovine insulin prepared by heating or agitating an acid solution of insulin showed an increased content of β-sheet and a decrease in the intensity of the α-helix band. In hydrochloric acid, the frequencies of the β-sheet bands depended on whether the fibrillation was induced by heating or agitation.

Liu et al. (2010) investigated the fibrillation of bovine insulin in bulk at a concentration of 2 mg/ml in 20% acetic acid incubated at 60 ˚C. They also obtained sigmoidal curves from their ThT fluorescence kinetic experiments which reached the equilibrium phase after 70 hours of incubation. Furthermore, they noticed four different structural transitions occurring during the process of insulin fibrillation. Namely, the initial transition, characterized by the dissolution of insulin and an increase in α-helices; the second transition, which may be attributed to changes in the insulin monomer during the nucleation phase; the third transition, in which a replacement of α-helices by β-sheets is evident and the final transition in which most of insulin solution was in a β-sheet conformation. Secondary structure percentages were not reported.

3.3. DYNAMIC LIGHT SCATTERING

An effort to follow insulin aggregation by dynamic light scattering (DLS) was made. The results are sensitive to bubbles and dust and therefore, some of them are inconclusive.

The autocorrelation functions were analyzed by means of the program CONTIN. Size distribution histograms were generated in which relative scattering intensities and relative scattering by number were plotted versus particle diameter. The aggregation of insulin in bulk and in the presence of surfaces incubated at 37 ˚C and 230 rpm for up to 55 hours was particularly challenging to follow.

Figure 3.12 shows two typical histograms. The left panel corresponds to intensity averages where the presence of dust is evident (the scattering is dominated by the largest particles). The right panel corresponds to number averages where the "dust signal" has disappeared and the size corresponds roughly to insulin monomer/dimer.

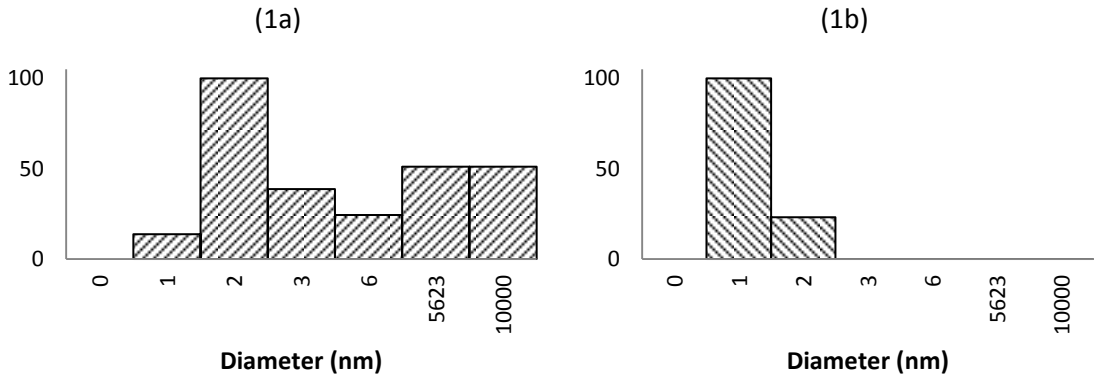

Figure 3.12. DLS analysis of bovine insulin (source 4) aggregation in bulk. Histograms represent relative scattering by intensity (a) and by number (b). Results shown are for: (1a) & (1b) before incubation. The signal at a few micrometers is due to dust.

The quality of most experimental runs was quite poor. We used a couple of simple tools to clean the data. First, data sets with differences between calculated and experimental base lines higher than 1% were eliminated. Second, all data sets poorly fitted by the CONTIN algorithm were excluded. Unfortunately, many sample sets lost their duplicates after this exercise. The "surviving" histograms are included in

Appendices B, C and D for completeness but they have not been thoroughly analyzed. None of the data taken at 37 ^{o}C survived.

3.4. CONGO RED HISTOLOGICAL DYE BINDING TO INSULIN FIBRILS

Congo red strongly stains amyloid aggregates by binding to the β-pleated sheet conformation of the protein (Klunk et al., 1989). This technique was used to confirm the presence of amyloid deposits at the end of each experiment. A representative absorbance spectrum of Congo red solution in the presence of β-pleated bovine insulin is shown in Figure 3.13. The remaining spectra are included in Appendix E.

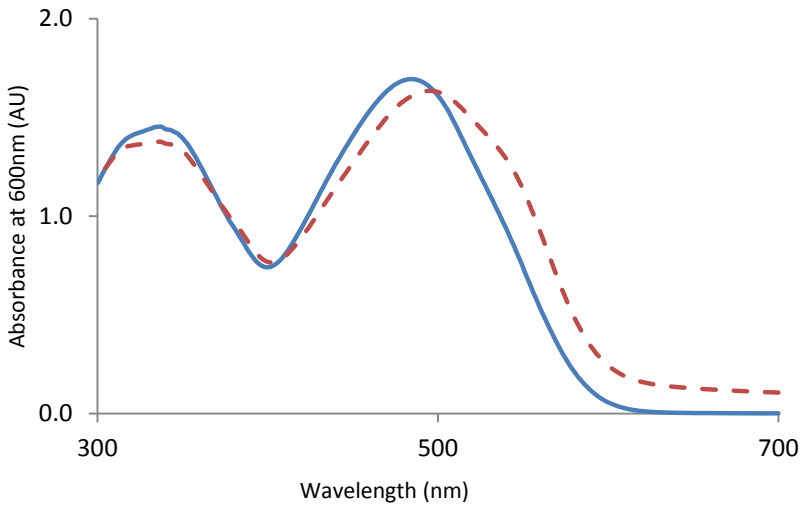

Figure 3.13. Congo red spectrum of bovine insulin incubated at 37 ˚C and 230 rpm for 55 hours: Blank (—); Sample (- - -).

3.5. TRANSMISSION AND SCANNING ELECTRON MICROSCOPY

All the micrographs were obtained from the same sample unless otherwise specified. All samples were prepared in 0.025 M HCl and 0.1 M NaCl (pH 1.6). Statistical analysis of the size distribution of the length of the fibrils was performed, when possible. It is well known that amyloid fibrils have a width of 10-20 nm (Knowles et al., 2007; White et al., 2009). Nevertheless, statistical analysis of the width of the

fibrils was conducted as well in order to fully characterize the amyloid fibrils and make a sound comparison of the obtained results to those from the literature. Negative stained micrographs of different samples under different incubation conditions in the presence and in the absence of surfaces were acquired for both bovine and human insulin.

Figure 3.14 shows micrographs of human and bovine insulin incubated at 60 ˚C for 6 hours; they show similar morphologies and sizes.

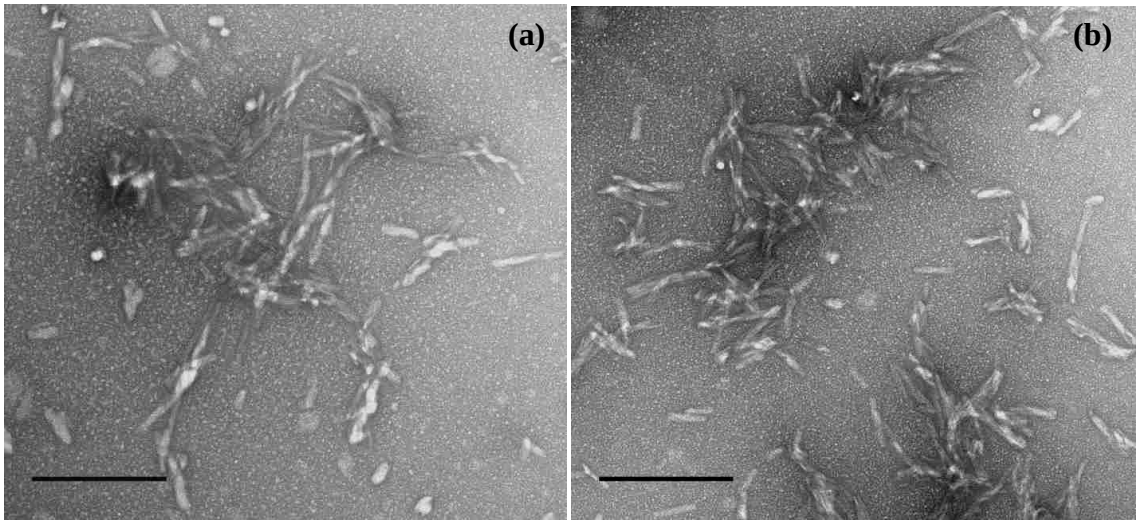

Figure 3.14. Negative staining transmission electron images of amyloid fibril formation of (a) human and (b) bovine insulin incubated at 60 ˚C for 6 hours. The scale bar represents 200 nm.

The data is summarized in Table 3.16 and Figure 3.15. The mean length of human insulin fibrils is 158±24 nm while that of bovine insulin is 155±33 nm, with the longest insulin fibril being 173 nm and that of bovine insulin 213 nm. The average width of the fibrils was measured to be 12±2 nm and 13±1 nm for human and bovine insulin, respectively. (Table 3.17 and Figure 3.16)

Table 3.16. Statistical analysis of the length of human and bovine insulin incubated at 60˚C for six hours.

Sample	Mean (nm)	Std Deviation (nm)	Minimum (nm)	Median (nm)	Maximum (nm)
(a)	158	24	102	169	173
(b)	155	33	118	146	213

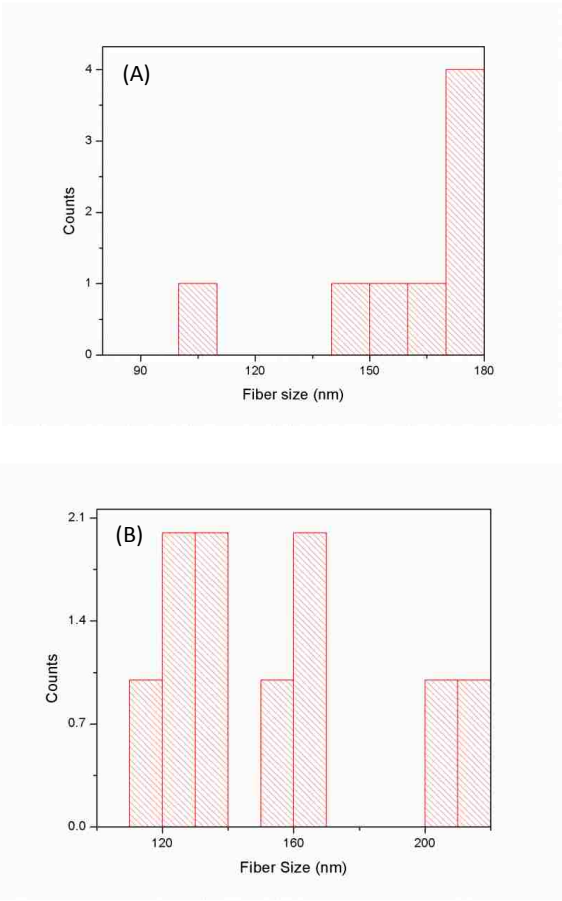

Figure 3.15. Length distribution of (A) human and (B) bovine insulin incubated at 60˚C for six hours.

Table 3.17. Statistical analysis of the width of human and bovine insulin incubated at 60˚C for six hours.

Sample	Mean (nm)	Std Deviation (nm)	Minimum (nm)	Median (nm)	Maximum (nm)
(a)	12	2	10	12	15
(b)	13	1	11	14	15

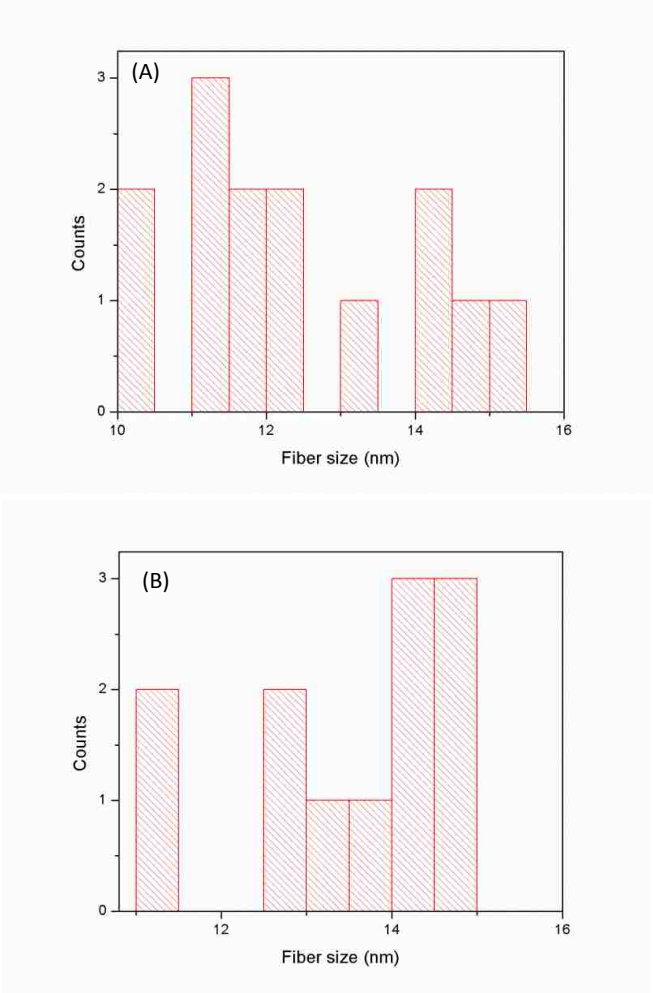

Figure 3.16. Width distribution of (A) human and (B) bovine insulin incubated at 60˚C for six hours.

In agreement with Liu et al., 2010, it was observed that fibrils attain a larger size when incubated for longer periods of time and under no mechanical stresses (i.e. stirring). These differences were observed between insulin incubated at 60˚C for 6 (Figure 3.14) and 40 (Figure 3.17) hours. Figures 3.17, 3.25, and 3.27 confirm these results. Liu et al. (2010) incubated the insulin for 26 hours at 60 ˚C in 20% acetic acid.

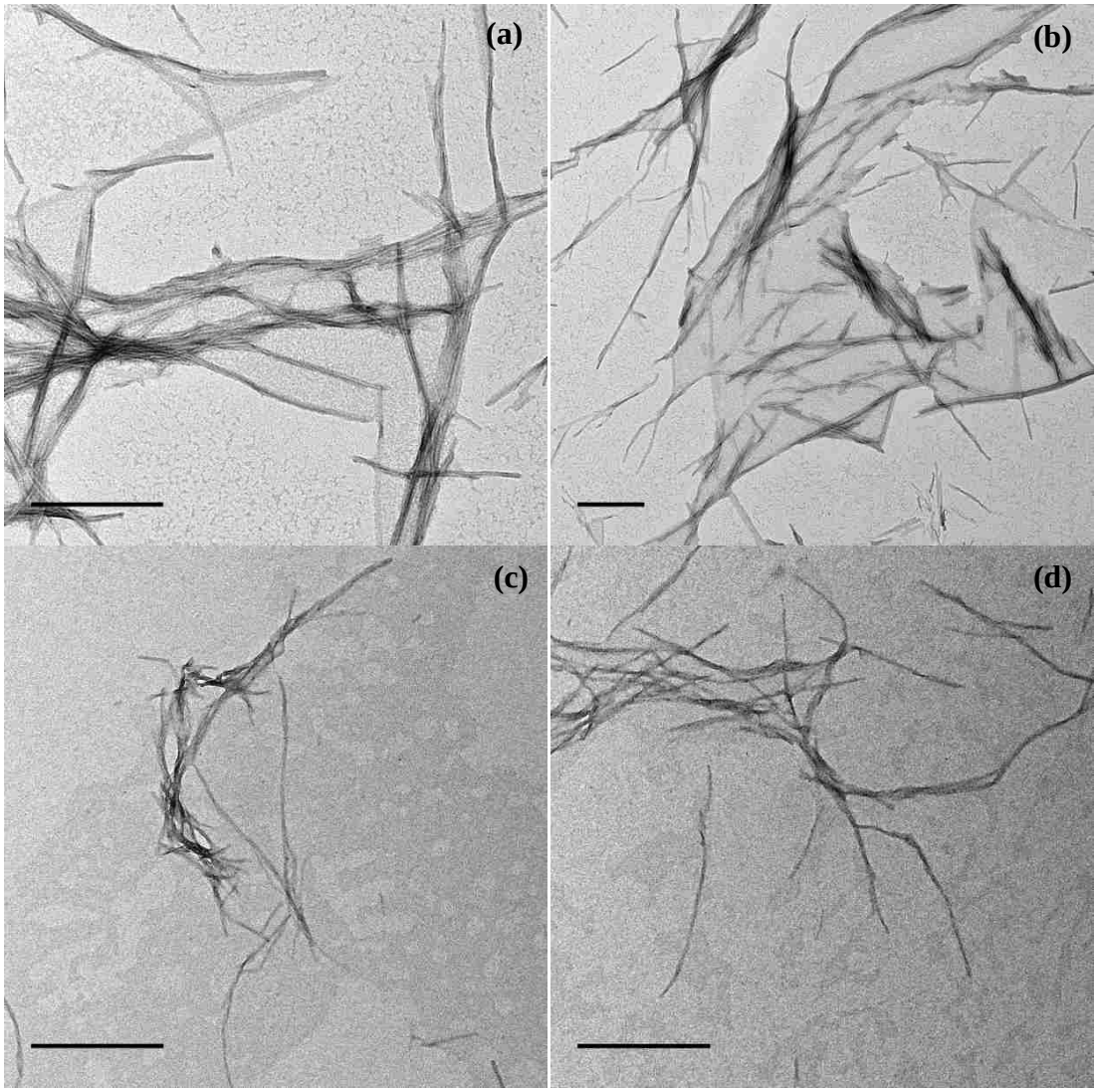

Figure 3.17. Negative staining transmission electron images of amyloid fibril formation of human and bovine insulin incubated at 60 ˚C for 40 hours. (a) and (b) human insulin. (c) and (d) bovine insulin. The scale bar represents 500 nm.

A statistical analysis of the length distribution of a few fibrils (most fibrils extend further outside the image) from Figure 3.17 was performed. The results are shown in Table 3.18. The mean length of human insulin fibrils is 1197±148 nm while that of bovine insulin is 1092±168 nm. These results clearly demonstrate the increase in length with increasing incubation time (without mechanical stresses). Figure 3.18 shows the histograms of the results obtained. It can be seen that the fibrils are several microns in length.

Table 3.18. Statistical analysis of the length of human and bovine insulin incubated at 60˚C for 40 hours.

Samples	Mean (nm)	Std Deviation (nm)	Minimum (nm)	Median (nm)	Maximum (nm)
(a) & (b)	1197	148	1046	1186	1432
(c) & (d)	1092	165	927	1047	1364

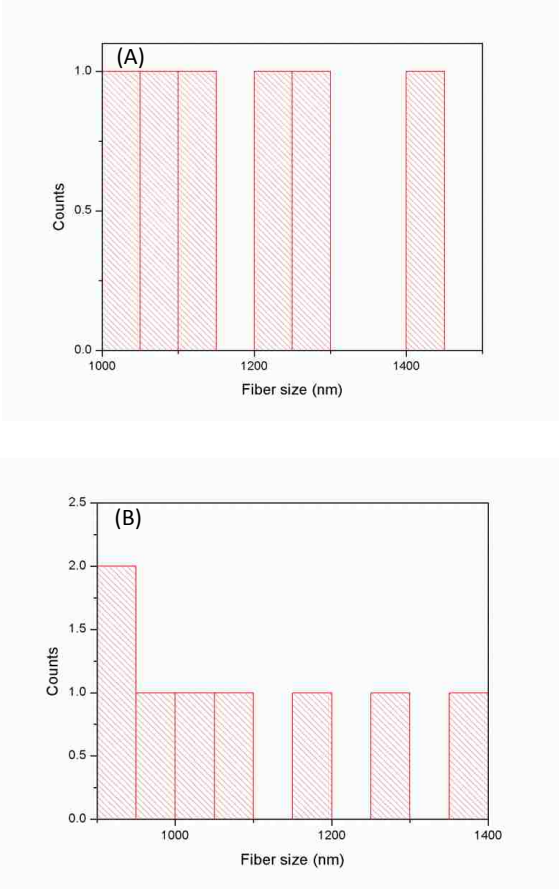

Figure 3.18. Length distribution of (A) human and (B) bovine insulin incubated at 60˚C for 40 hours.

The average width of the fibrils was measured to be 18±2 nm and 15±3 nm for human and bovine insulin, respectively (Table 3.19 and Figure 3.19).

Table 3.19. Statistical analysis of the width of human and bovine insulin incubated at 60˚C for 40 hours.

Samples	Mean (nm)	Std Deviation (nm)	Minimum (nm)	Median (nm)	Maximum (nm)
(a) & (b)	18	2	15	19	20
(c) & (d)	15	3	11	16	20

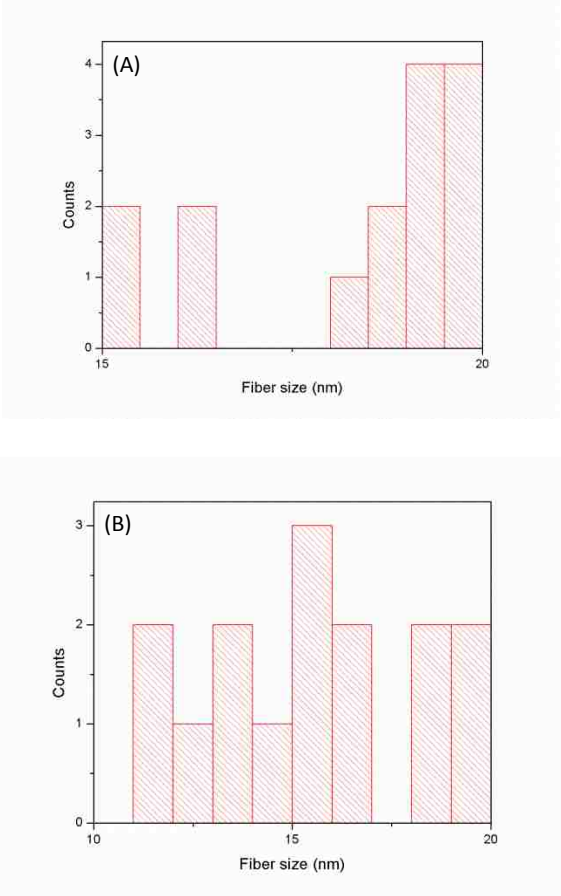

Figure 3.19. Width distribution of (A) human and (B) bovine insulin incubated at 60˚C for 40 hours.

Figure 3.20 shows that human insulin fibrils formed by incubation at 37 ˚C with stirring at 230 rpm for 55 hours look as if they had been "fragmented". Their size was significantly shorter than that of insulin human incubated for at 60 ˚C 40 hours. Hill

(1983) showed that fibril fragmentation is a mechanism that drastically minimizes fibril length depending on the length distribution of the fibrils being fragmented.

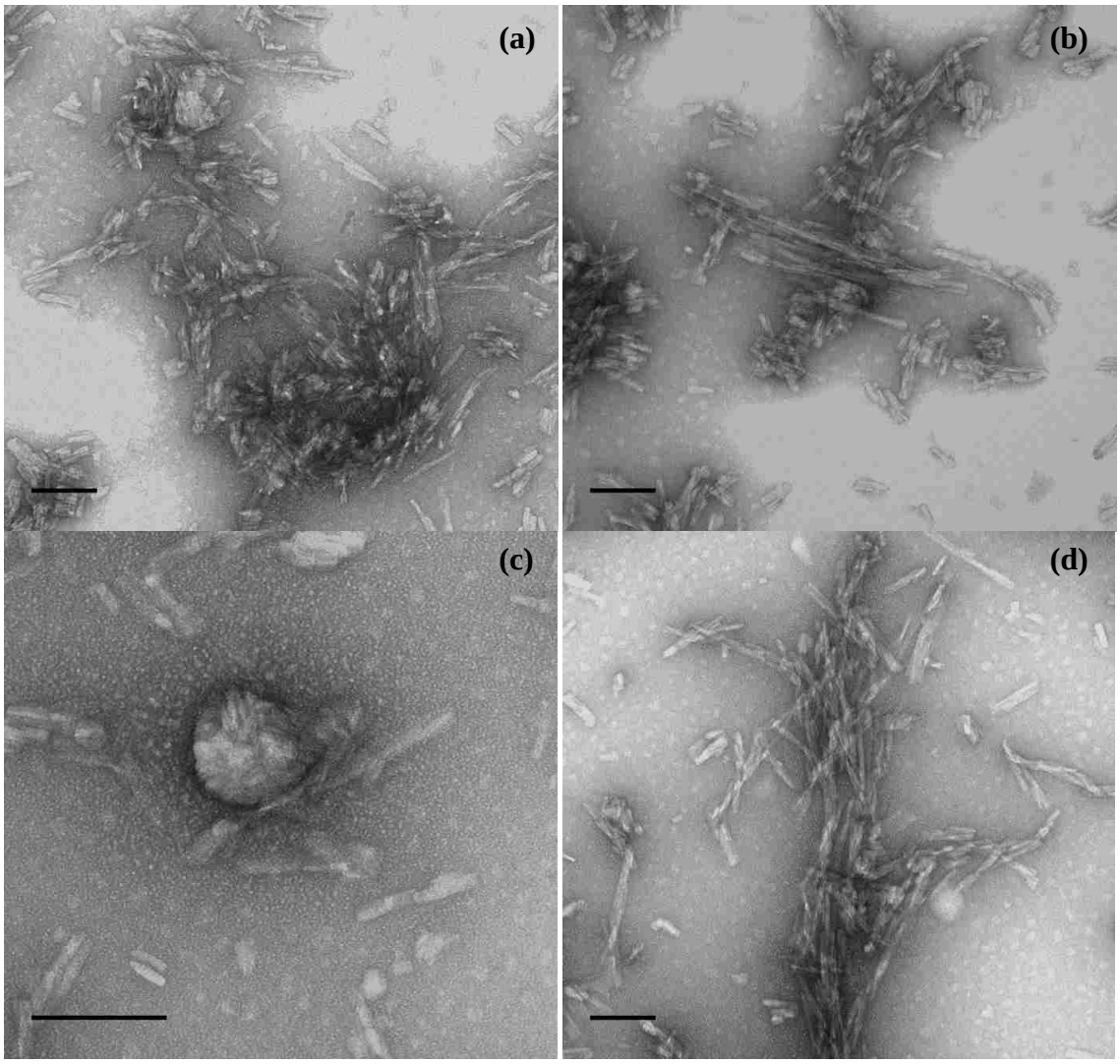

Figure 3.20. Negative staining transmission electron images of amyloid fibril formation of human insulin incubated for 55 hours at 37 ˚C and 230 rpm. The scale bar represents 100 nm.

When insulin is incubated at 37 ˚C with stirring at 230 rpm for 55 hours the median fibril length is 71±64 nm, with the smallest fibril length being 25 nm and the longest fibril attaining a size of 362 nm (Table 3.20 (A)). A few outliers (longer fibrils),

shown in the bimodal histogram in Figure 3.21 (A), were found between 200 to 400 nm. Therefore, a second analysis of the densest population (i.e. without taking into account fibrils larger than 300 nm) was performed (Figure 3.21 (B)) to obtain a more precise distribution of the length of the fibrils. The median fibril length became 68±44 nm. (Table 3.20 (B)). Overall, under these conditions, most of the fibrils do not reach an average size greater than 100 nm.

Table 3.20. Statistical analysis of the length of human insulin incubated at 37˚C and 230 rpm for 55 hours. (A) Bimodal and (B) Unimodal analysis.

Samples	Mean (nm)	Std Deviation (nm)	Minimum (nm)	Median (nm)	Maximum (nm)
(A): (a) to (d)	88	64	25	71	362
(B): (a) to (d)	80	44	25	68	208

Table 3.21 shows that the average width of the human insulin fibrils is 14±3 nm. Figure 3.22 depicts the histogram of such results. The same "fragmentation" occurred to bovine insulin under the same incubation conditions (37 ˚C and 230 rpm) (Figure 3.23).

Table 3.21. Statistical analysis of the width of human insulin incubated at 37˚C and 230 rpm for 55 hours.

Samples	Mean (nm)	Std Deviation (nm)	Minimum (nm)	Median (nm)	Maximum (nm)
(a) to (d)	14	3	10	13	20

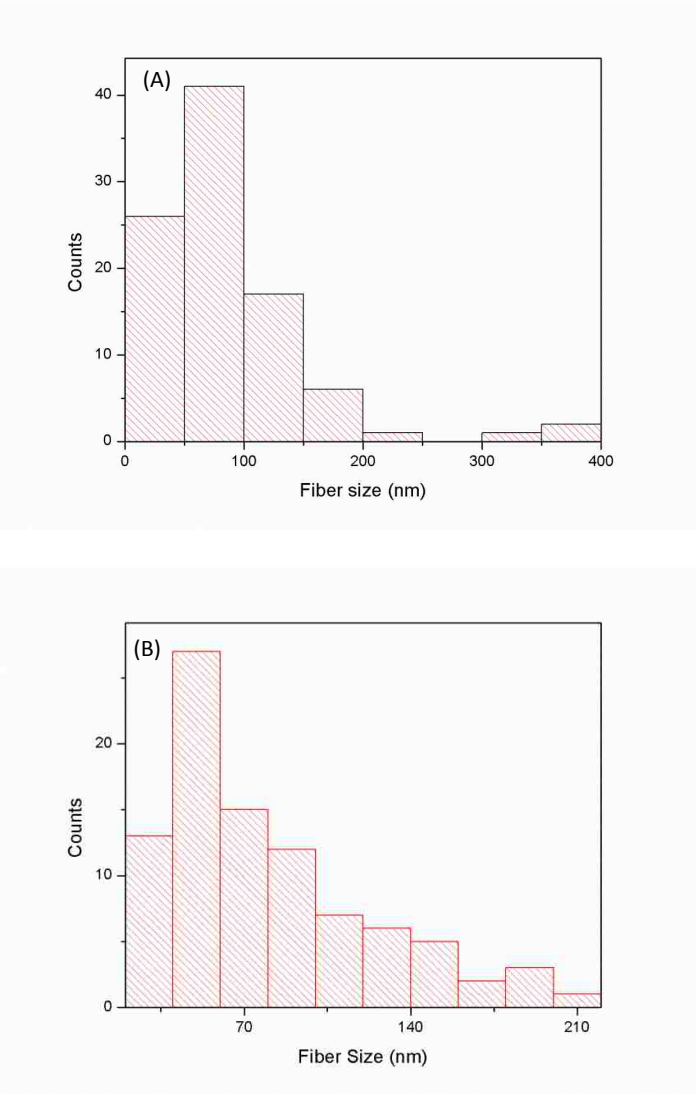

Figure 3.21. Length distribution of human insulin incubated at 37˚C and 230 rpm for 55 hours. (A) Bimodal and (B) Unimodal analysis.

Table 3.22. Statistical analysis of the length (A) and width (B) of bovine insulin incubated at 37˚C at 230 rpm for 55 hours.

Samples	Mean (nm)	Std Deviation (nm)	Minimum (nm)	Median (nm)	Maximum (nm)
(A): (a) to (d)	128	68	45	107	327
(B): (a) to (d)	11	1	10	11	15

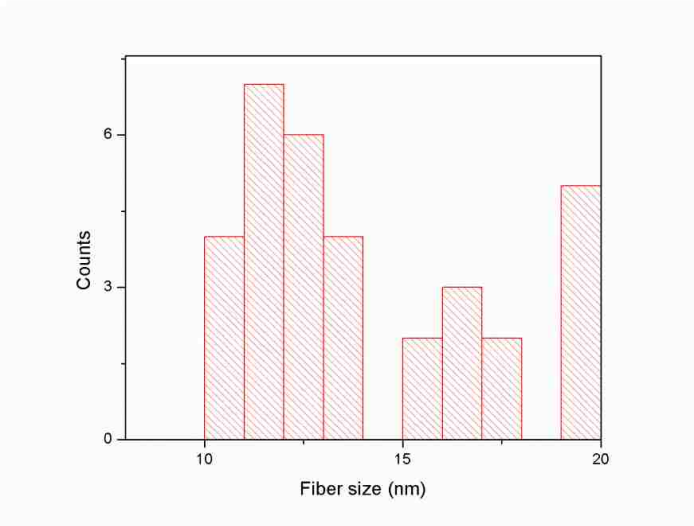

Figure 3.22. Width distribution of human insulin incubated at 37˚C and 230 rpm for 55 hours.

Comparing the length distributions of both insulins one may conclude that while bovine insulin fibrils were also fragmented, they are longer and thinner than human insulin fibrils. When human insulin is incubated at 37 ˚C with stirring at 230 rpm for 55 hours the median fibril length is 71±64 nm, with the smallest fibril length being 25 nm and the longest fibril attaining a size of 362 nm (Table 3.20 (A)). In contrast, the mean fibril length of bovine insulin is 128±68 nm with the shortest fibril being 45 nm and the longest fibril 327 nm (a few longer fibrils were present but they were curved, therefore, they were not measured) (Table 3.22, Figure 3.24). The average width of the human insulin fibrils is 14±3 nm (Table 3.21) whereas the average width of bovine insulin fibrils is 11±1 nm, under the same conditions.

Figure 3.25 shows images of amyloid fibril formation of human and bovine insulin in the presence of liposome 3 (80/20 PC/C) incubated at 60 ˚C for 40 hours. Regardless of the presence or the absence of surfaces, human and bovine insulin showed similar morphologies under the same incubation conditions.

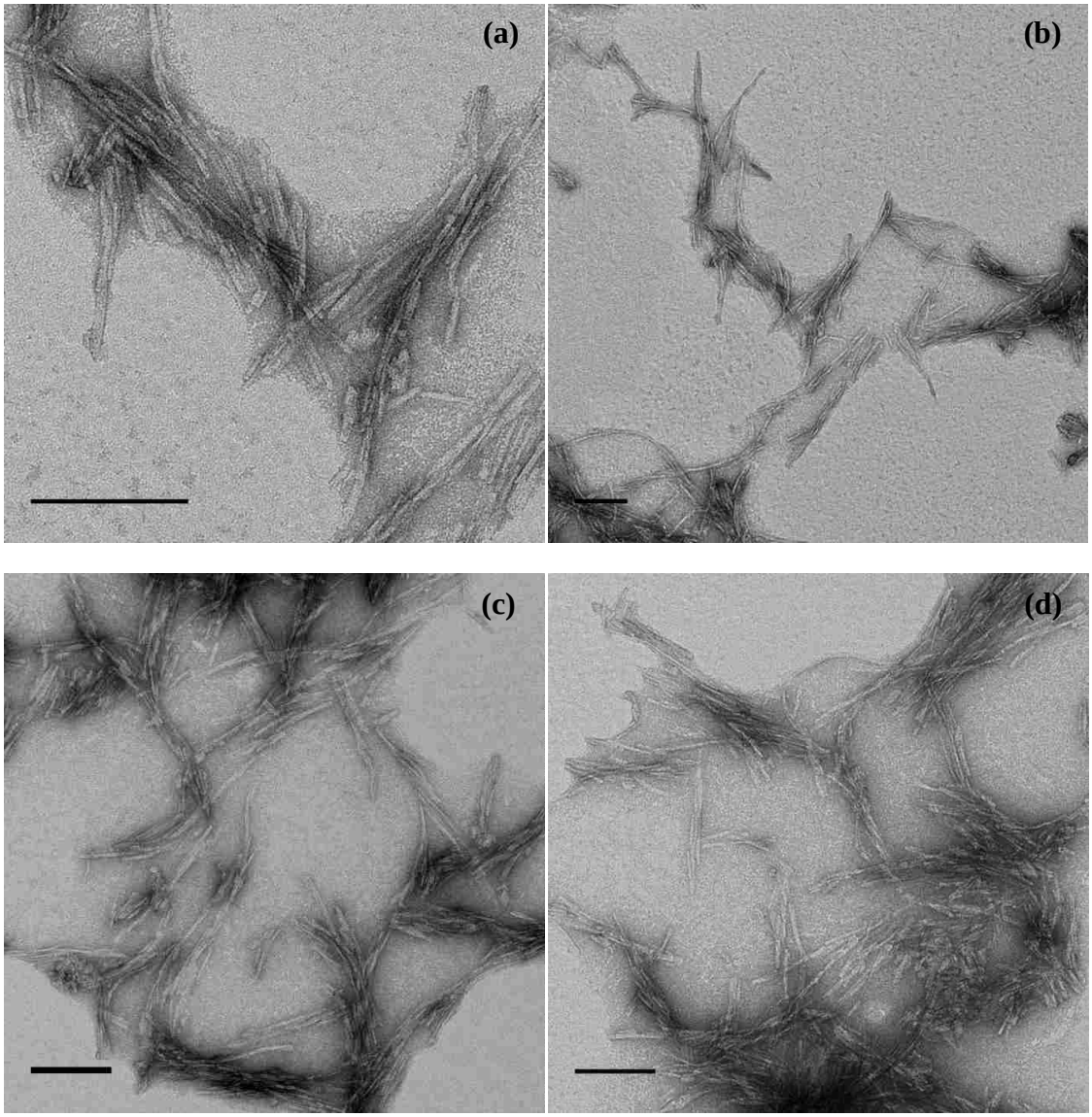

Figure 3.23. Negative staining transmission electron images of amyloid fibril formation of bovine insulin incubated for 55 hours at 37 ˚C and 230 rpm. The scale bar represents 200 nm.

A statistical analysis of the length distribution of the fibrils from Figure 3.25 was not possible due to the fact that most fibrils extend further outside the image. However, the fibrils have similar morphologies and nearly all fibrils are several microns in length. The average width of the fibrils was measured to be 15±3 nm and 15±3 nm for human and bovine insulin, respectively (Table 3.23 and Figure 3.26).

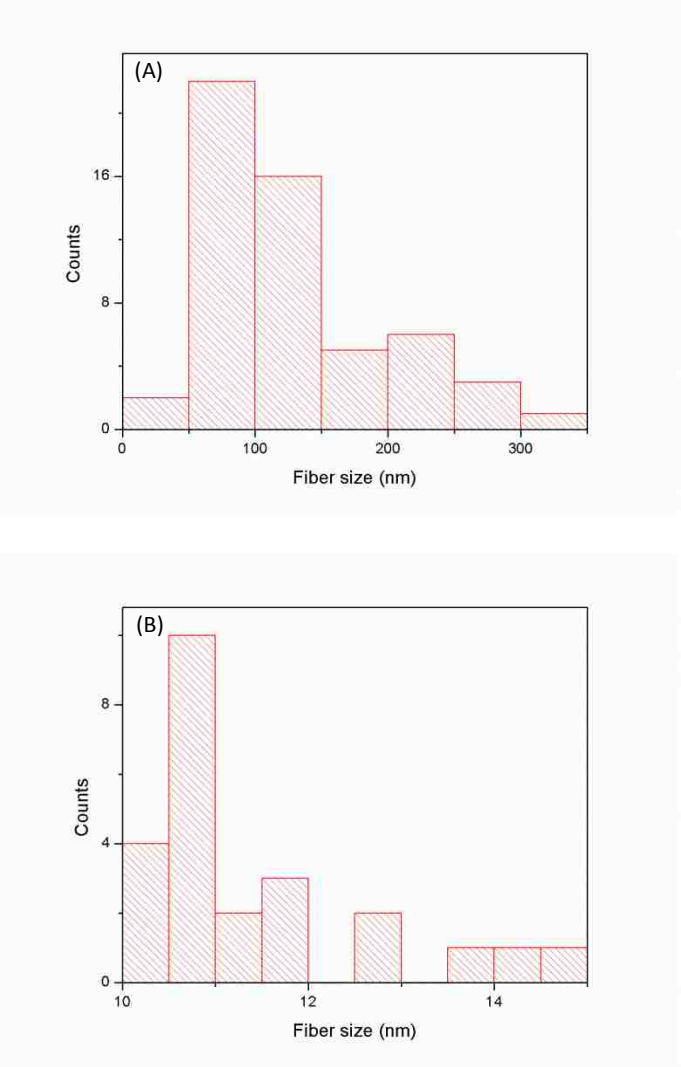

Figure 3.24. Length (A) and width (B) distributions of bovine insulin incubated and 37˚C at 230 rpm for 55 hours.

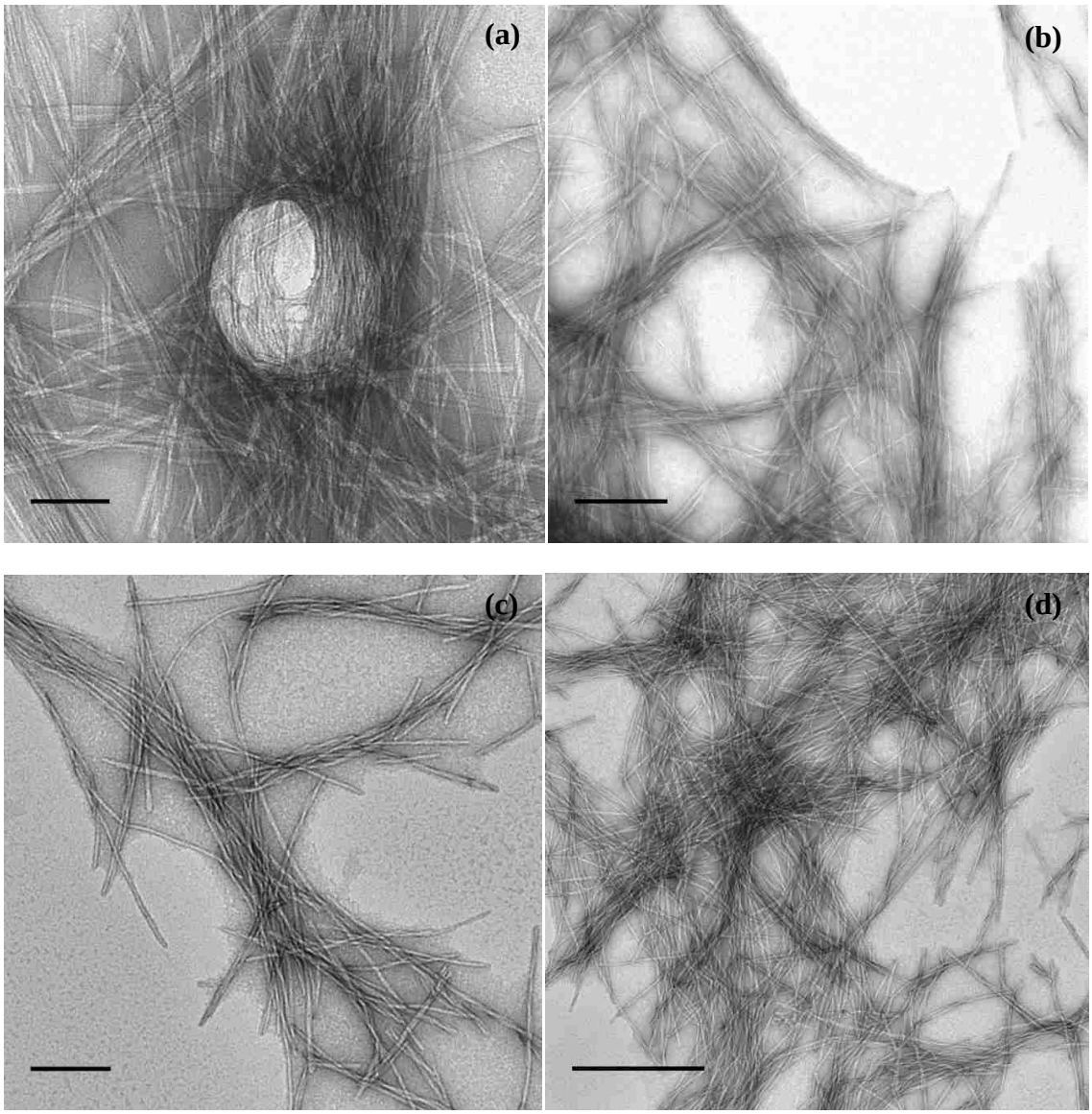

Figure 3.25. Negative staining transmission electron images of amyloid fibril formation of human and bovine insulin in the presence of liposome 3 (80/20 PC/C) incubated at 60 ˚C for 40 hours. (a) and (b) Human insulin. (c) and (d) Bovine insulin. The scale bar represents 100 nm (a) 500 nm (b) & (d) and 200 nm (c).

Table 3.23. Statistical analysis of the width of human and bovine insulin in the presence of liposome 3 (80/20 PC/C) incubated at 60 ˚C for 40 hours.

Sample	Mean (nm)	Std Deviation (nm)	Minimum (nm)	Median (nm)	Maximum (nm)
(a) & (b)	15	3	10	15	20
(c) & (d)	15	3	11	14	20

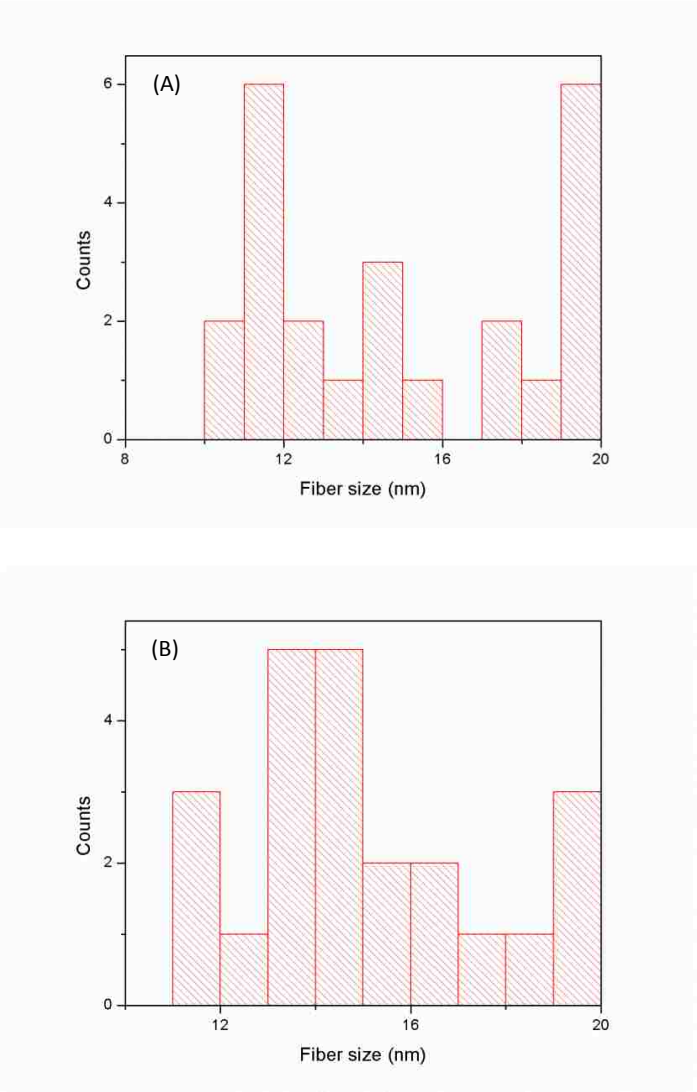

Figure 3.26. Width distribution of (A) human and (B) bovine insulin in the presence of liposome 3 (80/20 PC/C) incubated at 60 ˚C for 40 hours.

Figure 3.27 shows that in the presence of PS-COOH surfaces longer fibrils were also obtained when incubated for longer periods of time, without stirring. These differences were observed in human insulin incubated at 60˚C for 6 and 40 hours, respectively.

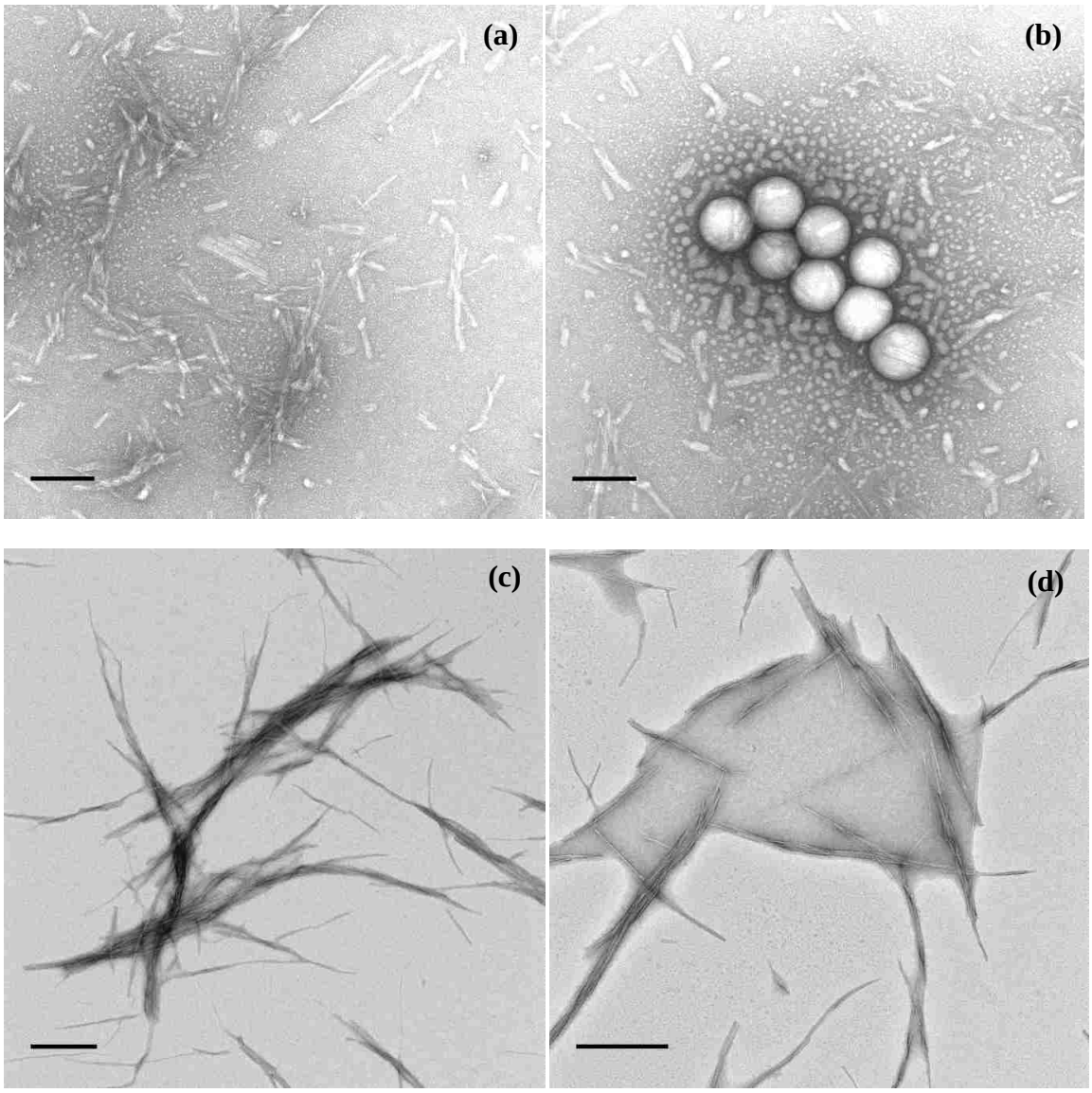

Figure 3.27. Negative staining transmission electron images of amyloid fibril formation of human insulin in the presence of PS-COOH. Images were obtained from two different samples: (a) and (b) were obtained from one sample while (c) and (d) were obtained from another sample. (a) and (b) incubated for 6 hours. (c) and (d) incubated for 40 hours. The scale bar represents 100 nm (a) and (b) and 500 nm (c) and (d).

When insulin (in the presence of PS-COOH) is incubated for six and 40 hours at 60 ˚C the fibrils attain an average length of 96±43 nm, and 1278±511 nm, respectively (Table 3.24 & Figure 3.28). When insulin (in the presence of PS-COOH) is incubated for

six and 40 hours at 60 ˚C the fibrils attain an average width of 13±2 nm and 15±4 nm, respectively (Table 3.25 and Figure 3.29).

Table 3.24. Statistical analysis of the length of human insulin in the presence of PS-COOH incubated for (A) six and (B) 40 hours.

Samples	Mean (nm)	Std Deviation (nm)	Minimum (nm)	Median (nm)	Maximum (nm)
(A): (a) & (b)	96	43	35	90	201
(B): (c) & (d)	1278	511	468	1251	2708

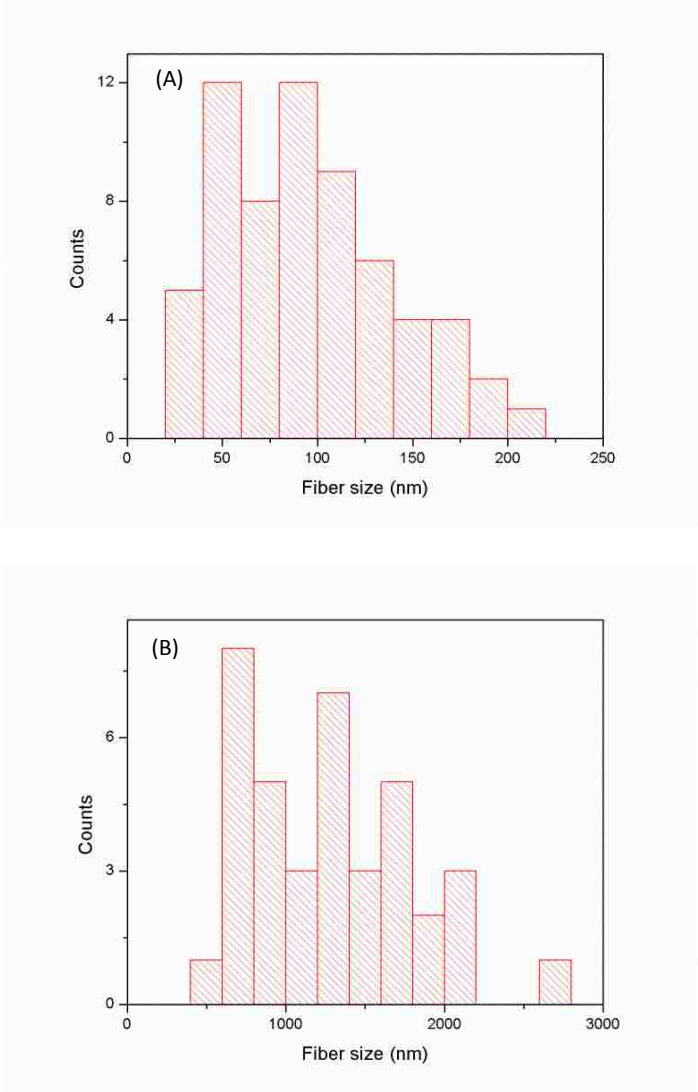

Figure 3.28. Length distribution of human insulin in the presence of PS-COOH incubated at 60˚C for (A) six and (B) 40 hours.

Table 3.25. Statistical analysis of the width of human insulin in the presence of PS-COOH incubated for (A) six and (B) 40 hours.

Sample	Mean (nm)	Std Deviation (nm)	Minimum (nm)	Median (nm)	Maximum (nm)
(A): (a) & (b)	13	2	10	12	18
(B): (c) & (d)	15	4	7	16	20

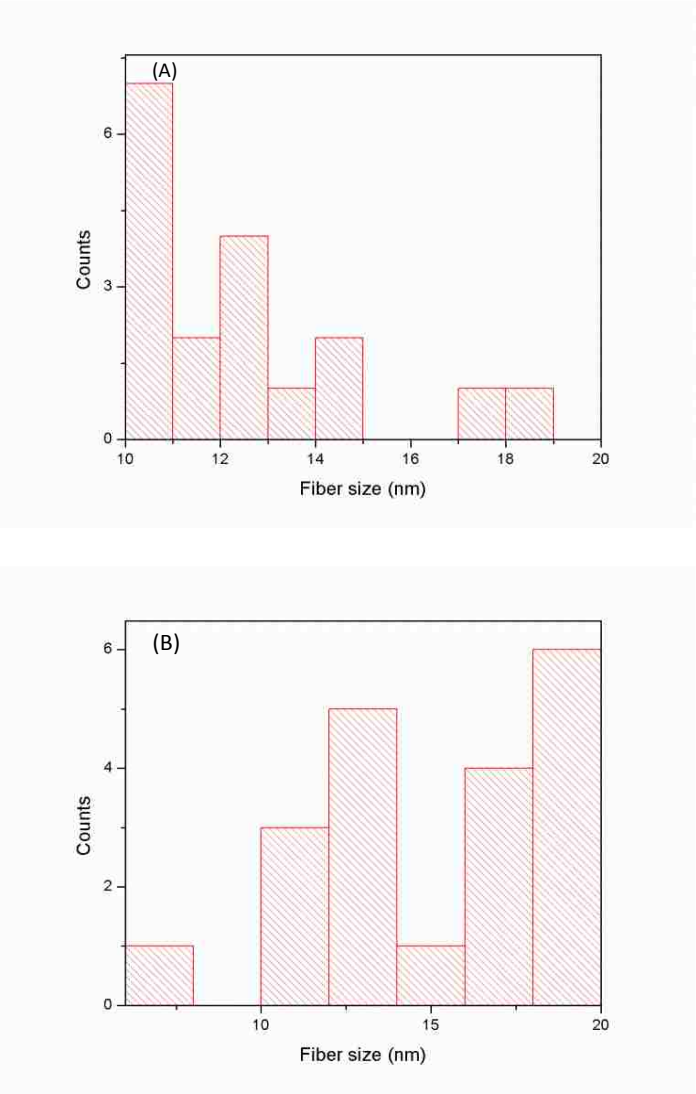

Figure 3.29. Width distribution of human insulin in the presence of PS-COOH incubated at 60˚C for (A) six and (B) 40 hours.

4. CONCLUSIONS

Not all the surfaces shorten the lag time (this is more evident for both insulins incubated at 60 ˚C). On the other hand, most surfaces had an impact (either significant or minute) on the growth rate of both insulins. The downhill mechanism can be used to describe the results represented by a sigmoidal curve while the "seeded" results can be described by the classical-nucleation polymerization model. An autocatalytic reaction may be plausible as well in which the formed fibril in solution can act as a preferential site for new nucleation or elongation events. Furthermore, several mechanisms may be necessary to fully describe the complex insulin aggregation process. In addition, it is probable that one mechanism is dominant at certain experimental conditions or at a certain stage in the aggregation process while another is more dominant at another stage.

Structural changes taking place during fibril formation were followed. In general, the initial transition in which the the insulin decreases from random coil into α-helix conformation may be attributed to the dissolution of the insulin. The second transition along with a constant or a continuous increase in α-helix structure could be due to the changes within the dimeric protein in the nucleation phase; throughout this transition, the reaction pathway may be chosen and the formation of the active centers may take place. However, which one occurs first? Is it the reaction the one that dictates the type of nucleus/active centers or is the nucleus/active centers the one that dictates the reaction pathway? We don't know but we do know that the choice of experimental conditions (temperature, mechanical stresses, pH, concentration, etc.) are a determinant factor in the rate of insulin aggregation and the amyloid fibril morphologies; this can give further insights into the reaction mechanism(s) and the subsequent build up of a model.

Since our results show different reactions (this is clear from the turbidimetry graphs) we have more than one mechanism present). The third transition in which a reduction in α-helix and an increase in β-turn and β-sheet take place may be attributed to the precipitation phase in which floccule formation could take place. The final transition in which the secondary structure of the insulin is predominantly β-sheet may depict,

depending on the incubation conditions, the elongation phase of the mature insulin fibrils or the formation of spherulites.

Both, human and bovine insulin formed fibril of similar morphologies (i.e. similar length, width, and structure) when treated under the same conditions in the presence and in the absence of surfaces with the exception of incubation at 37 ˚C and 230 rpm stirring for 55 hours. In addition, when human and bovine insulin are subjected to mechanical stresses the fibrils appear "fragmented" and hence their size is smaller when compared to insulin that has not been agitated. Bovine insulin fibrils were longer and thinner under these incubation conditions (37 ˚C and 230 rpm) than human insulin fibrils. Incubation temperatures were different between agitated insulin (37 ˚C) and non-agitated insulin (60 ˚C). It is also noticeable that at 60 ˚C larger fibrils formed at longer incubation times. The width of the fibrils ranged between 10 to 20 nm, there is not a noticeable dependence/correlation between fibril length and width for human or bovine insulin. On the other hand, based on the obtained images, the statistical analysis, and in agreement with literature the incubation methods utilized determined the fibril morphologies.

Nielsen et al. (2000b) have concluded that the fibrillation of bovine insulin has shorter lag times than human insulin. Our results partially agreed with that.

A**PPENDIX A**

INSULIN FIBRILS BY THE METHOD OF BURKE AND ROUGVIE

Usually, a 1 % solution of insulin in water is adjusted to pH 2.0 with hydrochloric acid and the solution is placed in a sealed-glass test tube. The tube is heated in a water bath to between 80 and 100 °C until a clear gel is formed. The time required for gelling is between 2 and 10 minutes depending on the exact temperature and pH. The sample is then cooled and frozen rapidly by immersion in a dry ice acetone bath, thawed under running tap water, and reheated (80-100°) for approximately 2 min. The procedure of freezing and reheating is repeated three or four times until a firm gel is formed. Total conversion of native to fibrillar insulin is possible by this process.

APPENDIX B

DYNAMIC LIGHT SCATTERING HISTOGRAMS

OF BOVINE INSULIN IN BULK AND IN THE PRESENCE OF POLYSTYRENE

LATEX INCUBATED AT 60 ˚C

1. BLANKS

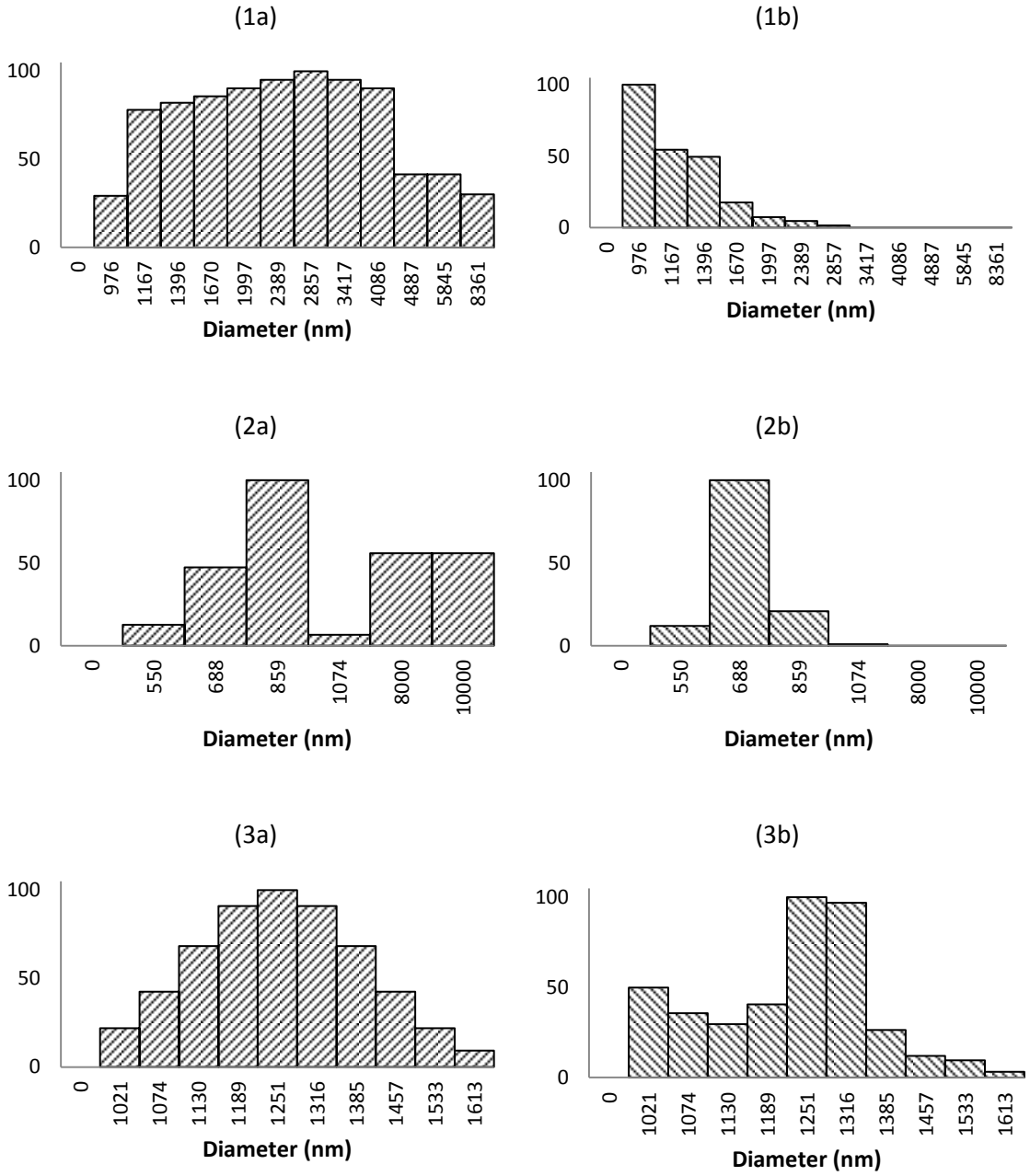

Figure B.1. DLS analysis of the blanks: histograms represent relative scattering by intensity (a) and by number (b). Results shown are for: (1a) & (1b) buffer solution after 7 hours; (2a) & (2b) buffer+PS after 7 hours; and (3a) & (3b) buffer+PSOH after 1 hour.

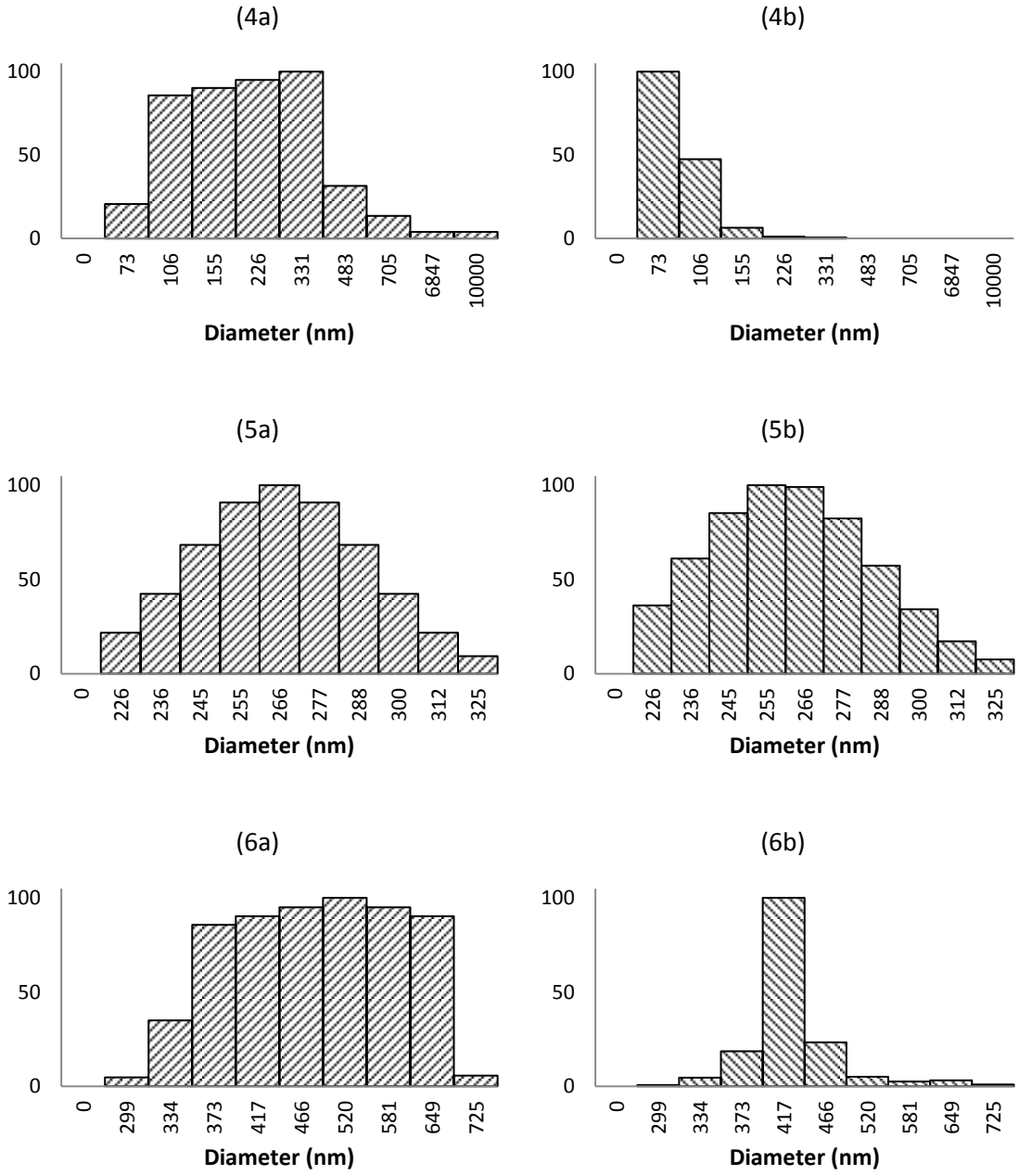

Figure B.2. DLS analysis of the blanks: histograms represent relative scattering by intensity (a) and by number (b). Results shown are for: (4a) & (4b) buffer+PSCOOH solution after 60 min; (5a) & (5b) buffer+PSNH2 before incubation; and (6a) & (6b) buffer+PSNH2 after 7 hours of incubation.

2. BOVINE INSULIN IN BULK

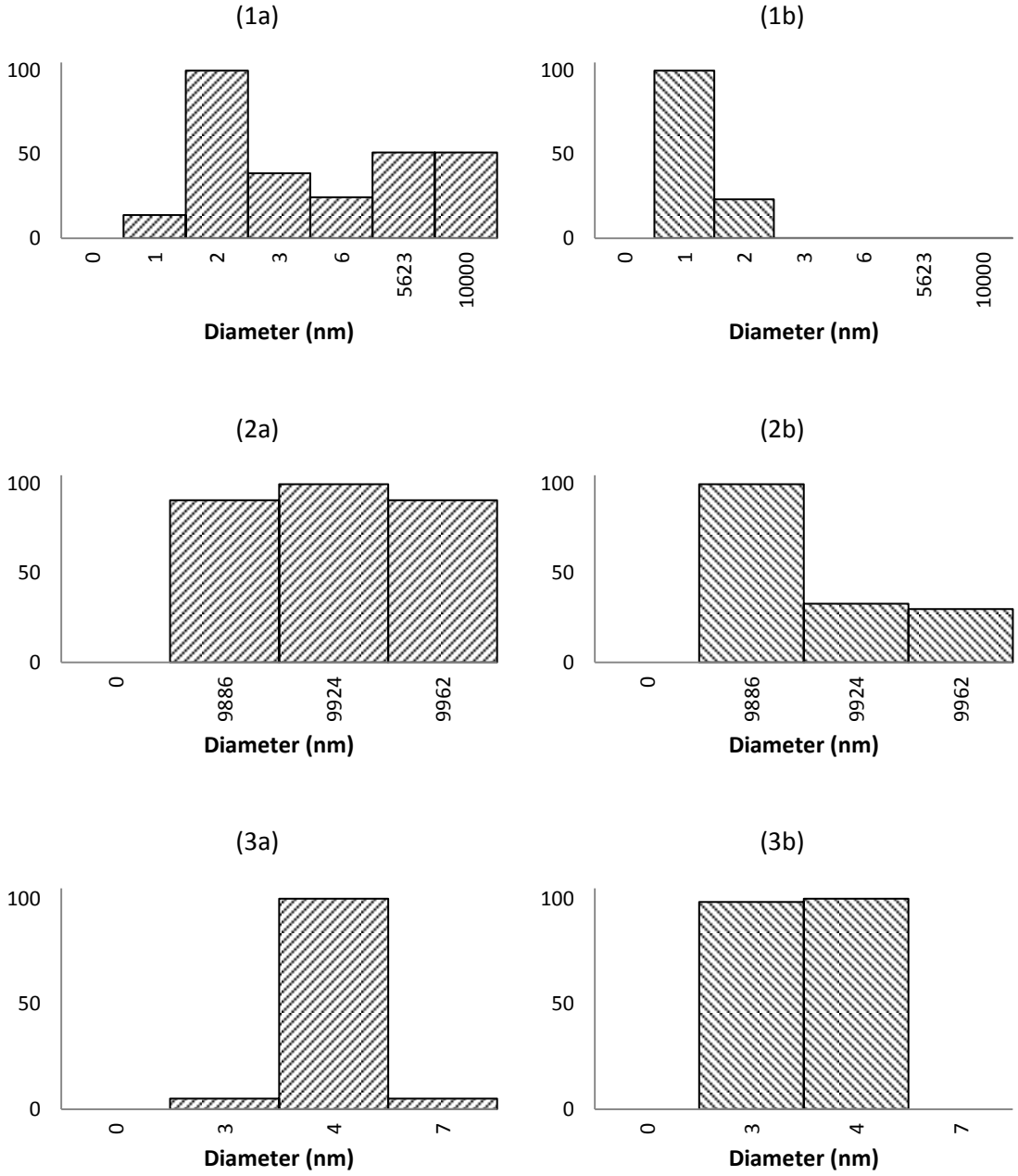

Figure B.3. DLS analysis of bovine insulin (SIGMA, Cat. #: I5500 (lot 019K17765V) aggregation in bulk: histograms represent relative scattering by intensity (a) and by number (b). Results shown are for: (1a) & (1b) before incubation; (2a), (2b), (3a) & (3b) after 25 minutes of incubation. Sample (3) is the duplicate of sample (2).

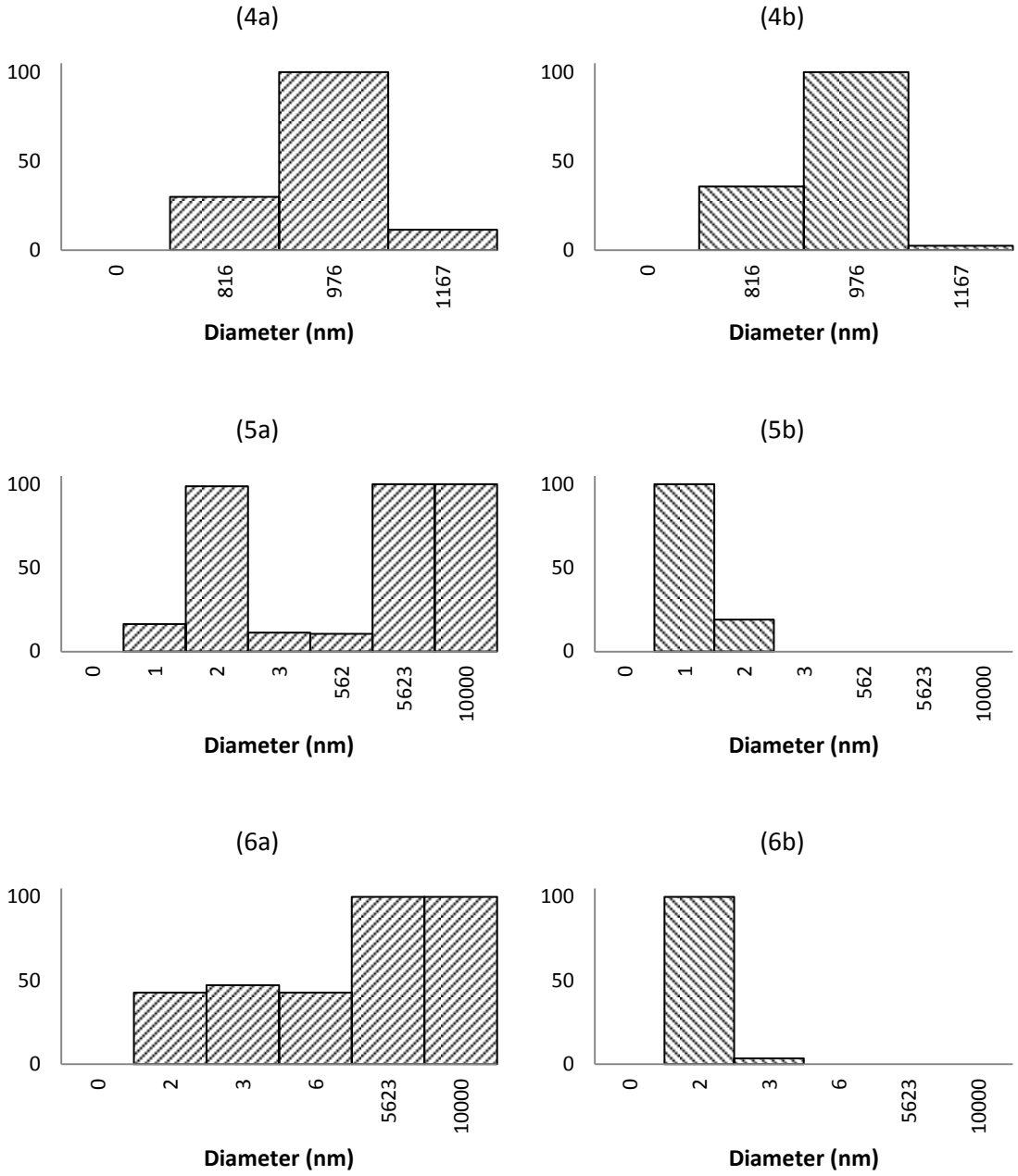

Figure B.4. DLS analysis of bovine insulin (SIGMA, Cat. #: I5500 (lot 019K17765V) aggregation in bulk: histograms represent relative scattering by intensity (a) and by number (b). Results shown are for: (4a) & (4b) after 45 minutes; (5a), (5b), (6a) & (6b) after 90 minutes of incubation. Sample (6) is the duplicate of sample (5).

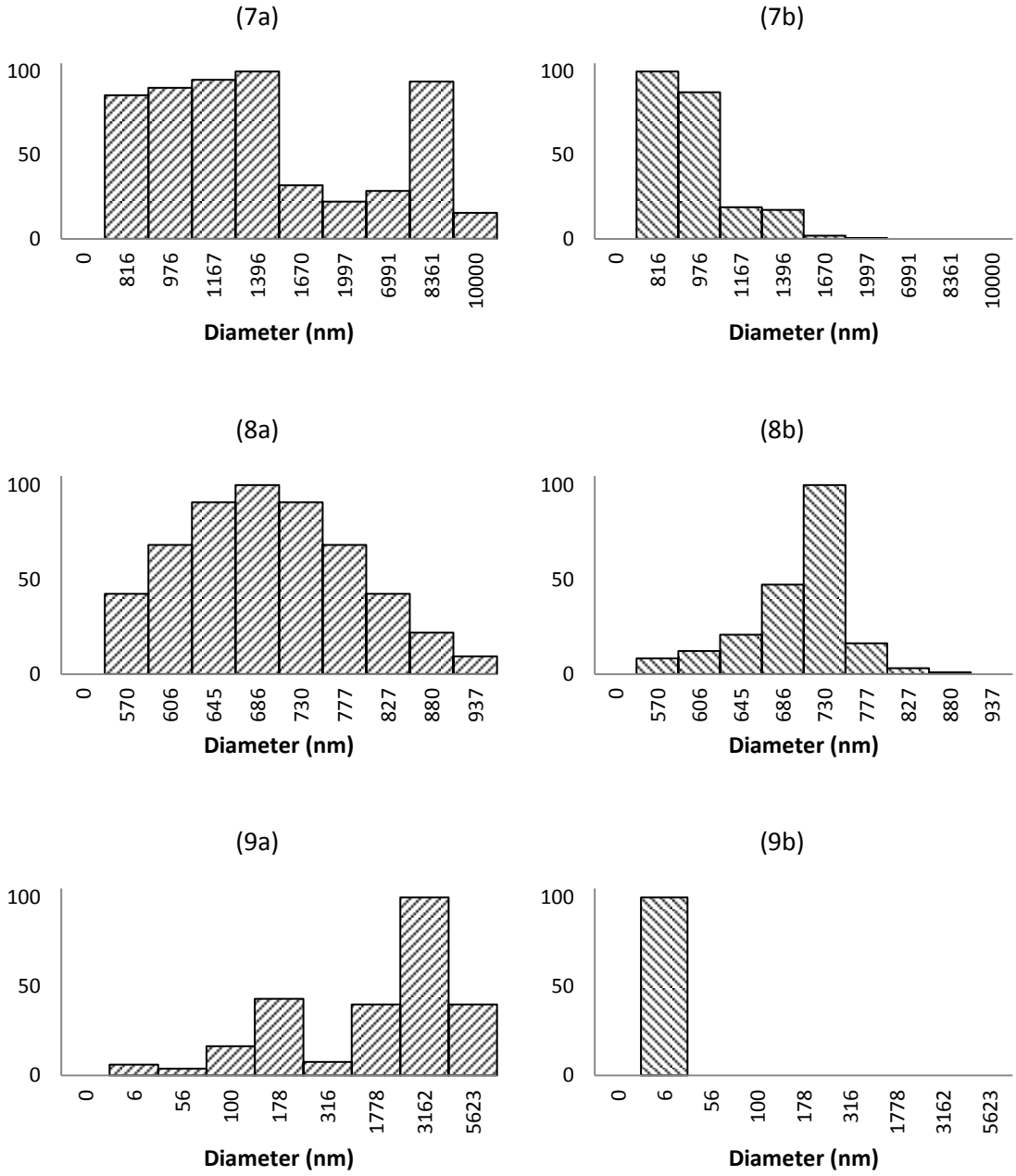

Figure B.5. DLS analysis of bovine insulin (SIGMA, Cat. #: I5500 (lot 019K17765V) aggregation in bulk: histograms represent relative scattering by intensity (a) and by number (b). Results shown are for: (7a), (7b), (8a) & (8b) after 120 minutes; and (9a) & (9b) after 150 minutes of incubation. Sample (8) is the duplicate of sample (7).

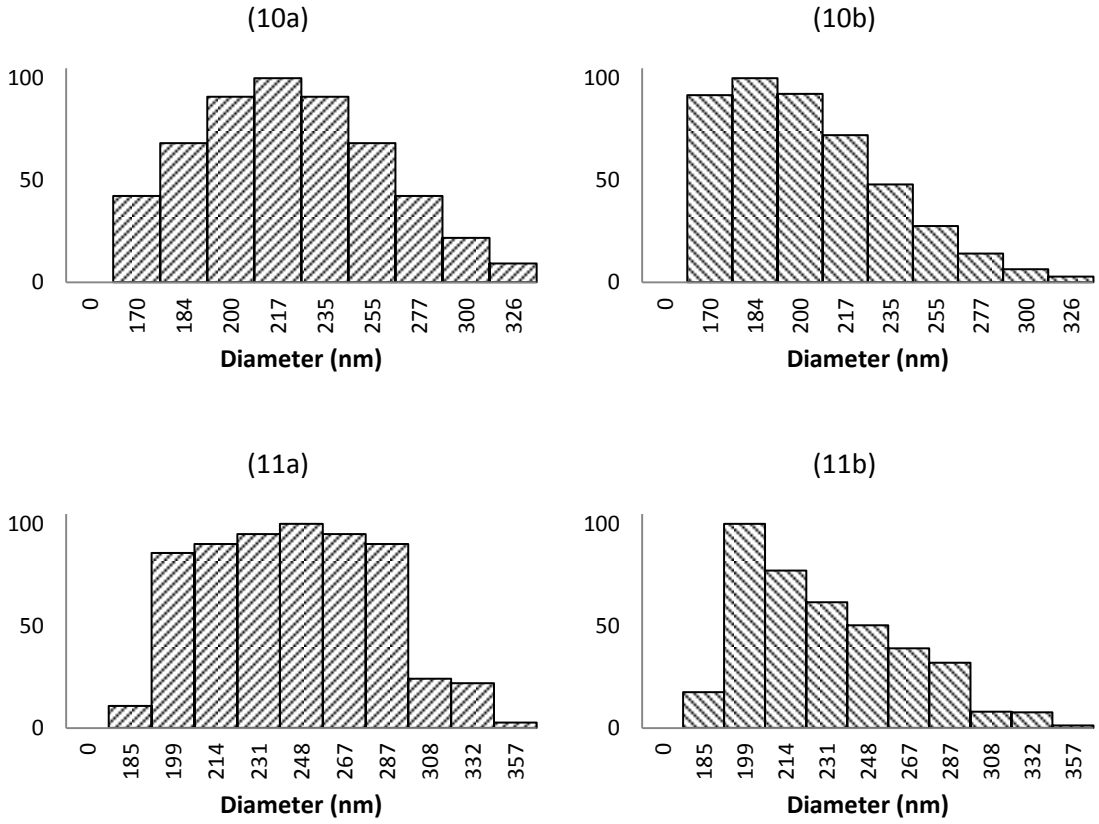

Figure B.6. DLS analysis of bovine insulin (SIGMA, Cat. #: I5500 (lot 019K17765V) aggregation in bulk: histograms represent relative scattering by intensity (a) and by number (b). Results shown are for: (10a) & (10b) after 180 minutes of incubation; and (11a) & (11b) after 210 minutes.

3. BOVINE INSULIN IN THE PRESENCE OF PS SURFACE

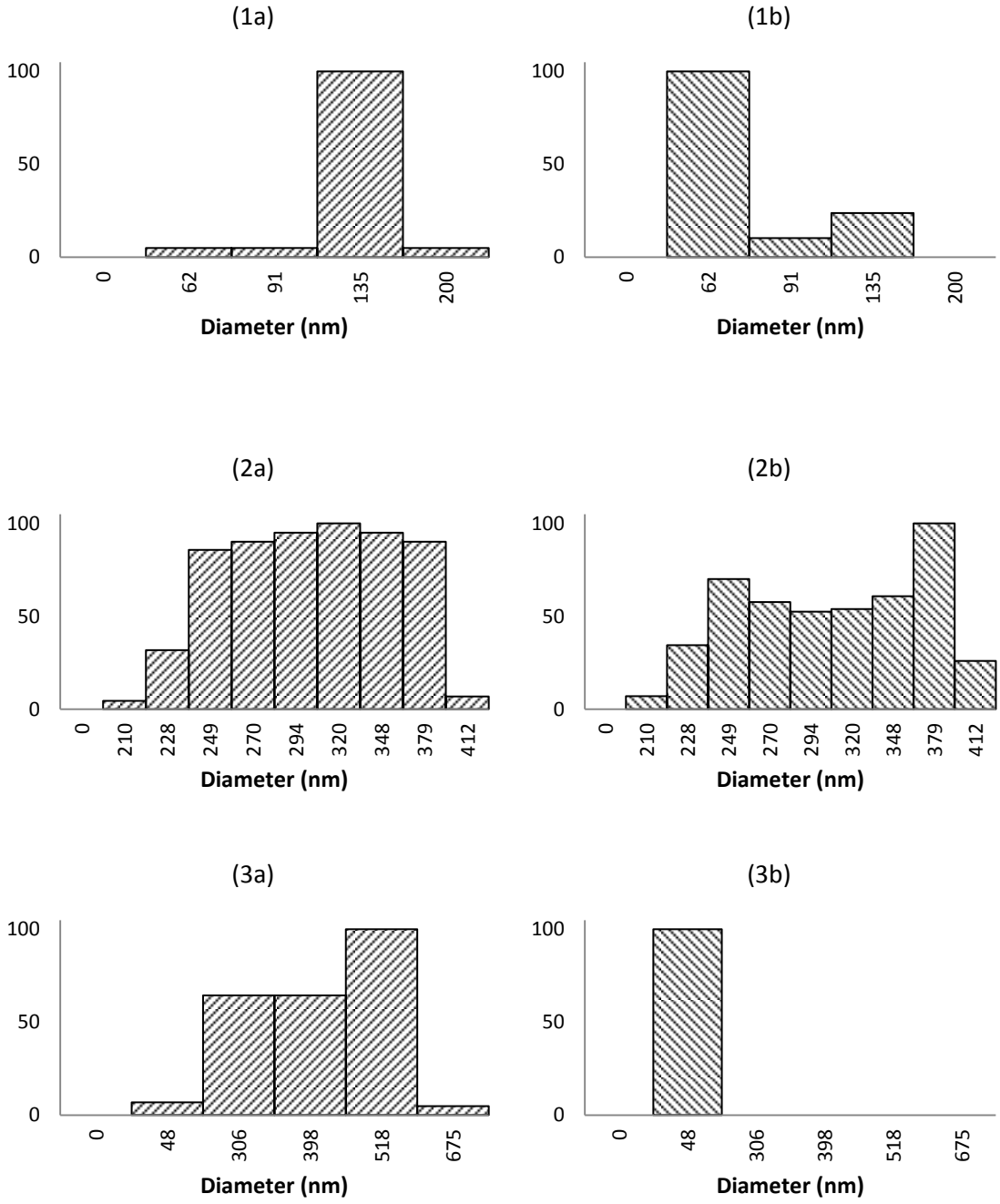

Figure B.7. DLS analysis of bovine insulin (SIGMA, Cat. #: I5500 (lot 019K17765V) aggregation in the presence of PS surface: histograms represent relative scattering by intensity (a) and by number (b). Results shown are for: (1a), (1b), (2a), (2b), (3a) & (3b) before incubation. Sample (2) is the duplicate of sample (1).

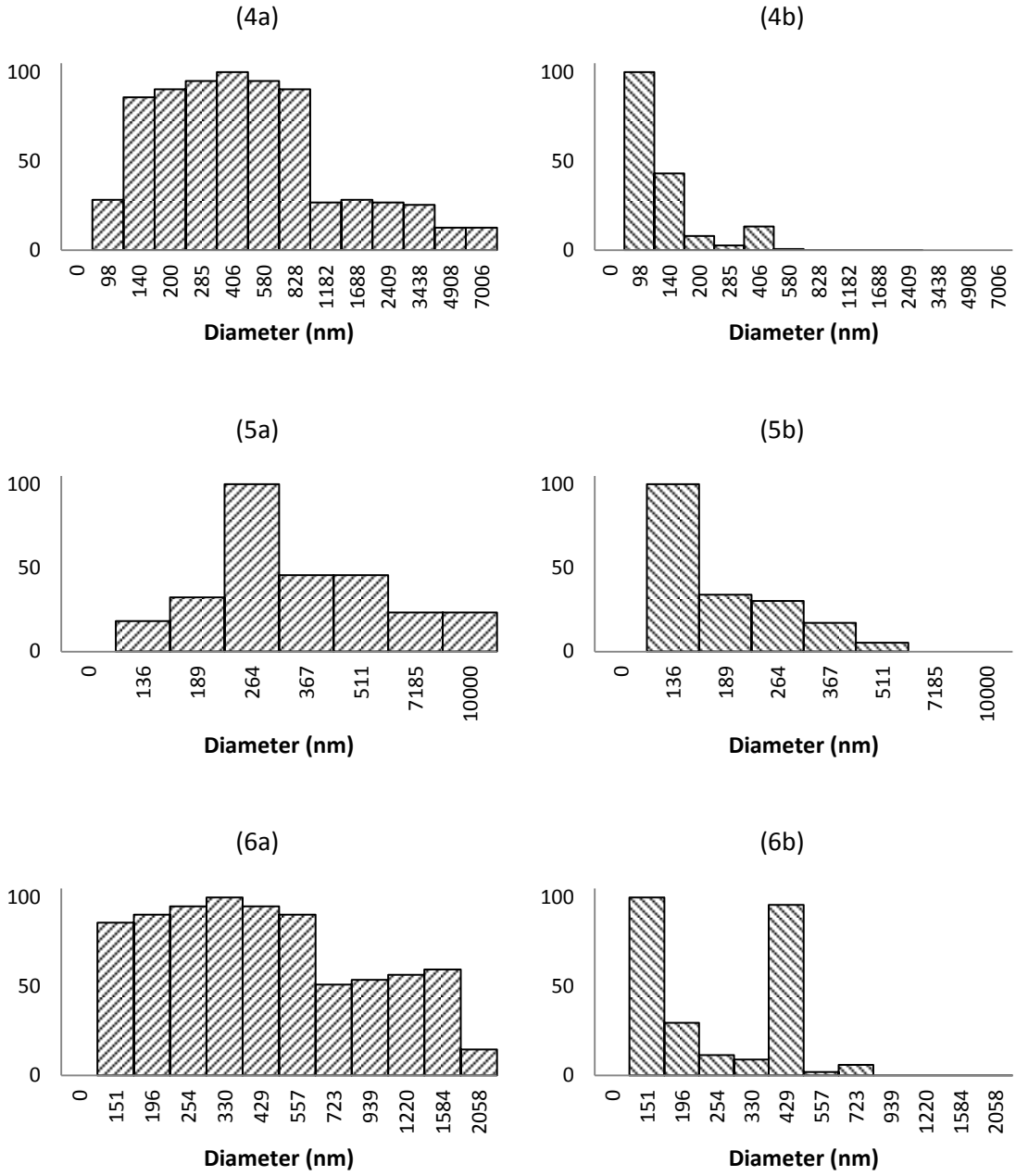

Figure B.8. DLS analysis of bovine insulin (SIGMA, Cat. #: I5500 (lot 019K17765V) aggregation in the presence of PS surface: histograms represent relative scattering by intensity (a) and by number (b). Results shown are for: (4a) & (4b) before incubation; (5a), (5b), (6a) & (6b) after 25 minutes of incubation. Sample (4) is the duplicate of sample (3) and sample (6) is the duplicate of sample (5).

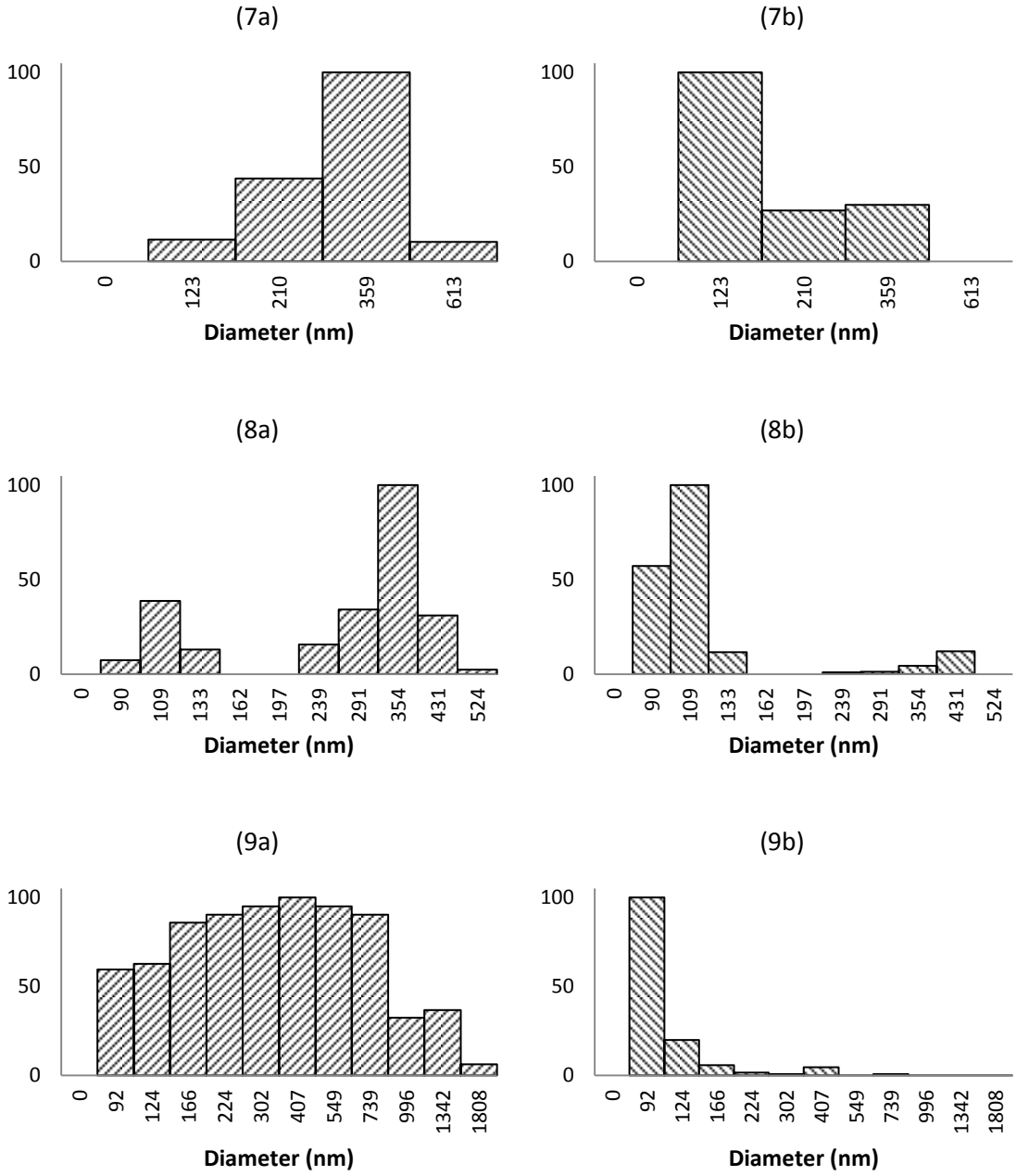

Figure B.9. DLS analysis of bovine insulin (SIGMA, Cat. #: I5500 (lot 019K17765V) aggregation in the presence of PS surface: histograms represent relative scattering by intensity (a) and by number (b). Results shown are for: (7a), (7b), (8a) & (8b) after 30 minutes; and (9a) & (9b) after 45 minutes of incubation. Sample (8) is the duplicate of sample (7).

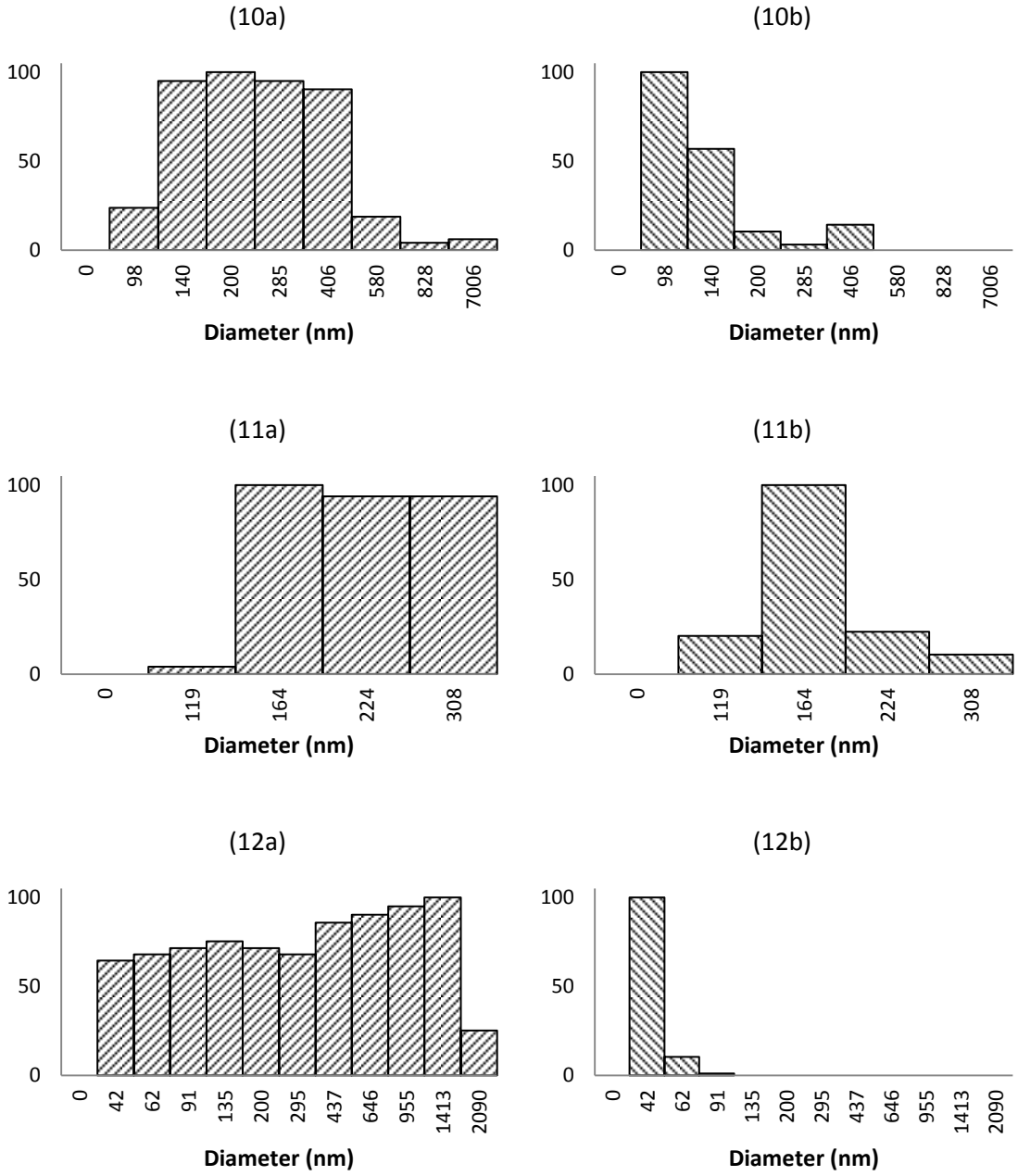

Figure B.10. DLS analysis of bovine insulin (SIGMA, Cat. #: I5500 (lot 019K17765V) aggregation in the presence of PS surface: histograms represent relative scattering by intensity (a) and by number (b). Results shown are for: (10a), (10b), (11a) & (11b) after 60 minutes; and (12a) & (12b) after 90 minutes of incubation. Sample (11) is the duplicate of sample (10).

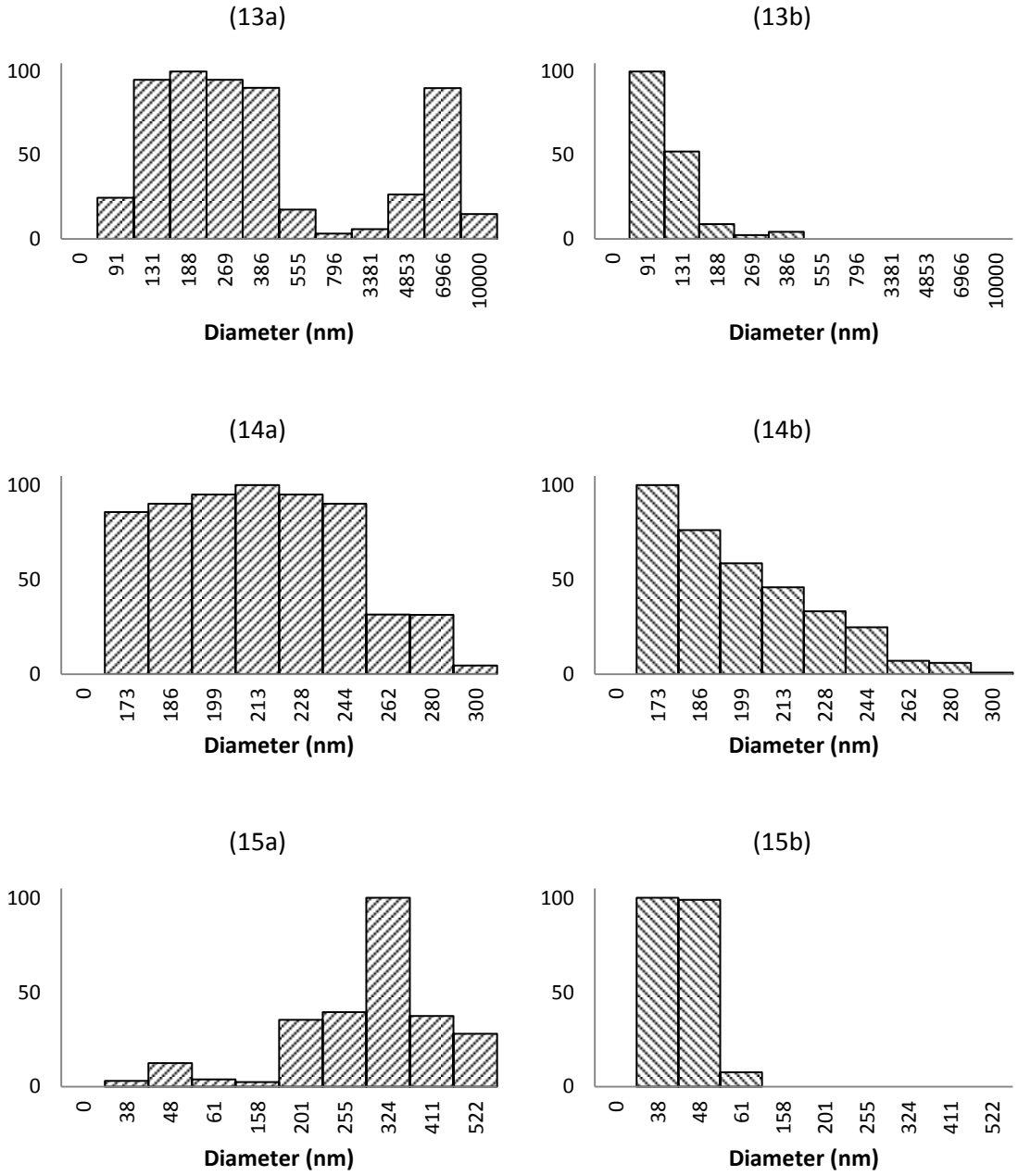

Figure B.11. DLS analysis of bovine insulin (SIGMA, Cat. #: I5500 (lot 019K17765V) aggregation in the presence of PS surface: histograms represent relative scattering by intensity (a) and by number (b). Results shown are for: (13a) & (13b) after 120 minutes; and (14a), (14b), (15a) & (15b) after 240 minutes. Sample (15) is the duplicate of sample (14).

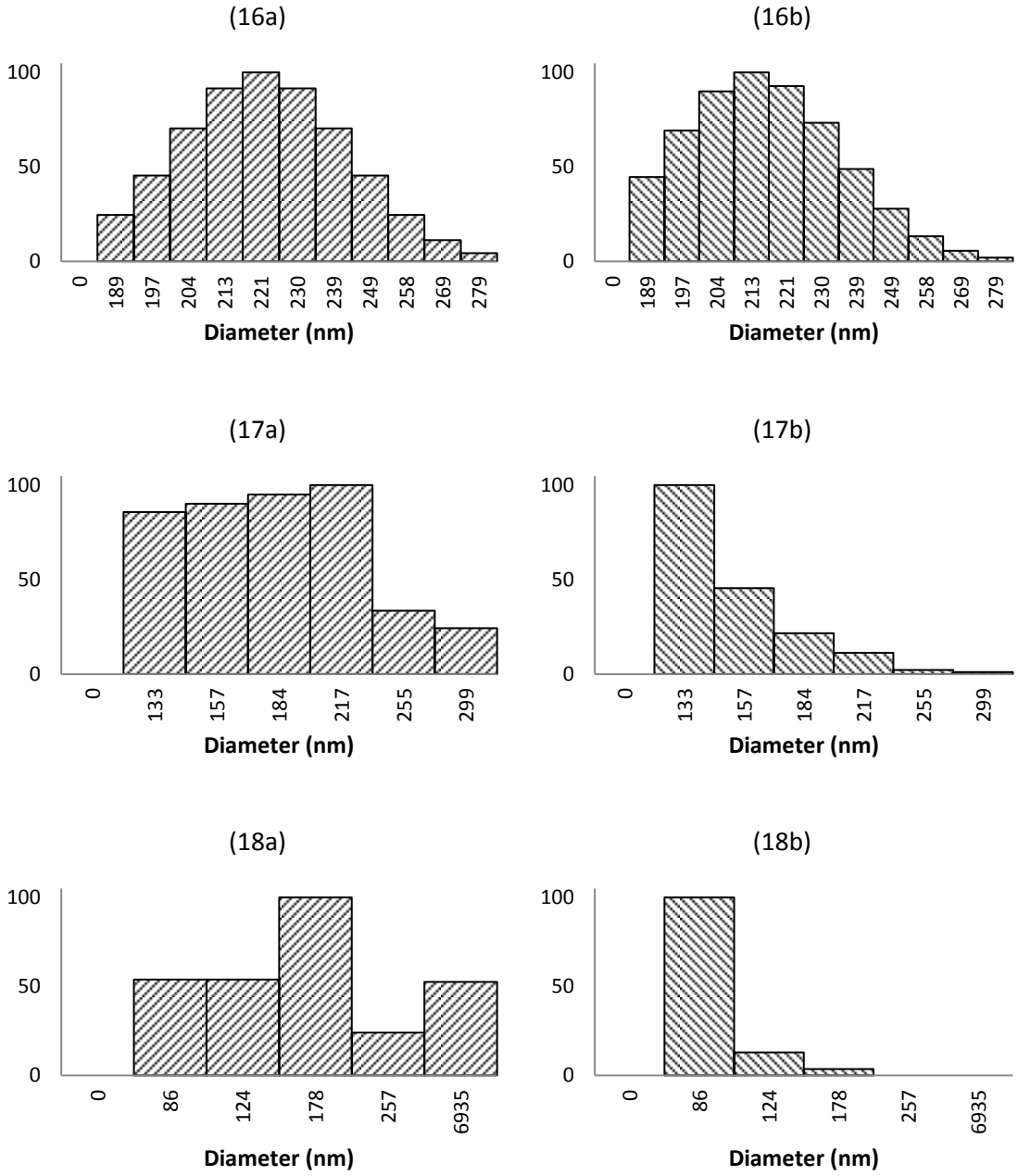

Figure B.12. DLS analysis of bovine insulin (SIGMA, Cat. #: I5500 (lot 019K17765V) aggregation in the presence of PS surface: histograms represent relative scattering by intensity (a) and by number (b). Results shown are for: (16a) & (16b) after 300 minutes; (17a) & (17b) after 330 minutes; and (18a) & (18b) after 360 minutes of incubation.

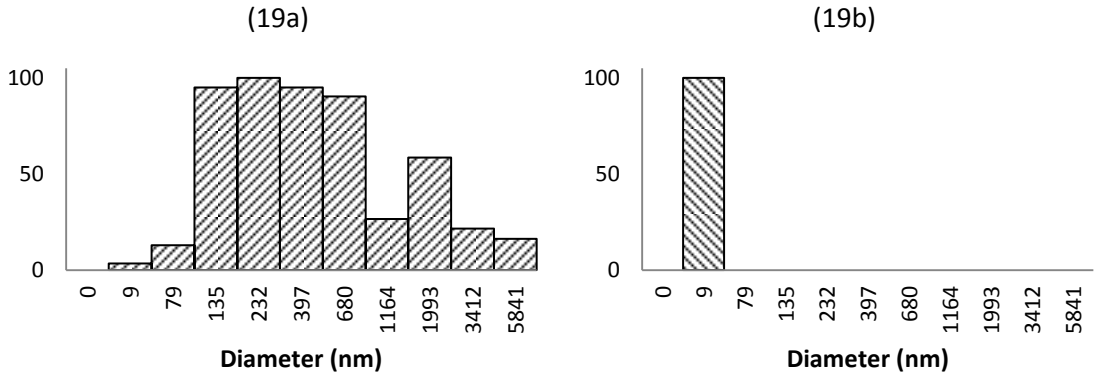

Figure B.13. DLS analysis of bovine insulin (SIGMA, Cat. #: I5500 (lot 019K17765V) aggregation in the presence of PS surface: histograms represent relative scattering by intensity (a) and by number (b). Results shown are for: (19a) & (19b) after 390 minutes of incubation.

4. BOVINE INSULIN IN THE PRESENCE OF PS-OH SURFACE

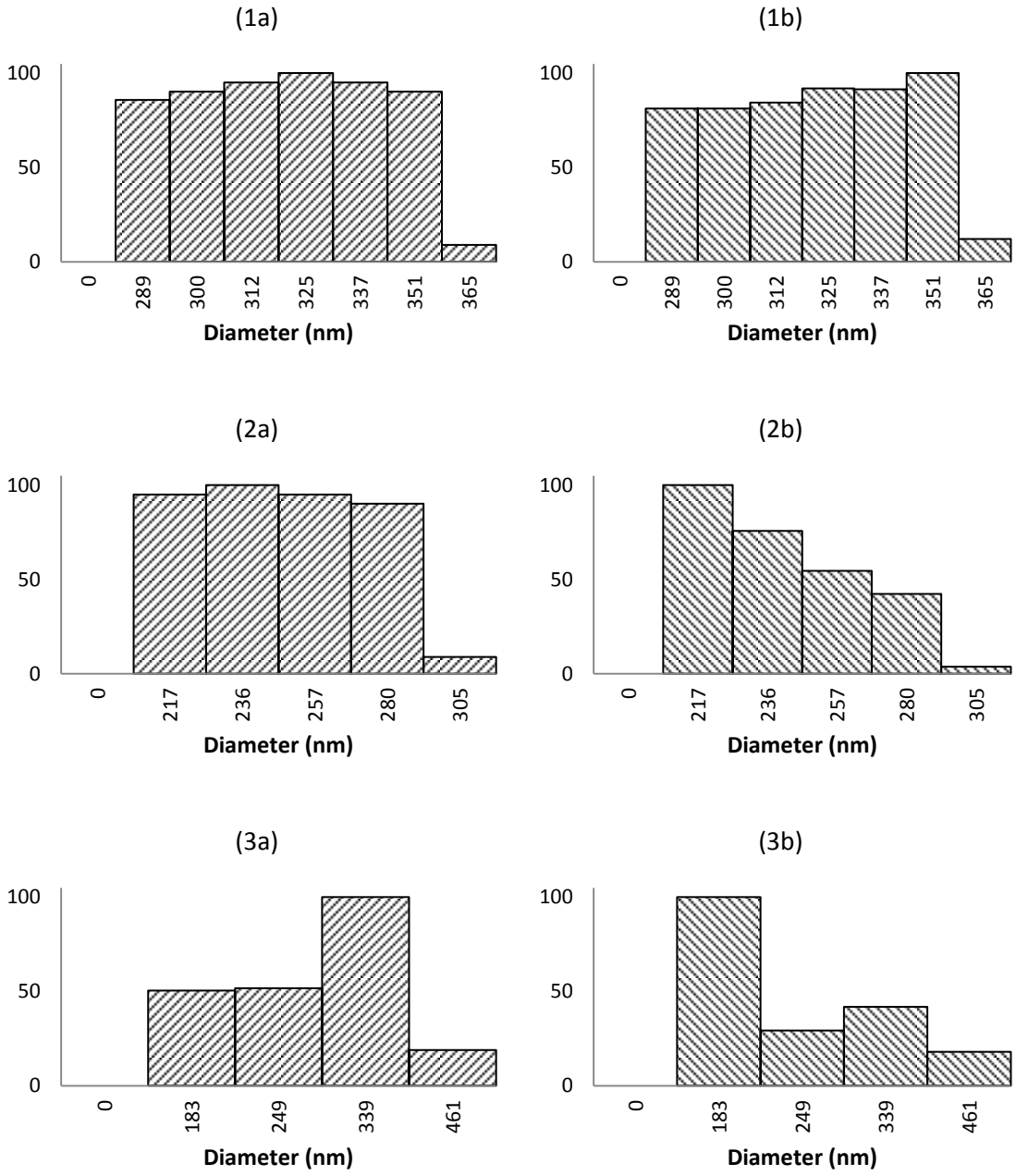

Figure B.14. DLS analysis of bovine insulin (SIGMA, Cat. #: I5500 (lot 019K17765V) aggregation in the presence of PS-OH surface: histograms represent relative scattering by intensity (a) and by number (b). Results shown are for: (1a), (1b), (2a), (2b), (3a) & (3b) before incubation. Sample (2) is the duplicate of sample (1).

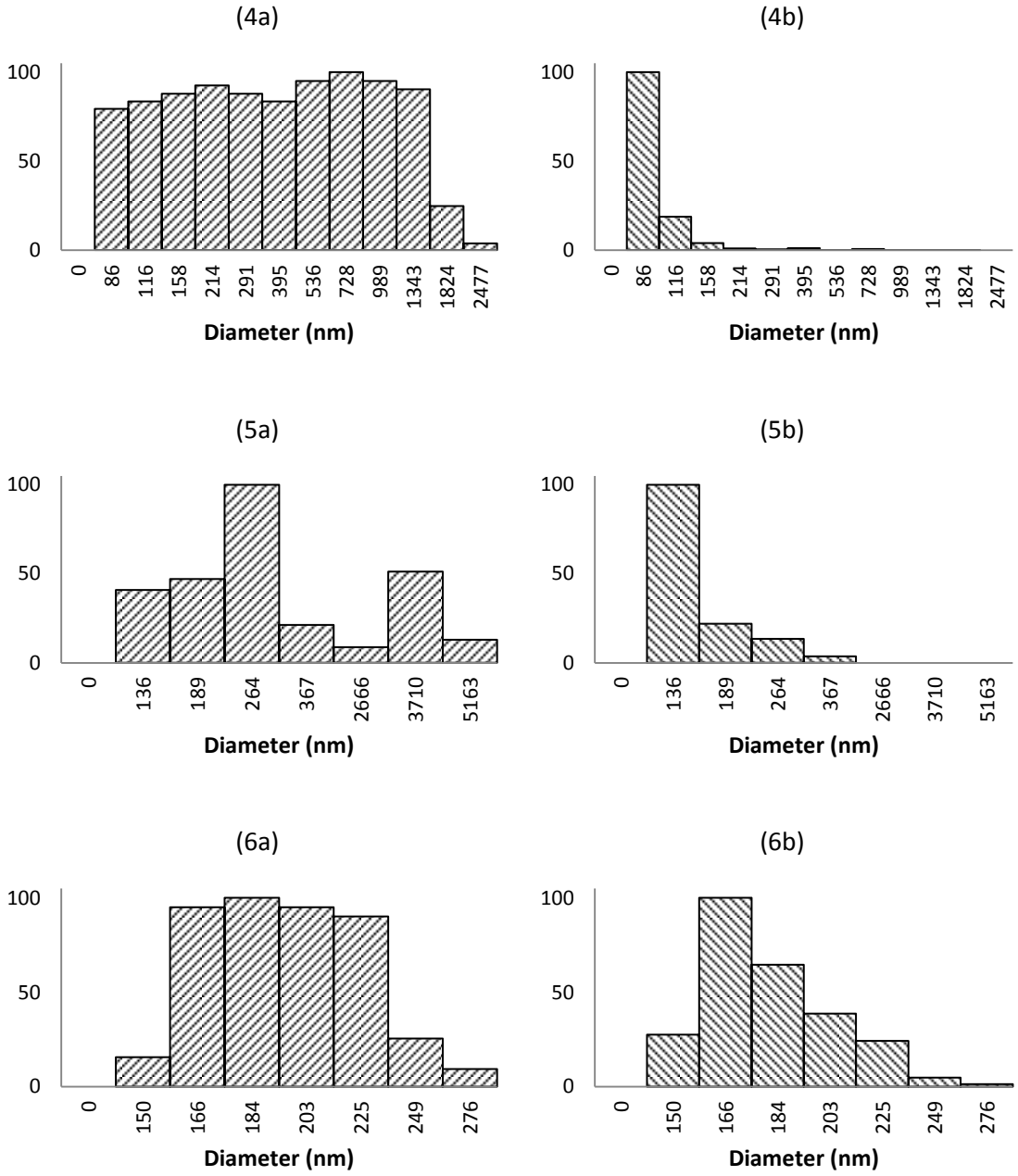

Figure B.15. DLS analysis of bovine insulin (SIGMA, Cat. #: I5500 (lot 019K17765V) aggregation in the presence of PS-OH surface: histograms represent relative scattering by intensity (a) and by number (b). Results shown are for: (4a), (4b), (5a) & (5b) after 25 minutes; and (6a) & (6b) after 30 minutes of incubation. Sample (5) is the duplicate of sample (4).

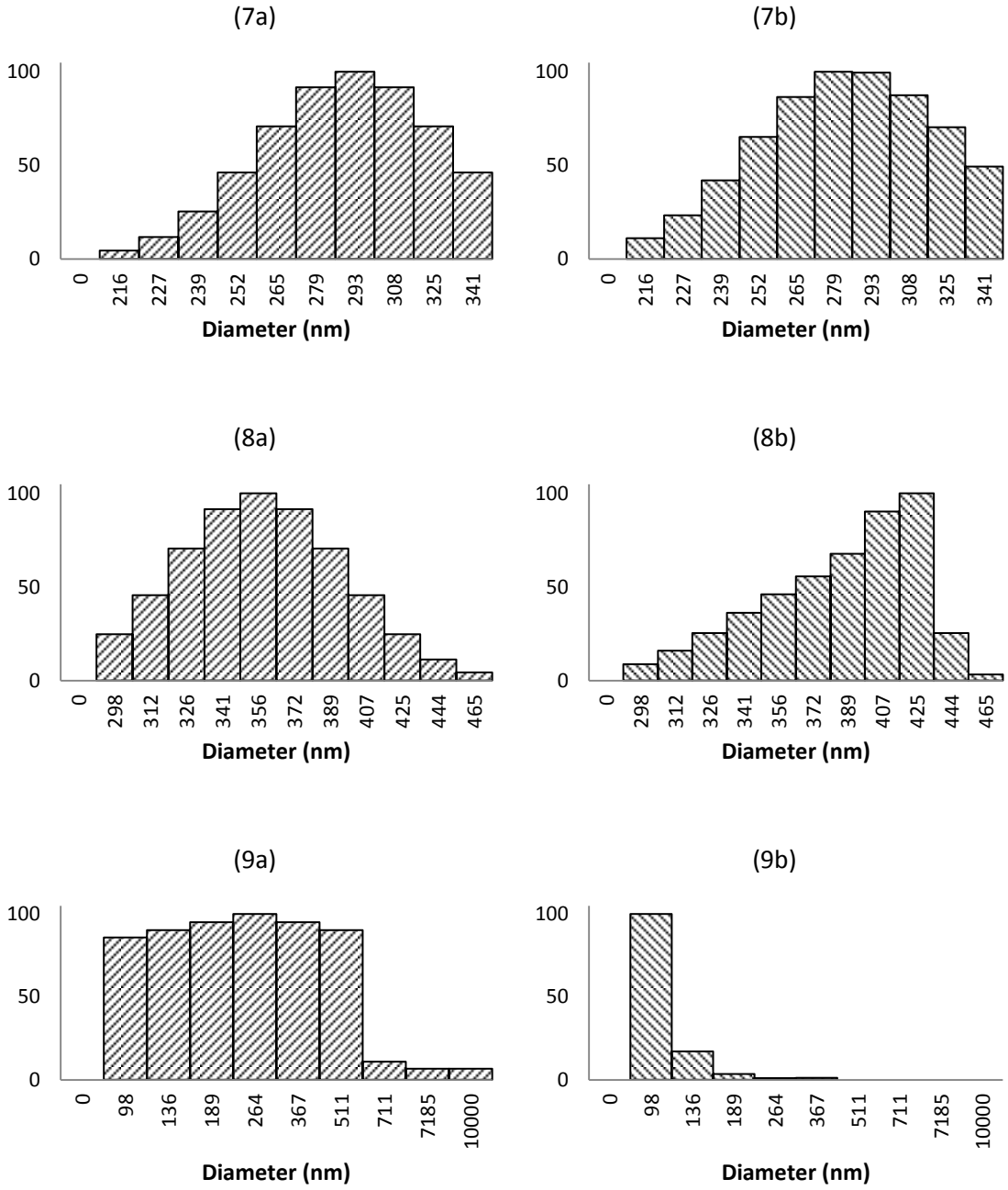

Figure B.16. DLS analysis of bovine insulin (SIGMA, Cat. #: I5500 (lot 019K17765V) aggregation in the presence of PS-OH surface: histograms represent relative scattering by intensity (a) and by number (b). Results shown are for: (7a) & (7b) after 30 minutes; (8a), (8b), (9a) & (9b) after 60 minutes of incubation. Sample (7) is the duplicate of sample (6) and sample (9) is the duplicate of sample (8).

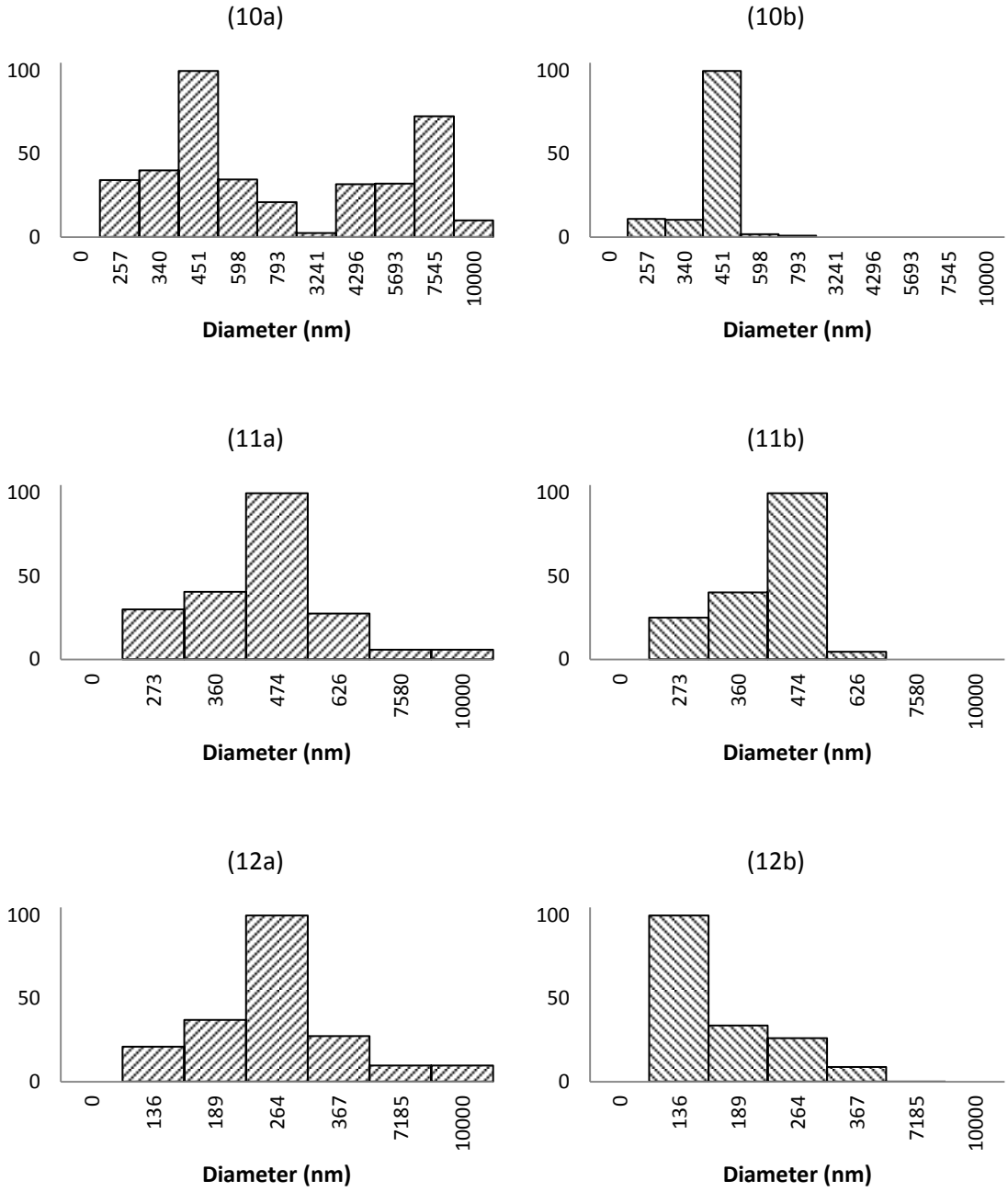

Figure B.17. DLS analysis of bovine insulin (SIGMA, Cat. #: I5500 (lot 019K17765V) aggregation in the presence of PS-OH surface: histograms represent relative scattering by intensity (a) and by number (b). Results shown are for: (10a), (10b), (11a) & (11b) after 65 minutes; and (12a) & (12b) after 85 minutes of incubation. Sample (11) is the duplicate of sample (10).

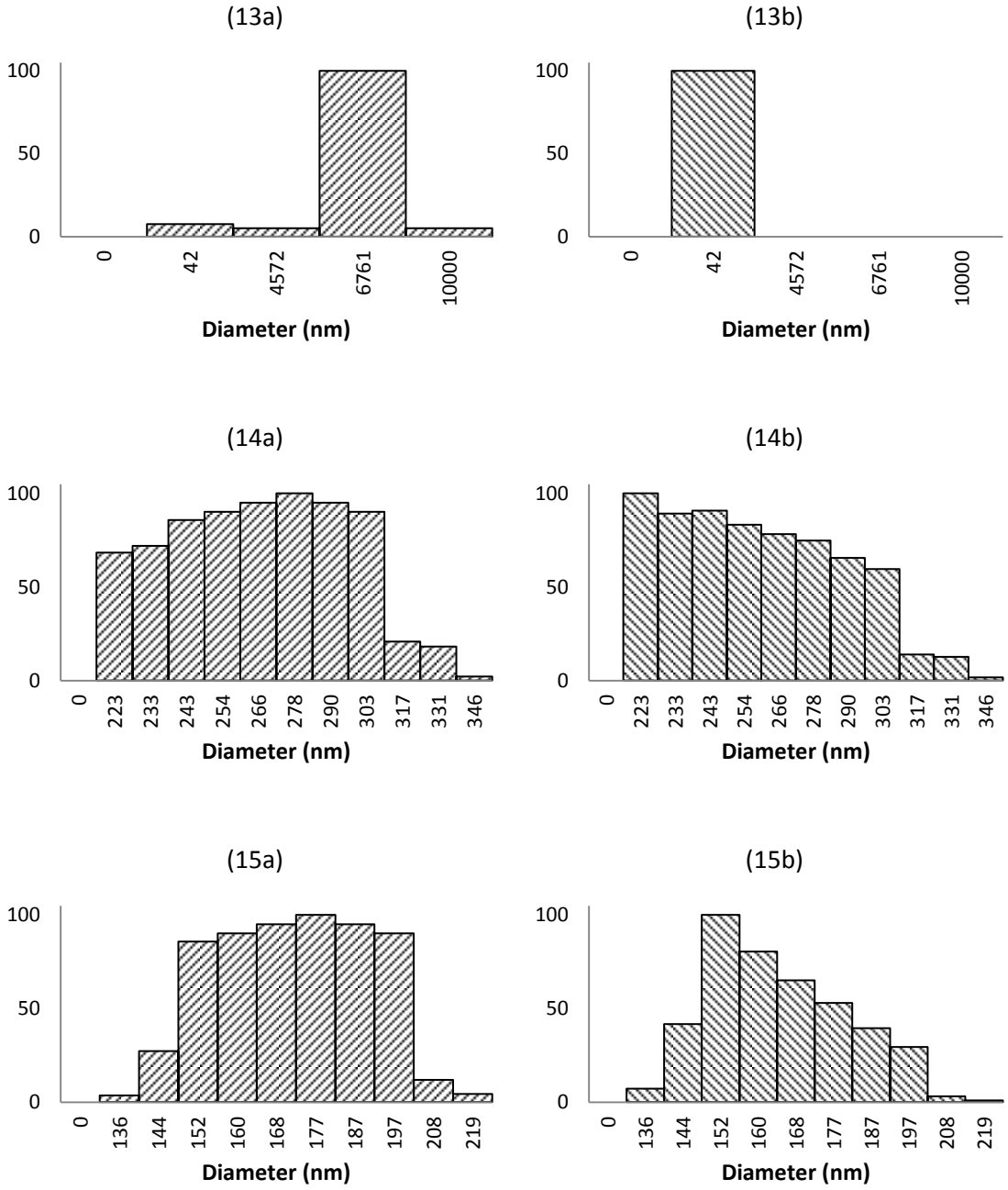

Figure B.18. DLS analysis of bovine insulin (SIGMA, Cat. #: I5500 (lot 019K17765V) aggregation in the presence of PS-OH surface: histograms represent relative scattering by intensity (a) and by number (b). Results shown are for: (13a) & (13b) after 90 minutes; (14a) & (14b) after 180 minutes; and (15a) & (15b) after 210 minutes of incubation.

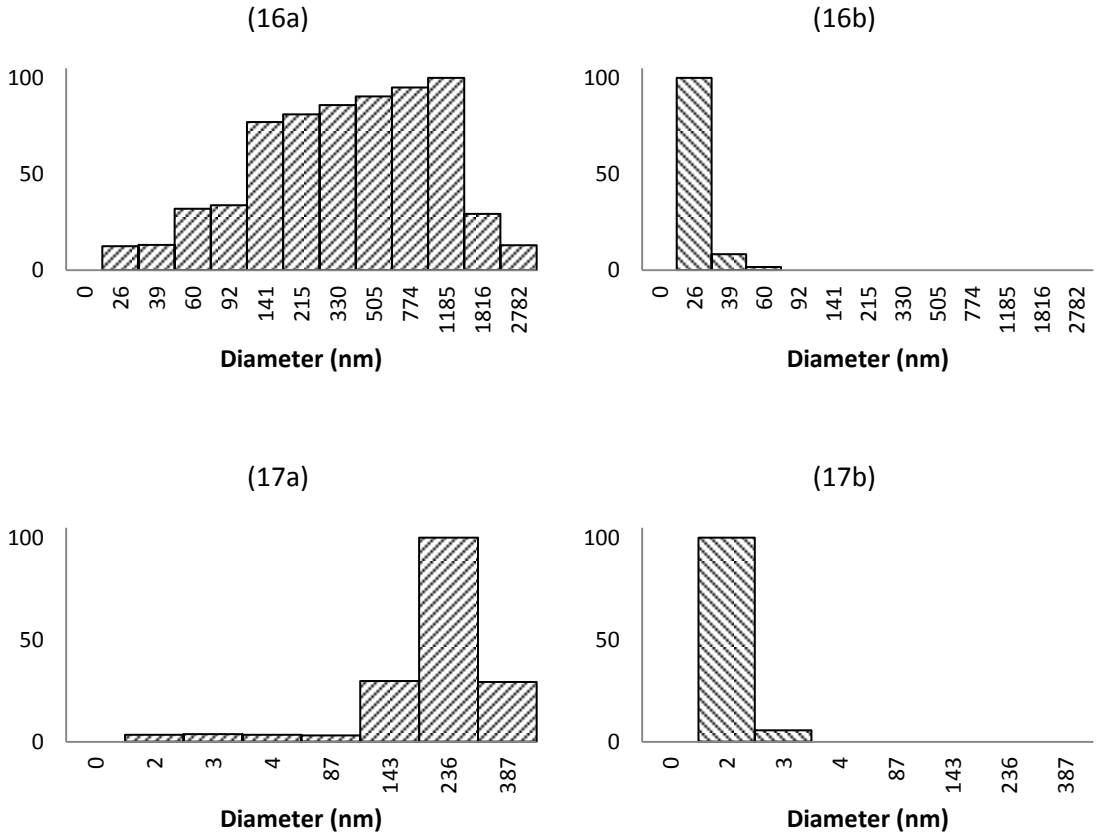

Figure B.19. DLS analysis of bovine insulin (SIGMA, Cat. #: I5500 (lot 019K17765V) aggregation in the presence of PS-OH surface: histograms represent relative scattering by intensity (a) and by number (b). Results shown are for: (16a) & (16b) after 330 minutes; and (17a) & (17b) after 210 minutes of incubation.

5. BOVINE INSULIN IN THE PRESENCE OF PS-COOH SURFACE

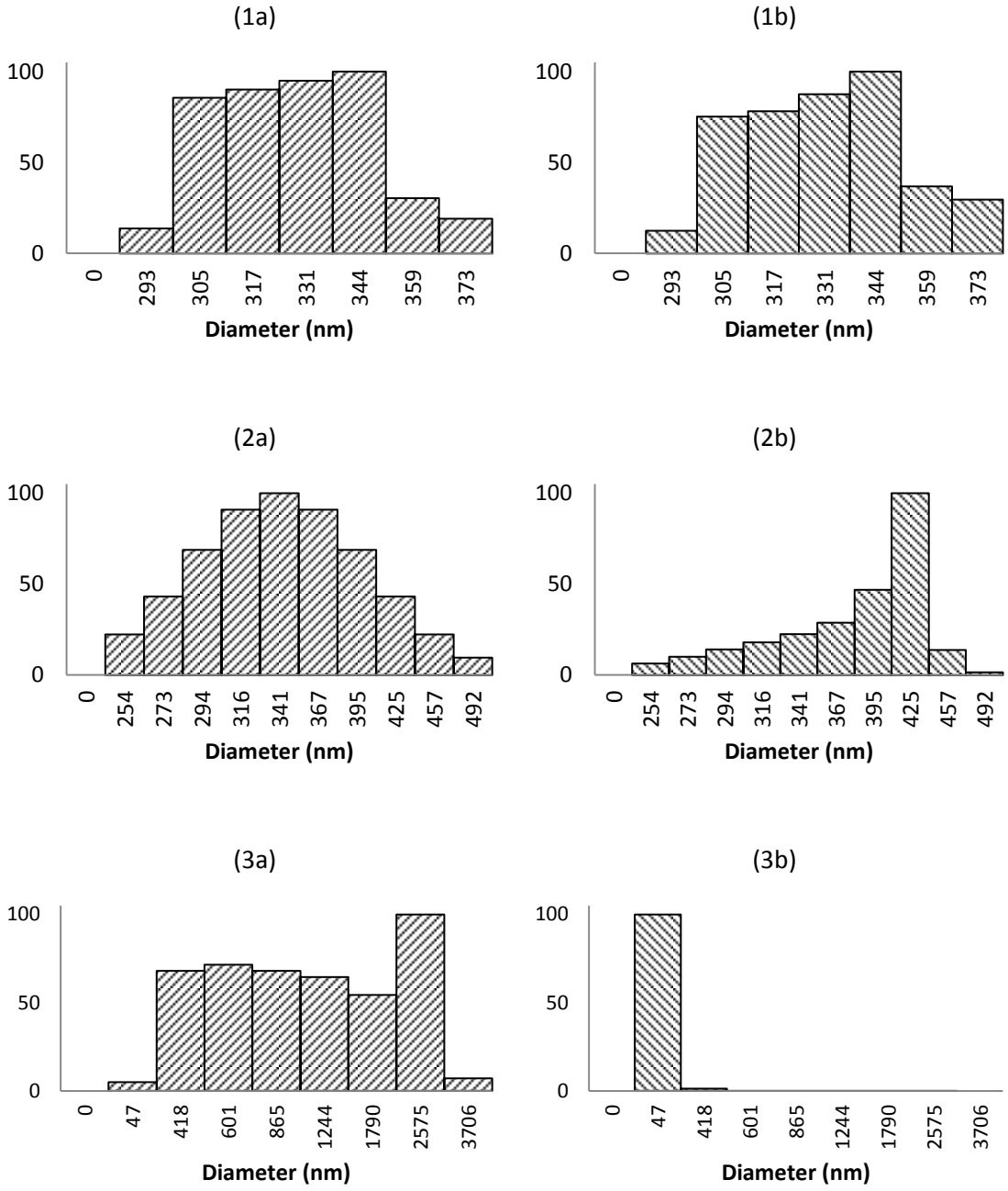

Figure B.20. DLS analysis of bovine insulin (SIGMA, Cat. #: I5500 (lot 019K17765V) aggregation in the presence of PS-COOH surface: histograms represent relative scattering by intensity (a) and by number (b). Results shown are for: (1a), (1b), (2a), (2b), (3a) & (3b) before incubation. Sample (2) is the duplicate of sample (1).

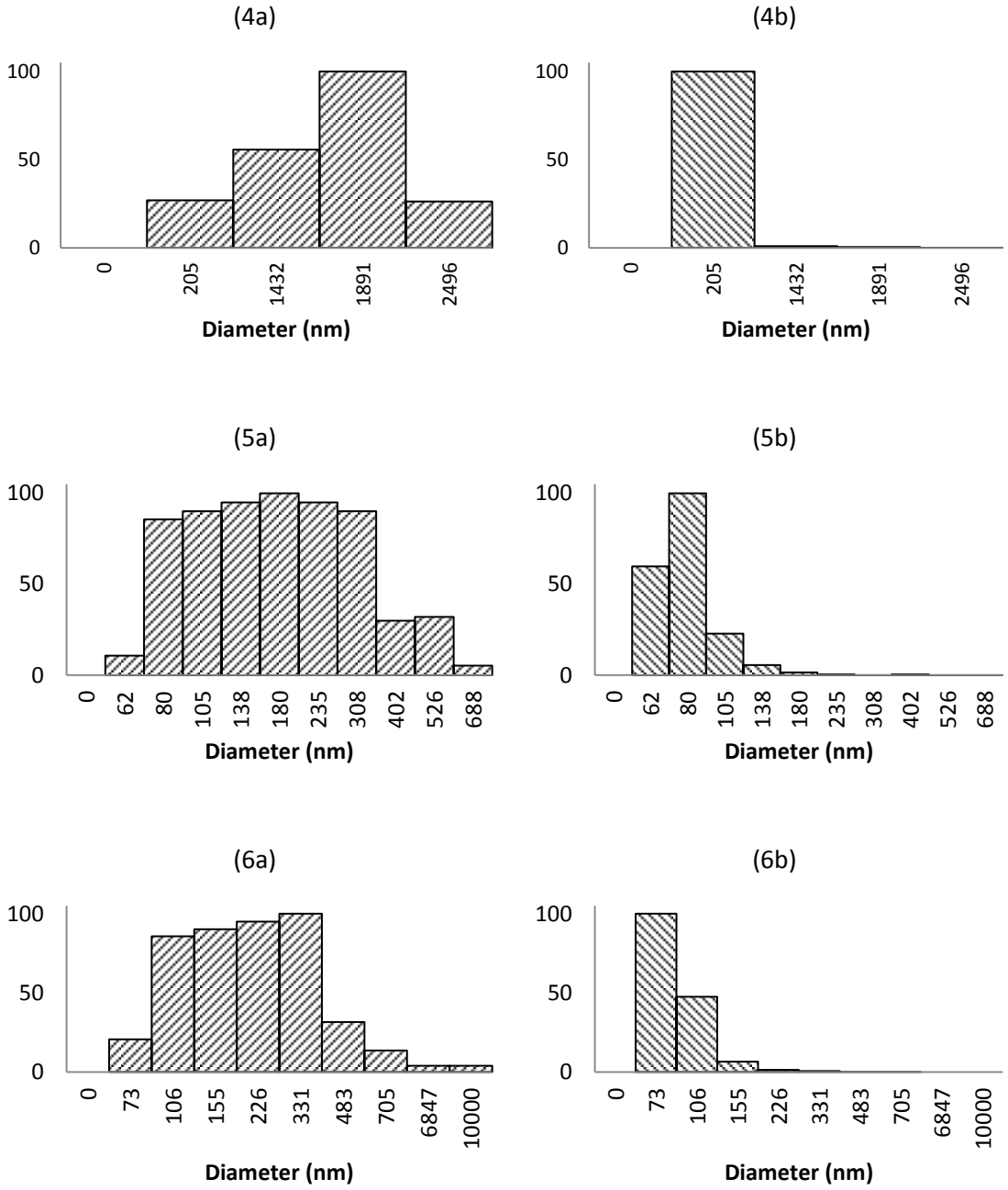

Figure B.21. DLS analysis of bovine insulin (SIGMA, Cat. #: I5500 (lot 019K17765V) aggregation in the presence of PS-COOH surface: histograms represent relative scattering by intensity (a) and by number (b). Results shown are for: (4a) & (4b) before incubation; (5a), (5b), (6a) & (6b) after 30 minutes of incubation. Sample (4) is the duplicate of sample (3) and sample (6) is the duplicate of sample (5).

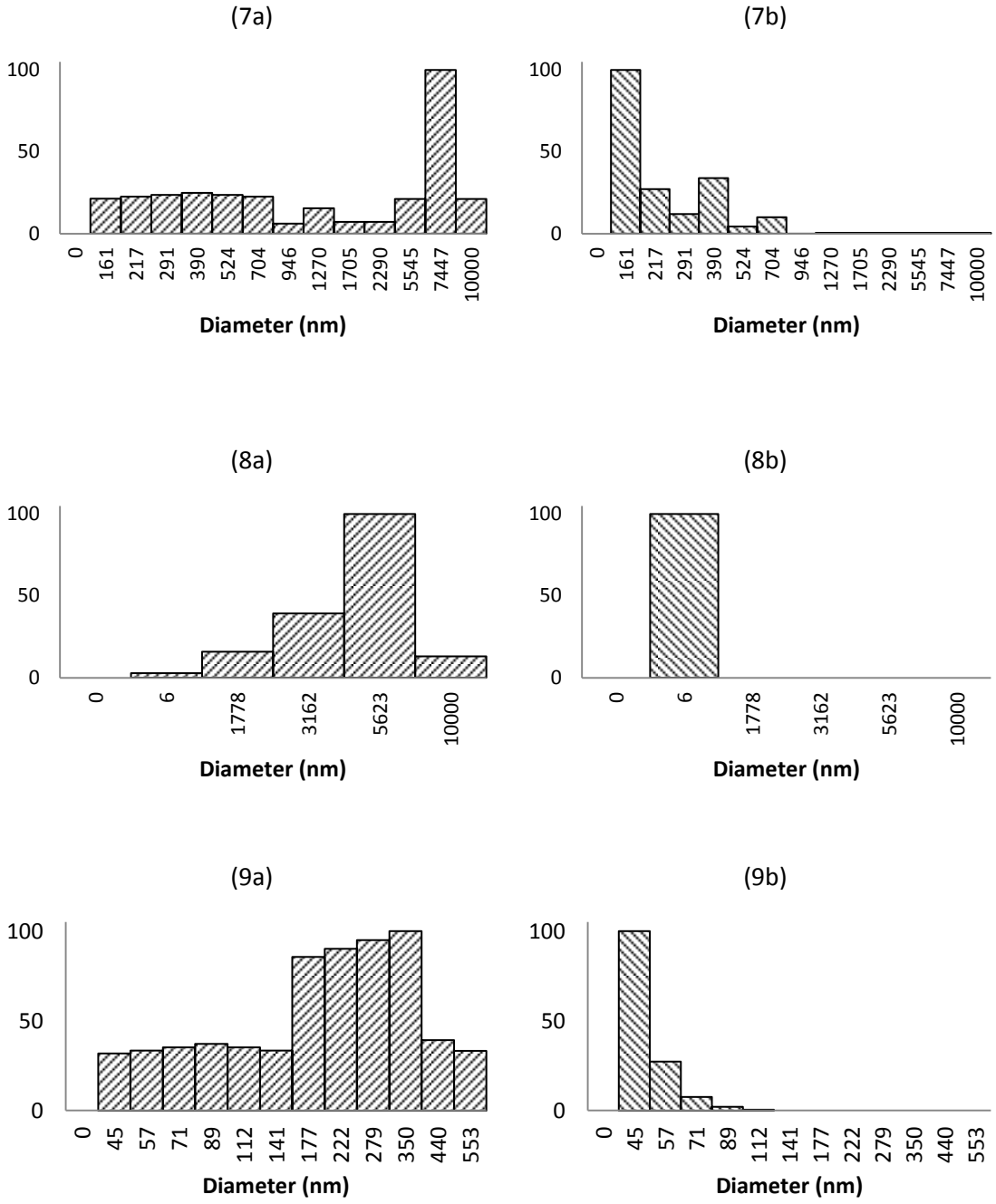

Figure B.22. DLS analysis of bovine insulin (SIGMA, Cat. #: I5500 (lot 019K17765V) aggregation in the presence of PS-COOH surface: histograms represent relative scattering by intensity (a) and by number (b). Results shown are for: (7a), (7b), (8a) & (8b) after 45 minutes; and (9a) & (9b) after 60 minutes of incubation. Sample (8) is the duplicate of sample (7).

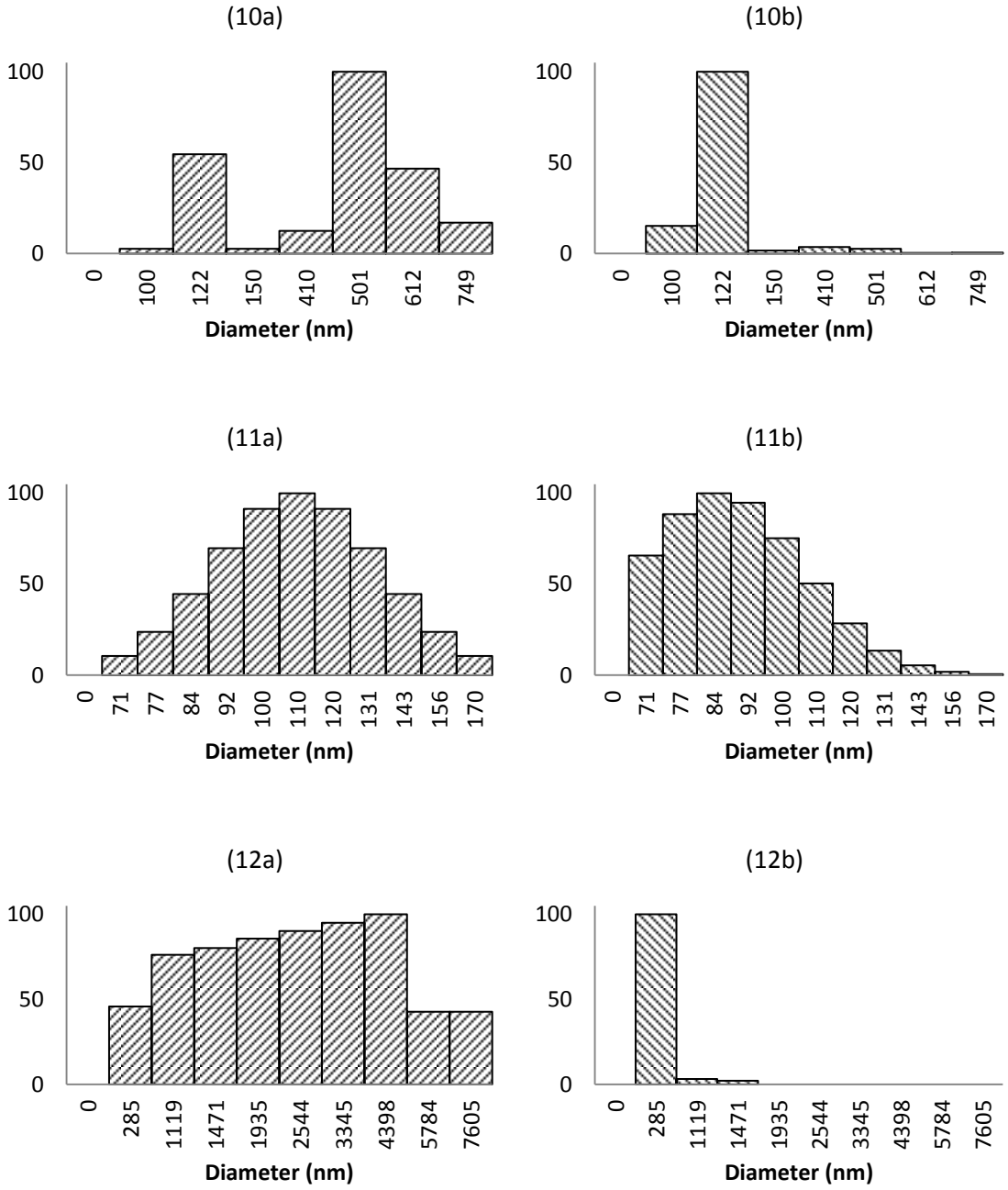

Figure B.23. DLS analysis of bovine insulin (SIGMA, Cat. #: I5500 (lot 019K17765V) aggregation in the presence of PS-COOH surface: histograms represent relative scattering by intensity (a) and by number (b). Results shown are for: (10a) & (10b) after 60 minutes; (11a) & (11b) after 90 minutes; and (12a) & (12b) after 150 minutes of incubation. Sample (10) is the duplicate of sample (9).

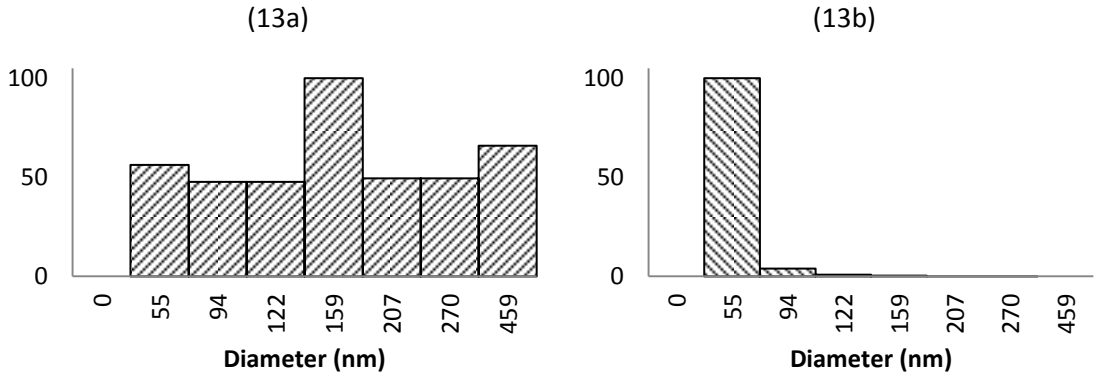

Figure B.24. DLS analysis of bovine insulin (SIGMA, Cat. #: I5500 (lot 019K17765V) aggregation in the presence of PS-COOH surface: histograms represent relative scattering by intensity (a) and by number (b). Results shown are for: (13a) & (13b) after 420 minutes of incubation.

6. BOVINE INSULIN IN THE PRESENCE OF PS-NH_2 SURFACE

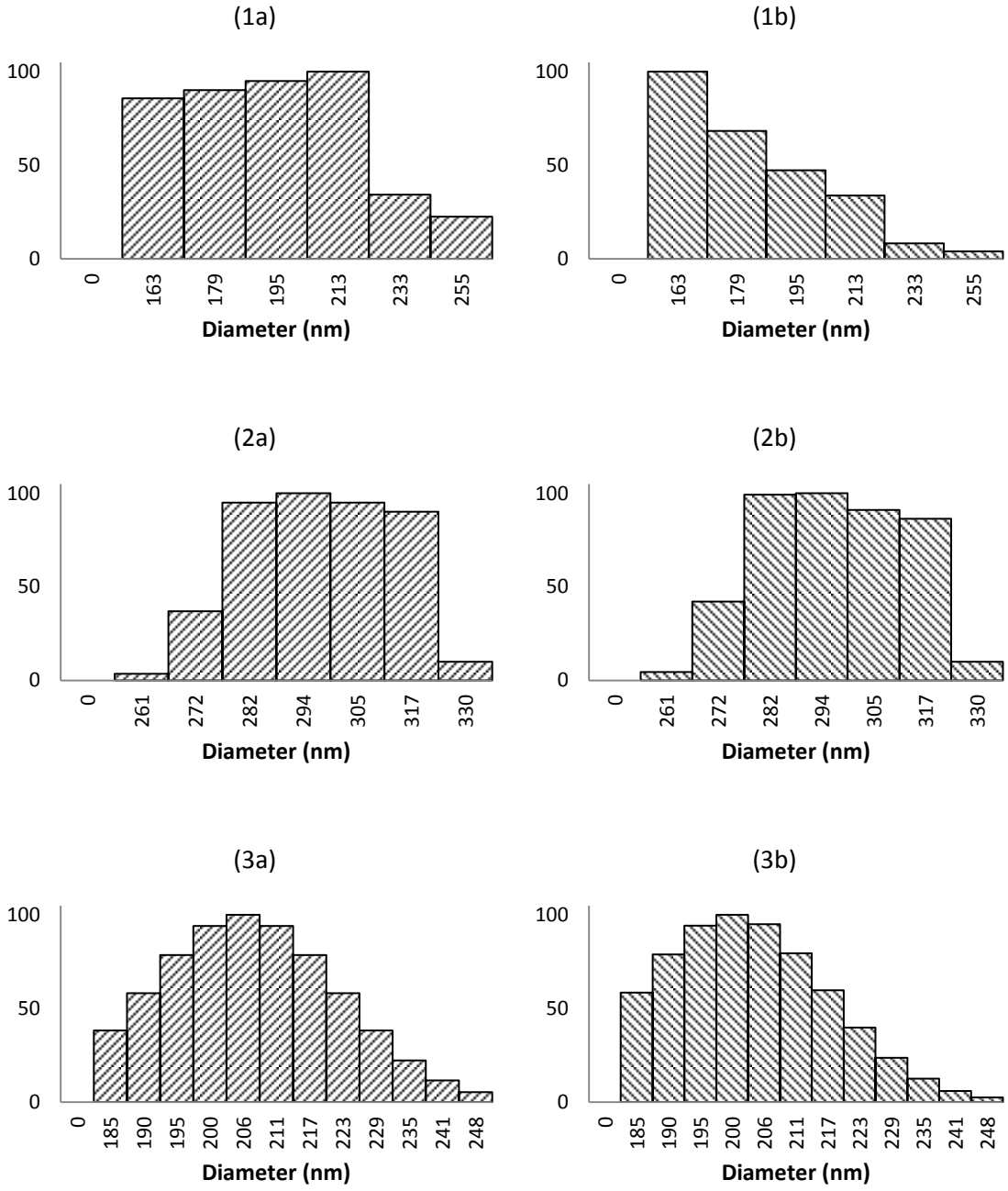

Figure B.25. DLS analysis of bovine insulin (SIGMA, Cat. #: I5500 (lot 019K17765V) aggregation in the presence of PS-NH2 surface: histograms represent relative scattering by intensity (a) and by number (b). Results shown are for: (1a), (1b), (2a), (2b), (3a) & (3b) before incubation. Sample (2) is the duplicate of sample (1).

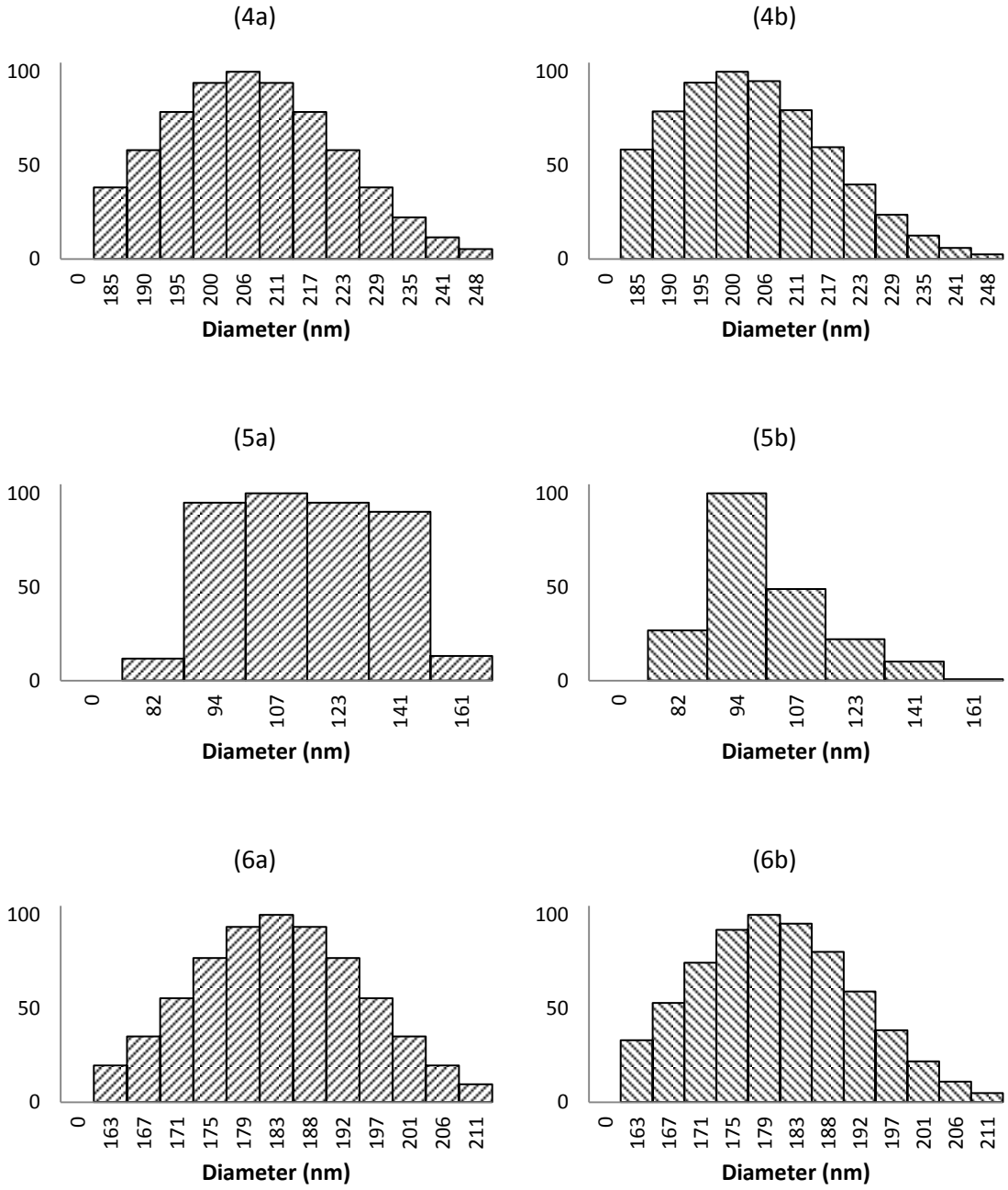

Figure B.26. DLS analysis of bovine insulin (SIGMA, Cat. #: I5500 (lot 019K17765V) aggregation in the presence of PS-NH2 surface: histograms represent relative scattering by intensity (a) and by number (b). Results shown are for: (4a) & (4b) before incubation; (5a), (5b), (6a) & (6b) after 30 minutes of incubation. Sample (4) is the duplicate of sample (3) and sample (6) is the duplicate of sample (5).

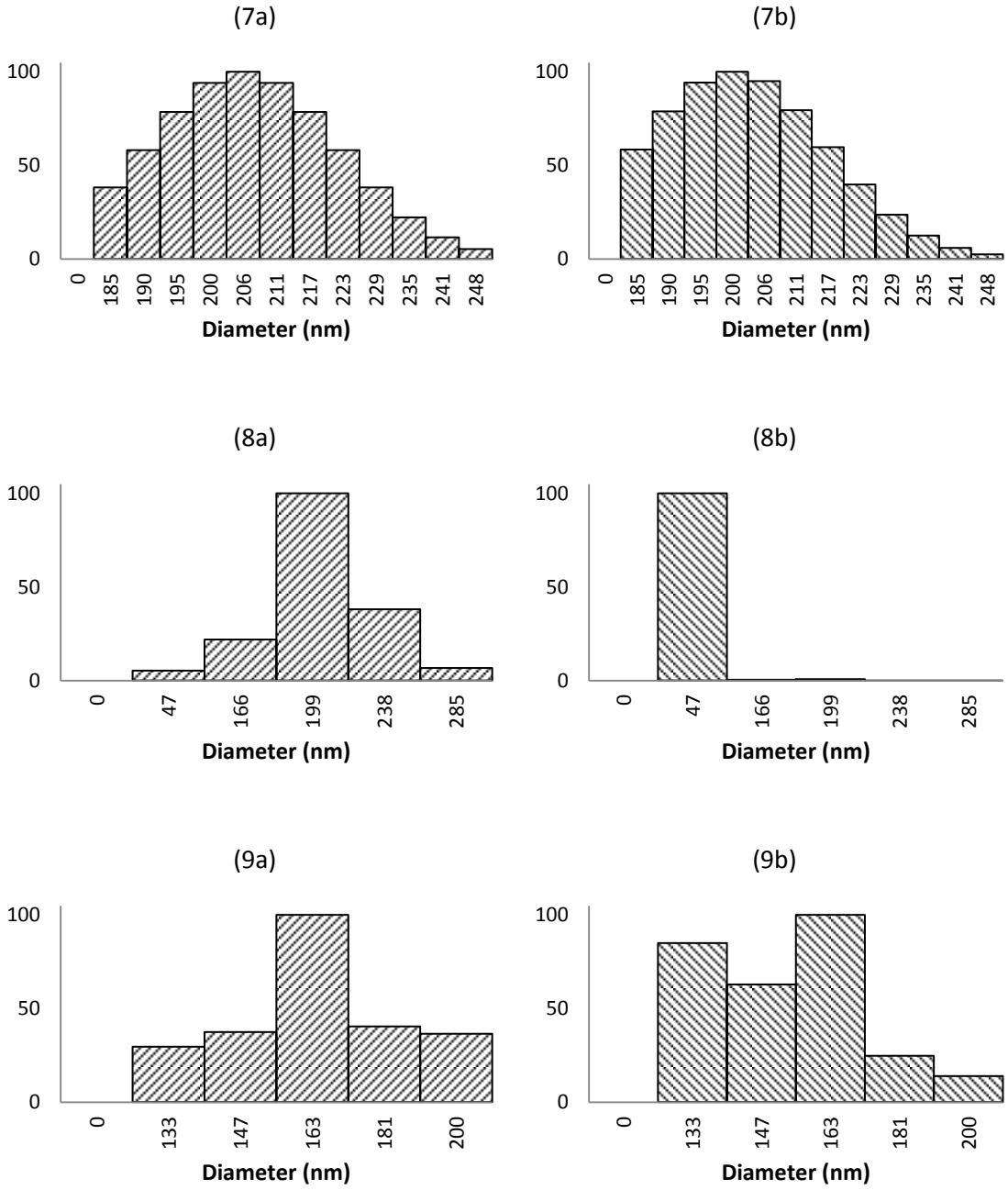

Figure B.27. DLS analysis of bovine insulin (SIGMA, Cat. #: I5500 (lot 019K17765V) aggregation in the presence of PS-NH2 surface: histograms represent relative scattering by intensity (a) and by number (b). Results shown are for: (7a) & (7b) after 45 minutes; (8a), (8b), (9a) & (9b) after 60 minutes of incubation. Sample (9) is the duplicate of sample (8).

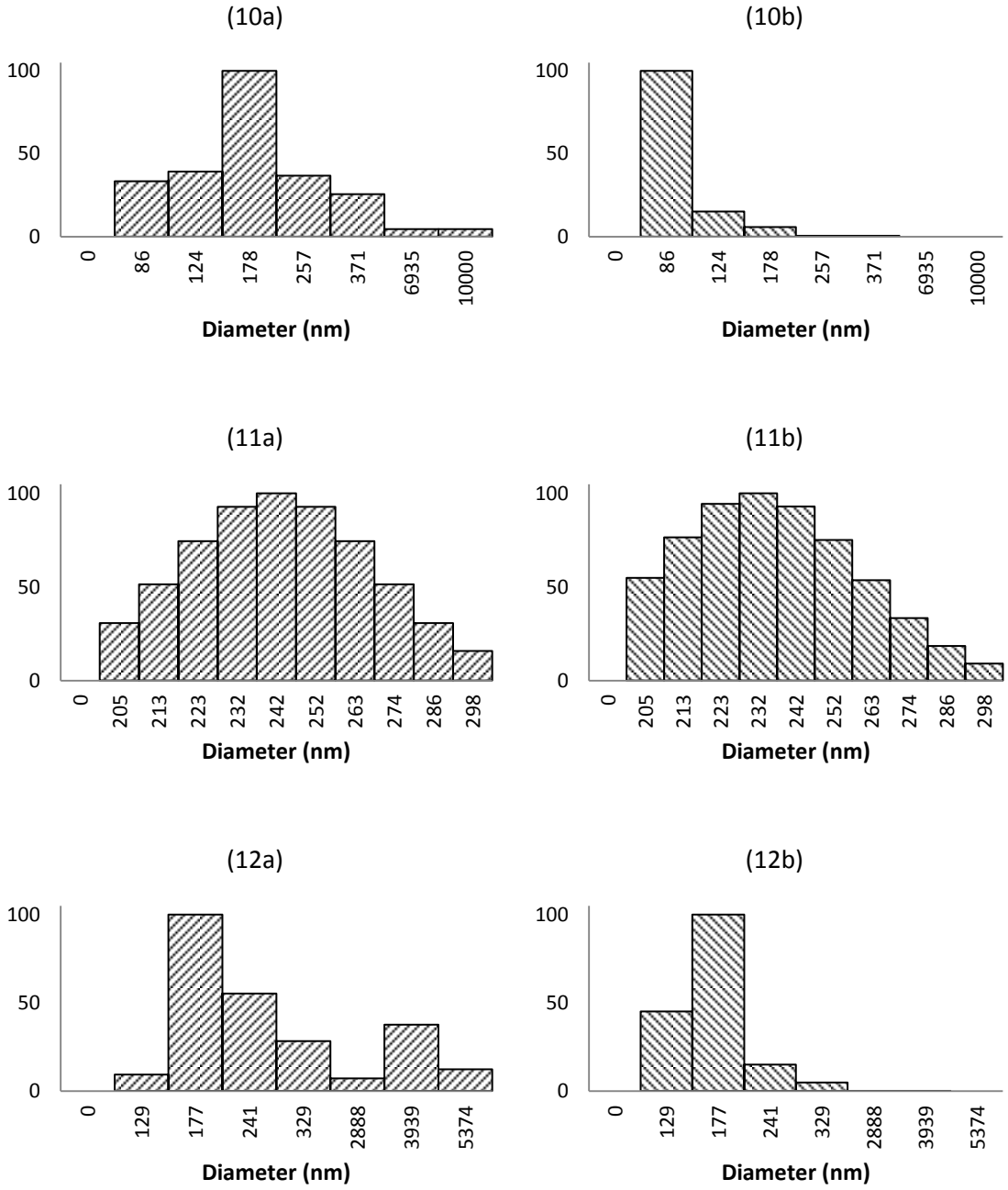

Figure B.28. DLS analysis of bovine insulin (SIGMA, Cat. #: I5500 (lot 019K17765V) aggregation in the presence of PS-NH2 surface: histograms represent relative scattering by intensity (a) and by number (b). Results shown are for: (10a), (10b), (11a) & (11b) after 90 minutes; and (12a) & (12b) after 120 minutes of incubation. Sample (11) is the duplicate of sample (10).

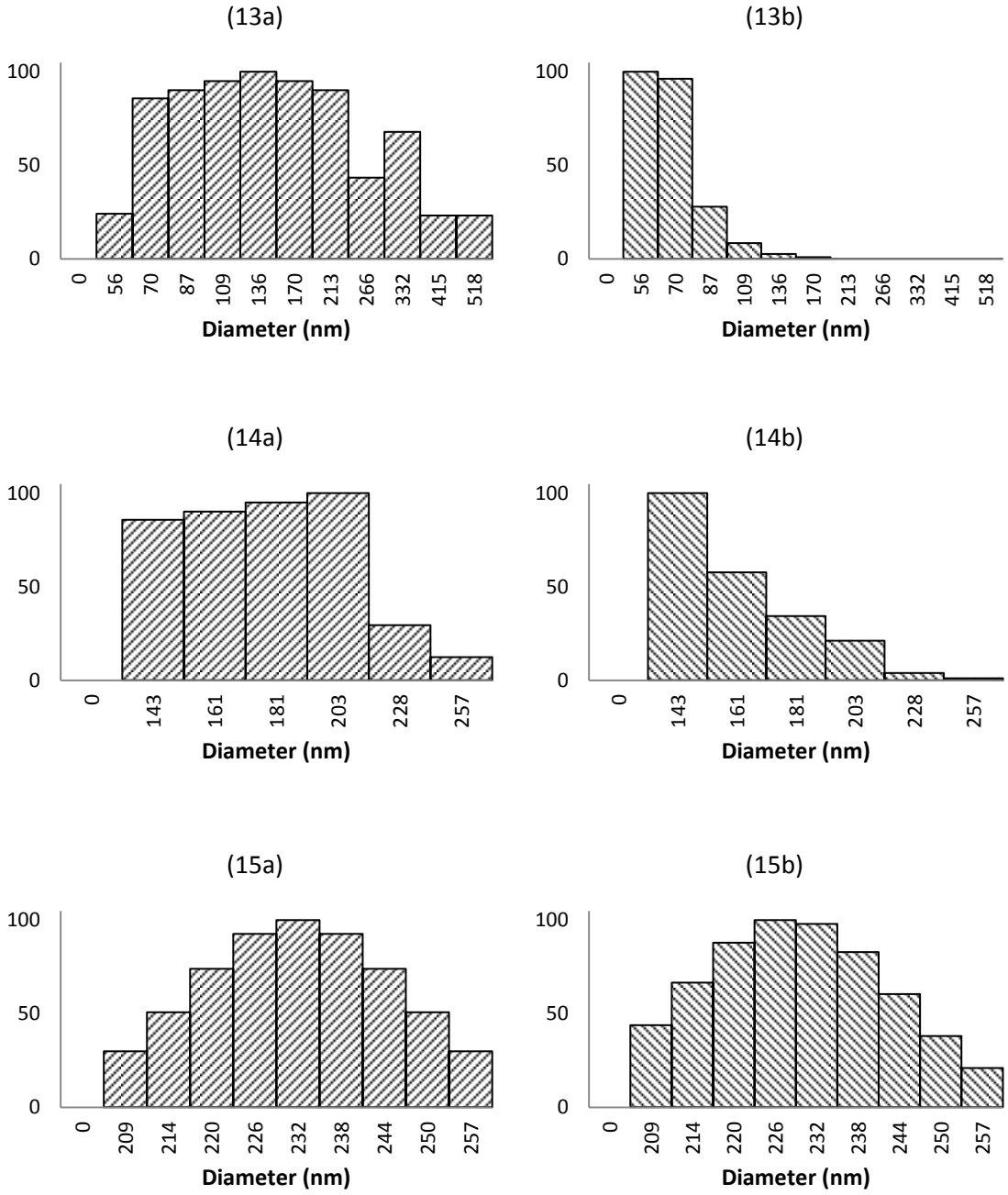

Figure B.29. DLS analysis of bovine insulin (SIGMA, Cat. #: I5500 (lot 019K17765V) aggregation in the presence of PS-NH2 surface: histograms represent relative scattering by intensity (a) and by number (b). Results shown are for: (13a) & (13b) after 120 minutes; (14a) & (14b) after 150 minutes; and (15a) & (15b) after 180 minutes of incubation. Sample (13) is the duplicate of sample (12).

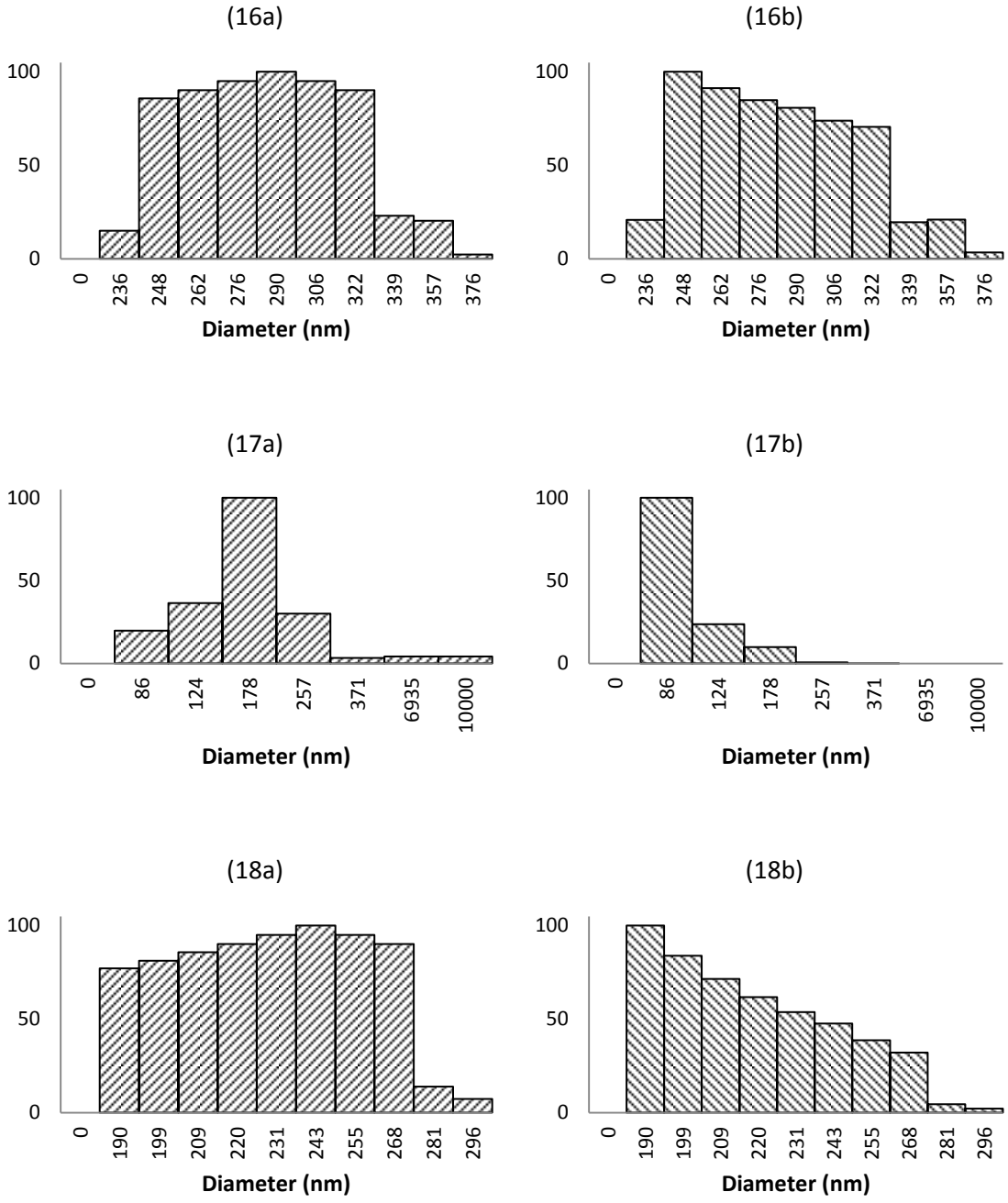

Figure B.30. DLS analysis of bovine insulin (SIGMA, Cat. #: I5500 (lot 019K17765V) aggregation in the presence of PS-NH2 surface: histograms represent relative scattering by intensity (a) and by number (b). Results shown are for: (16a) & (16b) after 180 minutes; (17a), (17b), (18a) & (18b) after 210 minutes of incubation. Sample (16) is the duplicate of sample (15) and sample (18) is the duplicate of sample (17).

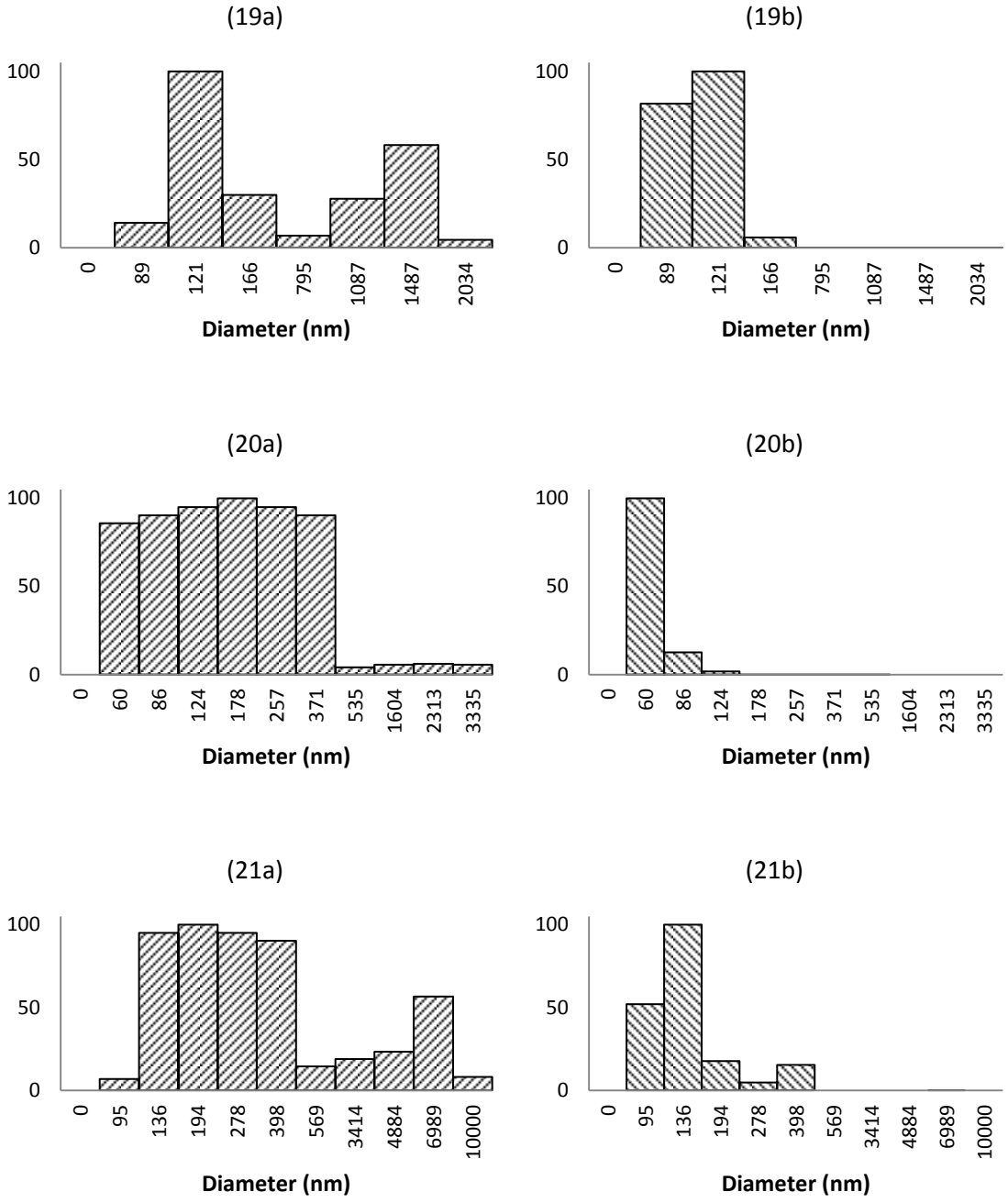

Figure B.31. DLS analysis of bovine insulin (SIGMA, Cat. #: I5500 (lot 019K17765V) aggregation in the presence of PS-NH2 surface: histograms represent relative scattering by intensity (a) and by number (b). Results shown are for: (19a) & (19b) after 240 minutes; (20a) & (20b) after 270 minutes; and (21a) & (21b) after 360 minutes of incubation.

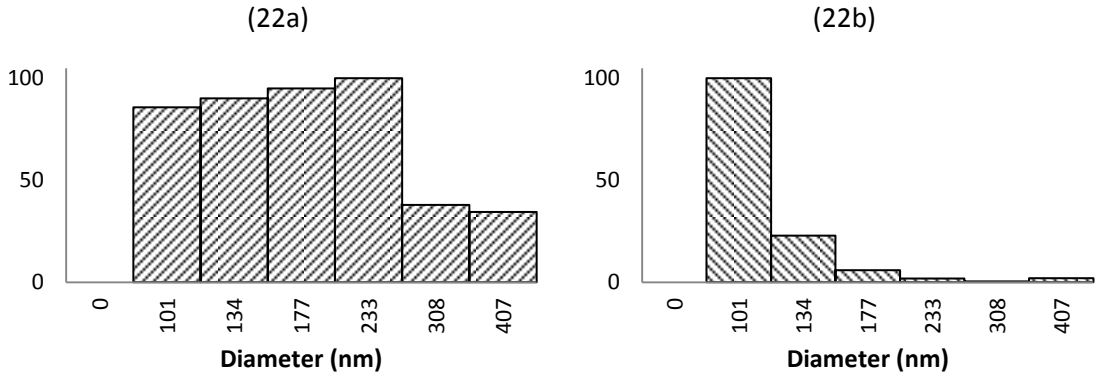

Figure B.32. DLS analysis of bovine insulin (SIGMA, Cat. #: I5500 (lot 019K17765V) aggregation in the presence of PS-NH2 surface: histograms represent relative scattering by intensity (a) and by number (b). Results shown are for: (22a) & (22b) after 420 minutes of incubation.

APPENDIX C

DYNAMIC LIGHT SCATTERING HISTOGRAMS

OF HUMAN ISULIN IN BULK AND IN THE PRESENCE OF POLYSTYRENE

LATEX INCUBATED AT 60 ˚C

1. HUMAN INSULIN IN BULK

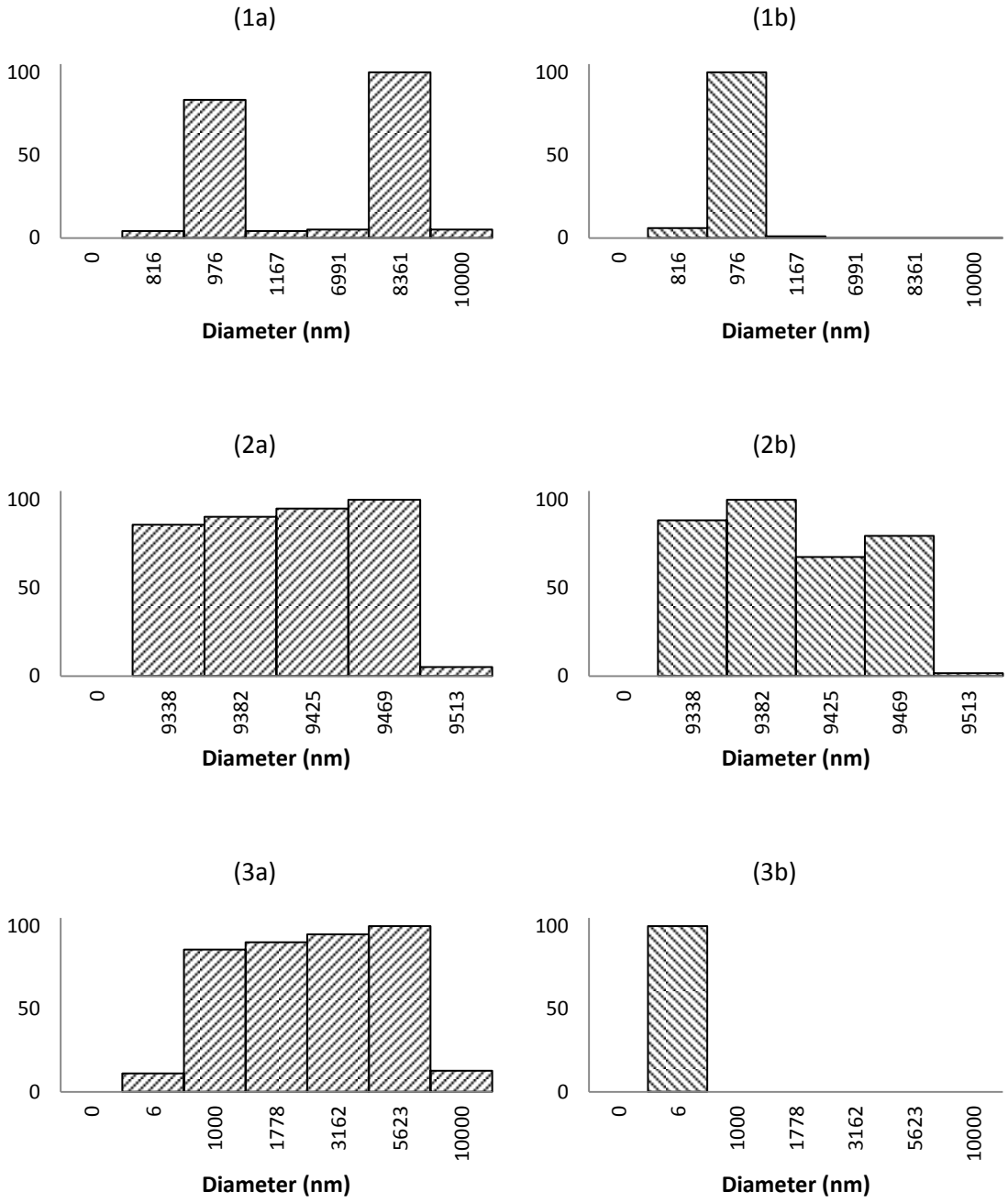

Figure C.1. DLS analysis of human insulin (SACF Biosciences, Cat. #: 91077 (lot 10L917) aggregation in bulk: histograms represent relative scattering by intensity (a) and by number (b). Results shown are for: (1a) & (1b) before incubation; (2a), (2b) 25 minutes; and (3a) & (3b) 65 minutes of incubation.

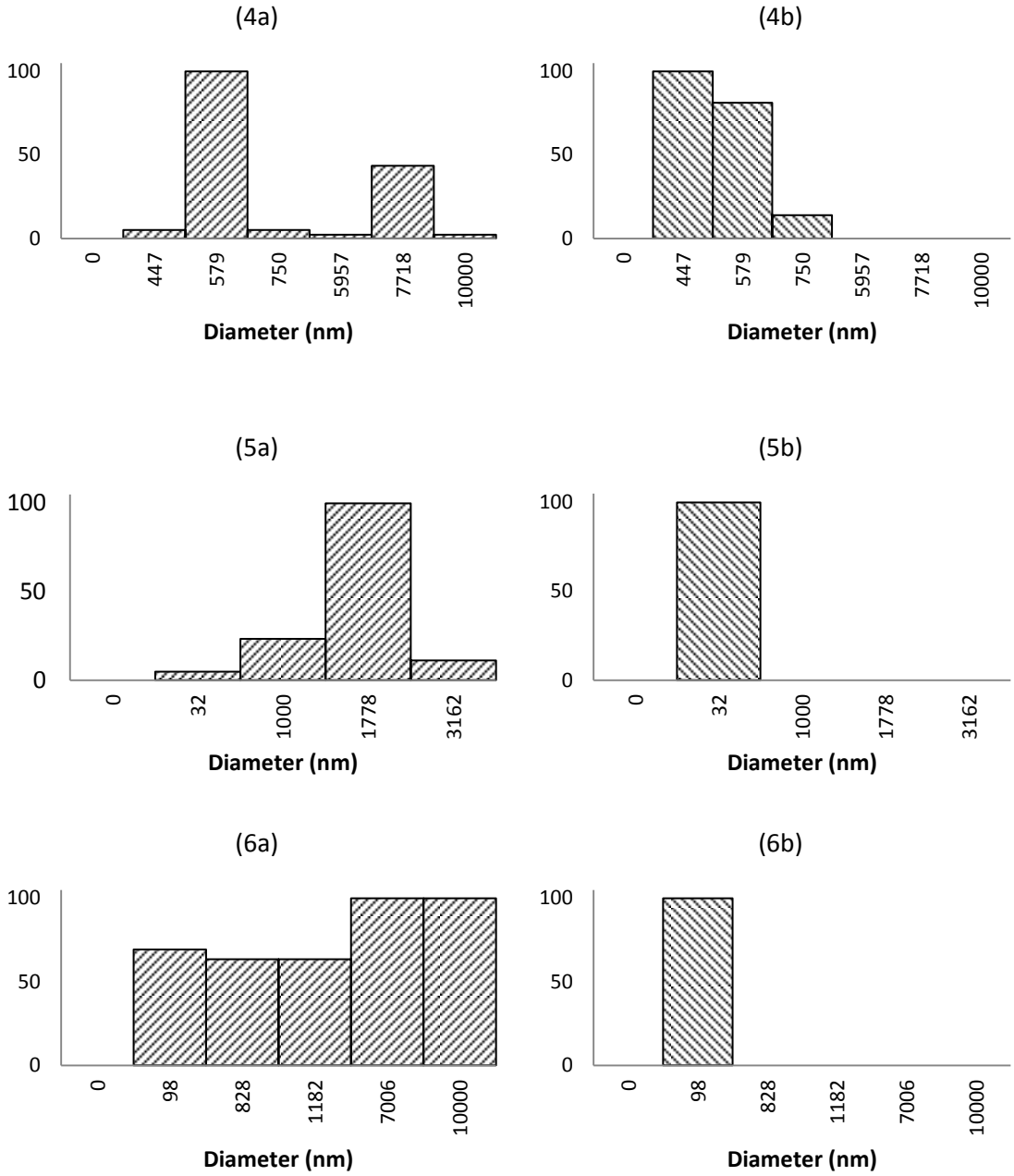

Figure C.2. DLS analysis of human insulin (SACF Biosciences, Cat. #: 91077 (lot 10L917)) aggregation in bulk: histograms represent relative scattering by intensity (a) and by number (b). Results shown are for: (4a) & (4b) 100 minutes; (5a), (5b) 110 minutes; and (6a) & (6b) 120 minutes of incubation.

2. HUMAN INSULIN IN THE PRESENCE OF PS SURFACE

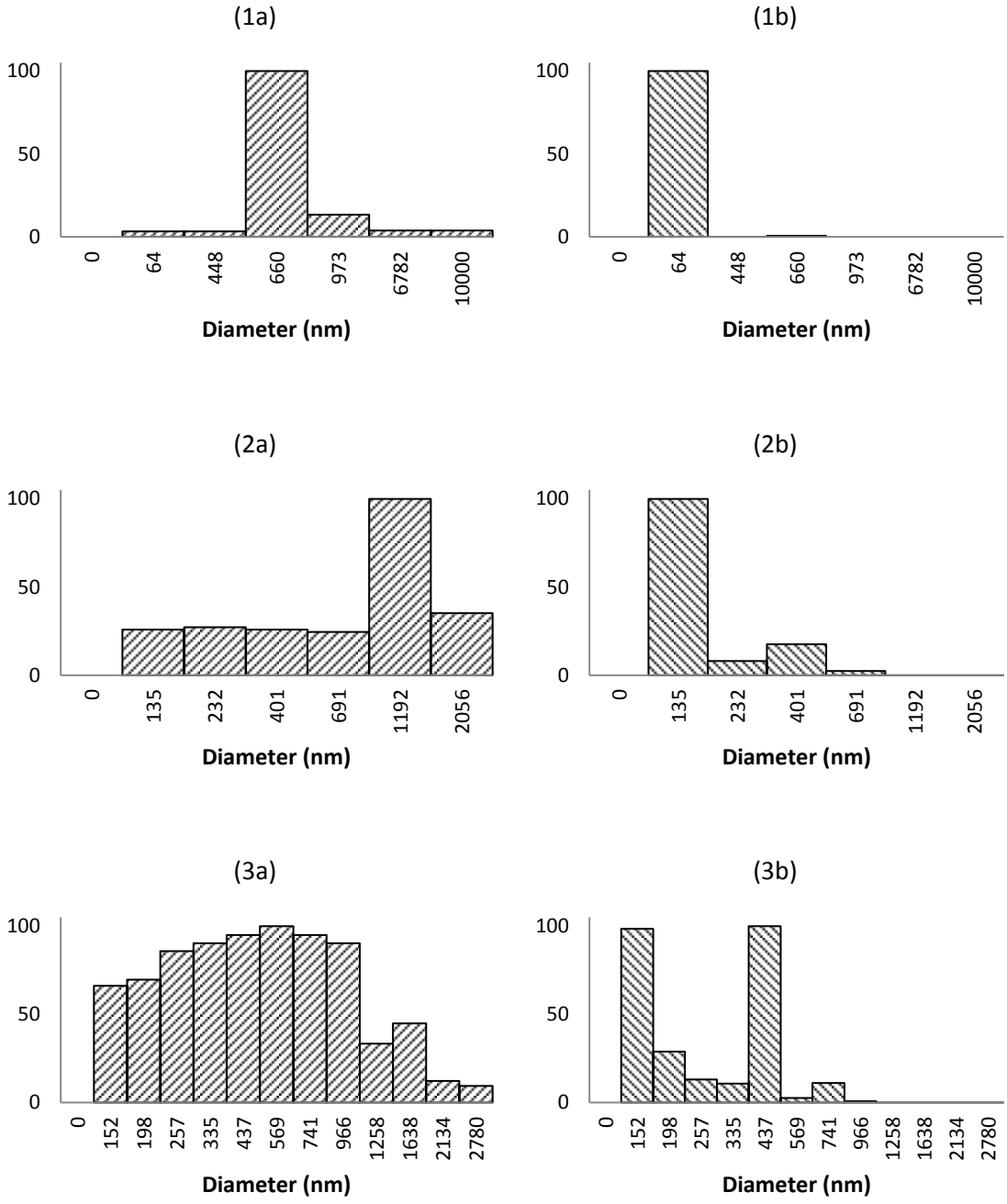

Figure C.3. DLS analysis of human insulin (SACF Biosciences, Cat. #: 91077, lot 10L917) aggregation in the presence of PS surface: histograms represent relative scattering by intensity (a) and by number (b). Results shown are for: (1a), (1b), (2a) & (2b) before incubation; and (3a) & (3b) 25 minutes of incubation. Sample (2) is the duplicate of sample (1).

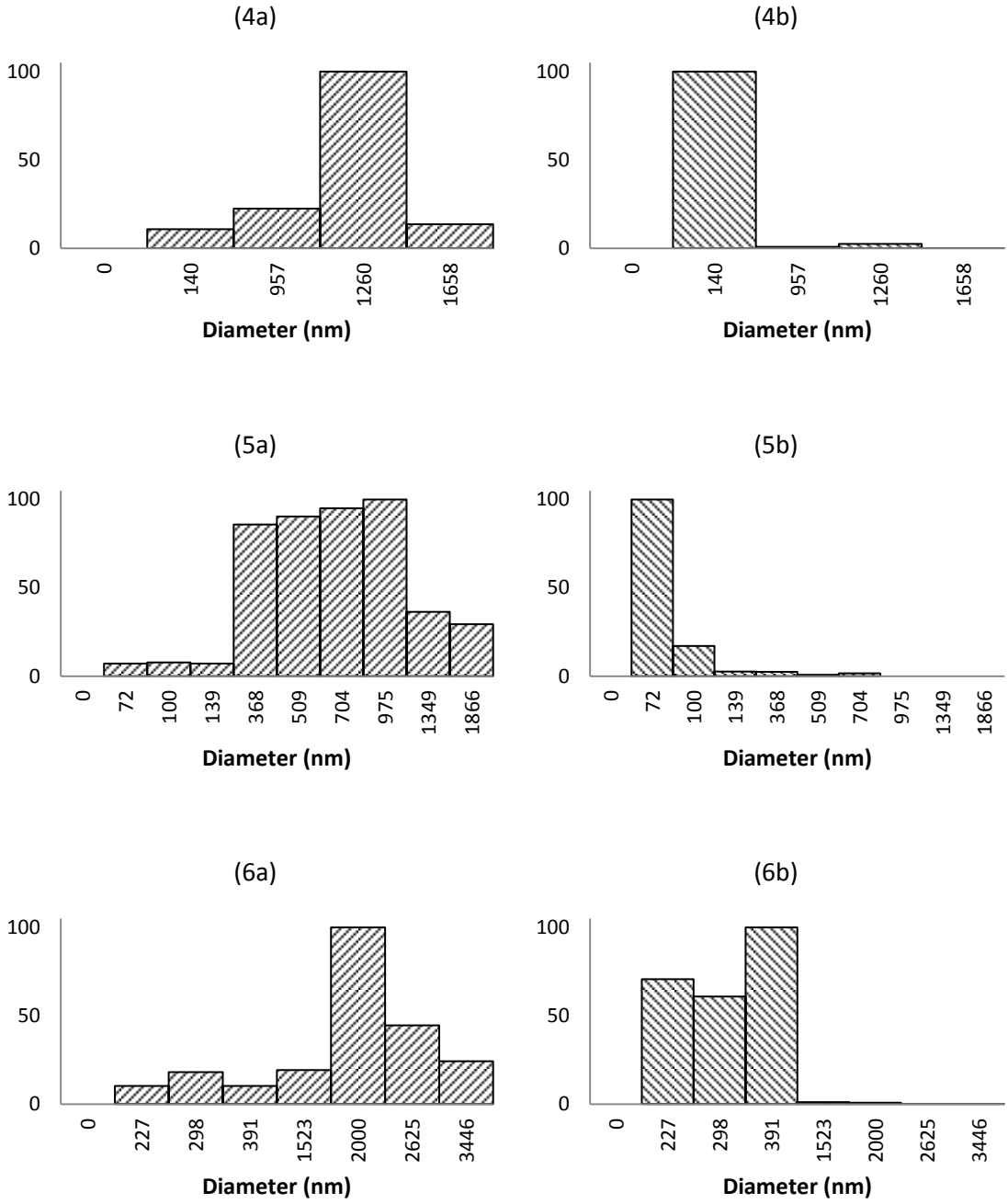

Figure C.4. DLS analysis of human insulin (SACF Biosciences, Cat. #: 91077, lot 10L917) aggregation in the presence of PS surface: histograms represent relative scattering by intensity (a) and by number (b). Results shown are for: (4a) & (4b) 25 minutes; and (5a), (5b), (6a) & (6b) 45 minutes of incubation. Sample (4) is the duplicate of sample (3) and sample (6) is the duplicate of sample (5).

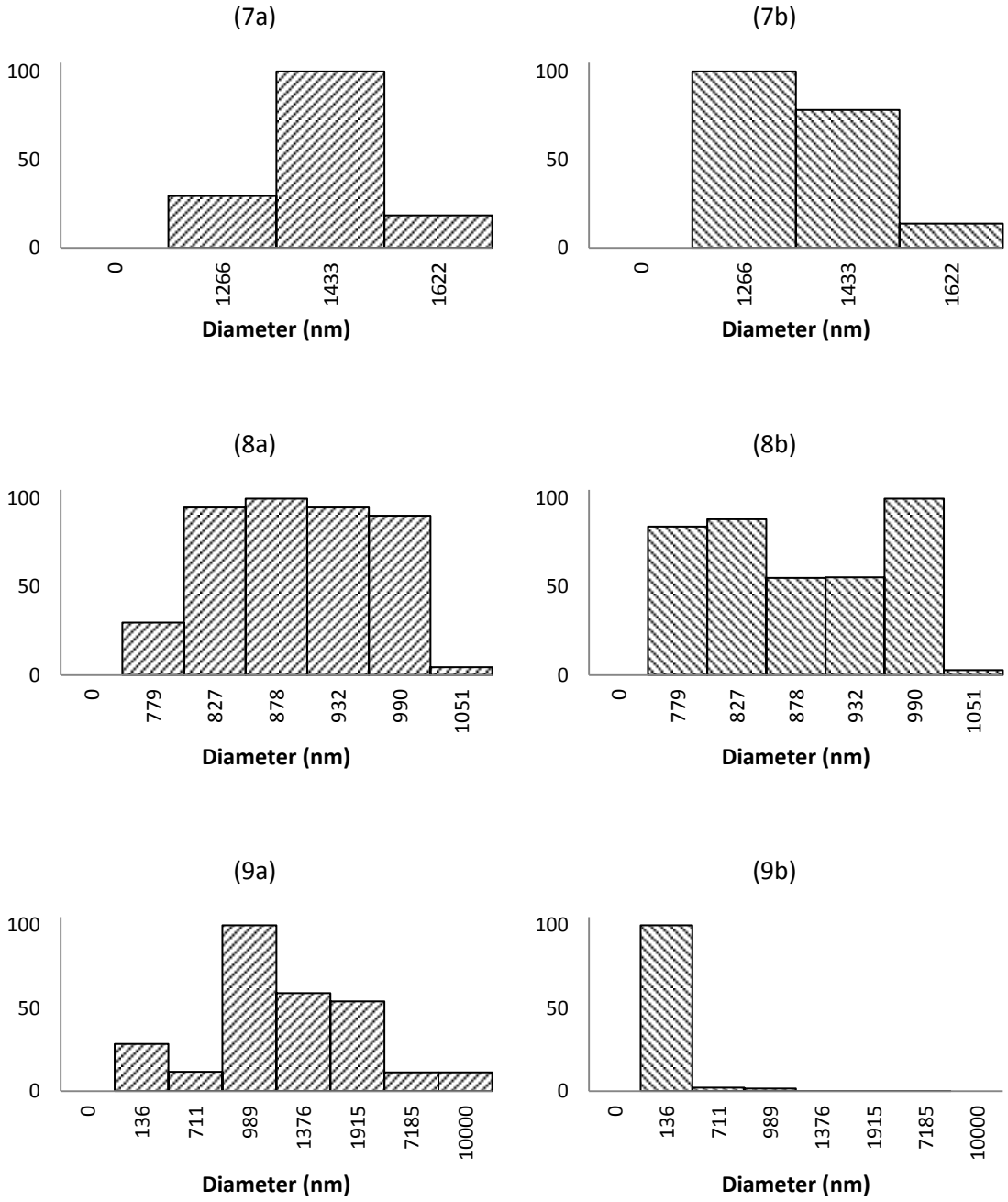

Figure C.5. DLS analysis of human insulin (SACF Biosciences, Cat. #: 91077, lot 10L917) aggregation in the presence of PS surface: histograms represent relative scattering by intensity (a) and by number (b). Results shown are for: (7a), (7b), (8a) & (8b) 65 minutes; and (9a) & (9b) 85 minutes of incubation. Sample (8) is the duplicate of sample (7).

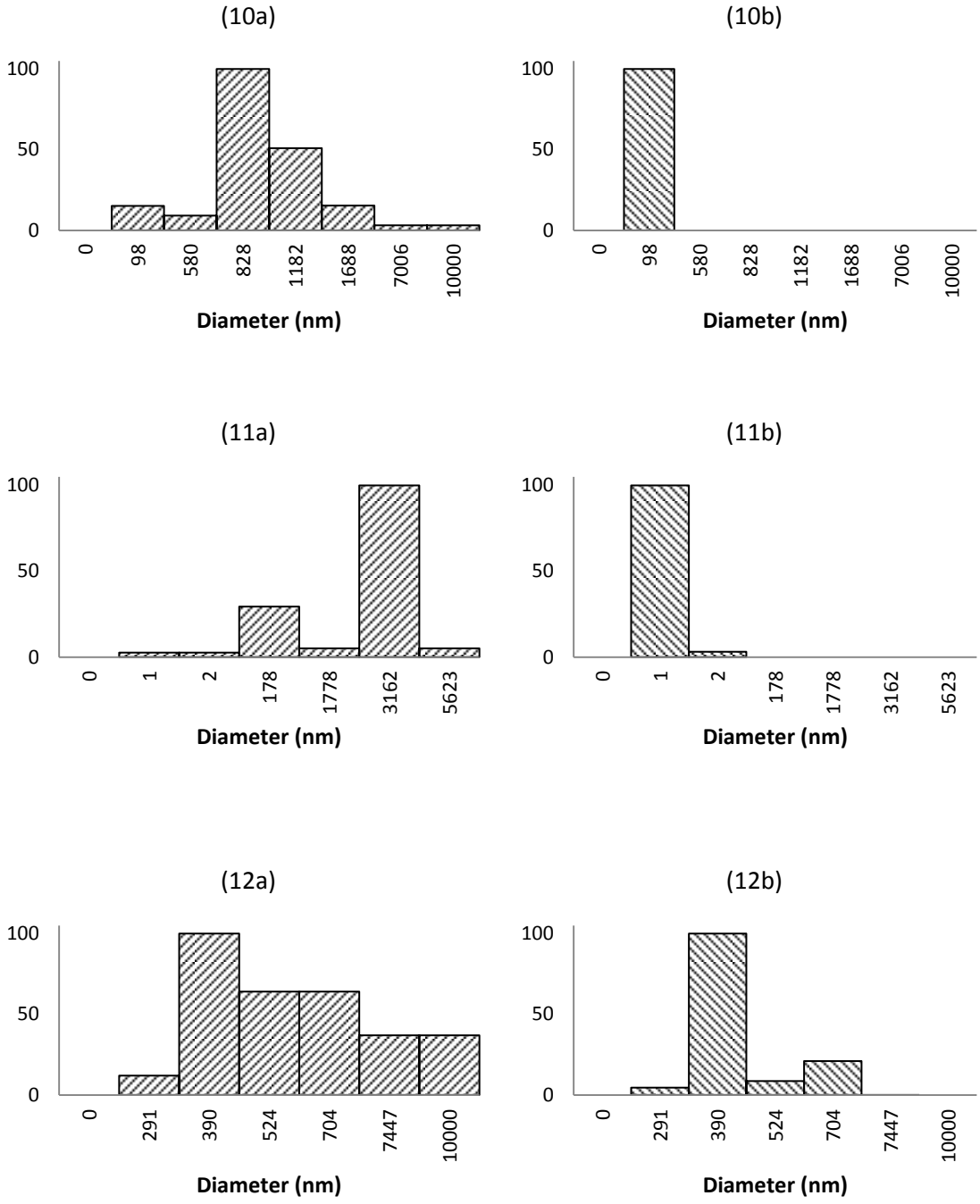

Figure C.6. DLS analysis of human insulin (SACF Biosciences, Cat. #: 91077, lot 10L917) aggregation in the presence of PS surface: histograms represent relative scattering by intensity (a) and by number (b). Results shown are for: (10a) & (10b) 85 minutes; and (11a), (11b), (12a) & (12b) 100 minutes of incubation. Sample (12) is the duplicate of sample (11).

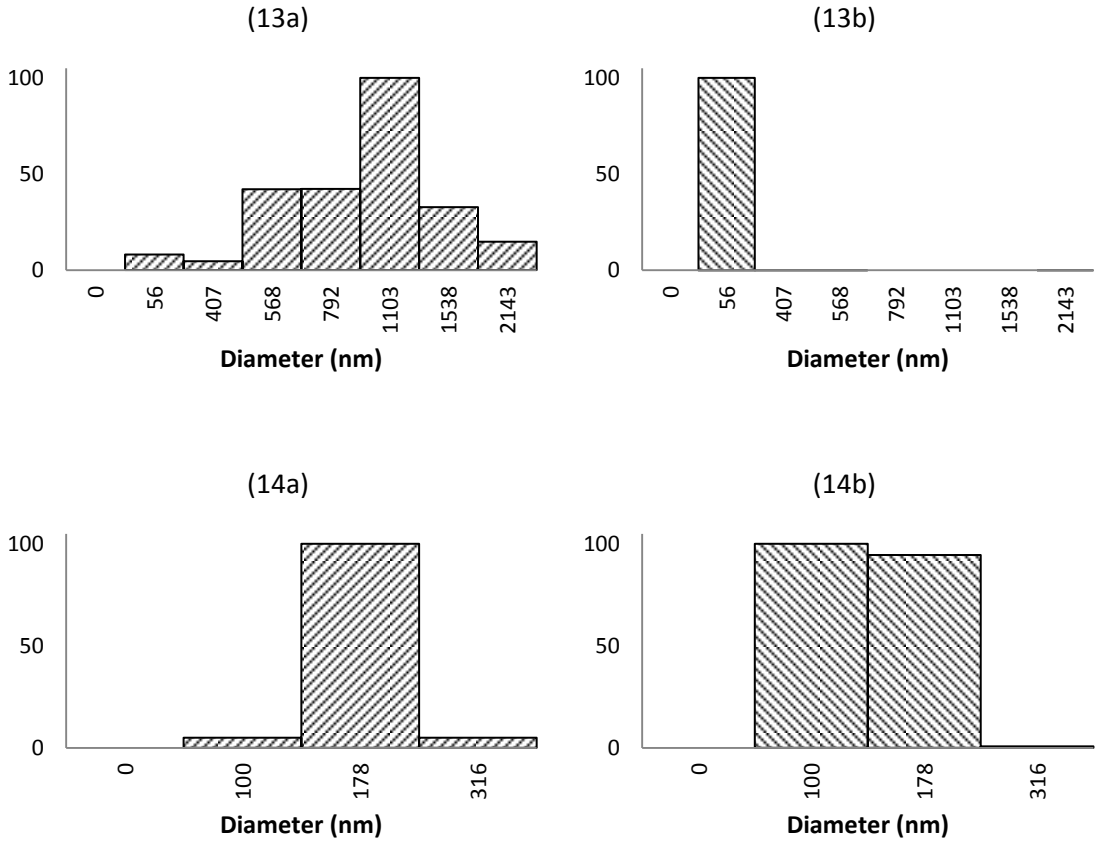

Figure C.7. DLS analysis of human insulin (SACF Biosciences, Cat. #: 91077, lot 10L917) aggregation in the presence of PS surface: histograms represent relative scattering by intensity (a) and by number (b). Results shown are for: (13a) & (13b) 110 minutes; and (14a) & (14b) 120 minutes of incubation.

3. HUMAN INSULIN IN THE PRESENCE OF PS-OH SURFACE

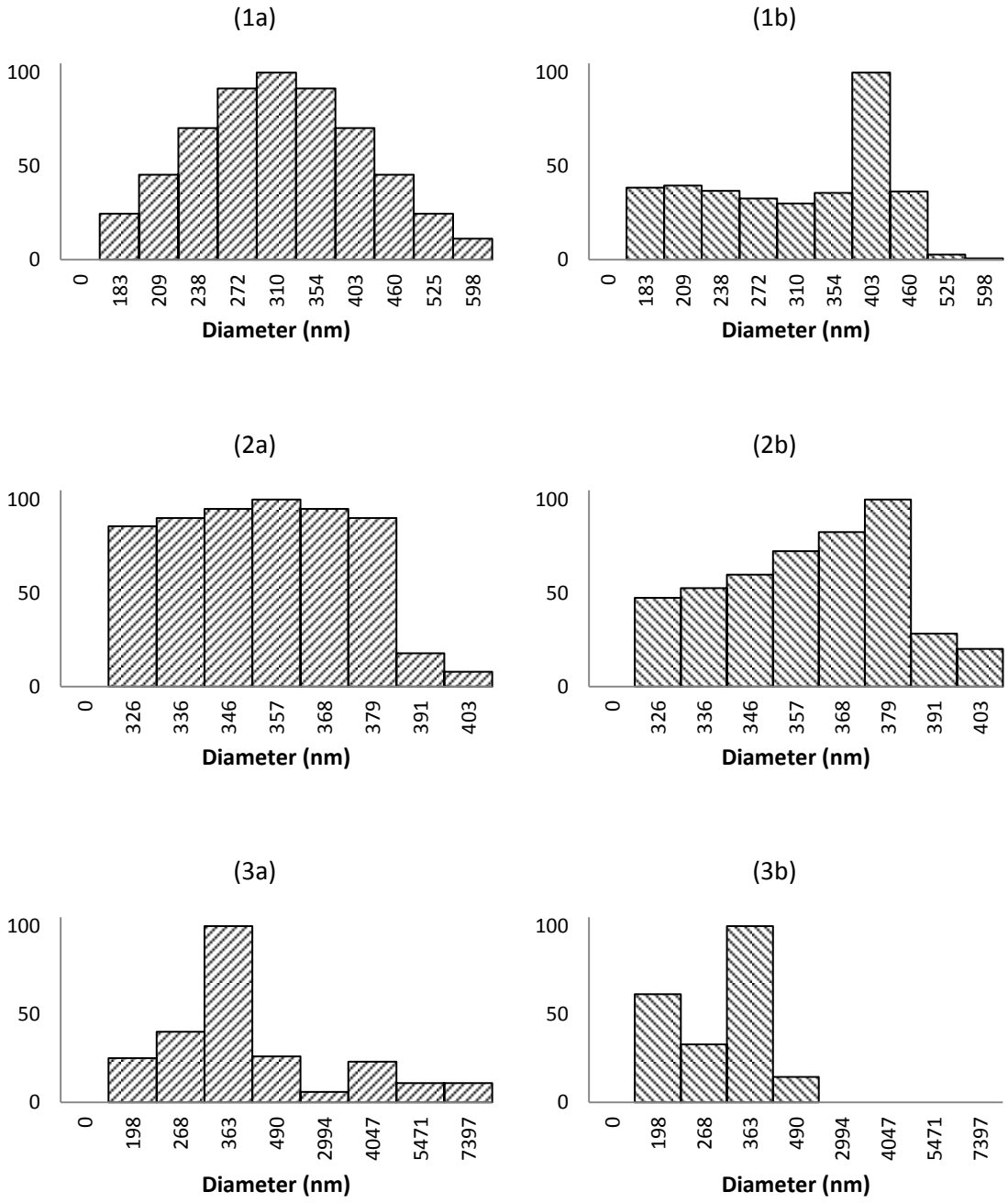

Figure C.8. DLS analysis of human insulin (SACF Biosciences, Cat. #: 91077, lot 10L917) aggregation in the presence of PS-OH surface: histograms represent relative scattering by intensity (a) and by number (b). Results shown are for: (1a), (1b), (2a) & (2b) before incubation; and (3a) & (3b) 25 minutes of incubation. Sample (2) is the duplicate of sample (1).

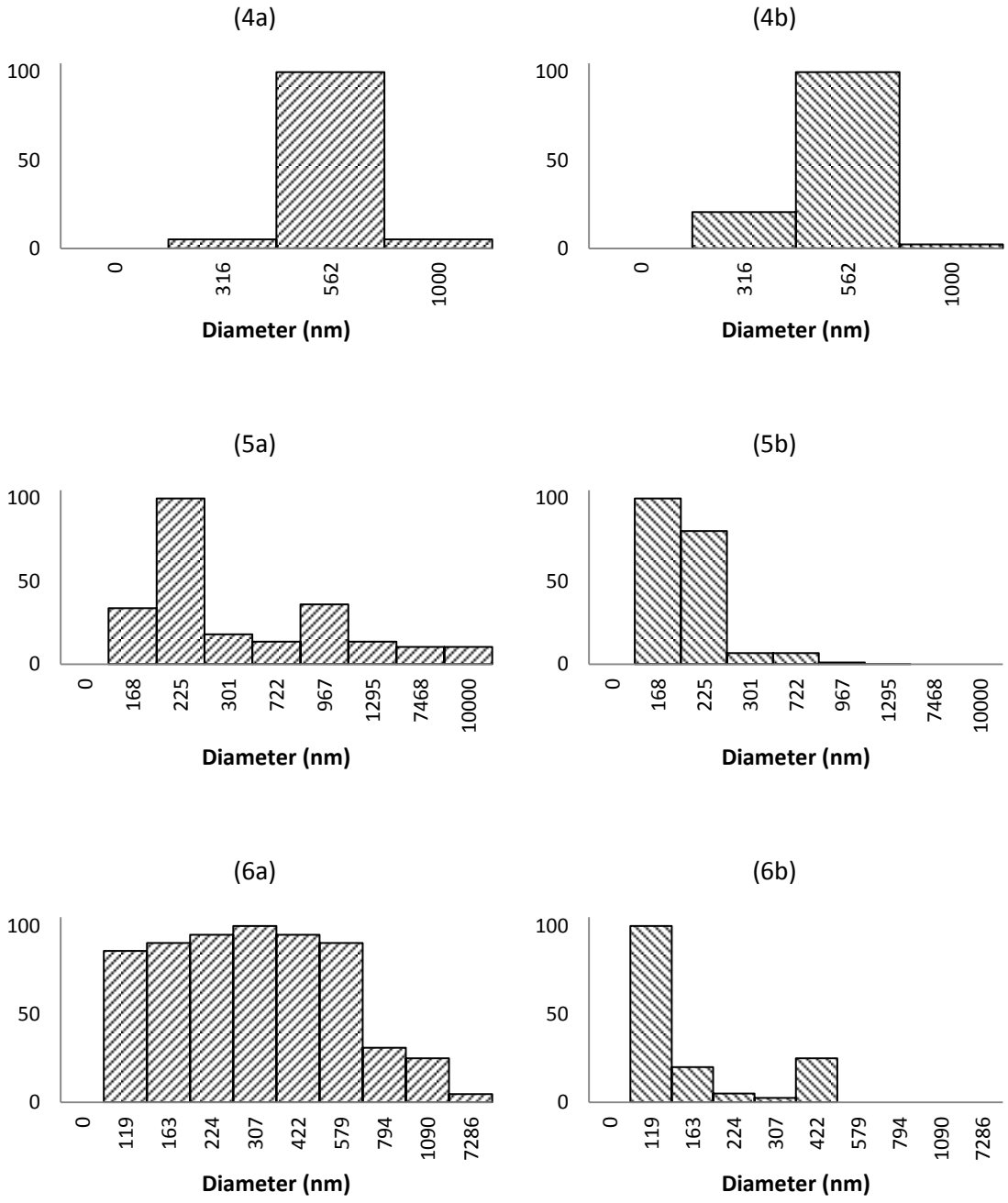

Figure C.9. DLS analysis of human insulin (SACF Biosciences, Cat. #: 91077, lot 10L917) aggregation in the presence of PS-OH surface: histograms represent relative scattering by intensity (a) and by number (b). Results shown are for: (4a) & (4b) 25 minutes; and (5a), (5b), (6a) & (6b) 45 minutes of incubation. Sample (4) is the duplicate of sample (3) and sample (6) is the duplicate of sample (5).

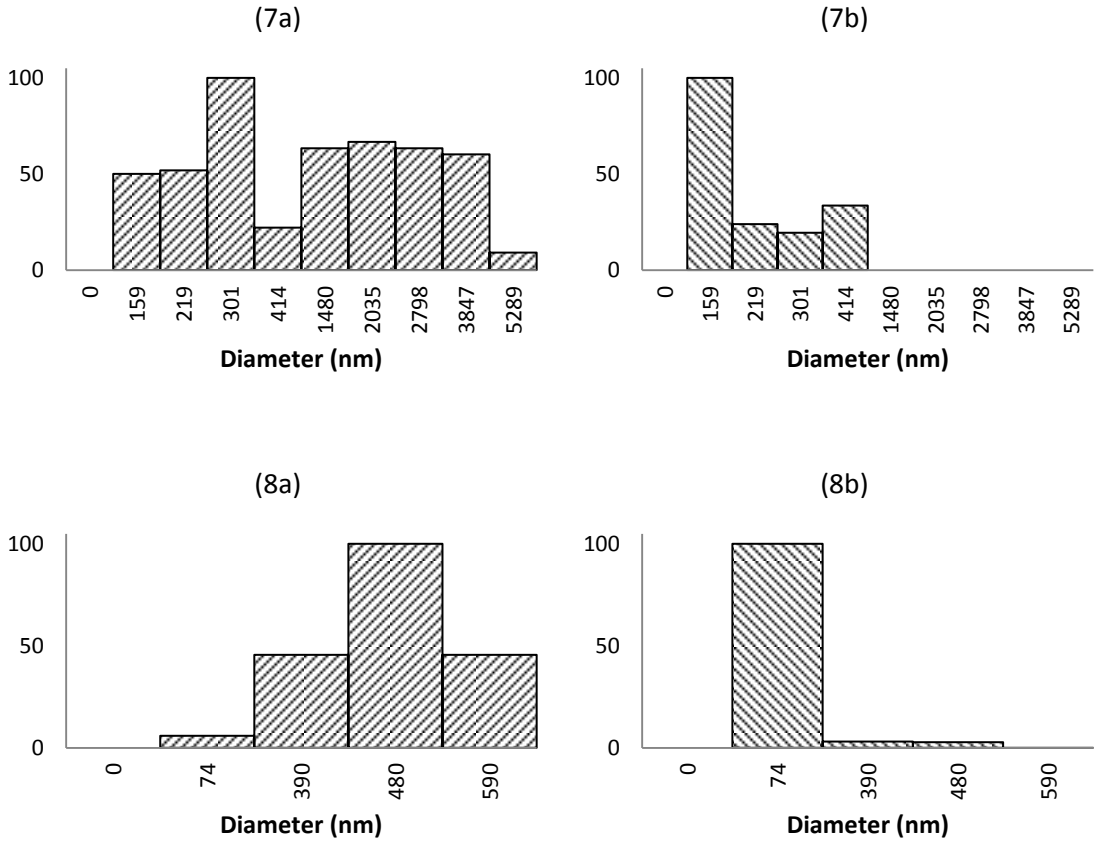

Figure C.10. DLS analysis of human insulin (SACF Biosciences, Cat. #: 91077, lot 10L917) aggregation in the presence of PS-OH surface: histograms represent relative scattering by intensity (a) and by number (b). Results shown are for: (7a), (7b), (8a) & (8b) 65 minutes of incubation. Sample (8) is the duplicate of sample (7).

4. HUMAN INSULIN IN THE PRESENCE OF PS-COOH SURFACE

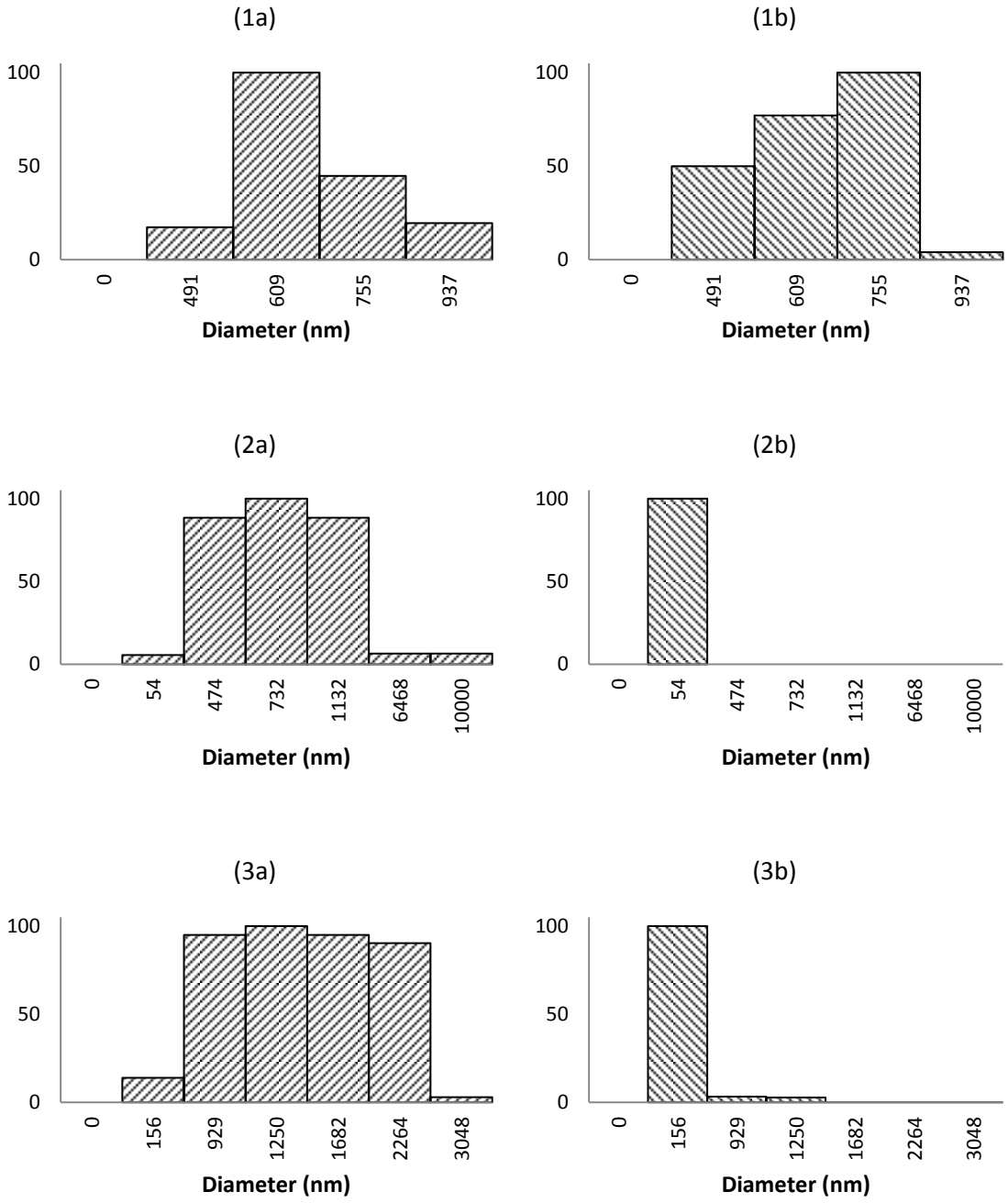

Figure C.11. DLS analysis of human insulin (SACF Biosciences, Cat. #: 91077, lot 10L917) aggregation in the presence of PS-COOH surface: histograms represent relative scattering by intensity (a) and by number (b). Results shown are for: (1a), (1b), (2a) & (2b) before incubation; and (3a) & (3b) 25 minutes of incubation. Sample (2) is the duplicate of sample (1).

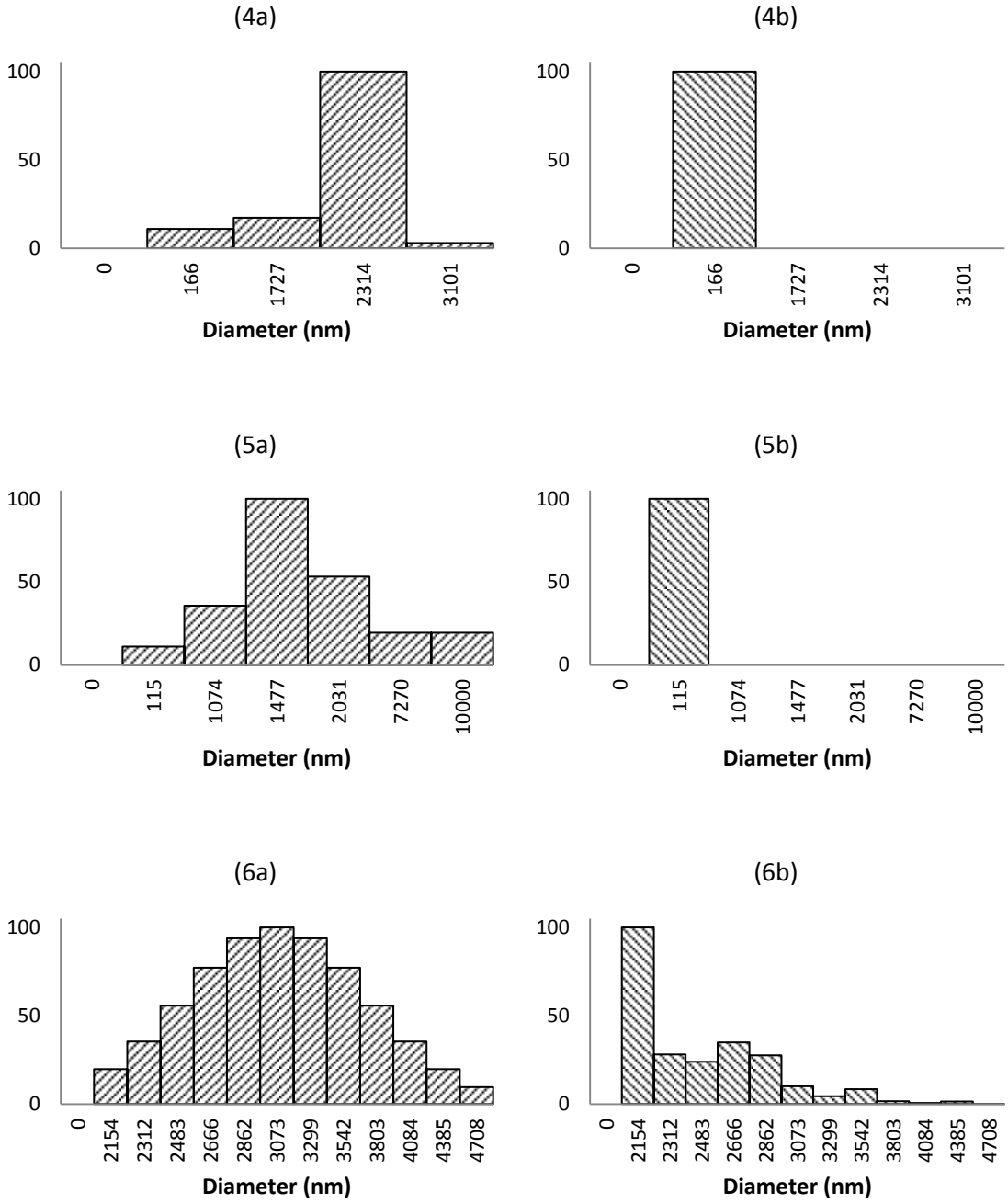

Figure C.12. DLS analysis of human insulin (SACF Biosciences, Cat. #: 91077, lot 10L917) aggregation in the presence of PS-COOH surface: histograms represent relative scattering by intensity (a) and by number (b). Results shown are for: (4a) & (4b) 25 minutes; and (5a), (5b), (6a) & (6b) 45 minutes of incubation. Sample (4) is the duplicate of sample (3) and sample (6) is the duplicate of sample (5).

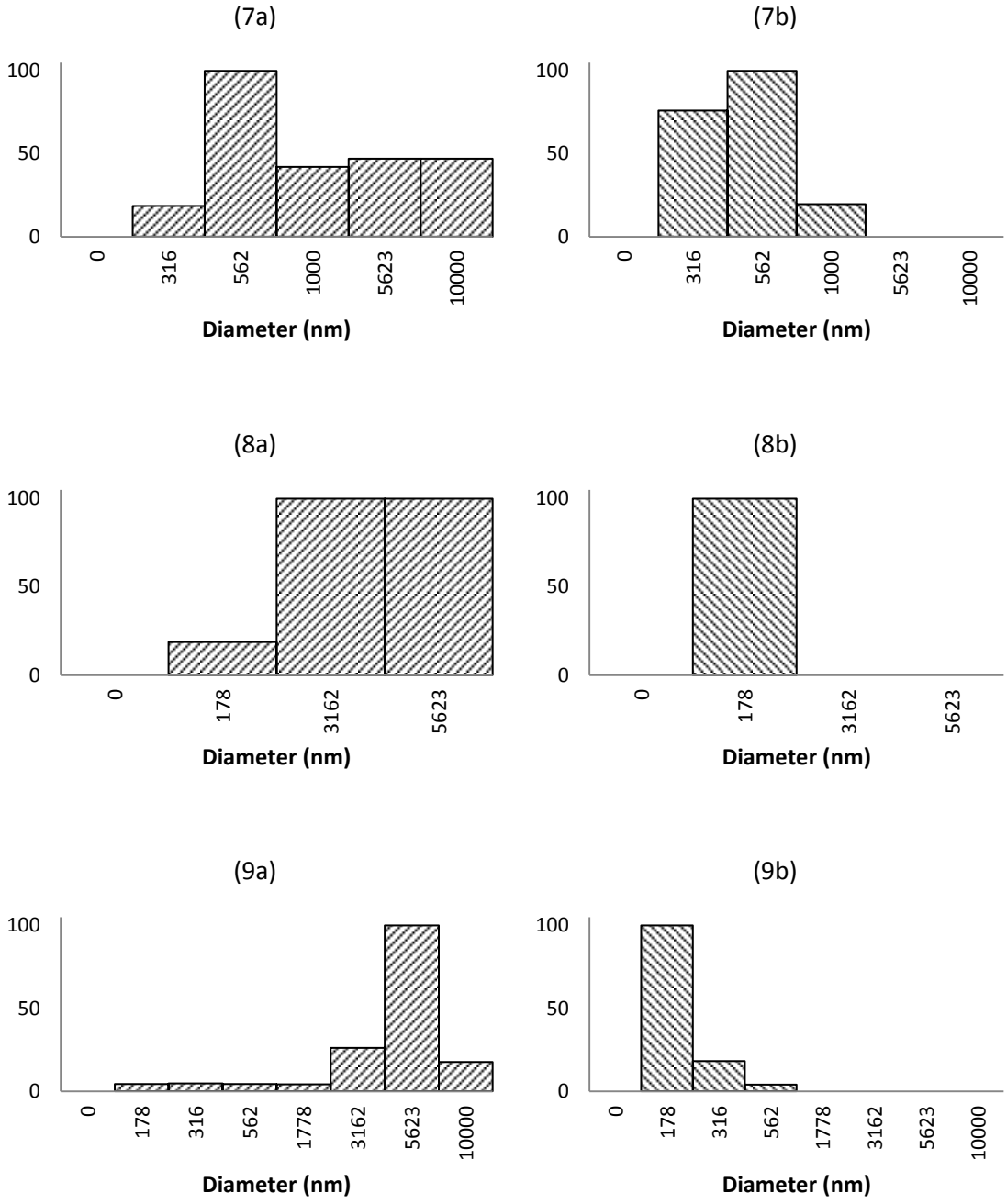

Figure C.13. DLS analysis of human insulin (SACF Biosciences, Cat. #: 91077, lot 10L917) aggregation in the presence of PS-COOH surface: histograms represent relative scattering by intensity (a) and by number (b). Results shown are for: (7a), (7b), (8a) & (8b) 65 minutes; and (9a) & (9b) 85 minutes of incubation. Sample (8) is the duplicate of sample (7).

5. HUMAN INSULIN IN THE PRESENCE OF PS-NH_2 SURFACE

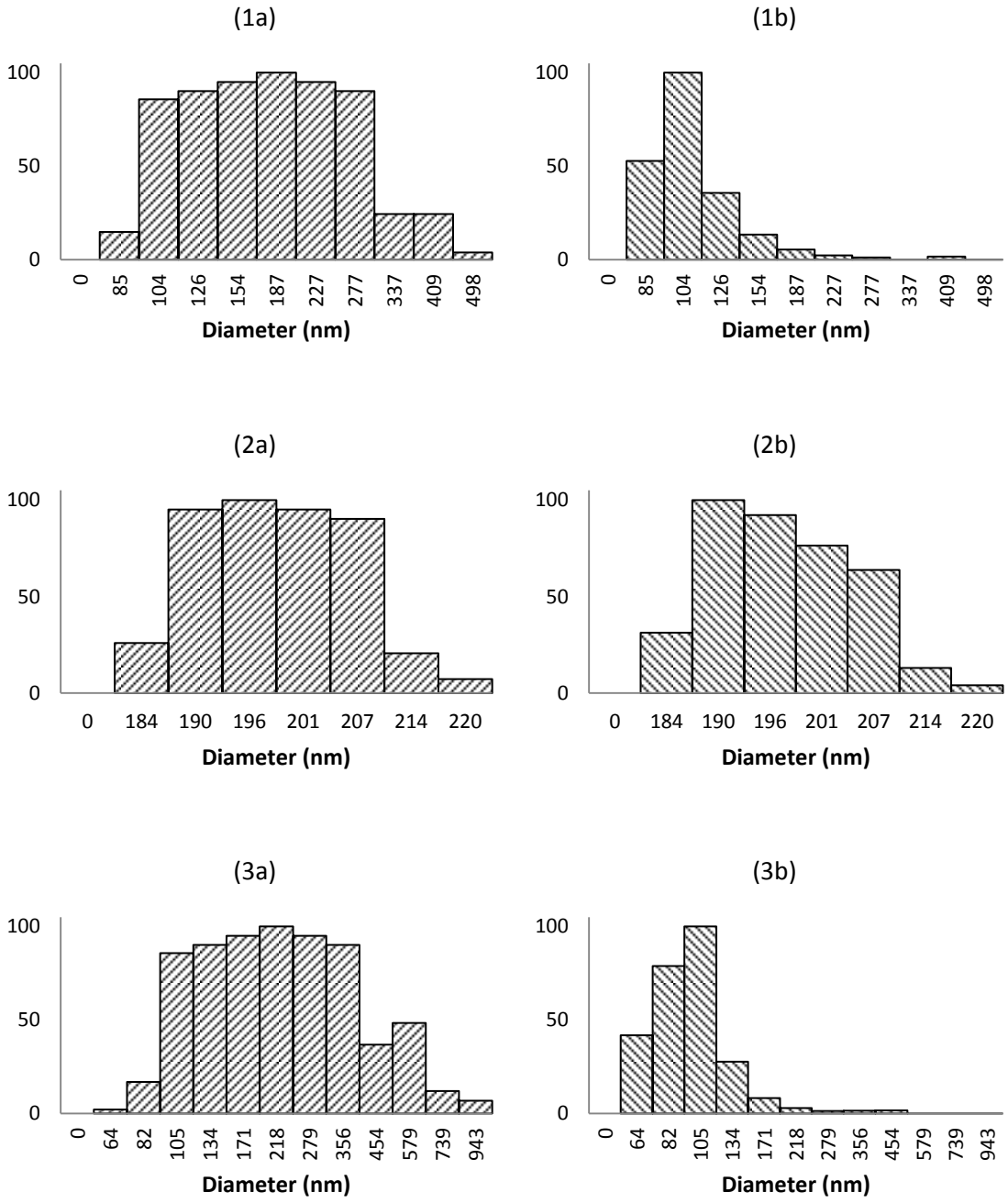

Figure C.14. DLS analysis of human insulin (SACF Biosciences, Cat. #: 91077, lot 10L917) aggregation in the presence of PS-NH2 surface: histograms represent relative scattering by intensity (a) and by number (b). Results shown are for: (1a), (1b), (2a) & (2b) before incubation; and (3a) & (3b) 25 minutes of incubation. Sample (2) is the duplicate of sample (1).

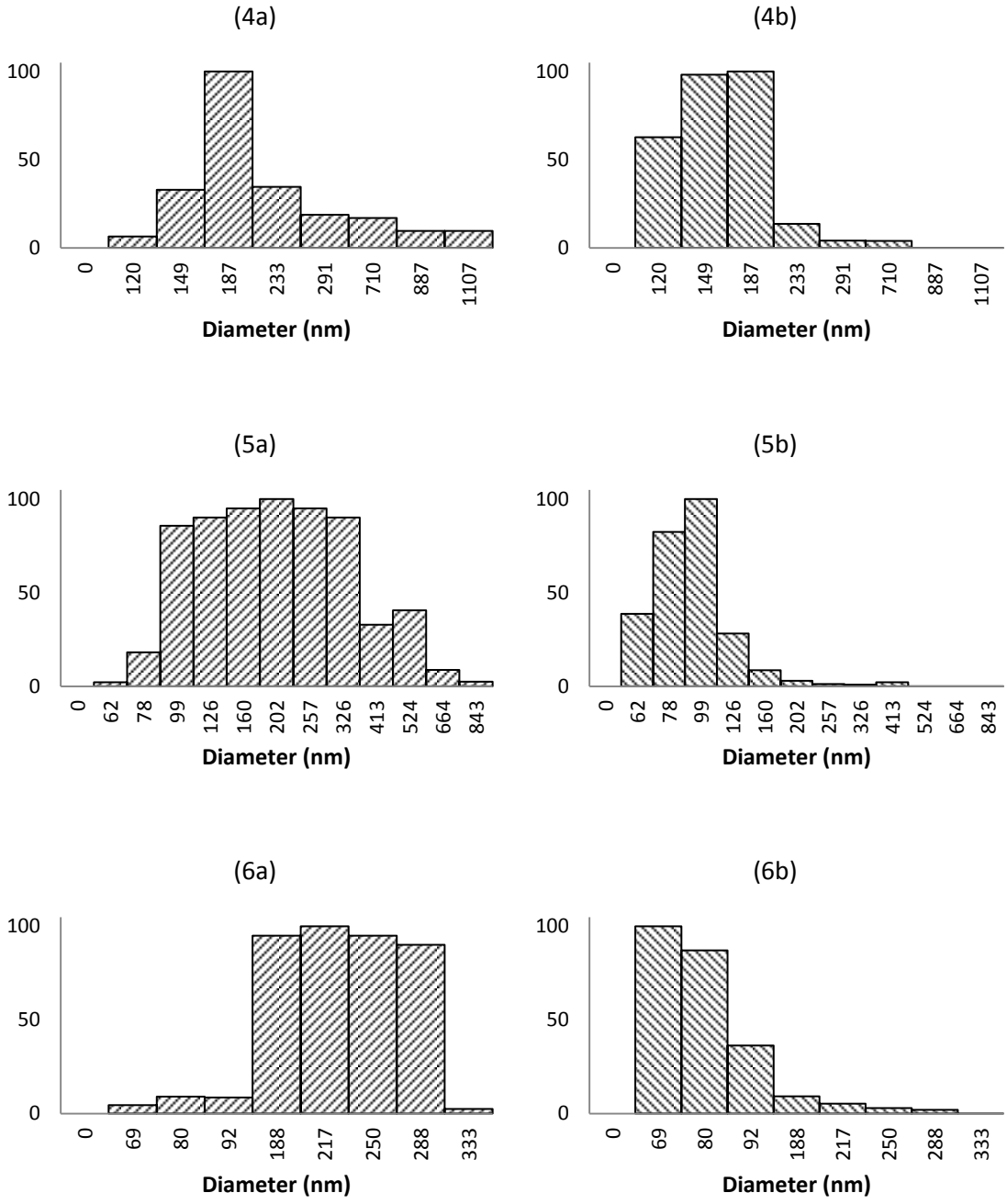

Figure C.15. DLS analysis of human insulin (SACF Biosciences, Cat. #: 91077, lot 10L917) aggregation in the presence of PS-NH2 surface: histograms represent relative scattering by intensity (a) and by number (b). Results shown are for: (4a) & (4b) 25 minutes; and (5a), (5b), (6a) & (6b) 45 minutes of incubation. Sample (4) is the duplicate of sample (3) and sample (6) is the duplicate of sample (5).

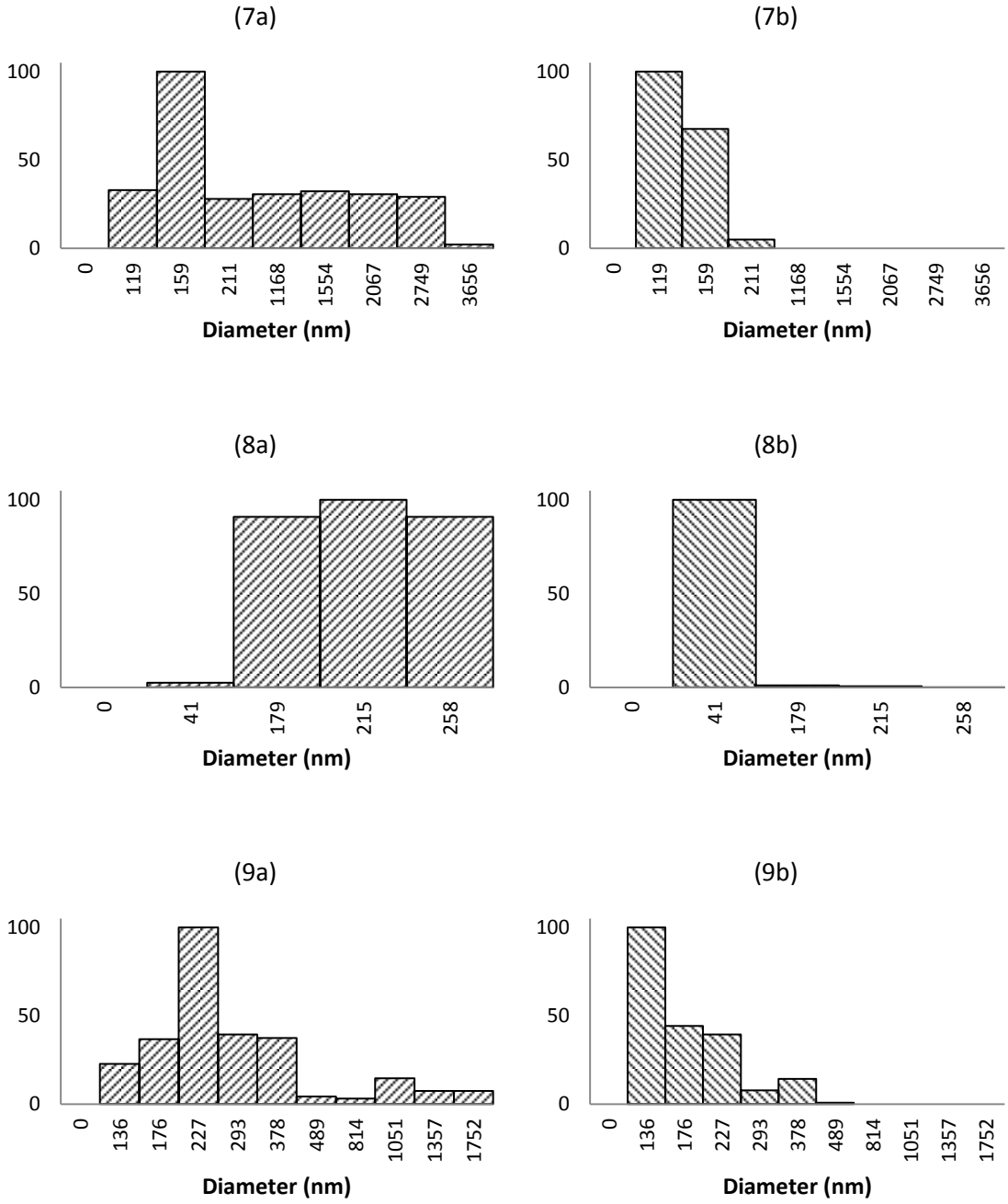

Figure C.16. DLS analysis of human insulin (SACF Biosciences, Cat. #: 91077, lot 10L917) aggregation in the presence of PS-NH2 surface: histograms represent relative scattering by intensity (a) and by number (b). Results shown are for: (7a), (7b), (8a) & (8b) 65 minutes; and (9a) & (9b) 85 minutes of incubation. Sample (8) is the duplicate of sample (7).

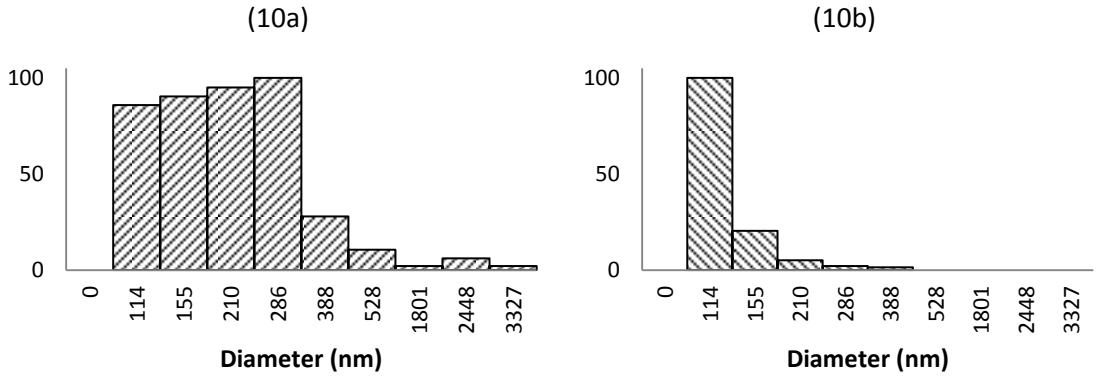

Figure C.17. DLS analysis of human insulin (SACF Biosciences, Cat. #: 91077, lot 10L917) aggregation in the presence of PS-NH2 surface: histograms represent relative scattering by intensity (a) and by number (b). Results shown are for: (10a) & (10b) 100 minutes of incubation.

APPENDIX D

DYNAMIC LIGHT SCATTERING HISTOGRAMS

OF BOVINE INSULIN IN BULK AND IN THE PRESENCE OF LIPOSOMES

INCUBATED AT 60 ˚C

1. BOVINE INSULIN IN BULK

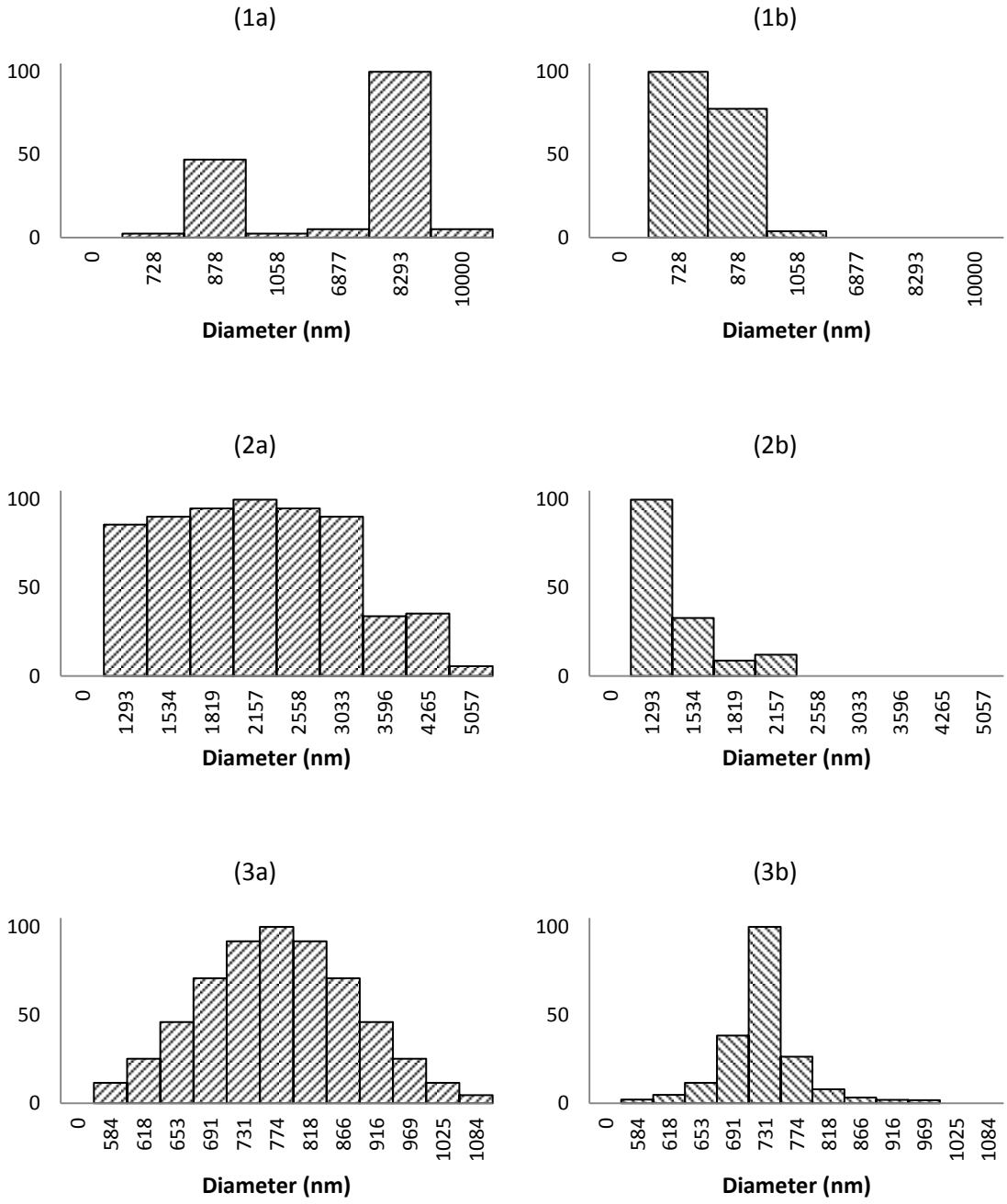

Figure D.1. DLS analysis of bovine insulin (SIGMA, Cat. #: I5500 (lot 019K17765V) aggregation in bulk: histograms represent relative scattering by intensity (a) and by number (b). Results shown are for: (1a) & (1b) 30 minutes; (2a) & (2b) 60 minutes; and (3a) & (3b) 150 minutes of incubation.

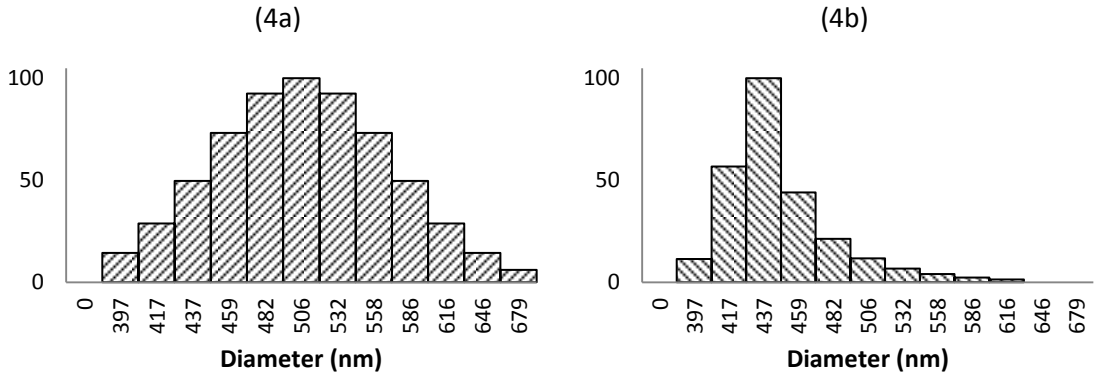

Figure D.2. DLS analysis of bovine insulin (SIGMA, Cat. #: I5500 (lot 019K17765V) aggregation in bulk: histograms represent relative scattering by intensity (a) and by number (b). Results shown are for: (4a) & (4b) 150 minutes of incubation. Sample (4) is the duplicate of sample (3).

2. BOVINE INSULIN IN THE PRESENCE OF LIPOSOME 1 (80/20)% PC/PS

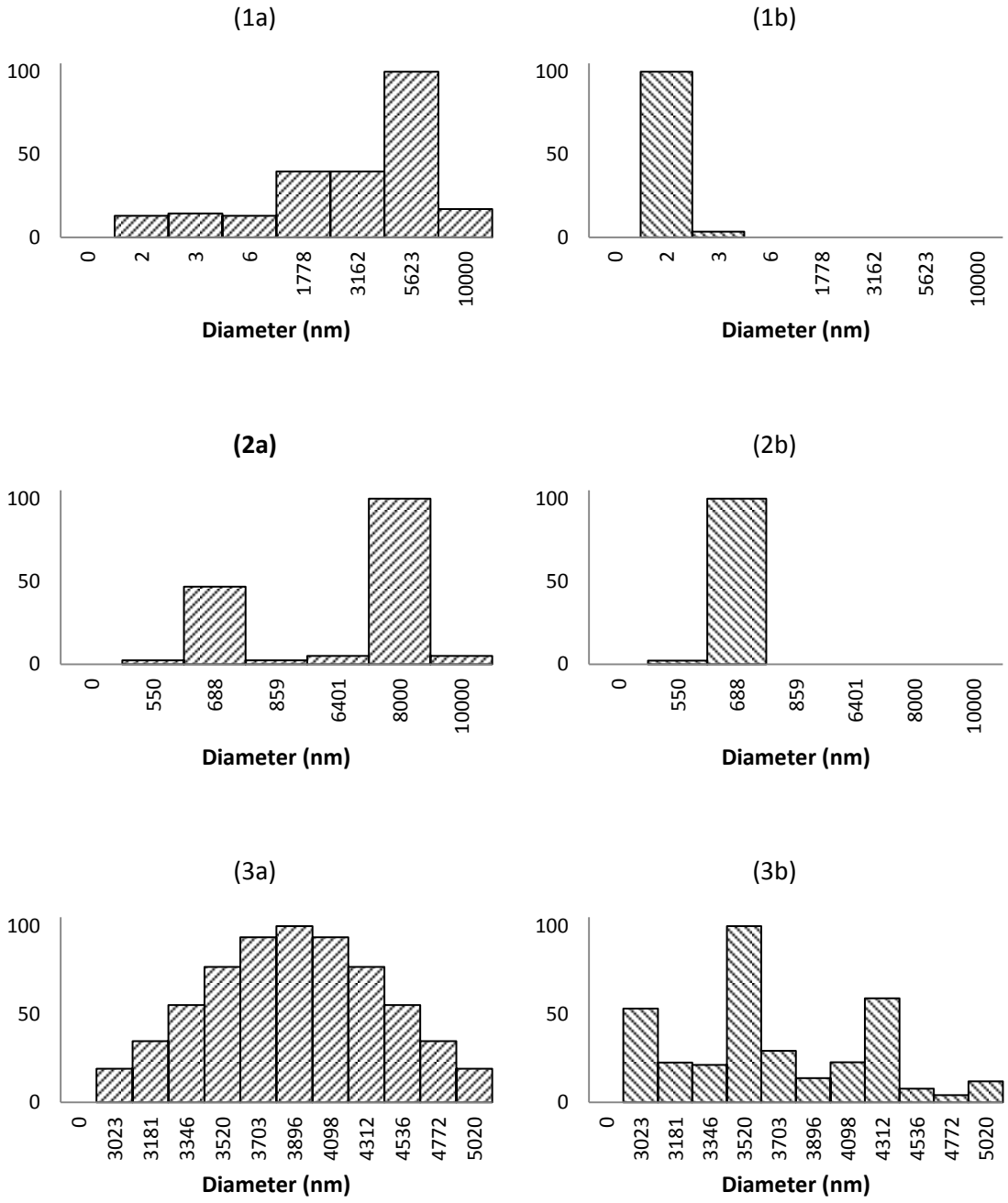

Figure D.3. DLS analysis of bovine insulin (SIGMA, Cat. #: I5500 (lot 019K17765V) aggregation in the presence of liposome 1 (80/20)% PC/PS: histograms represent relative scattering by intensity (a) and by number (b). Results shown are for: (1a), (1b), (2a) & (2d) 30 minutes; and (3a) & (3b) after 90 minutes of incubation.

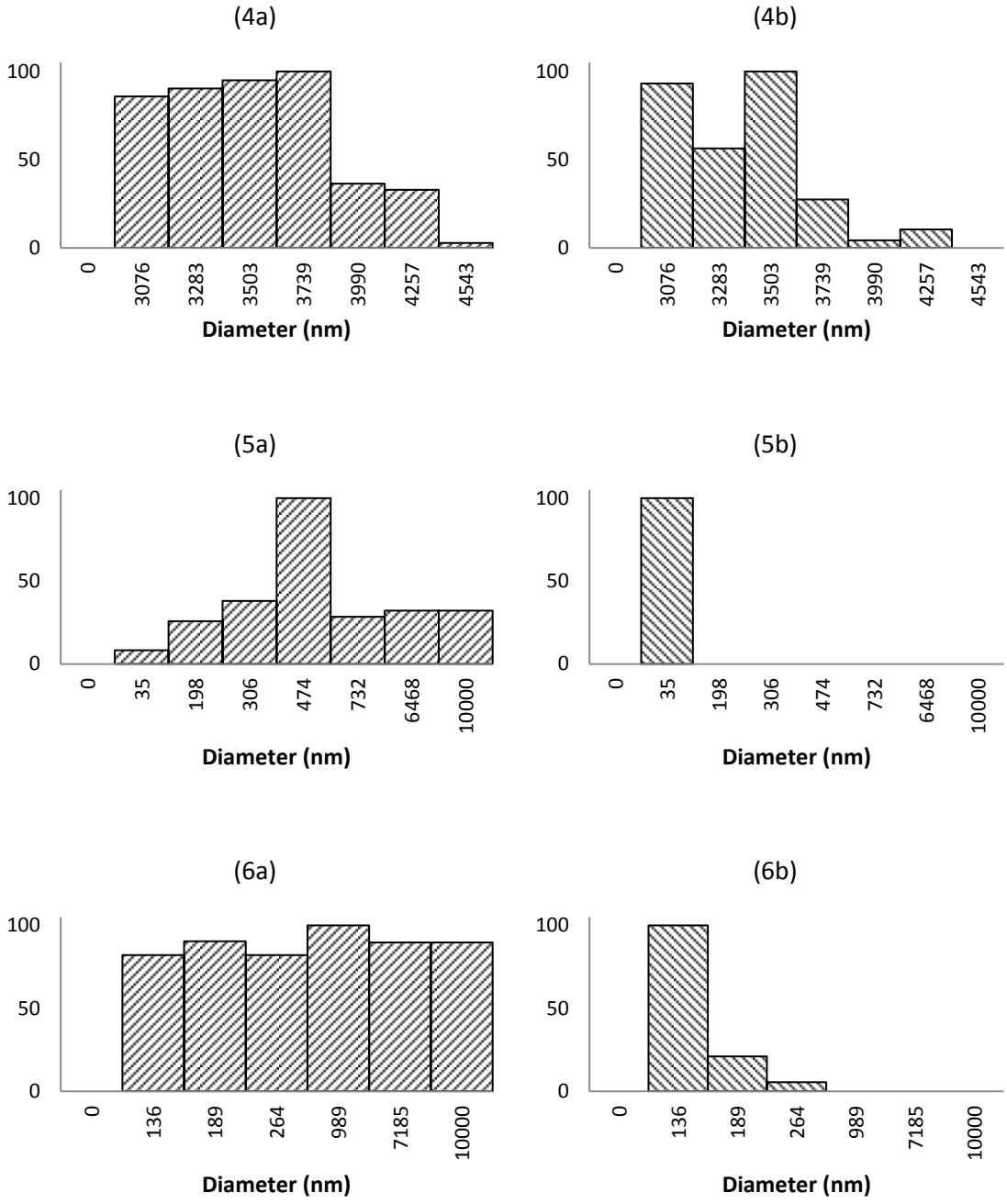

Figure D.4. DLS analysis of bovine insulin (SIGMA, Cat. #: I5500 (lot 019K17765V) aggregation in the presence of liposome 1 (80/20)% PC/PS: histograms represent relative scattering by intensity (a) and by number (b). Results shown are for: (4a) & (4b) 90 minutes; (5a) & (5b) 120 minutes and (6a) & (6b) after 150 minutes of incubation. Sample (4) is the duplicate of sample (3).

3. BOVINE INSULIN IN THE PRESENCE OF LIPOSOME 2 (20/80)% PC/C

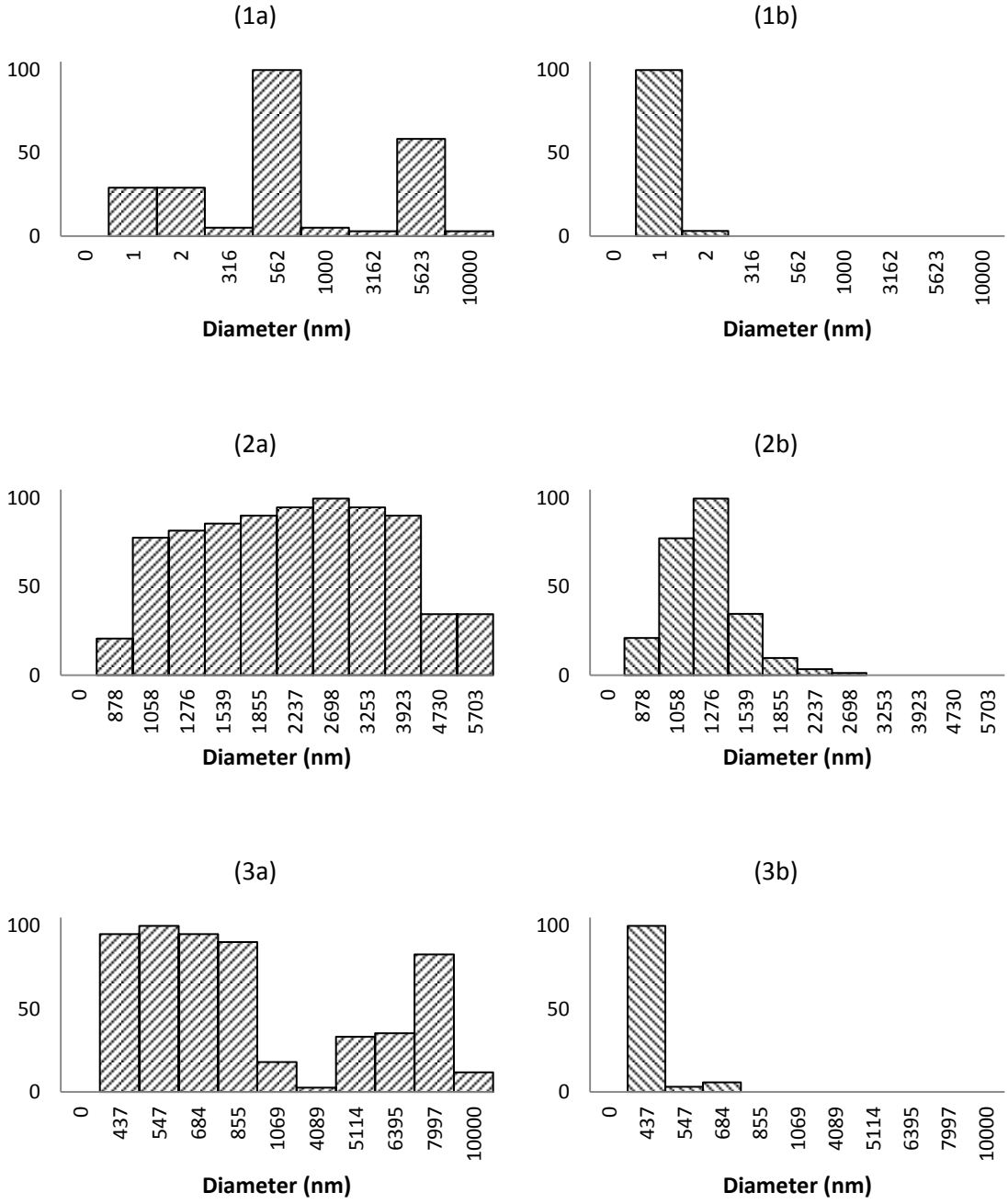

Figure D.5. DLS analysis of bovine insulin (SIGMA, Cat. #: I5500 (lot 019K17765V) aggregation in the presence of liposome 2 (20/80)% PC/C: histograms represent relative scattering by intensity (a) and by number (b). Results shown are for: (1a), (1b), (2a) & (2d) 30 minutes; and (3a) & (3b) after 90 minutes of incubation.

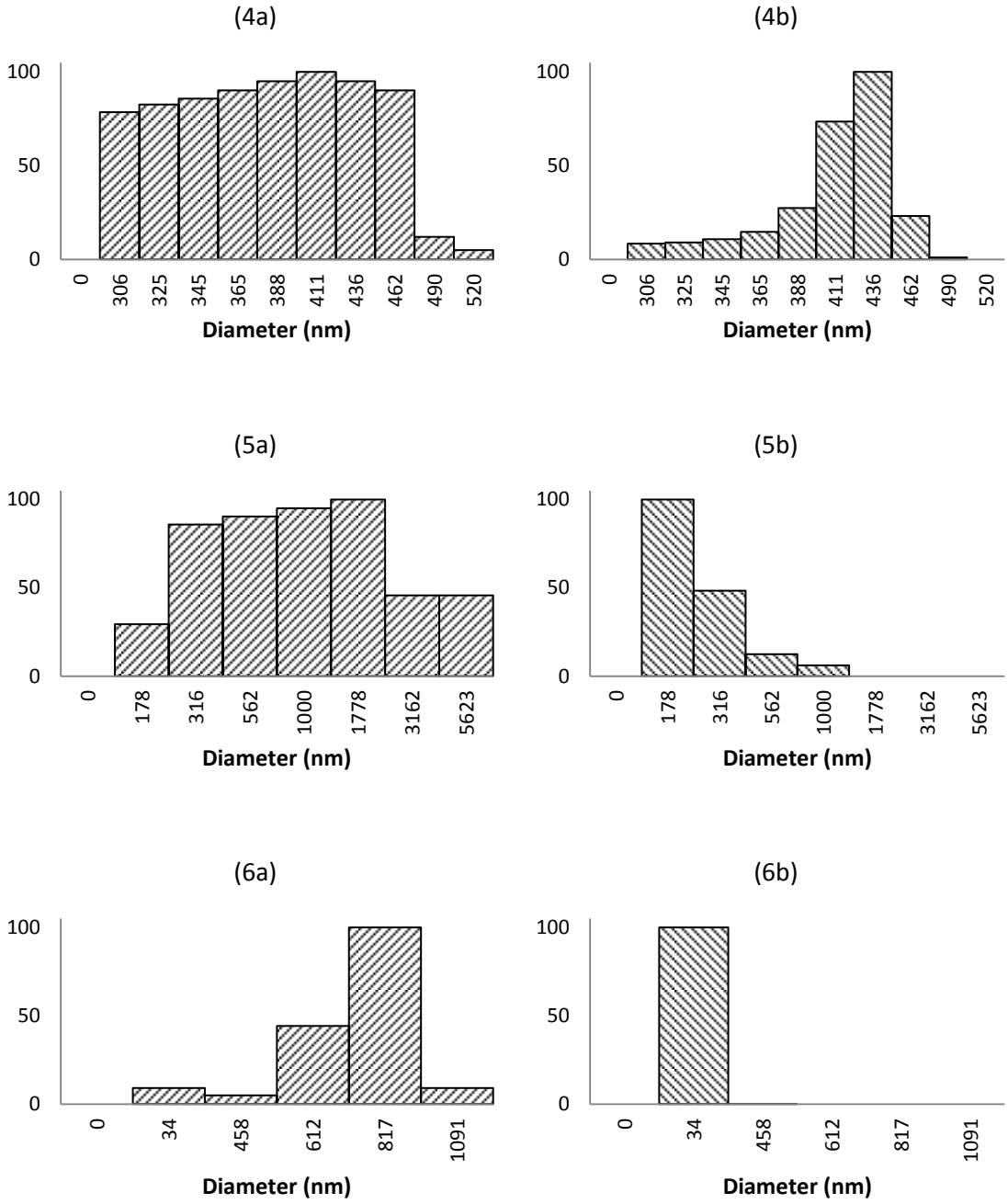

Figure D.6. DLS analysis of bovine insulin (SIGMA, Cat. #: I5500 (lot 019K17765V) aggregation in the presence of liposome 2 (20/80)% PC/C: histograms represent relative scattering by intensity (a) and by number (b). Results shown are for: (4a) & (4b) 90 minutes; (5a), (5b), (6a) & (6b) after 150 minutes of incubation. Sample (4) is the duplicate of sample (3) and sample (6) is the duplicate of sample (5).

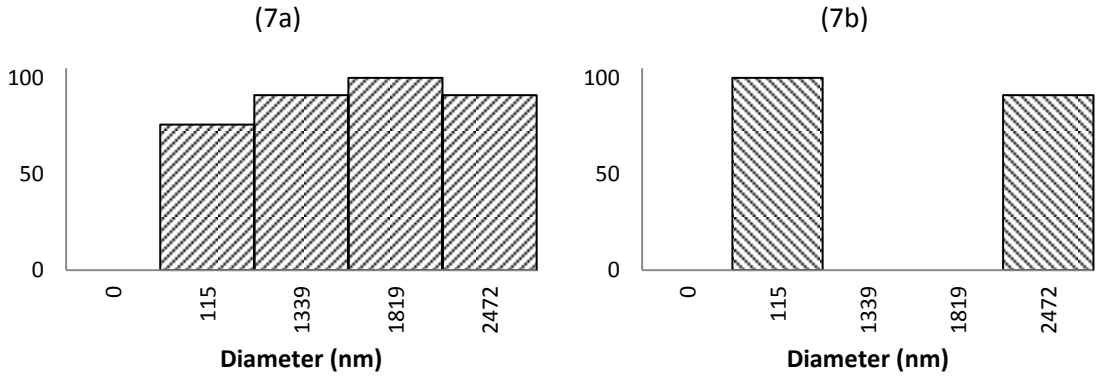

Figure D.7. DLS analysis of bovine insulin (SIGMA, Cat. #: I5500 (lot 019K17765V) aggregation in the presence of liposome 2 (20/80)% PC/C: histograms represent relative scattering by intensity (a) and by number (b). Results shown are for: (7a) & (7b) 180 minutes of incubation.

4. BOVINE INSULIN IN THE PRESENCE OF LIPOSOME 3 (80/20)% PC/C

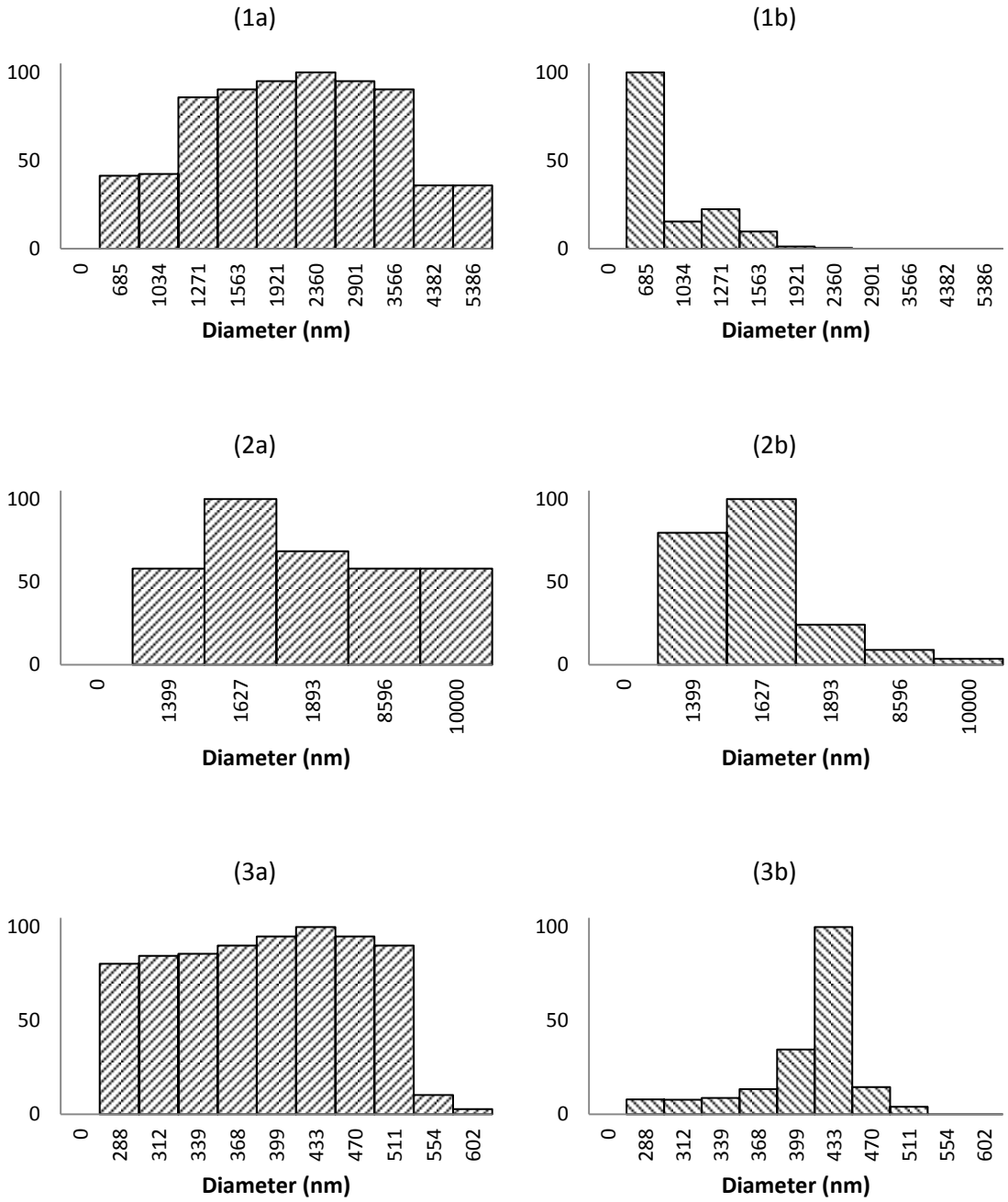

Figure D.8. DLS analysis of bovine insulin (SIGMA, Cat. #: I5500 (lot 019K17765V) aggregation in the presence of liposome 3 (80/20)% PC/C: histograms represent relative scattering by intensity (a) and by number (b). Results shown are for: (1a), (1b), (2a) & (2d) 60 minutes; and (3a) & (3b) 120 minutes of incubation. Sample (3) is a duplicate of sample (2).

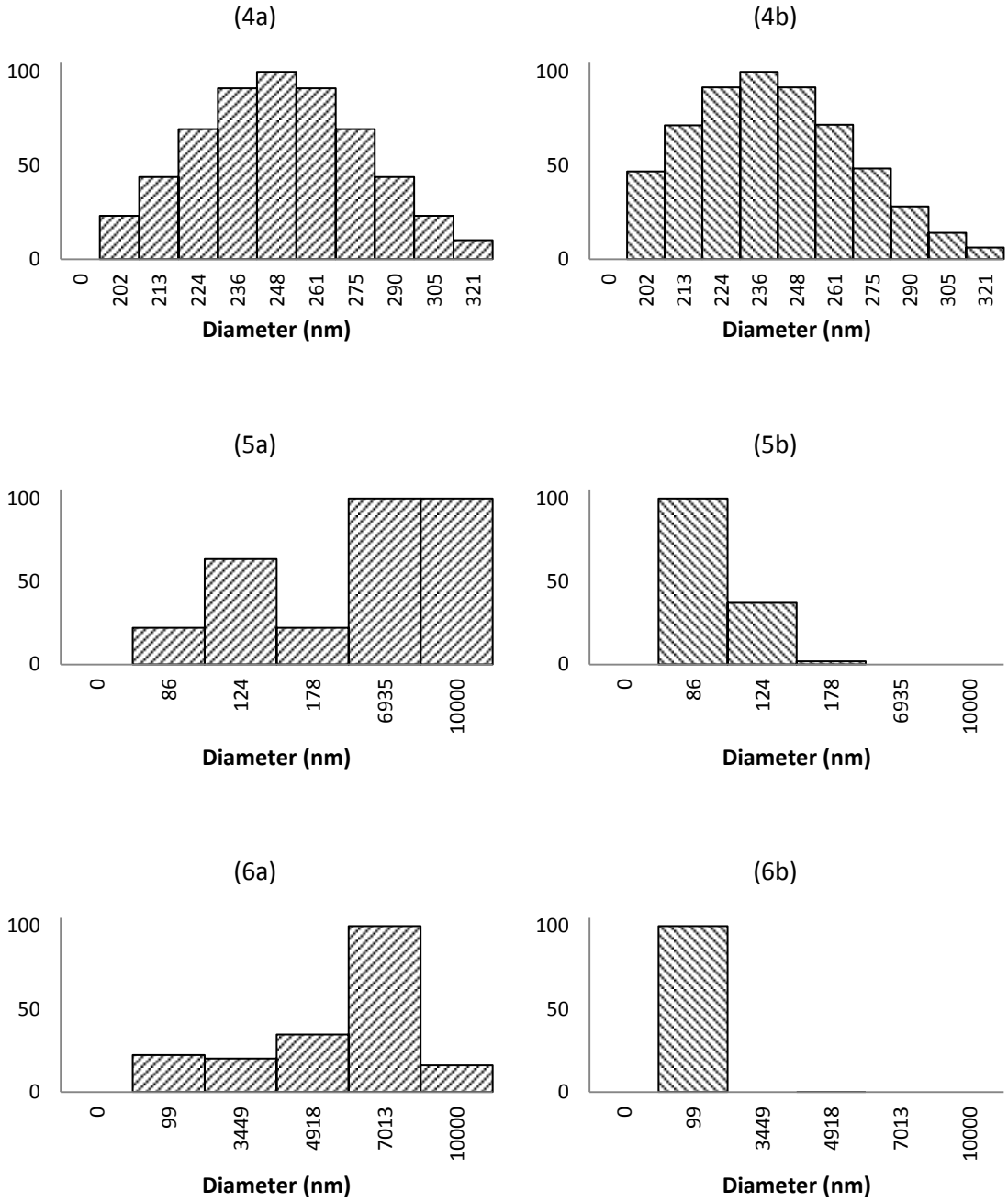

Figure D.9. DLS analysis of bovine insulin (SIGMA, Cat. #: I5500 (lot 019K17765V) aggregation in the presence of liposome 3 (80/20)% PC/C: histograms represent relative scattering by intensity (a) and by number (b). Results shown are for: (4a), (4b), (5a) & (5d) 180 minutes; and (6a) & (6b) 210 minutes of incubation. Sample (5) is a duplicate of sample (4).

5. BOVINE INSULIN IN THE PRESENCE OF LIPOSOME 4 (2:2:1:1) C/PC/PG/PE

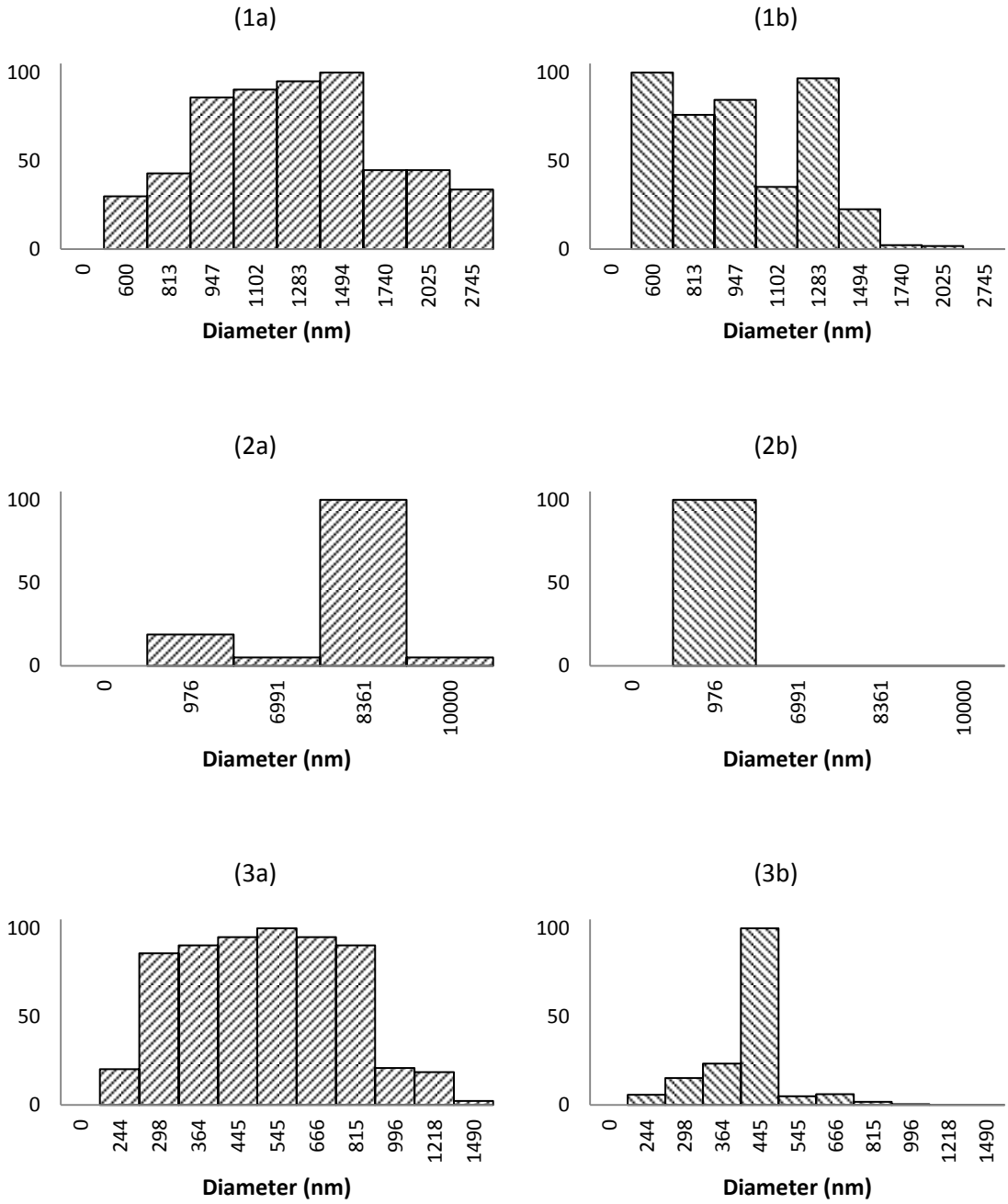

Figure D.10. DLS analysis of bovine insulin (SIGMA, Cat. #: I5500 (lot 019K17765V) aggregation in the presence of liposome 4 (2:2:1:1) C/PC/PG/PE: histograms represent relative scattering by intensity (a) and by number (b). Results shown are for: (1a) & (1b) 30 minutes; and (2a), (2b), (3a) & (3b) after 60 minutes of incubation. Sample (3) is the duplicate of sample (2).

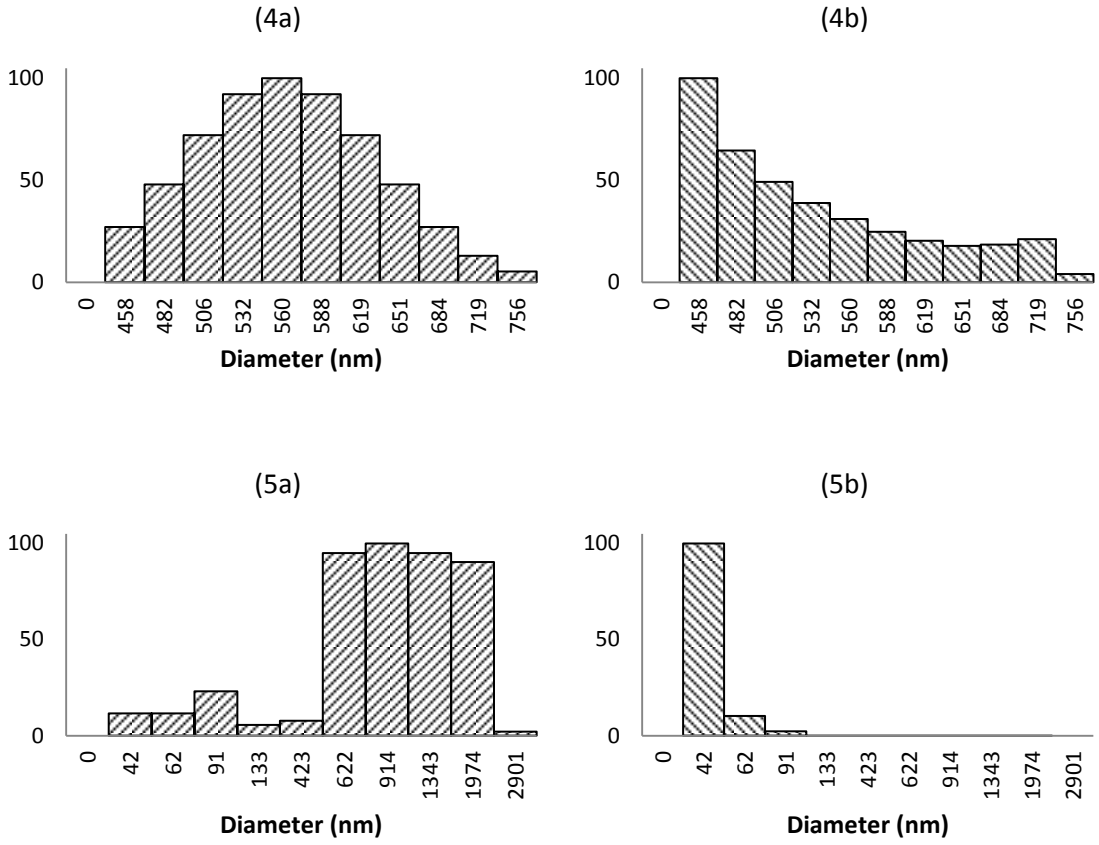

Figure D.11. DLS analysis of bovine insulin (SIGMA, Cat. #: I5500 (lot 019K17765V) aggregation in the presence of liposome 4 (2:2:1:1) C/PC/PG/PE: histograms represent relative scattering by intensity (a) and by number (b). Results shown are for: (4a) & (4b) 120 minutes; and (5a) & (5b) after 150 minutes of incubation.

6. BOVINE INSULIN IN THE PRESENCE OF LIPOSOME 5 (10:5:7.5:16) PC/PE/PS/C

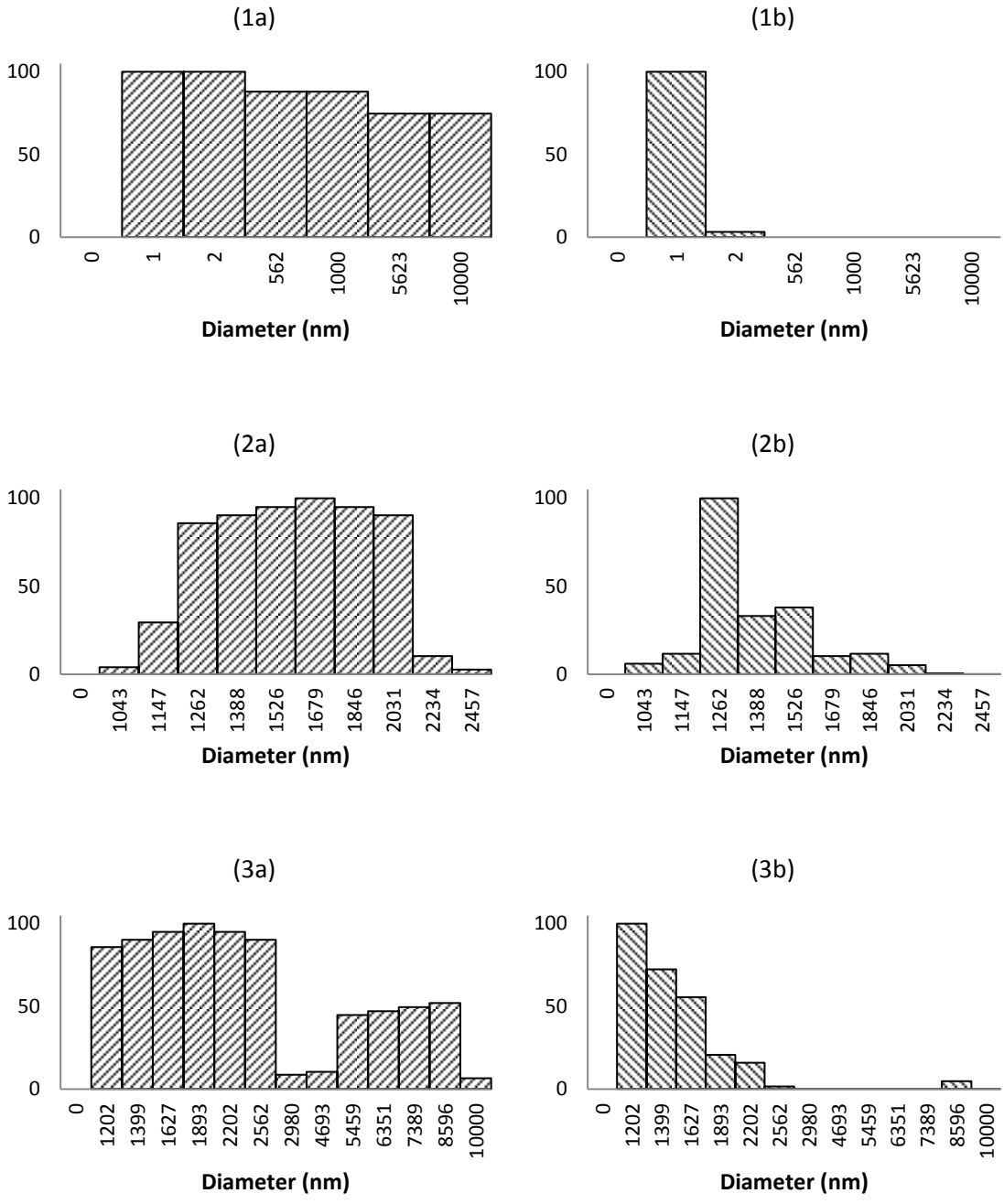

Figure D.12. DLS analysis of bovine insulin (SIGMA, Cat. #: I5500 (lot 019K17765V) aggregation in the presence of liposome 5 (10:5:7.5:16) PC/PE/PS/C: histograms represent relative scattering by intensity (a) and by number (b). Results shown are for: (1a) & (1b) 30 minutes; and (2a), (2b), (3a) & (3b) after 60 minutes of incubation. Sample (3) is the duplicate of sample (2).

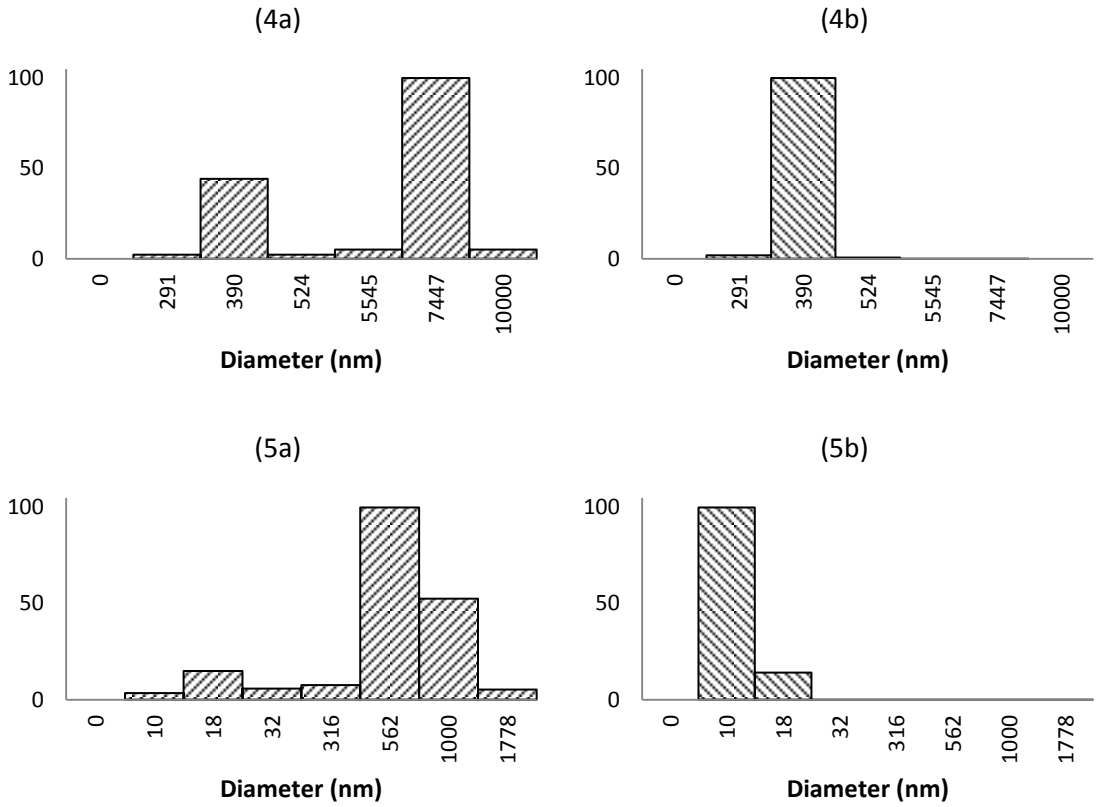

Figure D.13. DLS analysis of bovine insulin (SIGMA, Cat. #: I5500 (lot 019K17765V) aggregation in the presence of liposome 5 (10:5:7.5:16) PC/PE/PS/C: histograms represent relative scattering by intensity (a) and by number (b). Results shown are for: (4a) & (4b) 150 minutes; and (5a) & (5b) after 210 minutes of incubation.

APPENDIX E

CONGO RED SPECTRA

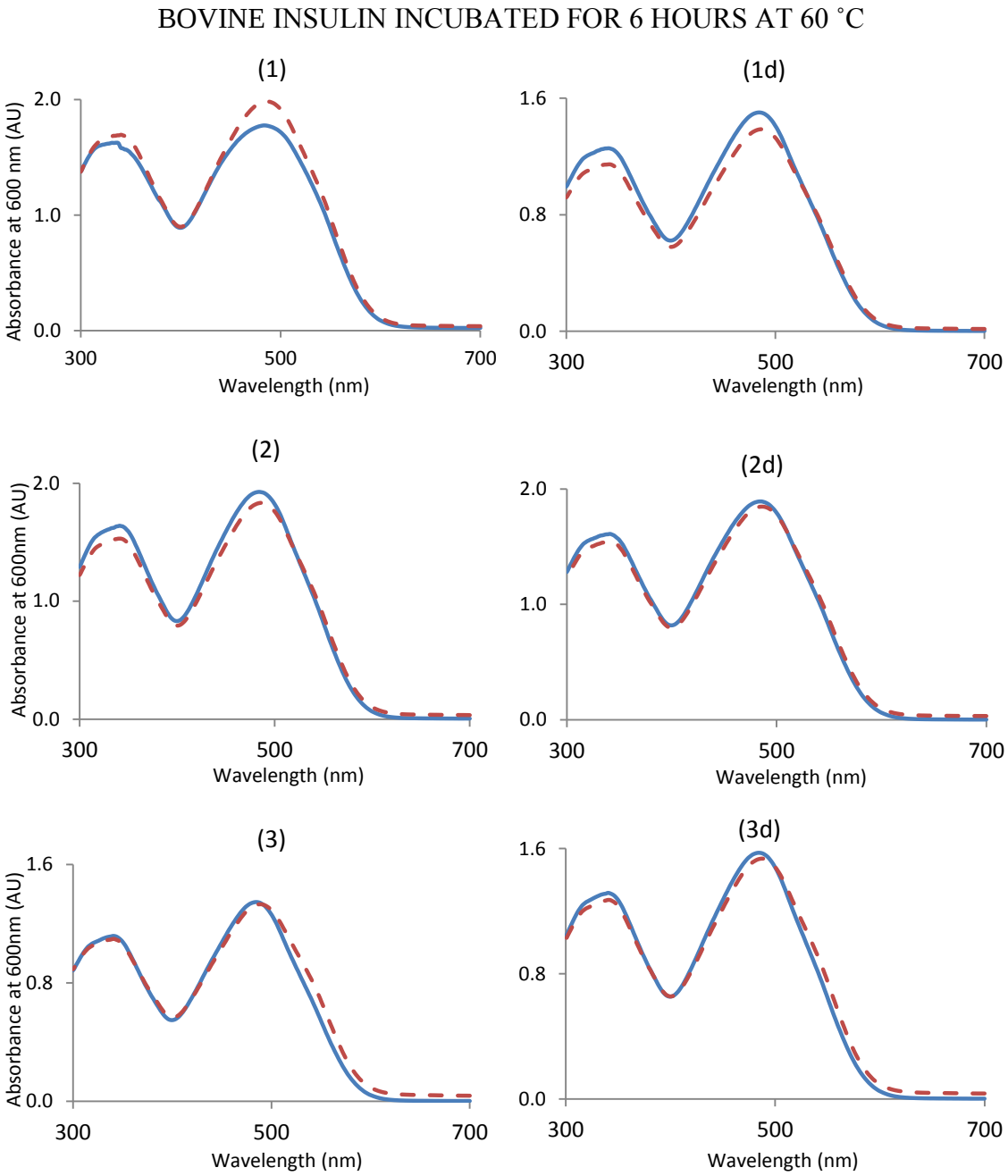

Figure E.1 Congo red results of bovine insulin in bulk and in the presence of surfaces: (CELL Applications, INC. Cat. #:128 -100 (lot 104), lyophilized): Blank (—); Sample (- - -). (1) and (1d) are bovine insulin and its duplicate; (2) and (2d) are bovine insulin and its duplicate in liposome 2 (20/80)% PC/C; (3) and (3d) are bovine insulin and its duplicate in liposome 3 (80/20)% PC/C.

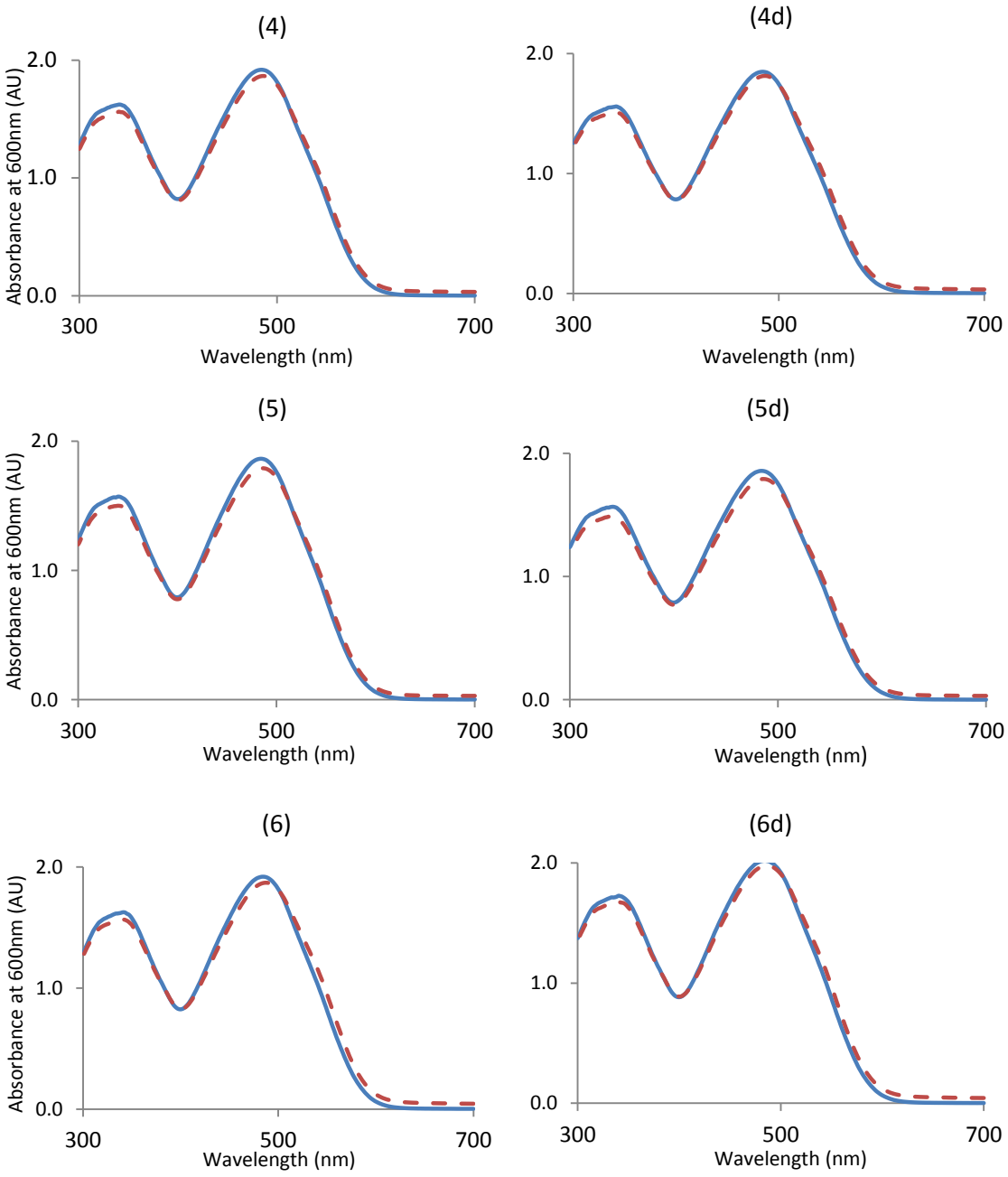

Figure E.2. Congo red results of bovine insulin in bulk and in the presence of surfaces: (CELL Applications, INC. Cat. #: 128 -100 (lot 104), lyophilized): Blank (—); Sample (- - -). (4) and (4d) are bovine insulin and its duplicate in liposome 5 (10:5:7.5:16) PC/PE/PS/C; (5) and (5d) are bovine insulin and its duplicate in liposome 6 (50/50)% PC/C; (6) and (6d) are bovine insulin and its duplicate in PS-NH2.

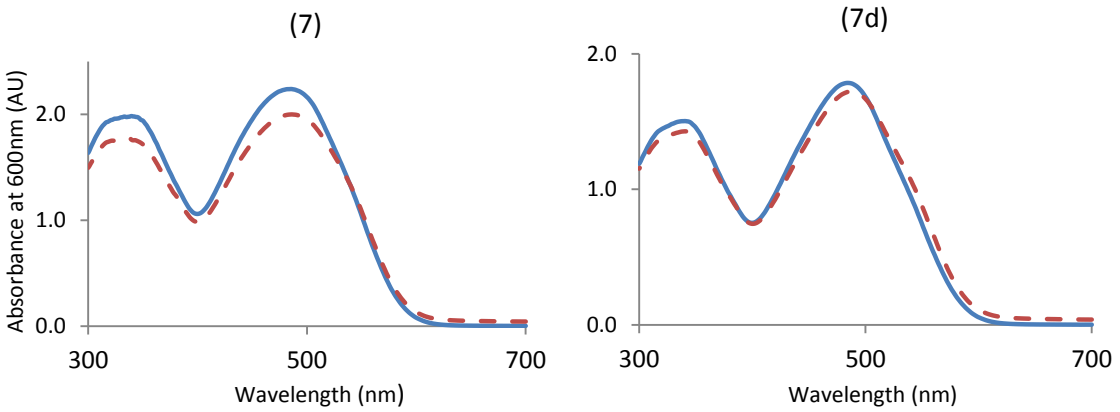

Figure E.3. Congo red results of bovine insulin in bulk and in the presence of surfaces: (CELL Applications, INC. Cat. #: 128 -100 (lot 104), lyophilized): Blank (—); Sample (- - -). (7) and (7d) are bovine insulin and its duplicate in PS-COOH.

BOVINE INSULIN INCUBATED FOR 55 HOURS AT 37 ˚C AND 230 RPM

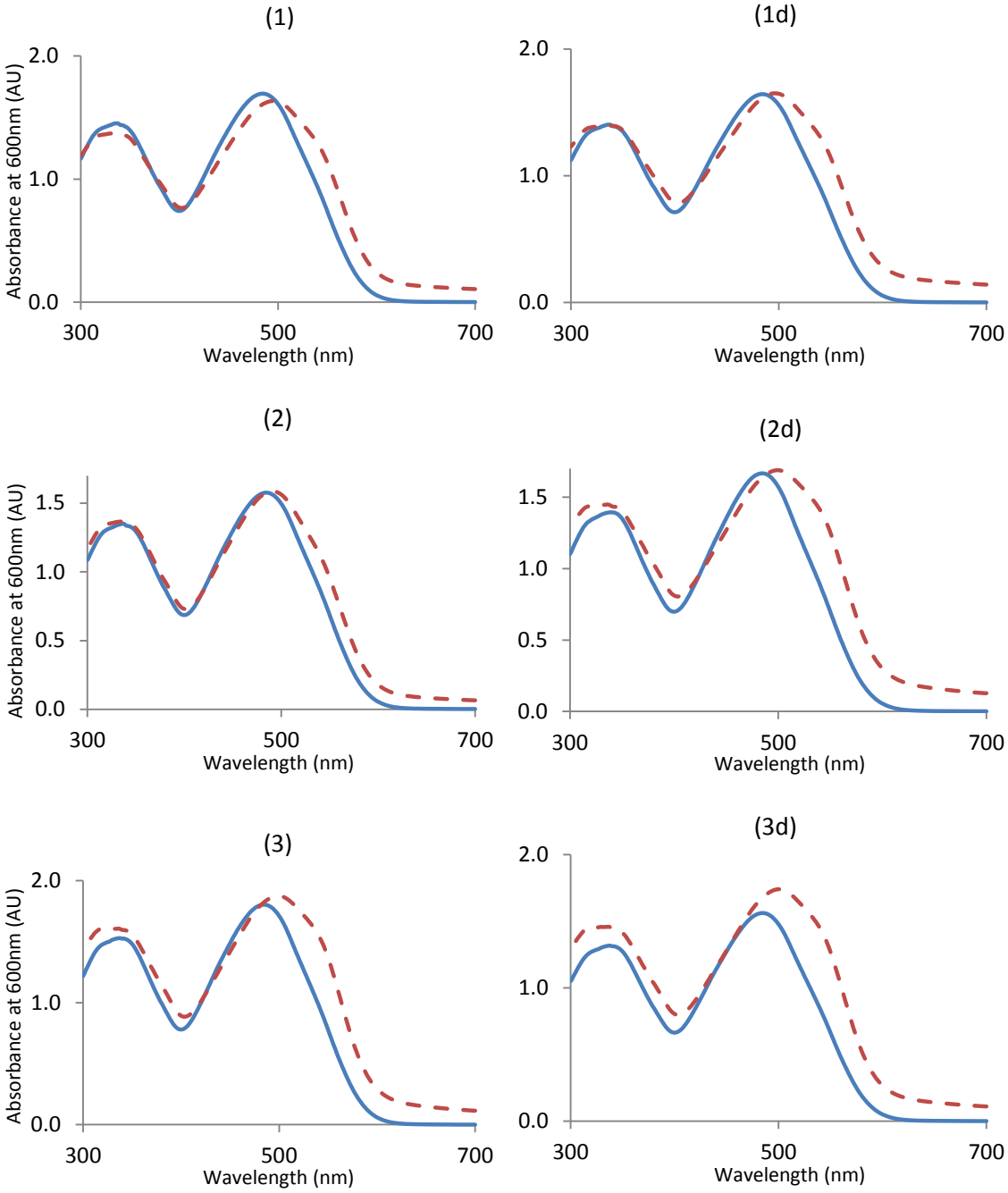

Figure E.4 Congo red results of bovine insulin in bulk and in the presence of surfaces: (CELL Applications, INC. Cat. #: 128 -100 (lot 104), lyophilized): Blank (—); Sample (- - -). (1) and (1d) are bovine insulin and its duplicate; (2) and (2d) are bovine insulin and its duplicate in liposome 2 (20/80)% PC/C; (3) and (3d) are bovine insulin and its duplicate in liposome 3 (80/20)% PC/C.

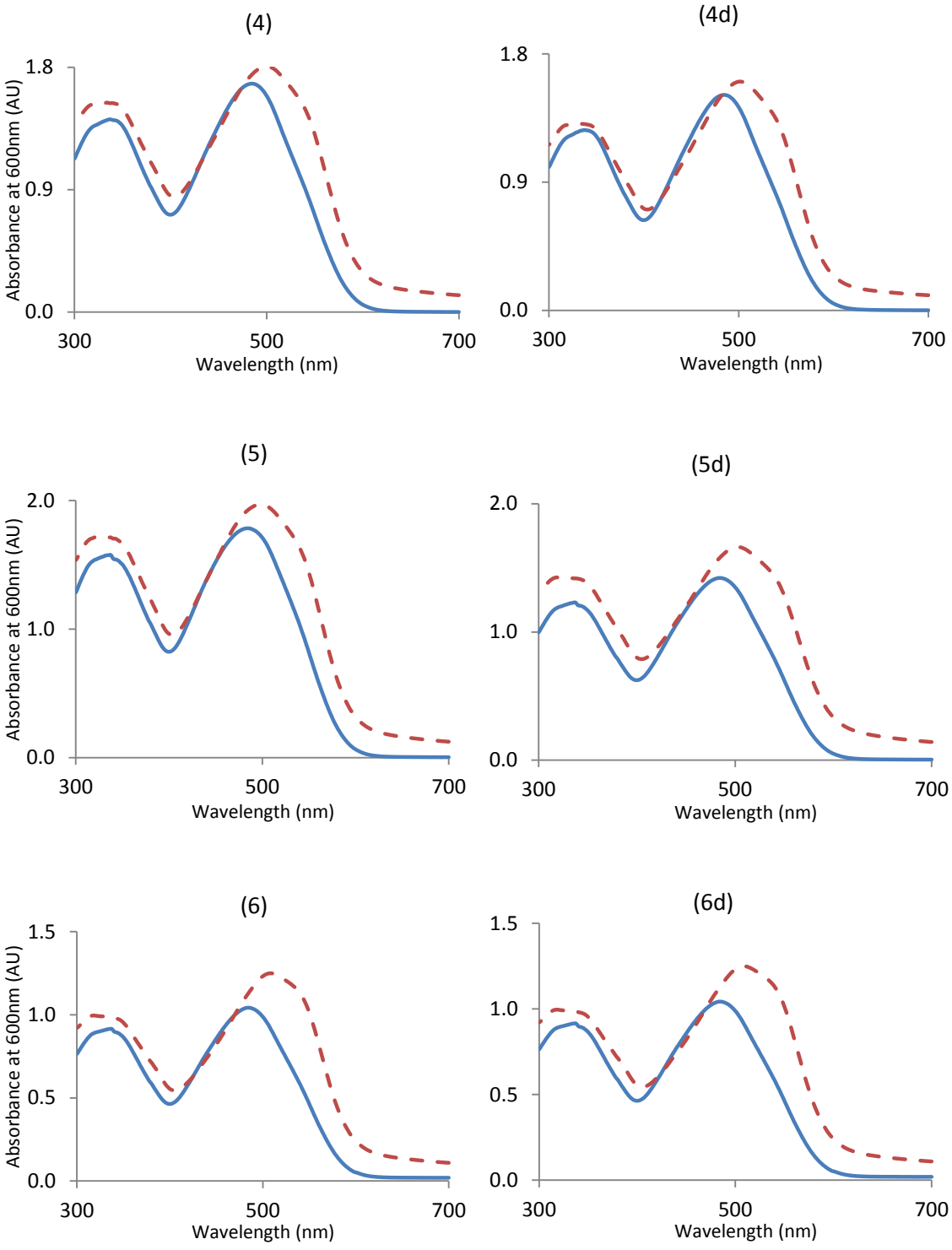

Figure E.5. Congo red results of bovine insulin in bulk and in the presence of surfaces: (CELL Applications, INC. Cat. #: 128 -100 (lot 104), lyophilized): Blank (—); Sample (- - -). (4) and (4d) are bovine insulin and its duplicate in liposome 5 (10:5:7.5:16) PC/PE/PS/C; (5) and (5d) are bovine insulin and its duplicate in liposome 6 (50/50)% PC/C; (6) and (6d) are bovine insulin and its duplicate in PS-NH_2.

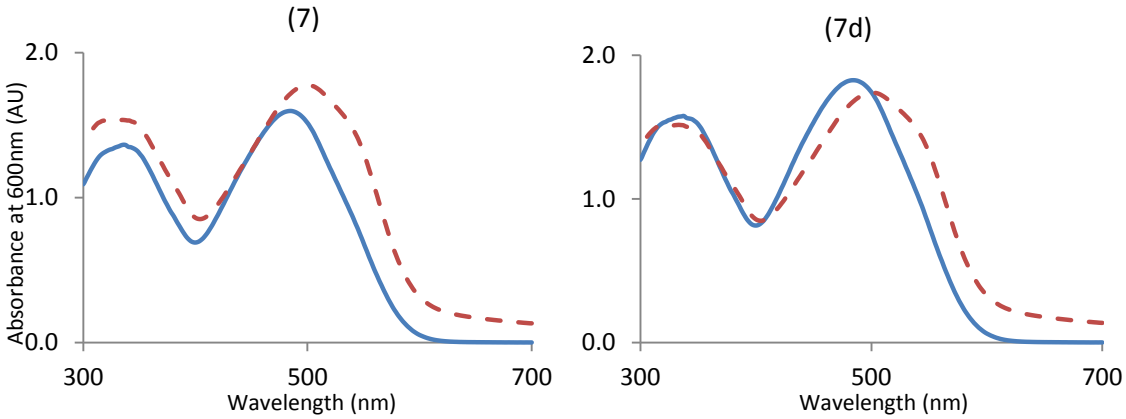

Figure E.6. Congo red results of bovine insulin in bulk and in the presence of surfaces: (CELL Applications, INC. Cat. #:128-100 (lot 104), lyophilized): Blank (—); Sample (- - -). (7) and (7d) are bovine insulin and its duplicate in PS-COOH.

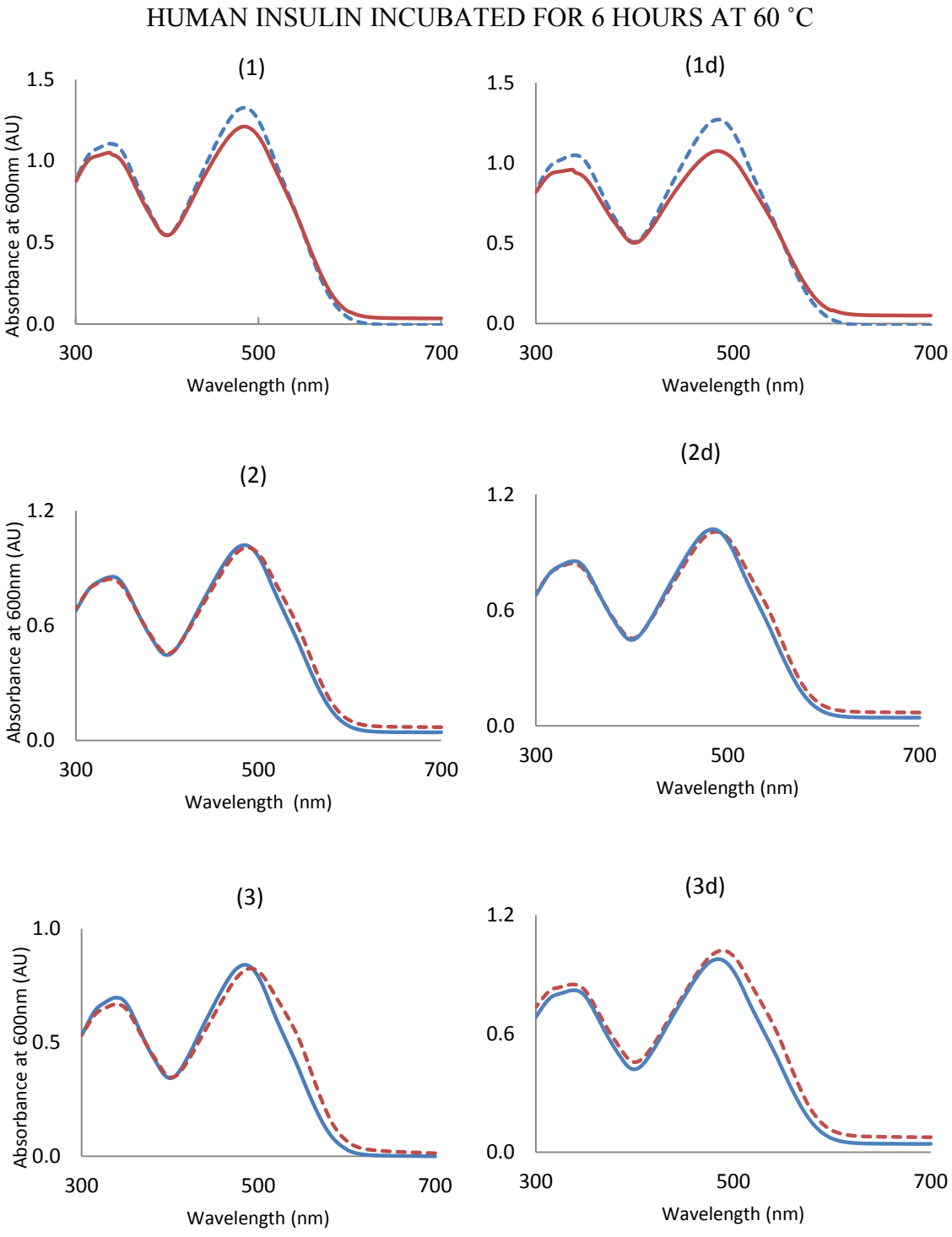

Figure E.7 Congo red results of human insulin in bulk and in the presence of surfaces (SACF Biosciences, Cat. #: 91077C-250MG (lot 10L917)): Blank (—); Sample (- - -). (1) and (1d) are human insulin and its duplicate; (2) and (2d) are human insulin and its duplicate in liposome 2 (20/80)% PC/C; (3) and (3d) are human insulin and its duplicate in liposome 3 (80/20)% PC/C.

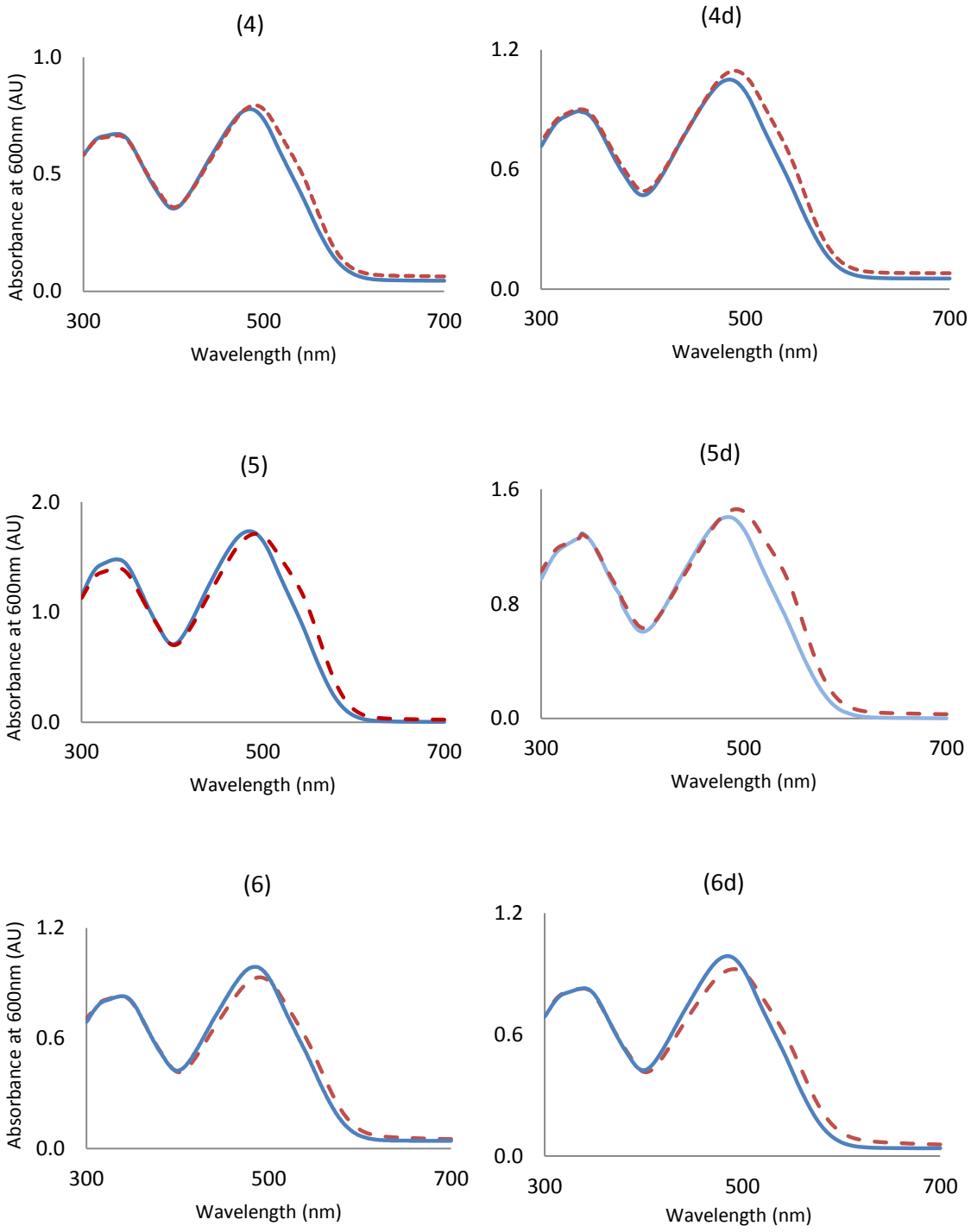

Figure E.8. Congo red results of human insulin in bulk and in the presence of surfaces (SACF Biosciences, Cat. #: 91077C-250MG (lot 10L917)): Blank (—); Sample (- - -). (4) and (4d) are human insulin and its duplicate in liposome 5 (10:5:7.5:16) PC/PE/PS/C; (5) and (5d) are human insulin and its duplicate in liposome 6 (50/50)% PC/C; (6) and (6d) are human insulin and its duplicate in PS-NH_2.

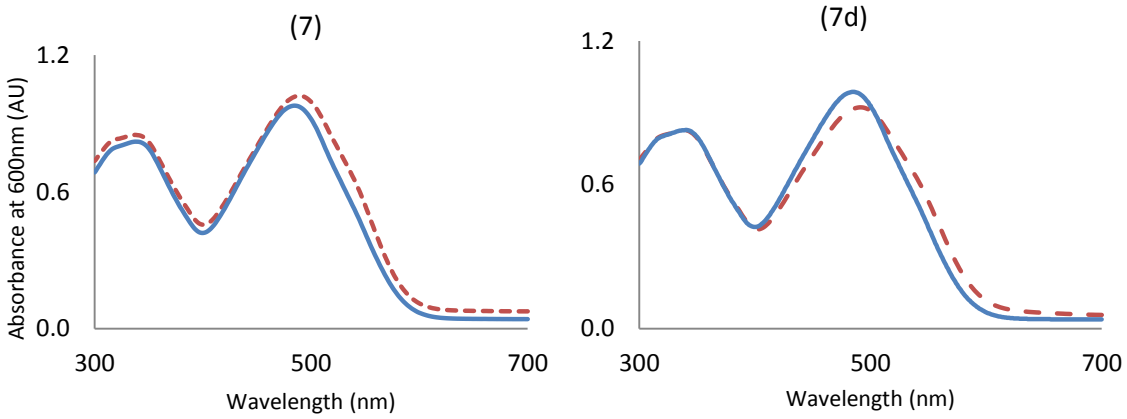

Figure E.9. Congo red results of human insulin in bulk and in the presence of surfaces (SACF Biosciences, Cat. #: 91077C-250MG (lot 10L917)): Blank (—); Sample (- - -). (7) and (7d) are human insulin and its duplicate in PS-COOH.

HUMAN INSULIN INCUBATED FOR 55 HOURS AT 37 ˚C AND 230 RPM

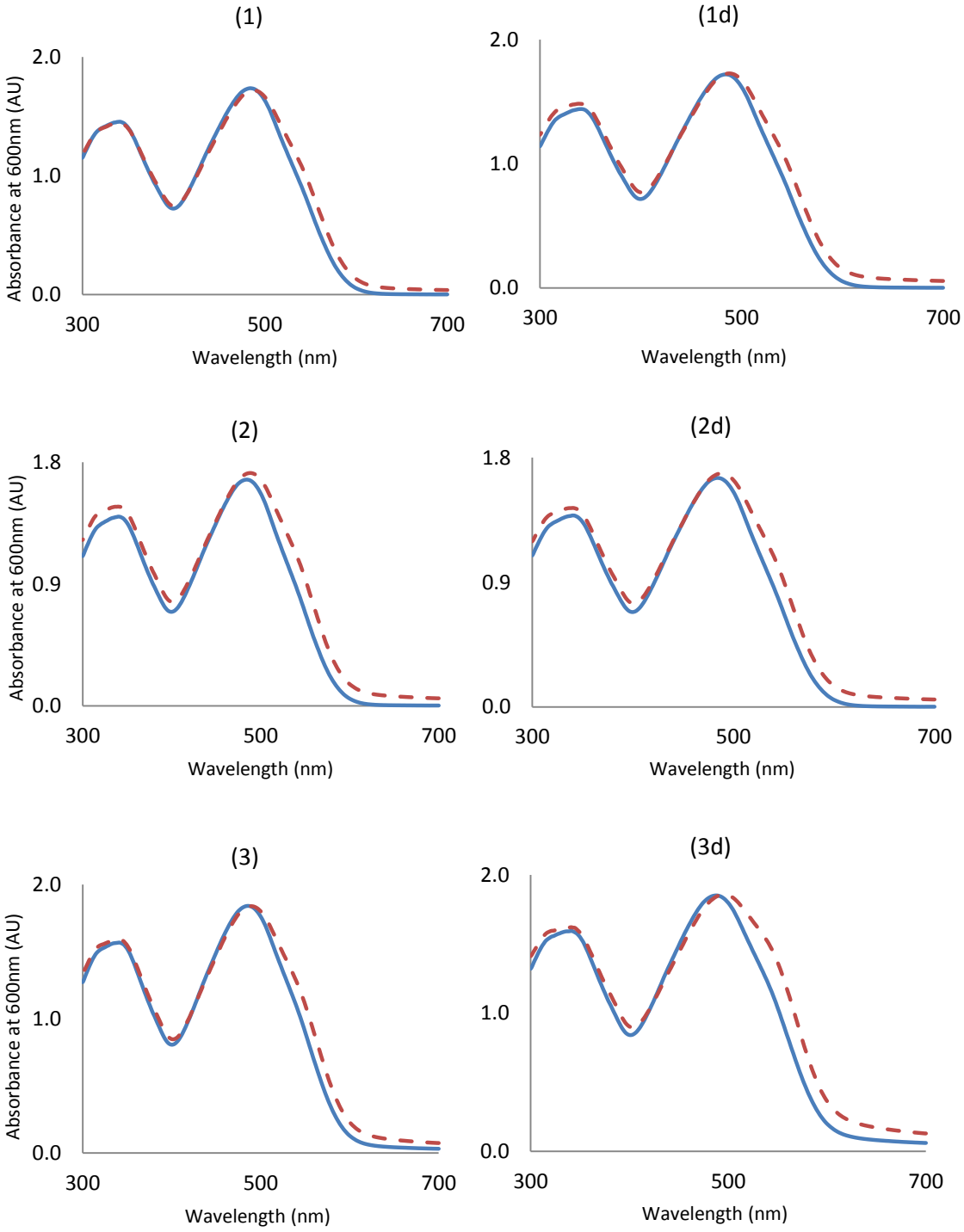

Figure E.10 Congo red results of human insulin in bulk and in the presence of surfaces (SIGMA I2643, lot (096K03811V)): Blank (—); Sample (- - -). (1) and (1d) are human insulin and its duplicate; (2) and (2d) are human insulin and its duplicate in liposome 2 (20/80)% PC/C; (3) and (3d) are human insulin and its duplicate in liposome 3 (80/20)% PC/C.

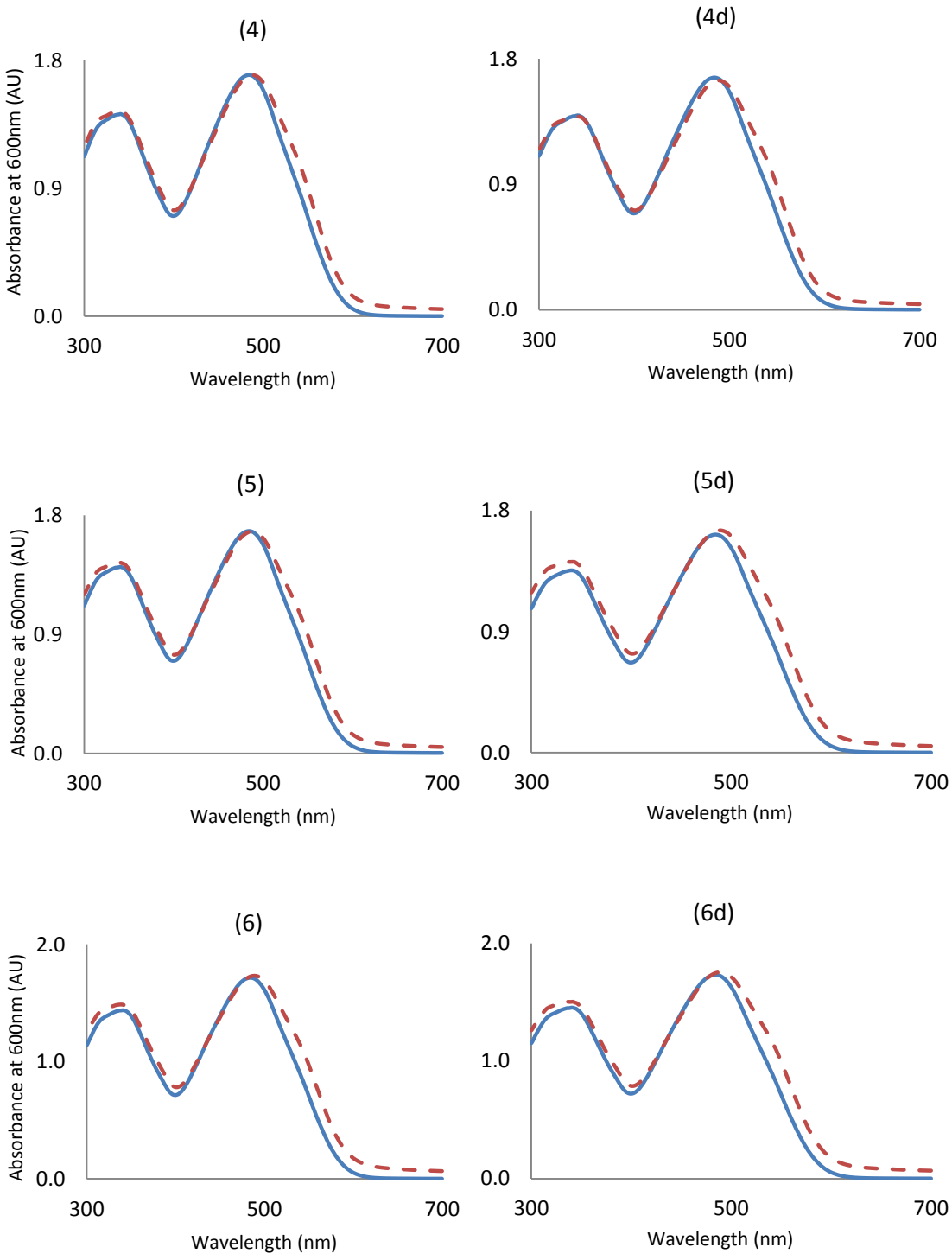

Figure E.11. Congo red results of human insulin in bulk and in the presence of surfaces: (SIGMA I2643, lot (096K03811V)): Blank (—); Sample (- - -). (4) and (4d) are human insulin and its duplicate in liposome 5 (10:5:7.5:16) PC/PE/PS/C; (5) and (5d) are human insulin and its duplicate in liposome 6 (50/50)% PC/C; (6) and (6d) are human insulin and its duplicate in PS-NH_2.

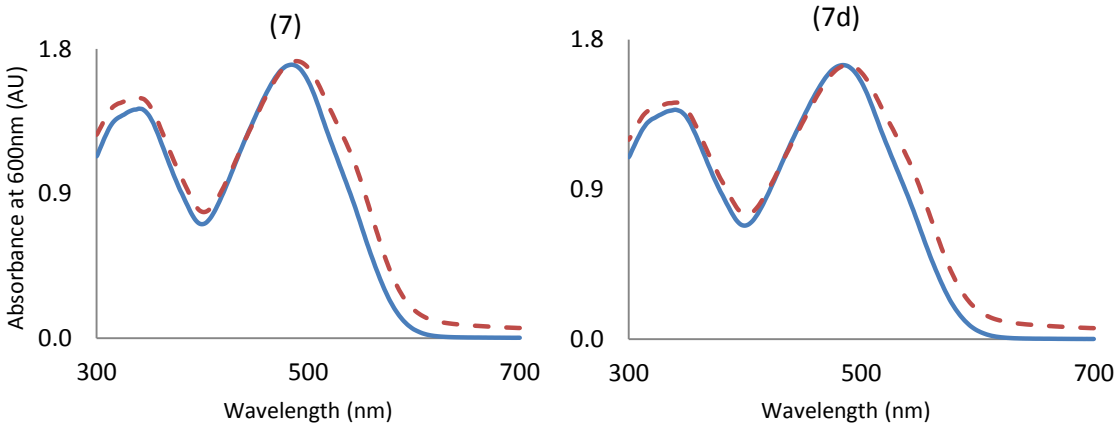

Figure E.12. Congo red results of human insulin in bulk and in the presence of surfaces: (SIGMA I2643, lot (096K03811V)): Blank (—); Sample (- - -). (7) and (7d) are human insulin and its duplicate in PS-COOH.

BIBLIOGRAPHY

1. Ahmad, A., Millett, I.S., Doniach, S., Uversky, V.N., Fink, A.L. 2003. Partially folded intermediates in insulin fibrillation. Biochemistry 42: 11404–11416.

2. Ban, T., Hoshino, M., Takahashi, S., Hamada, D., Hasegawa, K., Naiki, H., and Goto, Y. Direct Observation of AB Amyloid Fibril Growth and Inhibition. 2004. J. Mol. Biol. 344, 757-767.

3. Bauer, H.H., Aebi, U., Haener, M., Hermann, R., Mueller, M., Arvine, T., and Merkle, H.P. J. Struct. Biol. **115**, 1-15 (1995).

4. Blake, C. and Serpell, L.C. Structure (London) **4**, 989-998 (1996).

5. Bouchard, M., Zurdo, J., Nettleton, E.J., Dobson, C.M. and Robinson, C. (2000). Formation of insulin amyloid fibrils followed by FTIR simultaneously with CD and electron microscopy. Protein Science. 9, 1960-1967.

6. Brange, J., Andersen, L., Laursen, E. D., Meyn, G., and Rasmussen, E. 1997. Toward understanding insulin fibrillation. J. Pharm. Sci., 86, 517-525.

7. Brange, J., Skelbaek-Pedersen, B., Langkjaer, L., Damgaard, U., Ege, H., Havelund, S., Heding, L. G., Jorgensen, K. H.,Lykkeberg, J., Markussen, J., Pingel, M., and Rasmussen, E.(1987) Galenics of insulin. The physicochemical and pharmaceutical aspects of insulin and insulin preparations, Springer-Verlag, Berlin.

8. Bryant, C., Spencer, D. B., Miller, A., Bakaysa, D. L., McCune, K. S., Maple, S. R., Pekar, A. H., and Brems, D. N. 1993. Acid stabilization of insulin. Biochemistry, 32, 8075-8082.

9. Burke, MJ, Rougvie MA. 1972. Cross-beta protein structures. I. Insulin fibrils. Biochemistry, 11, 2435-2439.

10. Chirita, N.C., Congdon, E.E., Yin, H., Kuret, J. 2005. Triggers of full-length tau aggregation: a role for partially folded intermediates. Biochemistry, 44, 5862-5872.

11. Dobson, C. M., 1999. Protein misfolding, evolution and disease. Trends Biochem. Sci., 24, 329–332.

12. Dobson, C.M., Sail, A., and Karplus, M. 1998. Protein folding: a perspective from theory and experiment. Angew, Chem. Int. Ed. Eng. 37, 868-893.

13. Feingold, V., Jenkins, A. B., Kraegen, E. W. 1984. Diabetologia, 27, 373-378.

14. Flyvbjerg, H., Jobs, E., and Leibler, S. 1996. Kinetics of self-assembling microtubules: An "inverse problem" in biochemistry. Proc. Natl. Acad. Sci. 93. 5975-5979.

15. Grudzielanek, S., Jansen, R. and Winter, R. 2005. Solvational tuning of the unfolding, aggregation and amyloidogenesis of insulin. J. Mol. Biol. 351 (4), 879-894.

16. Goldsbury, C.S., Cooper, G.J.S., Goldie, K.N., Mueller, S.A., Saafi, E.L., Gruijters, W.T.M., Misur, M.P., Engel, A. and Aebi, U. 1997. Polymorphic fibrillar assembly of human amylin. J. Struct. Biol.119, 17-27.

17. Hill, T.L. 1983. Length dependence of rate constants for end-to-end association and dissociation of equilibrium linear aggregates. Biophys. J. 44, 285-288.

18. Jarrett, J.T. and Lansbury, P.T., Jr. 1992. Amyloid fibril formation requires a chemically discriminating nucleation event: Studies of an amyloidogenic sequence from the bacterial protein OsmB. Biochemistry. 31 (49), 12345-12352.

19. Jarrett, J.T. and Lansbury, P.T., Jr. 1993. Seeding "one-dimensional crystallization" of amyloid: a pathogenic mechanism in Alzheimer's disease and scrapie? Cell., 73, 1055-1058.

20. Jimenez, J.L., Nettleton, E. J., Bouchard, M., Robinson, C.V., Dobson, C.M., and Saibil, H.R. 2002. The protofilament structure of insulin amyloid fibrils. PNAS. 99 (14) 9196-9201.

21. Klunk, W. E., Pettergrew, J. W. and Abraham, D. J. 1989. Quantitative Evaluation of congo red binding to Amyloid like Protein with β-Pleated Sheet Conformation. J. Histchem. Cytochem. 37 (8), 1273-1281.

22. Knowles, T.P., Fitzpatrick, A.W., Meehan, S., Mott,H.R., Vendruscolo, M., Dobson, C.M. and Welland, M.E. 2007. Role of intermolecular forces in defining material properties of protein nanofibrils. Science, 318, 1900-1903.

23. Li, C. and Deng, Y. 2004. A novel method for the preparation of liposomes: Freeze drying of monophase solutions. J. Pharm. Sci., 93 (6) 1403-1414.

24. Librizzi, F. and Rischel, C. 2005. The kinetic behavior of insulin fibrillation is determined by heterogeneous nucleation pathways. Protein Sci. 14, 3129-3134.

25. Lui, R., He, M., Su, R., Yu, Y., Qi, W., and He, Z. 2010. Insulin amyloid fibrillation studied by terahertz spectroscopy and other biophysical methods. Biochemical and Biophysical Research Communications. 391. 862–867.

26. Matheus, S., Mahler, H-C. and Friess W. 2006. A critical evaluation of Tm(FTIR) measurements of high-concentration IgG1 antibody formulations as a formulation development tool. Pharm. Res. 23, 1617-1627.

27. McLaurin, J., Darabie, A.A., and Morrison, M.R. 2002. Cholesterol, a modulator of membrane-associated Aβ-fibrillogenesis. Ann. N.Y. Acad. Sci. 977, 376-383.

28. Moores, B., Drolle, E., Attwood, S., Simons, J., Leonenko, Z. 2011. Effect of Surfaces on Amyloid Fibril Formation. PLoS ONE 6(10): p1.

29. Naiki, H. and Nakakuki K. 1996. First-order kinetic model of Alzheimer's β-amyloid fibril extension in vitro. Laboratory Investigation, 74 (2), 374-383.

30. Nayak, A., Dutta, A. K., and Belfort, G. 2008. Surface-enhanced nucleation of insulin amyloid fibrillation. Biochemical and Biophysical Research Communications 369, 303-307.

31. Nettleton, E.J. (1998) Ph. D. thesis (Oxford University, Oxford).

32. Nielsen, L., Frokjaer, S., Carpenter, J.F. and Brange, J. (2000). Studies of the structure of insulin fibrils by Fourier transform infrared (FTIR) spectroscopy and electron microscopy. Journal of Pharmaceutical Sciences, 90, 29-37.

33. Nielsen L, Khurana R, Coats A, Frokjaer S, Brange J, Vyas S, Uversky VN, Fink A., 2001a. Effect of environmental factors on the kinetics of insulin fibril formation: elucidation of the molecular mechanism. Biochemistry. 40, 6036-6046.

34. Nielsen, L., Frokjaer, S., Brange, J., Uversky, V. N. and. Fink. A. L. 2001b. Probing the mechanism of insulin fibril formation with insulin mutants. Biochemistry, 40, 8397–8409.

35. Nilsson, M.R. 2004. Techniques to study amyloid fibril formation in vitro. Methods, 34, 151-160.

36. Oosawa, F. and Asakura, S. 1975. Thermodynamics of the Polymerization of Protein, Academic Press Inc.: London.

37. Relini. A., Cavalleri, O., Rolandi, R., and Gliozzi, A. 2008. The two-fold aspect of the interplay of amyloidogenic proteins with lipid membranes. Chemistry and Physics of Lipids. 158 1-9.

38. Sharp, J.S., Forrest, J.A., and Jones, R.A.L. Surface denaturation and amyloid fibril formation of insulin at model lipid-water interfaces. 2002. Biochemistry. 41, 15810-15819.

39. Shire, S.J., Shahrokh, Z. and Liu, J. 2004. Challenges in the development of high protein concentration formulations. J. Pharm. Sci. 93, 1390-1402.

40. Sluzky, V., Tamada J. A., Klibanov A. M., and Langer R. 1991. Kinetics of Insulin aggregation in aquesous solutions upon agitation in the presence of hydrophobic surfaces. Proc.Natl. Acad. Sci. USA. 88, 9377-9381.

41. Vestergaard, B., Groenning, M., Roessle, M., Kastrup J.S., van de Weert M. 2007. A helical structural nucleus is the primary elongating unit of insulin amyloid fibrils. PLoS Biol 5 (5): e134. doi:10.1371/journal.pbio.0050134.

42. Wang, W., Nema, S. and Teagarden, D. 2010. Protein aggregation- Pathways and influencing factors. International Journal of Pharmaceutics. 390, 89-99.

43. Waugh, D. F. 1940. Pressure-soluble and pressure-displaceable components of monolayers of native and denatured proteins. Langmuir, I. J Am. Chem. Soc. 62, 2771-2793.

44. Waugh, D.F. 1941. The properties of protein fibers produced reversibly from soluble protein molecules. A. J. Physiol. 133, 484-485.

45. Waugh, D. F. 1946a. A fibrous modification of insulin. I. The heat precipitate of insulin. J. Am. Chem. Soc. 68, 247-250.

46. Waugh, D. F. 1946b. Reactions involved in insulin fibril formation. Fed. Proc. 5, 111.

47. Waugh, D. F., Wilhelmson, D.F., Commerford, S. L., Sackler, M. L. 1953. Studies of the nucleation and growth reactions of selected types of insulin fibrils. J. Am. Chem. Soc. 75, 2592-2600.

48. White, H. E., Hodgkinson, J.L., Jahn, T.R., Cohen-Krausz, S., Gosal, W.S., Müller, S., Orlova, E.V., Radford, S.E. and Saibil, H.R. 2009. Globular tetramers of β2-microglobulin assemble into elaborate amyloid fibrils. J. Mol. Biol. 389, 48–57.

49. Wolynes, P.G., Onuchi, J.N. and Thirumalai, D. 1995. Navigating the folding routes. Science. 267, 1619-1620.

VITA

Paulina Barranco Morales was born in Mexico City, Mexico. She graduated with a Bachelor of Sciences in Chemical Engineering from Missouri University of Science and Technology (Missouri S&T) in the Fall of 2010. She joined Missouri S&T in the Spring of 2011 for her Master's degree in Chemical Engineering. During her graduate studies she obtained a Co-op position with Bayer HealthCare (Leverkusen, Germany) as an Engineer Trainee. She received her M.S. degree in Chemical Engineering in December 2013. Paulina joined Bayer HealthCare in the USA in the Fall of 2013.